ACOUSTIC AND THERMAL CHARACTERIZATION OF RIVER LANDSCAPES

Dissertation

for the degree of

Doctor of Sciences

submitted to

Department of Biology, Chemistry and Pharmacy

Freie Universität, Berlin, Germany

presented by

Diego Tonolla

Master of Science (Environmental Sciences)

Swiss Federal Institute of Technology, Zurich, Switzerland

Place of birth: Locarno (Switzerland)

April 2011

First referee **Prof. Dr. Klement Tockner**

Director of the Leibniz-Institute of Freshwater Ecology and Inland Fisheries (IGB), Berlin, Germany. Professor of Aquatic Ecology at the Freie Universität, Berlin.

Second referee **Dr. Mark S. Lorang**

Research Associate Professor, The University of Montana, Flathead Lake Biological Station (FLBS), Polson, Montana, USA.

Date of the dissertation defense: 16 June 2011.

TABLE OF CONTENTS

SUMMARY

The study of rivers and their heterogeneity at the landscape scale has been recognized by many scientists as crucial for advancing our understanding of ecology, and for establishing adequate restoration and conservation strategies. This doctoral thesis used advanced acoustic and infrared sensors to quantify acoustic and thermal attributes of river landscapes and relate these properties to the ecological relevance in river science.

Acoustic characterization of river landscapes

For many decades, rivers and streams have been the subject of intense research into their hydrologic, geomorphic, and ecological characteristics. However, the physical generation of underwater sound as an essential property of fluvial landscapes and as a source of information for aquatic biota has been neglected. This work provides the first quantitative insights into the underwater acoustics of river landscapes (Chapters 1 to 3).

In the first study, the effects of hydrogeomorphic parameters (e.g. discharge, water velocity, bed structures) and induced turbulence on acoustic signal generation was quantified under controlled laboratory conditions (Chapter 1). The lessons learned from this flume study were then applied in the field to five common river habitat types along 12 rivers. These Eulerian data were analyzed and their acoustic, as well as their hydraulic and geomorphic variables were compared (Chapter 2). The third approach to assessing the link between acoustic signals and hydraulic flow conditions took the Lagrangian approach by continuously recording data while floating downstream on a raft. Data were collected during intermediate flow conditions for 5-24 km along the downstream axis of the main channels of five hydrogeomorphic different river segments. In order to determine the effects of flow on the acoustic signal, two segments were again floated at different discharge levels (Chapter 3).

Acoustic signals beneath the water surface were recorded using two submerged hydrophones (one hydrophone in Chapter 3) with the head facing upstream, and analyzed using a signal-processing software over 31 third-octave bands (0.020-20 kHz), and then combined in 10 octave bands (0.0315-16 kHz).

The primary goals of Chapters 1 to 3 were (i) to identify the main hydraulic and geomorphic features that best explain the generation and propagation of underwater acoustic signals in flowing water, (ii) to characterize and compare river habitat types and river

segments based on their acoustic signature, and (iii) to discuss the potential ecological relevance of different acoustic signatures for freshwater organisms.

The results from Chapters 1 to 3 revealed that distinct underwater acoustic landscapes (so-called "soundscapes") exist and can be used to quantify hydrogeomorphic processes and differentiate between aquatic habitats (e.g. pools, runs, riffles) and river types (e.g. channelized, bedrock-constrained, unconstrained). These distinctions are based on sound heterogeneity and sound pressure level of 10 octave bands. Distinct soundscapes were detected at spatial scales ranging from centimeters (Chapter 1) to meters (Chapter 2), and to kilometers (Chapter 3) with hydraulically and morphologically heterogeneous habitats and river segments showing more complex soundscapes than more homogeneous ones. I found that the significant differences in the acoustic signatures between habitat and river types are primarily determined by relative roughness, flow velocity, flow depth, and particle collisions during streambed sediment transport (Chapters 1 to 3). Specifically, increases in water velocity resulted in increased sound pressure levels over a wide range of frequencies; increases in relative roughness led to a predominant increase in the middle-frequency sound pressure level (~0.063-1 kHz), while an increase in streambed sediment transport increased the sound pressure level at high frequencies (~2-16 kHz). The latter two factors were responsible for most of the heterogeneity in the acoustic signals. Furthermore, changes in the flow level modified relative roughness, turbulence, and streambed sediment transport, thus modifying the soundscape by influencing acoustic heterogeneity and the sound pressure level of distinct frequencies (Chapter 3).

The results of Chapters 1 to 3 clearly showed that physically generated underwater sound is a complex and robust signal, and hence, should be considered as an important and unique property of riverine ecosystems. It is well known that inter- and intraspecific communication is not the only role of sound in aquatic ecosystems, but that many organisms use acoustic cues for spatial orientation and for positioning themselves within suitable habitats. I am convinced that physically generated underwater soundscapes contain important information for freshwater organisms about their riverine environment, and therefore may potentially influence their behavior and ecology, as well as ecosystem processes. Moreover, underwater soundscapes could be used to assess and quantify the heterogeneity of rivers, because they reflect important hydraulic (turbulence levels) and geomorphic (bedload mobility) dynamics. Acoustic signals could potentially be used to monitor river restoration measures that impact or change the flow field and subsequent streambed sediment transport-deposition processes.

Thermal characterization of river landscapes

River floodplains are composed of a shifting mosaic of interconnected aquatic and terrestrial habitats that differ in their ecosystem functions and biodiversity patterns. Temperature is a master variable that drives ecosystem processes and influences the dispersal and behavior of organisms. However, assessing thermal heterogeneity at the floodplain scale using only in-situ point measurements greatly limits our ability to understand the thermal effects on ecological processes. Therefore, alternative methods that provide high spatial and temporal resolution are needed to characterize the thermal heterogeneity of entire river landscapes such as floodplains (Chapters 4 and 5).

In the first study (Chapter 4), ground-based thermal infrared (IR) imagery was used to quantify surface temperature patterns at 12-15 minute intervals over diel cycles in two near-natural Alpine floodplains (Roseg and Tagliamento Rivers). Vertical temperature distribution was measured with thermocouples at 3-5 minute intervals in the top layer (at 1 cm intervals; 0-29 cm depth) of unsaturated gravel sediment deposits. In the second study (Chapter 5), airborne thermal IR imagery was used to quantify thermal heterogeneity and water extent under two flow conditions in a lowland floodplain (Oder River). At the same time, all major river and floodplain water bodies were electro-fished in order to identify the composition of associated fish assemblages. Furthermore, temperature loggers were deployed from March to July across the entire range of floodplain water bodies to assess seasonal thermal dynamics (recording interval: 20 minutes).

The common goals of Chapters 4 and 5 were (i) to quantify spatiotemporal thermal heterogeneity of entire river floodplains at high spatial resolution, and (ii) to evaluate whether or not high resolution thermal IR imagery is a useful tool for quantifying thermal heterogeneity in complex river landscapes. In addition, Chapter 4 aimed (iii) to thermally characterize specific aquatic and terrestrial types of floodplain habitat, and (iv) to quantify vertical temperature patterns within unsaturated gravel sediment deposits. Chapter 5 aimed (v) to evaluate the potential link between thermal heterogeneity and the structure of fish assemblages at the river floodplain scale, and (vi) to assess the effect of different flow levels on surface temperature patterns.

Both studies revealed complex spatiotemporal thermal patterns in river floodplains that varied considerably over a 24-hour period (Chapter 4), and between mean and high flow conditions (Chapter 5). Specific properties (e.g. surface type, coverage, morphology, hydrological connectivity) of the different terrestrial and aquatic habitat types were responsible for the distinct thermal signatures that created the complex thermal mosaic. The

vertical and temporal variation of temperature in unsaturated gravel sediments was almost as large as horizontal variation across the entire floodplain surface (Chapter 4). A high level of congruence was found between thermal properties of floodplain water bodies (derived from analysis of airborne thermal IR images) and fish assemblages, which could not have been determined with in-situ temperature measurements (Chapter 5).

Chapters 4 and 5 clearly demonstrated that sub-meter resolution thermal IR imagery provides the unique capacity to detect and quantify the composition and the spatial configuration of thermal patches in complex river landscapes such as floodplains. This study indicated that standard in-situ surveys are likely to underestimate the spatiotemporal thermal heterogeneity of floodplains, as well as of individual habitat types. The large spatial scale of the overview gained via thermal IR imagery may be used to decide where to concentrate the most detailed and time-consuming in-situ investigations. Moreover, this method allowed for the identification of both natural and anthropogenic drivers that influence thermal heterogeneity, as well as the detection of ecologically important warm and cold patches and distinct temperature gradients. This information is expected to be crucial for quantifying and interpreting the effects of thermal heterogeneity on key ecosystem processes and biodiversity. Finally, it can improve our understanding of the factors that control the composition and behavior of organisms across various spatial and temporal scales. The method itself is an important monitoring tool crucial for planning adequate conservation and river restoration strategies.

ZUSAMMENFASSUNG

Das Studium von Fließgewässern und deren Heterogenität auf der Landschaftsebene wird von vielen Ökologen als entscheidend eingestuft, um einerseits unser Verständnis der Gewässerkomplexität zu erweitern und zudem um die Etablierung angemessener Renaturierungs- und Naturschutzstrategien zu ermöglichen. In dieser Doktorarbeit wurden moderne akustische und Infrarot-Sensoren eingesetzt, um akustische und thermische Eigenschaften von Fließgewässerlandschaften zu quantifizieren und darüber hinaus die potentielle ökologische Relevanz dieser grundlegenden Eigenschaften zu beleuchten.

Akustische Charakterisierung von Fließgewässerlandschaften

Über viele Jahrzehnte waren Flüsse und Bäche Gegenstand intensiver Forschung, die auf deren hydraulischen, geomorphologischen und ökologischen Eigenschaften basierten. Jedoch wurde bislang die spezifische physikalische Erzeugung des Unterwasserschalls als eine wesentliche Eigenschaft von Fließgewässerlandschaften und als eine kritische Informationsquelle für aquatische Fauna zumeist vernachlässigt. Somit liefert diese Arbeit den ersten quantitativen Einblick in die Unterwasserakustik von Fließgewässerlandschaften (Kapitel 1 bis 3).

In der ersten Studie wurden unter kontrollierten Laborbedingungen die Effekte hydraulischer und geomorphologischer Parameter (z.B. Abflussmenge, Wassergeschwindigkeit, Flussbettstrukturen) sowie induzierter Wirbelströmungsbildung auf die akustische Signalerzeugung quantifiziert (Kapitel 1). Die aus diesen Fließrinnen-Studien gewonnenen Erkenntnisse wurden in einem nächsten Schritt auf das Feld übertragen und in fünf verbreitet vorkommenden Fließgewässer-Habitaten von 12 Flüssen getestet. Die so gewonnenen Eulerschen-Daten wurden analysiert und unter Beachtung ihrer akustischen, hydraulischen und geomorphologischen Variablen verglichen (Kapitel 2). Als dritter Ansatz zur Bewertung der akustischen Signale und hydraulischen Strömungsverhältnisse wurde der Lagrange-Ansatz verwendet, für den die Daten kontinuierlich von einem Floß aus erfasst wurden. Die Daten wurden während mittlerer Abflussbedingungen auf einer Länge von 5-24 km entlang der Hauptflussrinne Richtung flussabwärts an fünf Flussabschnitten unterschiedlicher hydraulischer und geomorphologischer Ausprägung gesammelt. Um den Einfluss der Abflusserhöhung auf das akustische Signal bestimmen zu können, wurde die o.g.

Datenerfassung für zwei der fünf Abschnitte auch unter verschiedenen Abflussmengen durchgeführt (Kapitel 3).

Die akustischen Unterwassersignale wurden von je zwei stromaufwärts ausgerichteten Hydrophonen aufgezeichnet (nur ein Hydrophon in Kapitel 3), diese unter Verwendung einer Signalverarbeitungssoftware mit über 31 Terzbändern (0.020-20 kHz) analysiert und später in zehn Oktavbändern (0.0315-16 kHz) kombiniert.

Die Hauptziele von Kapitel 1 bis 3 waren (i) die Identifizierung der wichtigsten hydraulischen und geomorphologischen Merkmale, die die Erzeugung und Verbreitung von Unterwasserschallsignalen in Fließgewässern am besten erklären, (ii) die Charakterisierung und der Vergleich von Fließgewässer-Habitaten und Fließgewässerabschnitten aufgrund ihrer akustischen Eigenschaften, und (iii) die Diskussion der potenziellen ökologischen Relevanz verschiedener akustischer Eigenschaften für Süßswasserorganismen.

Ergebnisse aus Kapitel 1 bis 3 zeigten, dass bestimmte akustische Unterwasser-Landschaften - so genannte Klanglandschaften - existieren, die zur Quantifizierung hydrologischer und geomorphologischer Prozesse, sowie zur Unterscheidung aquatischer Habitate (z.B. Stille, Gleite, Schnelle) und Fließgewässertypen (z.B. kanalisiert, natürlich verengt, freifließend) auf Grundlage ihrer akustischer Heterogenität und ihres Schalldruckpegels in zehn Oktavbändern verwendet werden können. Ausgeprägte Klanglandschaften wurden in räumlichen Größen von Zentimetern (Kapitel 1), Metern (Kapitel 2), bis zu mehreren Kilometern (Kapitel 3) erfasst, wobei hydraulisch und geomorphologisch heterogenere Habitate und Fließgewässerabschnitte komplexere Klanglandschaften aufwiesen als homogenere. Ferner konnte bestimmt werden, dass die bedeutendsten Unterschiede in den akustischen Eigenschaften von Habitaten und Fließgewässertypen im Wesentlichen von der relativen Rauheit, der Wassergeschwindigkeit, der Wassertiefe und den Partikelkollisionen während des Sedimenttransports am Flussbett abhängen (Kapitel 1 bis 3). Insbesondere die Zunahme der Wassergeschwindigkeit führte zu einem erhöhten Schalldruckpegel über ein breites Band von Frequenzen, die Zunahme der relativen Rauheit führte vor allem zu einer Erhöhung des Schalldruckpegels in den mittleren Frequenzbereichen (~0.063-1 kHz), während eine Zunahme des Sedimenttransports am Flussbett in einer Erhöhung des Schalldruckpegels in den oberen Frequenzbereichen (~2-16 kHz) resultierte. Die beiden letztgenannten Faktoren waren für den Großteil der Heterogenität des akustischen Signals verantwortlich. Darüber hinaus haben Abflussänderungen Modifizierungen der relativen Rauheit, der Turbulenz und des Sedimenttransportes

hervorgerufen und modifizierten folglich die Klanglandschaften durch eine Beeinflussung der akustischen Heterogenität und des Schalldruckpegels in bestimmten Frequenzen (Kapitel 3).

Die Ergebnisse der Kapitel 1 bis 3 zeigten deutlich, dass der physikalisch erzeugte Unterwasserschall ein komplexes und robustes Signal ist und deshalb als eine wichtige und einzigartige Eigenschaft von Fließgewässer-Ökosystemen betrachtet werden sollte. Weiterhin ist bekannt, dass die inter- und intraspezifische Kommunikation nicht die einzige Rolle des Schalls in aquatischen Ökosystemen darstellt, sondern dass viele Organismen auch akustische Signale für die räumliche Orientierung und die Auffindung passender Habitate benutzen können. Daher bin ich davon überzeugt, dass die physikalisch erzeugten Unterwasser-Klanglandschaften für Süsswasserorganismen wichtige Informationen über ihre Umgebung liefern und daher deren Verhalten und Ökologie, sowie auch Ökosystemprozesse beeinflussen können. Darüber hinaus könnten Klanglandschaften zur Bewertung und Quantifizierung der Heterogeneität von Fließgewässern verwendet werden, da sie wichtige hydraulische (Turbulenz-Ebenen) und geomorphologische (Sediment-Mobilität) Eigenschaften reflektieren. Das bedeutet, dass akustische Signale potenziell zur Überwachung der Maßnahmen zur Flussrevitalisierung verwendet werden könnten, da diese das Strömungsfeld und folglich auch Sedimenttransport- und Sedimentablagerungsprozesse beeinflussen oder ändern.

Thermische Charakterisierung von Fließgewässerlandschaften

Flussauen bestehen aus einem sich kontinuierlich veränderndem Mosaik miteinander verbundener aquatischer und terrestrischer Habitate, die sich in ihren Ökosystemfunktionen und ihrer biologischer Vielfalt unterscheiden. Eine Hauptvariable, die Ökosystemprozesse antreibt und die Verbreitung und das Verhalten von Organismen beeinflusst, ist die Temperatur. Jedoch ist die Bestimmung der Temperaturheterogenität in Flussauen zumeist auf lokale Punktmessungen beschränkt. Dies limitiert die Möglichkeiten erheblich, thermische Auswirkungen auf ökologische Prozesse zu verstehen. Um die Temperaturheterogenität von Fließgewässerlandschaften, wie etwa Flussauen, zu charakterisieren (Kapitel 4 und 5), sind alternative Methoden erforderlich, die sowohl eine hohe räumliche wie auch zeitliche Auflösung bieten.

In der ersten Studie (Kapitel 4) wurden thermische Infrarotbilder (IR-Bilder) einer stationären Kamera verwendet, um Oberflächentemperaturmuster in 12-15-minütigen Abständen über 24-stündige Zyklen in zwei nahezu natürlichen alpinen Flussauen (die Flüsse Roseg und Tagliamento) zu quantifizieren. Außerdem wurde mit Hilfe von Temperatursensoren die kinetische Temperaturverteilung in 3-5-minütigen Intervallen in der

obersten Schicht (in 1 cm Abständen; 0-29 cm Tiefe) von ungesättigten Flusssedimenten gemessen. In der zweiten Studie (Kapitel 5) wurden thermische IR-Bilder aus der Luft aufgenommen, um die Temperaturheterogenität und die Überflutungsfläche bei zwei verschiedenen Abflussmengen in einer Tiefland-Flussaue (Fluss Oder) zu quantifizieren. Gleichzeitig wurden alle großen Fluss- und Auengewässer elektrisch befischt, um die Zusammensetzung der assoziierten Fischfauna zu erfassen. Ferner wurden von März bis Juli Temperatursensoren in allen wesentlichen Auengewässer eingesetzt, um zeitlich hochauflösende Temperaturmuster zu erfassen (Aufzeichnungsintervall: 20 Minuten).

Die gemeinsamen Ziele der Kapitel 4 und 5 waren (i) die Quantifizierung der räumlichen und zeitlichen Temperaturheterogenität von Flussauen mit hoher räumlicher Auflösung und (ii) die Evaluierung, ob hochauflösende thermische IR-Bildaufnahmen als ein nützliches Werkzeug für die Quantifizierung der Temperaturheterogenität in komplexen Fließgewässerlandschaften dienen können. Des Weiteren hatte Kapitel 4 die Intention, (iii) spezifische aquatische und terrestrische Flussauen-Habitate thermisch zu charakterisieren und (iv) die vertikalen Temperaturmuster innerhalb ungesättigter Flusssedimenten zu quantifizieren. Kapitel 5 sollte (v) potenzielle Zusammenhänge zwischen der Temparaturheterogenität und der Verteilungsmuster der Fische in Auengewässern bewerten und (vi) die Rolle verschiedener Abflussverhältnisse auf die thermische Heterogenität beurteilen.

Beide Studien zeigten komplexe räumliche und zeitliche Temperaturmuster in Flussauen, die sich über 24 Stunden (Kapitel 4) und zwischen mittleren und hohen Abflussverhältnissen (Kapitel 5) deutlich änderten. Für die unterschiedlichen thermischen Muster waren spezifische Eigenschaften (z.B. Oberflächenbeschaffenheit, Vegetationsabdeckung, Morphologie, hydrologische Konnektivität) terrestrischer und aquatischer Habitate verantwortlich. Die vertikalen und zeitlichen Unterschiede der Temperatur in ungesättigten Flusssedimenten waren annähernd so hoch wie die horizontalen Unterschiede über die gesamte Oberfläche der Flussaue (Kapitel 4). Zwischen den thermischen Eigenschaften der Auengewässer (abgeleitet aus der Analyse der thermischen IR-Luftbilder) und der Fischgemeinschaften wurde ein hohes Kongruenzniveau festgestellt, welches mit lokalen Temperaturmessungen allein nicht hätte bestimmt werden können (Kapitel 5).

Kapitel 4 und 5 zeigten deutlich, dass thermische IR-Bilder mit einer Auflösung im Zentimeter Bereich die einzigartige Möglichkeit zur Feststellung und Quantifizierung von Zusammensetzung und räumlicher Konfiguration thermischer Muster in komplexen Fließgewässerlandschaften, wie etwa Flussauen, aufweisen. Diese Studie zeigte, dass die

herkömmlichen lokalen Messungen die räumliche und zeitliche Temparaturheterogenität von Flussauen, sowie deren Habitate wahrscheinlich unterschätzen. Die räumliche Dimension, die mit thermischen IR-Bildaufnahmen erzielt wurde, könnte benutzt werden, um zu entscheiden, wo detaillierte und zeitaufwendige lokale Untersuchungen durchzuführen sind. Außerdem erlaubt diese Methode die Identifizierung natürlicher und anthropogener Ursachen, die die Temperaturheterogenität beeinflussen, sowie die Erfassung von ökologisch wichtigen Temperaturrefugien und von eindeutigen Temperaturgradienten. Diese Informationen werden als entscheidend für die Quantifizierung und Interpretation der Auswirkungen von Temperaturheterogenität auf wichtige Ökosystemprozesse und die Biodiversität eingestuft. Letztlich können diese Informationen das Verständnis bezüglich jener Faktoren verbessern, die die Struktur und das Verhalten von Organismen auf unterschiedlichen räumlichen und zeitlichen Skalen maßgeblich kontrollieren. Diese Methodik stellt daher ein wichtiges Werkzeug zur Planung angemessener Naturschutz- und Revitalisierungsmaßnahmen von Fließgewässern dar.

THESIS OUTLINE

This doctoral thesis is organized as a cumulative work, presented in the form of three published, peer-reviewed articles and two submitted manuscripts currently under review. Each manuscript forms a separate chapter (Chapters 1 to 5) of this thesis and has its own introduction, methodology, results, discussion, and reference sections. As a result of this structure, each chapter can be read independently from the others. The present thesis also contains general introduction and discussion sections that provide the context and the perspectives based on the findings. These sections overlap with the content of the different chapters. The references used in the introduction and discussion are listed at the end of the discussion section.

The layout of peer-reviewed articles which have already been published or submitted has been modified (from the original journal layout) in order to ensure a consistent layout throughout the entire thesis.

Chapter 1

Tonolla D, Lorang MS, Heutschi K, Tockner K. 2009. A flume experiment to examine underwater sound generation by flowing water. *Aquatic Sciences* 71: 449-462. Doi: 10.1007/s00027-009-0111-5.

Author contributions

DT designed the study, organized and performed the flume experiments, analyzed the data and compiled the paper. MSL co-designed the study and contributed to the text. KH contributed to the acoustic data analyses and provided advice on acoustic methodology. KT co-designed the study and contributed to the final version of the text.

Chapter 2

Tonolla D, Acuña V, Lorang MS, Heutschi K, Tockner K. 2010. A field-based investigation to examine underwater soundscapes of five common river habitats. *Hydrological Processes* 24: 3146-3156. Doi: 10.1002/hyp.7730.

Author contributions

DT designed the study, organized and performed the field work, analyzed the data and compiled the paper. VA advised on the compilation of the manuscript and on data analysis and contributed to the text. MSL co-designed the study and contributed to the text. KH contributed to the acoustic data analyses and advised on acoustic methodology. KT contributed to the final version of the text.

Chapter 3

Tonolla D, Lorang MS, Heutschi K, Gotschalk CC, Tockner K. 2011. Underwater soundscapes along river corridors. *Limnology and Oceanography*. In revision.

Author contributions

DT designed the study, organized and performed the field work, analyzed the data and compiled the paper. MSL co-designed the study, assisted with data sampling in the USA and contributed to the text. KH contributed to the acoustic data analyses and advised on acoustic methodology. CCG assisted with data sampling in the USA and contributed to the preparation of raw data. KT contributed to the final version of the text.

Chapter 4

Tonolla D, Acuña V, Uehlinger U, Frank T, Tockner K. 2010. Thermal heterogeneity in river floodplains. *Ecosystems* 13: 727-740. Doi: 10.1007/s10021-010-9350-5.

Author contributions

DT analyzed the data and compiled the paper. VA contributed to the data analyses and the text. UU managed the field work and collected the data. TF contributed to the IR data analyses and advised on IR methodology. KT initiated and co-designed the study and contributed to the final version of the text.

Chapter 5

Tonolla D, Wolter C, Ruhtz T, Tockner K. 2011. Thermal heterogeneity and fish assemblages in a dynamic river floodplain mosaic (Oder River, Germany). Submitted to *Ecography: Pattern and Diversity in Ecology*.

Article reprinted with kind permission of the managing Editor of Ecography.

Author contributions

DT designed the study, organized and performed the field work, organized the remote sensing sampling, analyzed the data and compiled the paper. CW co-organized the field work, was responsible for electro-fishing and contributed to the text. TR collected the remotely-sensed images and contributed to image processing and the text. KT contributed to the final version of the text.

GENERAL INTRODUCTION AND GOALS

The study of rivers and their heterogeneity at the landscape scale is crucial for advancing our understanding of river ecology and for establishing adequate conservation strategies (Fausch et al. 2002; Wiens 2002). The physical structure of rivers may change significantly along spatiotemporal scales (Thorp et al. 2006) and can reveal hierarchically-organized structures that incorporate, on successively lower levels, segment, reach, habitat, and microhabitat subsystems, each one playing a particular structural and functional role (both physical and biological) in a river (Frissell et al. 1986). Furthermore, the flow of energy and sediment, the morphology, and the hydraulic exchange between and within rivers is neither uniform nor simple. Complex variations in these key factors will influence ecological processes and ultimately the composition and distribution of organisms.

In recent decades, many valid field and remote sensors for the study of freshwater ecology have been developed (Mertes 2002; Marcus and Fonstad 2010; and references therein). These tools are rapidly improving our understanding of ecosystems by greatly expanding the spatial scale upon which they can be analyzed. These tools provide a new set of "eyes" through which we may obtain unexpected results that may help to develop new paradigms (Porter et al. 2009). They are expected to not only advance the discipline of river ecology, but to enhance the effectiveness of conservation and restoration measures as well.

This thesis was designed to explore the use of new acoustic and thermal tools as they apply to the ecological study of river landscapes through a multidisciplinary research approach that blends purely physical studies of acoustic and thermal landscape patterns with the potential ecological outcomes. This required the formation of partnerships and ideas among ecologists, acoustic engineers, thermal IR experts, hydrologists and morphologists. Such an approach has been recognized as important for the advancement of science (Benson et al. 2010).

Acoustic characterization of river landscapes

The hydraulic, morphological, ecological and visual aspects of rivers have been the subject of intense research for over 50 years. Rivers and their habitats have traditionally been characterized based on hydraulic (e.g. flow depth, flow velocity) and geomorphic (e.g. slope, sediment composition, bed roughness) properties, and grouped into downstream sequences (e.g. riffle-pool) (Leopold and Maddock 1953; Montgomery and Buffington 1997; Wohl and

Merritt 2008). However, the hydraulically-generated sound beneath the surface of the water, and its potential as a quantitative indicator of the unique features of rivers and their habitats have only recently received attention from researchers (Lugli and Fine 2003; Amoser and Ladich 2005; Wysocki et al. 2007; Amoser and Ladich 2010). Indeed, sound seems to be a robust signal in fluvial ecosystems and may provide a potentially important source of information in underwater environments because of its lower attenuation rate compared to light and chemical substances, and because it can be transmitted rapidly over long distances (Hawkins and Myrberg 1983; Rogers and Cox 1988; Popper and Carlson 1998).

Underwater acoustic signals are mainly generated by turbulence, breaking waves, and entrainment of air and the subsequent collapse of air bubbles (Urick 1983; Lurton 2002). Moreover, as the acoustic signal travels, it is affected by the interactions with its underwater environment. The signal can be reflected, scattered and absorbed at the bottom or at the surface and when encountering obstructions to the flow or air bubbles in the water column (Hawkins and Myrberg 1983; Urick 1983; Lurton 2002). Furthermore, sound propagation in shallow water is constrained by flow depth and the nature of the material at the bottom. As a consequence, sounds cannot propagate as acoustic waves in water that is shallower than about one-fourth of the wavelength over a rigid bottom (cutoff theory: Officier 1958; Urick 1983; Rogers and Cox 1988). For example, the lowest frequency that will propagate in water of 0.5 m depth (with a rigid bottom and a sound velocity of 1,500 m s^{-1}) is approximately 0.75 kHz; lower frequencies will decay exponentially with distance from the source (Fine and Lenhardt 1983; Lugli and Fine 2003, 2007). All of these interactions may generate complex soundscapes at different spatial scales (centimeters: Chapter 1; meters: Chapter 2; several kilometers: Chapter 3), which may include information on other environmental variables that are directly relevant to the organisms (e.g. food availability, temperature conditions).

Although few fish species actively use acoustic signals for communication, almost all species studied to date are able to detect sound (Fay and Popper 2000; Popper et al. 2003) and may gain information about their surroundings by listening to acoustic signals from abiotic and biotic sources (Popper and Hastings 2009a). It is well known that fish are able to locate the sources of sound (Hawkins and Myrberg 1983; Popper and Carlson 1998) and to gain information about wind or water currents (Popper and Fay 1993; Lagardere et al. 1994). Furthermore, many investigations have shown that various aquatic organisms such as frogs, newts, fish larvae, and crustacean larvae are able to use the sounds in their environment for the purposes of spatial orientation and positioning themselves within suitable habitats (e.g. Simpson et al. 2005; Pupin et al. 2007; Radford et al. 2007; Swanson et al. 2007).

It has recently been suggested that soundscapes act as "acoustic daylight" for fish by providing important information that can substitute a visual assessment of the immediate surroundings. It is highly likely that many aquatic organisms use sound as more than just a means to communicate with other organisms (Fay 2009). Underwater acoustic signals are expected to strongly influence the ecology and behavior of many freshwater organisms.

In order to improve our understanding of the influence of physical sound on the behavior of freshwater biota and to help in designing appropriate field experiments, it is first necessary to investigate and to better understand the physical characteristics of underwater soundscapes and their spatial and temporal heterogeneity (Chapters 1 to 3). The key questions of the thesis are: Do rivers and their specific aquatic habitats have similar "white-noise" signatures, or do they have mixed, or even unique, acoustic signatures (e.g. do riffles and pools or channelized and unconstrained rivers sound similar)? Which hydraulic and geomorphic conditions are responsible for the generation of sound in flowing water? Do different factors that contribute to the generation of sound have an influence on single frequencies, or a range of frequencies? How do the complexity and arrangement of the energy gradients, coupled with the nature and degree of flow obstruction, combine with the availability and size of sediment particles within entire river segments to influence the composition and distribution of acoustic signals?

Thermal characterization of river landscapes

Temperature has long been recognized as a pivotal environmental variable within aquatic and terrestrial ecosystems, regulating physical, biochemical, and ecological processes such as the solubility of gases, primary production, decomposition, photosynthesis, and respiration (Webb 1996; Caissie 2006; McCullough et al. 2009), as well as structuring communities and influencing the dispersal of organisms, their biology, and survival (Wolter 2007; Buisson et al. 2008; Indermaur et al. 2009; Tiffan et al. 2009). In the coming decades, a general increase in the air temperature has been predicted (IPCC 2007). As a result, the scientific relevance of temperature is increasing, and it is becoming a subject of worldwide environmental research (Webb et al. 2008a).

The thermal regime of river ecosystems is influenced by incoming shortwave solar radiation, air temperature, flow conditions, riparian structures, streambed substrata, and the exchange of surface and subsurface water (Webb and Zhang 1999; Malard et al. 2001; Webb et al. 2003). Although the seasonal, annual and diel temperature cycles of lotic systems in medium to high latitudes have been studied thoroughly (for a review, see Caissie 2006), the spatiotemporal heterogeneity of temperature in complex river landscapes such as floodplains

has not yet been quantified. Furthermore, the River Continuum Concept (Vannote et al. 1980) as well as the universal river zonation scheme (Illies and Botosaneau 1963) emphasized the major role of temperature in structuring biotic communities along the course of rivers. However, the lateral and vertical thermal heterogeneity has been almost completely neglected.

In river floodplains, complex temperature patterns occur over broad scales, but the characterization of the spatial patterns is limited because most studies used only in-situ point measurements (e.g. Arscott et al. 2001; Uehlinger et al. 2003; Acuña and Tockner 2009). In fact, given the large size and heterogeneity of floodplain systems, conventional in-situ surveys can only discontinuously characterize complex landscapes (Marcus and Fonstad 2008). Therefore, these studies have not fully quantified the heterogeneous character of river floodplains. Quantifying floodplain-scale thermal heterogeneity in terms of the size, distribution and abundance of patches, including gradients between hot and cold patches, is pivotal for understanding the utilization of thermal patches by both aquatic and terrestrial organisms. This includes fishes but also animals with complex life cycles like amphibians and aquatic insects that use both environments.

Ground-based and remotely-sensed thermal IR imagery has been used to address longitudinal temperature variation within and among rivers (Faux et al. 2001; Torgersen et al. 2001; Cristea and Burges 2009), to calibrate and validate stream temperature models (Loheide and Gorelick 2006; Cristea and Burges 2009), and to analyze the relationships between continuous stream temperature and fish assemblage, as well as in locating warm and cold water patches (Belknap and Naiman 1998; Torgersen et al. 1999; Madej et al. 2006). However, none of these studies assessed temperature heterogeneity of entire floodplain sections.

For a comprehensive thermal characterization of complex river floodplains and an assessment of the thermal patterns that may affect biota and ecosystem processes, it is first necessary to map and quantify floodplain-scale spatiotemporal thermal heterogeneity and to understand the processes that may drive habitats and thermal mosaics (Chapters 4 and 5). The key questions of the thesis are: How thermally heterogeneous is a river floodplain? Does thermal heterogeneity change during a diel cycle and if so, in which manner? Is high-resolution thermal IR imagery a valuable tool for quantifying thermal heterogeneity of large, complex ecosystems? Do different floodplain habitat types have different thermal signatures? How do temperature and flow dynamics interact and control thermal patchiness?

Goals

With the present thesis, I aimed primarily to advance the current understanding of the acoustic and thermal characteristics of river landscapes, two key properties that are poorly understood in river science. This study sought to improve the scientific understanding of river ecosystems and applied unexplored techniques (underwater acoustic and thermal IR imagery) in order to advance our understanding of ecosystem processes at the local and at the landscape level. Furthermore, new insights into the complexities of aquatic ecosystems are provided, and the potential relevance of acoustic and thermal landscapes to the ecology and behavior of freshwater organisms is demonstrated.

Chapter 1

The main goal of this chapter was to quantify the generation of acoustic signals, and of turbulence and bubble formation, by varying hydrogeomorphic drivers (such as water velocity, discharge, flow obstruction, and relative submergence) under controlled laboratory conditions. It was an important step in identifying the hydrogeomorphic factors that influence the sound of flowing water. This information proved to be relevant to the design of the field experiments (Chapters 2 and 3).

Chapter 2

The overall goals of this chapter were to characterize the hydrogeomorphology and acoustics of five typical types of aquatic river habitat including pools, runs (with and without streambed sediment transport), riffles, and step-pools, as well as to quantify the relationship between acoustic signatures and hydrogeomorphic characteristics. This study confirmed the results reported from the artificial flume (Chapter 1) through stationary field experiments, and helped to evaluate the soundscapes in Chapter 3.

Chapter 3

In Chapters 1 and 2, the physical factors that determine acoustic signals in flowing water were identified. In this chapter, I investigated the way in which the composition and arrangement of these key factors along the longitudinal gradient of rivers influence the composition and distribution of acoustic signals over the distance of kilometers. The primary goal was to analyze the characteristics of underwater acoustic patterns at the river segment scale (5-24 km long), and to determine the effect of different flow conditions on sound generation in a spatially explicit way.

Chapter 4

The primary aim of this chapter was to use ground-based thermal IR imagery and in-situ temperature measurements to quantify spatiotemporal thermal heterogeneity over 24-hour cycles in two near-natural Alpine river floodplains (Roseg and Tagliamento Rivers). Furthermore, I aimed to quantify vertical temperature patterns within unsaturated gravel sediment deposits.

Chapter 5

The primary goal of this chapter was to combine aerial thermal IR imagery with in-situ temperature loggers in order to quantify the spatiotemporal heterogeneity of temperature in a lowland river floodplain (Oder River). Thermal IR imagery was applied under two different flow conditions. Furthermore, I aimed to evaluate the potential linkage between thermal heterogeneity and structure of fish assemblages at the floodplain scale.

CHAPTER 1

A flume experiment to examine underwater sound generation by flowing water

Abstract

The hydrogeomorphology and ecology of rivers and streams has been subject of intensive research for many decades. However, hydraulically-generated acoustics have been mostly neglected, even though this physical attribute is a robust signal in fluvial ecosystems. Physical generated underwater sound can be used to quantify hydrogeomorphic processes, to differentiate among aquatic habitat types, and it has implications on the behavior of organisms. In this study, acoustic signals were quantified in a flume by varying hydrogeomorphic drivers and the related turbulence and bubble formation. The acoustic signals were recorded using two hydrophones and analyzed using a signal processing software, over 31 third-octave bands (0.020-20 kHz), and then combined in 10 octave bands. The analytical method allowed for a major improvement of the signal-to-noise ratio, therefore greatly reducing the uncertainty in our analyses. Water velocity, relative submergence, and flow obstructions were manipulated in the flume and the resultant acoustic signals recorded. Increasing relative submergence ratio and water velocity were important for reaching a turbulence threshold above which distinct sound pressure levels were generated. Increases in water velocity resulted in increased sound pressure levels over a wide range of frequencies. The increases in sound pressure levels due to relative submergence of obstacles were most pronounced in midrange frequencies (0.125-2 kHz). Flow obstructions in running waters created turbulence and air bubble formation, which again produced specific sound signatures.

Introduction

Many organisms are adapted to hear and react to sound, hence sound provides important information about habitats and the ecosystem. Indeed, sound has been subject of intense scientific research. For example, acoustic techniques have been successfully applied to determine constraints upon acoustic communication in the aerial environment (Ellinger and Hödl 2003), for studying social communication among organisms (Slater and Catchpole 1990; Ruiz-Miranda et al. 2002; Da Cunha and Jalles 2007), and for determining the effect of anthropogenic noise on birds (Reijnen et al. 1997; Forman et al. 2002), bears (Gibeau et al. 2002; Dyck and Baydack 2004), amphibians (Sun and Narins 2005), and squirrels (Rabin et al. 2006). Research has also examined the human perception of sound (Southworth 1969; Carles et al. 1999), coupling visual and acoustic preferences (Anderson et al. 1983; Porteous and Mastin 1985; Yang and Kang 2005), in order to better understand noise as an impairing sound (Kariel 1990; Staples 1997; Gramann 1999).

In aquatic systems, acoustic research started with great vigor during WWI and II for military applications (Urick 1983). More recently, underwater acoustic measures have been used for assessing the diversity and distribution of marine mammals (McDonald et al. 1995; DiSciara and Gordon 1997; Clark and Clapham 2004) and for quantifying the effect of ship noise (Scholik and Yan 2002a; Wysocki et al. 2006; Vasconcelos et al. 2007) and ambient noise (Scholik and Yan 2001, 2002b; Popper 2003; Amoser and Ladich 2005) on fishes. Underwater acoustic recordings have also been used for estimating sediment transport (Rouse 1994; Rickenmann 1997; Mason et al. 2007), and substrate size distributions (Nitsche et al. 2004), analyzing rainfall events and drop size distribution (Nystuen 2001; Ma and Nystuen 2005; Ma et al. 2005), monitoring internal solitary waves produced in the ocean (Apel et al. 2007), and for measuring water temperature through differences in sound speed and propagation in the ocean (Terrill and Melville 1997; Vagle and Burch 2005). In addition, acoustic techniques were applied above the water surface for estimating reaeration (Morse et al. 2007).

The flowing water of rivers and streams is turbulent and often entrains air further released as bubbles that generates sound. This physical generated sound has captivated people for centuries as expressed in rhythmic poems and lyrics using well-sounding words. Rivers and streams bubble, gurgle, splash, whoosh, or roar, depending on water velocity and discharge, as well as on obstructions to flow created by different hydrogeomorphic features in the stream channel. Whereas hydrologic, morphologic, ecological, and also visual aspects of rivers have

been the subject of intense research, the specific physical generated sound recorded beneath the water surface, and its potential as a quantitative indicator of habitat uniqueness, have only recently received few attention (Amoser and Ladich 2005; Wysocki et al. 2007).

In this study we quantified, for the first time, acoustic signals related to hydrogeomorphic parameters and induced turbulence in flowing water under controlled laboratory conditions. First, we examined the influence of increasing water velocity and discharge on sound pressure levels. Second, we studied the role of flow obstruction and submergence on sound production. Third, we measured physical generated sound at different positions relative to the sound source to study how the sound signature changes relative to distance from its source. Specifically, we asked if different processes of physical sound generation influenced unique frequencies, or if they resulted in a broad band noise that spread equally throughout the channel. In particular, we sought to identify whether hydrogeomorphic factors influence sound in flowing water.

Materials and methods

Theoretical background

Turbulence created by strong velocity gradients and obstruction to flow by various structural elements that exist in a channel are ubiquitous sources of physical generated sound in flowing waters. Though an infinite number of interactions exist between flow and specific obstructions and bedforms, we limited our study to longitudinally non-uniform open-channel flow, which often occurs in natural streams (Figure 1), and can be easily modeled in the laboratory. Moreover, this type of flow has a theoretical background that can be used as the framework for the interpretation of the experimental results.

Open channel flow in a non-uniform channel, composed of two parts with unequal depth (Figure 1B), is represented by the Bernoulli equation:

$$p + \frac{\rho u^2}{2} + \rho g h = const \qquad (1)$$

where p is pressure, u is bulk water (flow) velocity, ρ is density of water, g is the acceleration due to gravity, and h is flow depth. The Bernoulli equation is derived as a one-dimensional approximation of the Navier-Stokes equations and expresses the law of conservation of energy. Equation 1 can be rewritten in a dimensionless form as:

$$\frac{p}{\rho g h} + \frac{u^2}{2 g h} + 1 = c_0 \qquad (2)$$

where c_0 is a constant. If pressure difference is small or attributed to the same effects of roughness, as can be assumed for river conditions, Equation 2 simplifies to:

$$Fr = \sqrt{2(c_0 - 1)}, \; Fr = \frac{u}{\sqrt{g\,h}} \tag{3}$$

where Fr is Froude number, which represents the ratio between inertia to gravity. Fr = 1 is considered as the critical state of flow (i.e. when water velocity is equal to the celerity c, or speed of a wave in a channel, so the waves have velocity $2c$ in the direction of flow), whereas, the flow can be in supercritical (i.e. when the velocity of the waves is greater than the critical flow: velocity > celerity; Fr >1) or subcritical condition (i.e. when the velocity of the waves is less than the critical flow but greater than zero: velocity < celerity; Fr <1). The transition from flow with larger Froude number to flow with smaller Froude number is accomplished with increased losses of energy through the adjustment of the pressure head and/or subsequent changes in depth. When both parts of the flow are in the subcritical condition, the transition zone is represented by a turbulent vortex. In the transition of flow from supercritical to subcritical regime, the transition zone is deformed into highly turbulent zone known as hydraulic jump, which is especially effective in entraining the air and releasing it as bubbles (Figure 1).

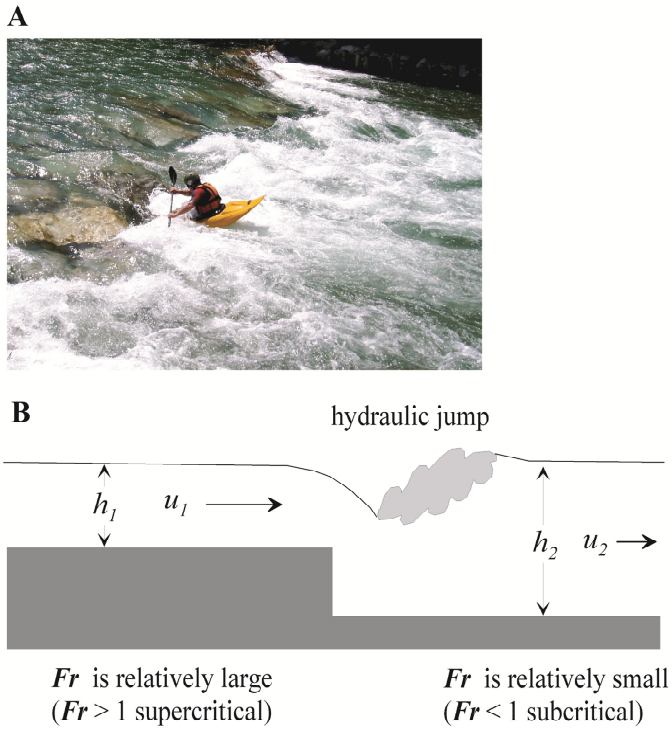

Figure 1. A) Picture example of a non-uniform open channel flow in a stream (Tiroler Achen, Tirol, Austria) (photo by Anna Sukhodolova). B) Schematic representation of a non-uniform open-channel flow composed of two parts with unequal flow depth (h_1 and h_2) and flow velocity (u_1 and u_2) (illustration by Alexander N. Sukhodolov).

In small streams to large rivers, hydraulic jumps can be very powerful and produce a loud roaring sound. The same condition exists for breaking waves in riffles and rapids. These whitewater flow features arise because supercritical flow conditions (Fr >1) have been reached resulting in wave breaking that traps and entrains air, which ultimately generates the sound of a roaring river. Moreover, this process of sound generation through wave breaking is a vastly more ubiquitous process of turbulent energy dissipation and generation of sound that exists in rivers and streams.

Froude number can be more effective for detecting the energetic state and transition zones in laboratory studies in which the Reynolds number ($Re = \frac{u\,h}{\nu}$), where ν is kinematic viscosity of water) is often relatively small due to limited size of laboratory facilities. Equation 3 also provides the theoretical background for scaling flow depth and water velocity between laboratory studies and for comparing with field conditions. Indeed, as it can be readily demonstrated that we need to run experiments in which the velocity in the two parts of the flow (over elevated obstacles and deeper in the downstream part) will be varied over a certain range of values. Another measure, depth, should be varied and for the part of the flow over an obstacle, it will provide the range of relative submergences. Thus, the main aim of the present experimental research was to determine the relation between flow characteristics and the sound generated by turbulent structures in the transition zone between longitudinally developing flows.

Experimental design

Between January and April 2007, three experiments were set up in a flume located in the Laboratory of Hydraulics, Hydrology and Glaciology (VAW) at the Swiss Federal Institute of Technology (ETH) Zurich. The flume was six meters long and 40 cm wide. The bottom consisted of concrete, the walls of Plexiglas. Discharge was adjustable between 0 and 70 l s^{-1}. Water velocity could be manipulated by changing the slope and/or by damming the water at the end of the flume. First, we manipulated water velocity (~10 cm s^{-1} to ~170 cm s^{-1}) at five different discharge levels (10 to 50 l s^{-1}) to assess its effect on sound generation. At each discharge level, 7-13 different flow velocities were generated (Table 1). Second, 5 cobbles of approximately the same size were arranged at the flume bottom (Figure 2) to model the flow over the elevated area similar as depicted in Figure 1. This experiment was repeated using two size classes of cobbles (average *c*-axis (=height): 11 and 16.8 cm) at a discharge of 20 l s^{-1} and of constant slope. Flow depth was manipulated to create relative submergence values of

approximately 1, 0.8, 0.5, and 0 (without cobbles). Relative submergence was calculated as the ratio of average substrate size (average *c*-axis of cobbles) to flow depth (Table 1).

Table 1. Summary of the experimental conditions of the three experiments: water velocity, relative submergence, and bed structures.

Experiment	Q ($l\ s^{-1}$)	u ($m\ s^{-1}$)	H (m)	D (m)	$D\ h^{-1}$	Fr	Re ($x10^4$)	Pos.
Water velocity	10.00	0.08-1.01 (7)	NA	NA	NA	NA	NA	NA
	20.00	0.26-1.56 (11)	NA	NA	NA	NA	NA	NA
	30.00	0.33-1.66 (13)	NA	NA	NA	NA	NA	NA
	40.00	0.26-1.69 (11)	NA	NA	NA	NA	NA	NA
	50.00	0.37-1.69 (11)	NA	NA	NA	NA	NA	NA
Relative submergence	20.00	0.56	0.11	0.11	1.00	0.54	6.16	NA
	20.00	0.48	0.14	0.11	0.79	0.41	6.72	NA
	20.00	0.37	0.22	0.11	0.50	0.25	8.14	NA
	20.00	0.26	0.17	0.17	0.99	0.20	4.42	NA
	20.00	0.20	0.21	0.17	0.80	0.14	4.20	NA
	20.00	0.05	0.32	0.17	0.53	0.03	1.60	NA
	20.00	0.25	0.22	0.00[A]	0.00	0.17	5.50	NA
Bed structures	20.00	0.24	0.22	0.19	0.89	0.16	5.28	1
	20.00	0.31	0.22	0.19	0.89	0.21	6.82	2
	20.00	0.48	0.22	0.19	0.89	0.33	10.56	3
	20.00	0.44	0.22	0.19	0.89	0.30	9.68	4
	20.00	0.48	0.22	0.19	0.89	0.33	10.56	5
	20.00	0.32	0.22	0.19	0.89	0.22	7.04	6
	20.00	0.16	0.22	0.19	0.89	0.11	3.52	7
	20.00	0.29	0.16	0.19	1.22	0.23	4.64	1
	20.00	0.46	0.16	0.19	1.22	0.37	7.36	2
	20.00	0.72	0.16	0.19	1.22	0.57	11.52	3
	20.00	0.90	0.16	0.19	1.22	0.72	14.40	4
	20.00	0.63	0.16	0.19	1.22	0.50	10.08	5
	20.00	0.53	0.16	0.19	1.22	0.42	8.48	6
	20.00	0.12	0.16	0.19	1.22	0.10	1.92	7
	20.00	0.35	0.22	0.00[A]	0.00	0.24	7.70	NA

Q: Discharge; *u*: water (flow) velocity (in bracket number of velocity measurements); *h*: flow depth; *D*: submerged object size (*c*-axis: height), [A] no submerged objects; $D\ h^{-1}$: relative submergence; *Fr*: Froude number; *Re*: Reynolds number; Pos.: positions of the acoustic recording in the flume (see Figure 9A); NA: not applicable.

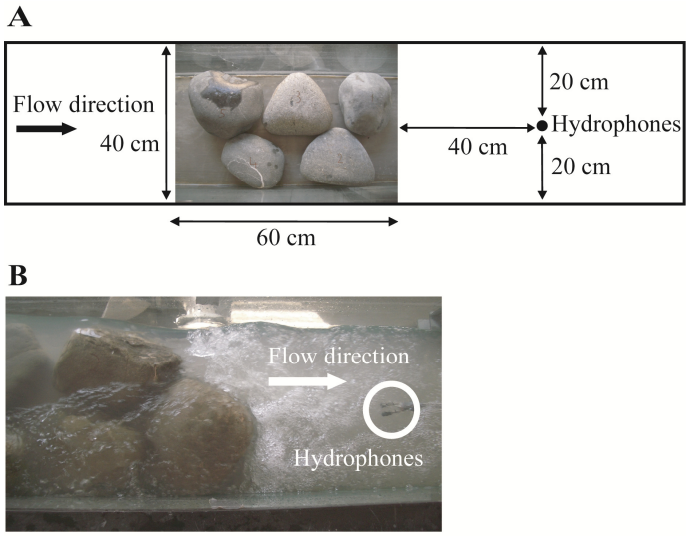

Figure 2. A) Top view schematic of the relative submergence experiment with a photograph insert showing one cobble arrangement. B) Photograph taken from the side of the flume showing turbulence created, and the position of the two hydrophones. Relative submergence in the present photograph was 1.

Third, geomorphic bed structures were created using bricks with length, width, and height of 25, 12, and 6.5 cm, respectively. A set of three bricks was used to create a more complex flow pattern by allowing spaces between obstacles (Figure 3), thus providing a greater degree of three-dimensionality compared to the basic scheme (Figure 1). The acoustic signal was recorded at different locations relative to the position of the bricks (Figure 9A). The experiment was repeated at a discharge of 20 l s^{-1} and at constant slope but at varying flow depths (22 and 16 cm) (Table 1). Additionally, *Re* and *Fr* were calculated to assess relative levels of turbulence and transition zones, respectively.

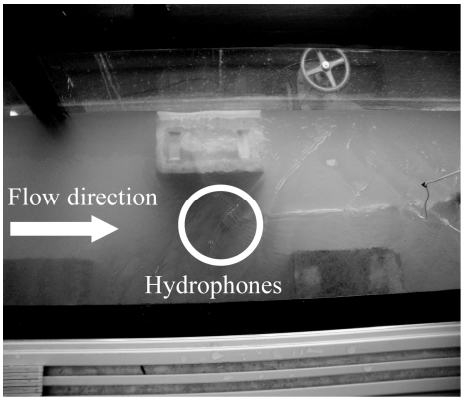

Figure 3. Top view photograph showing the position of the hydrophones and relative level of turbulence produced by a three bricks arrangement (position 3 in Figure 9A).

Data collection

Acoustic signals were recorded using two hydrophones (Type 8103, Brüel and Kjaer, Denmark), with the head facing upstream (Figures 2B, 3). Hydrophone depth was set at 60% flow depth, and distance between the two heads was ~2 cm. An amplifier (Type Nexus 2692 OS2, Brüel and Kjaer, Denmark), with sensitivity set at 3.16 mV Pa^{-1}, was used to amplify the signal sent by the hydrophones and stored with a digital recorder (Type R-4, Edirol, Japan). Sampling frequency was 44.1 kHz and amplitude resolution was 16 bits. This setting assured a frequency range between 0.020 and 20 kHz and a dynamic range of >90 dB, and it guaranteed maximum compatibility with other digital sound devices (e.g. Compact Disc). Recording time was approximately five minutes and 30 s. Water velocity was measured with a handheld FlowTracker (Acoustic Doppler Velocimeter; SonTek, San Diego, USA) or a propeller velocity meter (MiniAir2, Schiltknecht, Switzerland). Water velocity and flow depth were measured in front of the hydrophones.

Acoustic data analysis

The first step in the analysis of acoustic data collected was to separate the signals that were produced by flowing water from the ambient noise generated by other sources. However, a common difficulty in recording and analyzing underwater sound is a low signal-to-noise ratio. This is due to a high background noise caused by turbulent flow around the hydrophones and internal noise of sensors and amplifiers. Our approach to improve the signal-to-noise ratio was the use of two hydrophones located close to each other. The advantage of this configuration is that by multiplying these two signals instead of taking the square of just one sensor, incoherent components between the two hydrophones are nullified (Norton 1989). This reduces internal noise components and contributions of turbulence around the hydrophones, resulting in a significantly improved signal-to-noise ratio. As a consequence, the spectral analysis of the actual sound produced by flowing water is much more robust. The suppression of noise by usage of two hydrophones is demonstrated in Figure 4. Both sensors recorded the same sinusoidal signal with additional uncorrelated noise. Figure 4A shows the squared signal of hydrophone 1, $(s_1 + n)^2$, and the corresponding averaged time response, $(s_1 + n)^2$ – average. This curve lies clearly above the squared pure sinusoidal signal, s_1^2. On the other hand Figure 4B shows the product of the two hydrophone signals, $(s_1 + n)(s_2 + n)$, and the corresponding averaged time response, $(s_1 + n)(s_2 + n)$ – average, which is very close to and thus a good estimate of the squared pure sinusoidal signal, s_1^2.

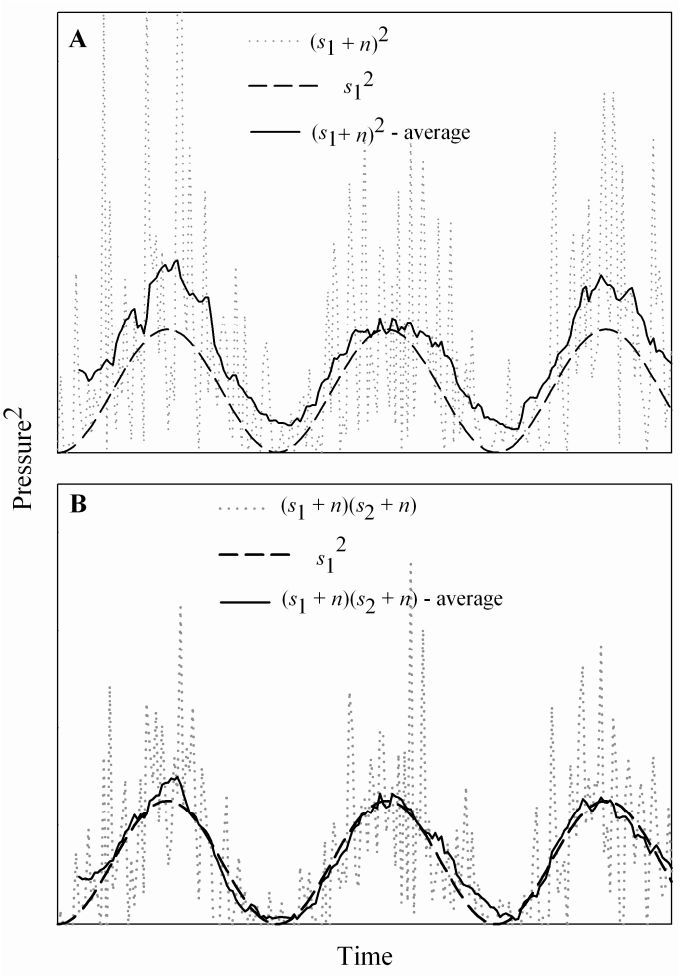

Figure 4. Improvement of the signal-to-noise by usage of two hydrophones (see text for details). A) One hydrophone. B) Two hydrophones.

Acoustic data analysis evaluated the hydrophone signal power as a function of frequency and time where signal power is defined as the mean value of the square of the signal. We evaluated the time-series of the hydrophone signal power by using a Fast Fourier Transform (FFT) analyzer to spectrally decompose the time-series. The FFT results in a spectrum with frequency resolution that is constant throughout the frequency range of recorded sound. By summing up the corresponding frequency lines, one-third octave band and octave band representations were evaluated (IEC 1995). Octave bands have a bandwidth that equals ~70% of the center frequency while the bandwidth of one-third octave bands is about 23%. Three-one-third octave bands span one octave, hence the resolution of this spectrum is three times finer than the octave band spectrum. A 44.1 kHz sampling frequency was chosen because it is a standard value for audio applications. With a 16,384 point FFT, the audio stream is transformed on a frame by frame basis into the frequency domain to get a description of it's spectral content. Three consecutive spectra were averaged at a time, which implies a temporal resolution of about 1.1 s.

The analysis of the hydrophone signals was performed with a signal processing audio analyzer software package written and developed by K. Heutschi specifically for this project. The audio analyzer captures audio data either directly from a sound card (real time mode) or from a wave file (post processing mode), as in the present study. Randomly selected 300 s of each audio file were analyzed with the audio analyzer for relative submergence and bed structures experiments and 30 s for velocity experiments. Shorter sound samplers were determined to be sufficient because of the immense amount of data collected for the velocity experiments after comparing the variance between a smaller subset of 300 and 30 s intervals.

Reduction of the acoustic data

Acoustic data were classified by a third-octave band analysis over 31 frequency bands (0.02-20 kHz). The evaluation of a power-band limited noise-like signal has uncertainty that depends reciprocally on the product of averaging time and bandwidth. The signal power in an octave band could be determined by adding up the signal power of the three corresponding third-octave bands. For constant averaging time, a reduction of the spectral resolution from third-octave bands to octaves lowered the uncertainty significantly. Therefore, for final analysis, we decided to combine the 31 third-octave bands in 10 octave bands. The average (energetic average) for each octave band was calculated. The averaging process is based on the square of the hydrophone pressure signal.

A reference value of the environmental noise in the laboratory was recorded with standing water (zero flow) and subtracted from the physical generated sound. Reliability of recorded data was checked by a threshold criterion to eliminate disturbing noise (generated by pumps and motors). The sound recordings in the flume were also influenced by noise produced by the fact that water cascades from the flume to a collection box at the end of the channel. We reduced this influence by placing an absorption mattress (of sponge rubber) at the end of the flume, thereby greatly reducing the level of background noise generated that had to be subtracted from the experimental data.

All data were expressed on a logarithmic scale as dB values relative to 1 micro-Pascal as a reference. The calibration of the measurement system was performed with a Brüel and Kjaer calibrator (Type 4223, Brüel and Kjaer, Denmark), which generates a highly reproducible nominal sound pressure level of 166 dB at 0.25 kHz. Selected acoustic analysis results were plotted as 3-D sound graphs, where frequency bands were plotted along the x-axis, time along the y-axis and sound pressure level (dB re 1 μPa) along the z-axis.

Statistical analysis

Analysis of variance between groups (one-way ANOVA) was applied to evaluate the effect of velocity on sound pressure level. The fixed factor variables (discharge) divided the samples into five groups (10-50 l s^{-1}). Using a general linear model procedure, the null hypotheses about the effects of factor covariate (independent variable: velocity) on the means of various groupings of single dependent variables (sound pressure level of each octave band) were tested. In addition, Pearson moment correlation analyses were used to identify the direction and strength of relationships. One-way ANOVA was also applied to evaluate the effect of relative submergence (independent variable) on sound pressure level (dependent variable). Data were checked to test if variables clearly deviate from normality with a Kolmogorov-Smirnov test. All analyses were performed with SPSS (version 14.0, SPSS Inc., Chicago, USA).

Results

Effect of water velocity on sound pressure level

There was a positive relation between water velocity and sound pressure level for all frequency bands (ANOVA: $4.42 \leq F_{1,49} \leq 114.08$; $p < 0.05$), except for 16 kHz. Discharge exhibited a significant effect on all frequency bands (ANOVA: $2.93 \leq F_{4,49} \leq 23.46$; $p < 0.05$). However, post-hoc tests showed that in our flume, a sound pressure level created by discharge of 10 l s^{-1} differed from levels created by higher discharge rates. Moreover, variation in water velocity had a more pronounced influence (higher F-value) on sound pressure level than variation in discharge, except for 8 and 16 kHz.

Increasing the water increased the sound pressure level in a wide range of frequencies, except at a discharge of 10 l s^{-1} (Figure 5). At 10 l s^{-1} the sound pressure level of middle to high frequencies (0.5-2 kHz and 8 kHz) decreased with increasing velocity (Table 2). At discharge rates ≥20 l s^{-1}, sound pressure level increased with velocity (Figure 5B-E). The increase was significant for all frequency bands, except for 0.063 kHz (for 40 and 50 l s^{-1}), 1 kHz (for 20 l s^{-1}), 8 kHz (for 20 and 30 l s^{-1}), and 16 kHz (for 20, 40 and 50 l s^{-1}) (Table 2).

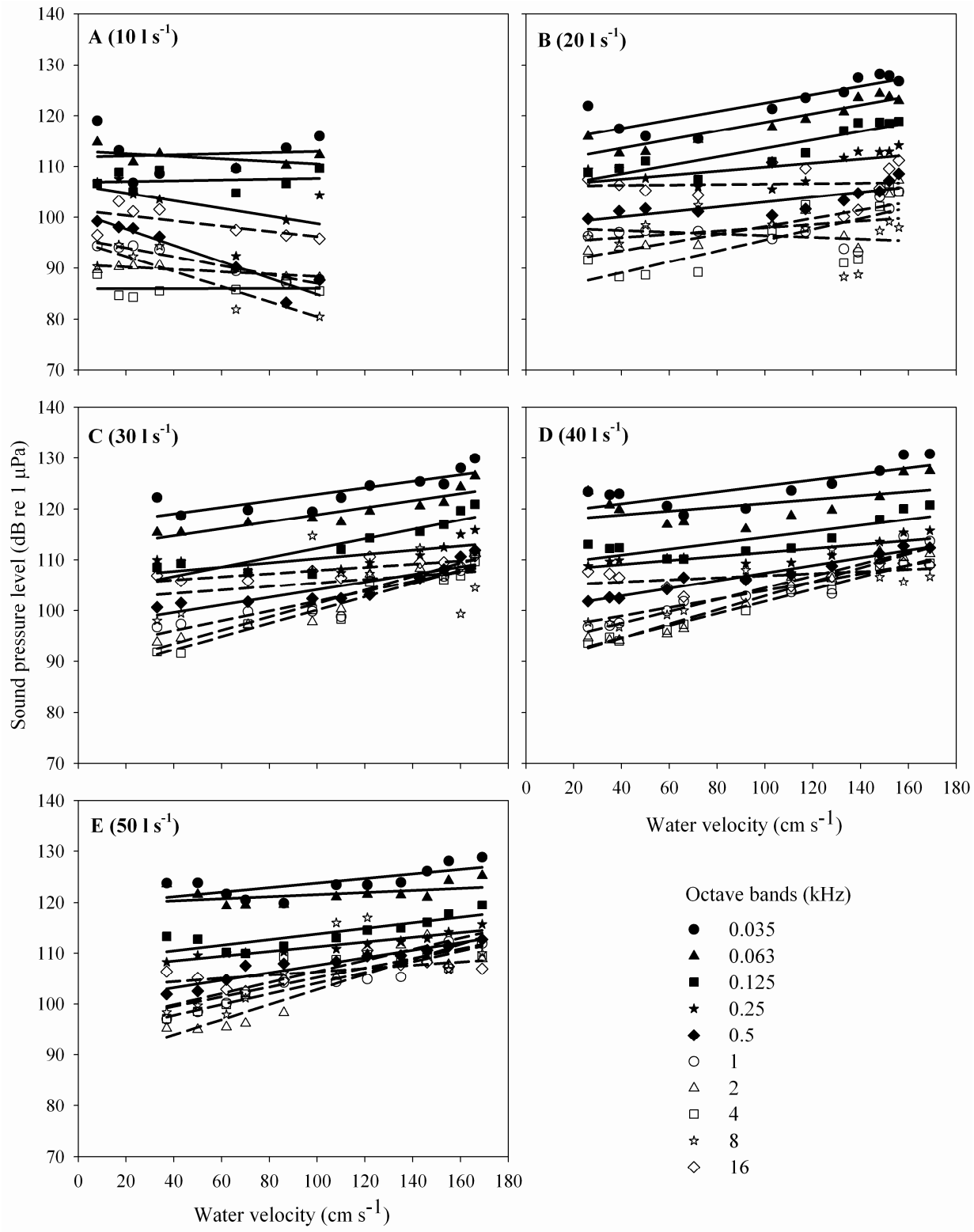

Figure 5. Relationship between sound pressure level (dB, decibels; dB re 1 µPa) of 10 octave bands and flow velocity (cm s^{-1}) at five discharge conditions (10-50 l s^{-1}). Closed symbols and solid regressions lines show the octave bands from 0.0315 to 0.5 kHz, open symbols and dashed regression lines show the octave bands from 1 to 16 kHz.

Table 2. Pearson moment correlation analysis to test direction and strength of the relationship (r) between water velocity and sound pressure level (10 octave bands) at five discharge conditions (10 to 50 l s^{-1}).

Octave band (kHz)	r (10 l s^{-1})	r (20 l s^{-1})	r (30 l s^{-1})	r (40 l s^{-1})	r (50 l s^{-1})
0.0315	0.096	0.836**	0.825**	0.762**	0.713*
0.063	-0.529	0.934**	0.908**	0.510	0.461
0.125	0.141	0.897**	0.880**	0.811**	0.828**
0.25	-0.524	0.620*	0.679*	0.829**	0.960**
0.5	-0.947**	0.815**	0.880**	0.981**	0.957**
1	-0.970**	0.406	0.926**	0.950**	0.959**
2	-0.830**	0.747**	0.960**	0.980**	0.914**
4	0.018	0.731*	0.970**	0.991**	0.847**
8	-0.886**	-0.195	0.300	0.822**	0.722*
16	-0.634	0.052	0.800**	0.496	0.599

$*p < 0.05$; $**p < 0.01$.

Effect of relative submergence on sound pressure level

An increase in relative submergence led to a significant increase in middle-frequency sound pressure levels (0.125-2 kHz) (ANOVA: $7.93 \leq F_{1,6} \leq 10.01$; $p < 0.05$). At low relative submergence values, both low and high frequencies showed higher sound pressure levels compared to midrange frequencies, where a "quiet" zone occurred (Figures 6, 7). As relative submergence and turbulence increased (from 0 to 1 and from $Re = 5.50 \times 10^4$; $Fr = 0.17$ to $Re = 6.16 \times 10^4$; $Fr = 0.54$, respectively) (Table 1), sound pressure levels increased in the midrange frequencies (0.125-2 kHz) more than in the higher and lower frequencies (Figures 6, 7). Moreover, an increase in relative submergence generally led to an increase in acoustic temporal variability (calculated as variance) across frequency bands and time. For example, at a relative submergence 1 the variance over time in the midrange frequencies 0.125, 0.25, 0.5, 1, and 2 kHz was 3.17, 5.39, 4.30, 4.26, and 11.33, respectively. At a relative submergence 0, the respective variances were 2.37, 0.5, 0.59, 1.52, and 0.46 respectively (Figure 7).

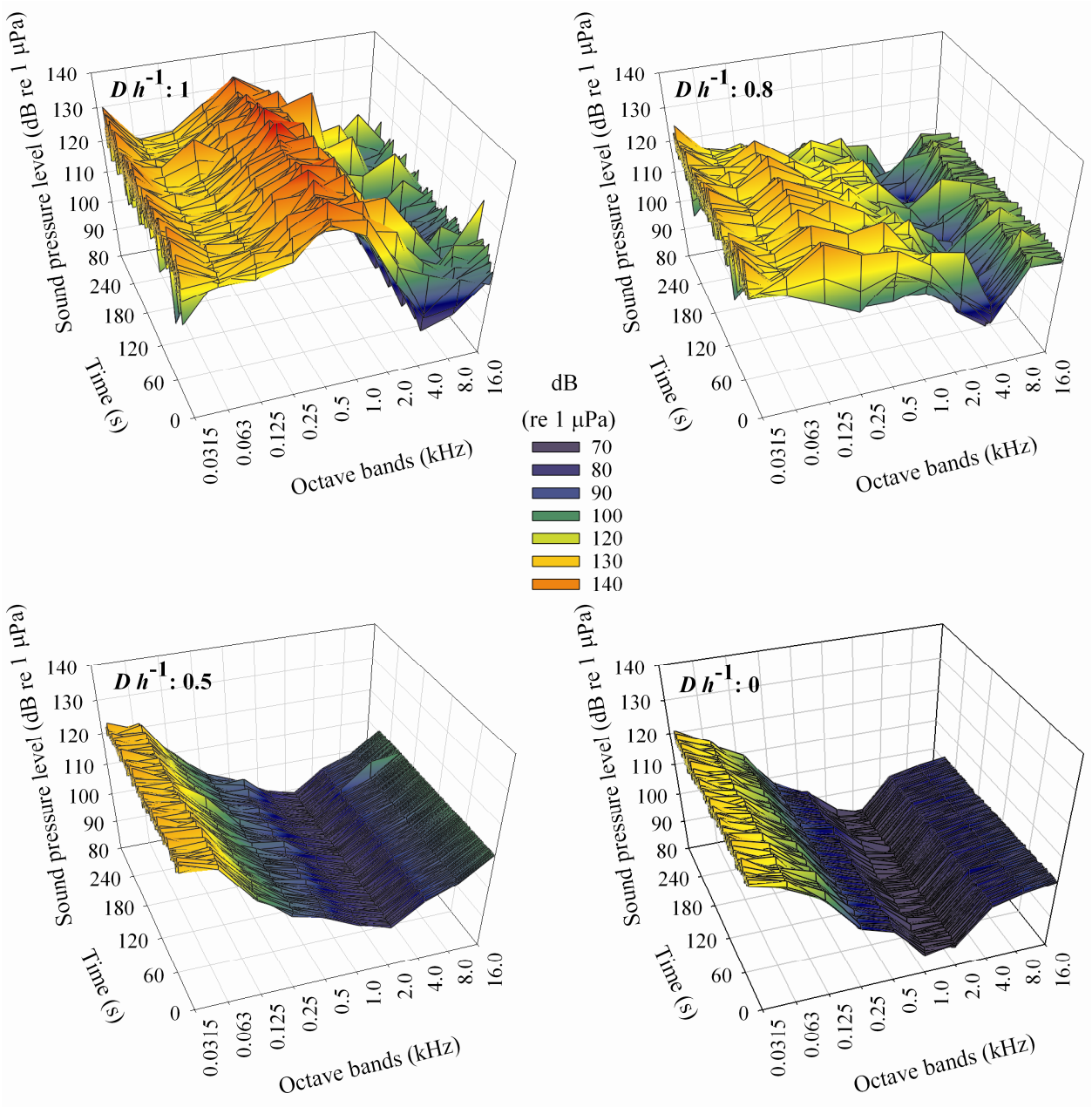

Figure 6. 3-D sound graphs (*x*-axis: 10 octave bands; *y*-axis: analyzed time, 300 s; *z*-axis: sound pressure level expressed in decibels (dB re 1 µPa)) generated through four relative submergence levels ($D\ h^{-1}$: 1, 0.8, 0.5, 0; where *D* submerged object size (*c*-axis: height) and *h* flow depth) at a constant discharge of 20 l s^{-1}. Average cobbles size (*c*-axis: height): 11 cm.

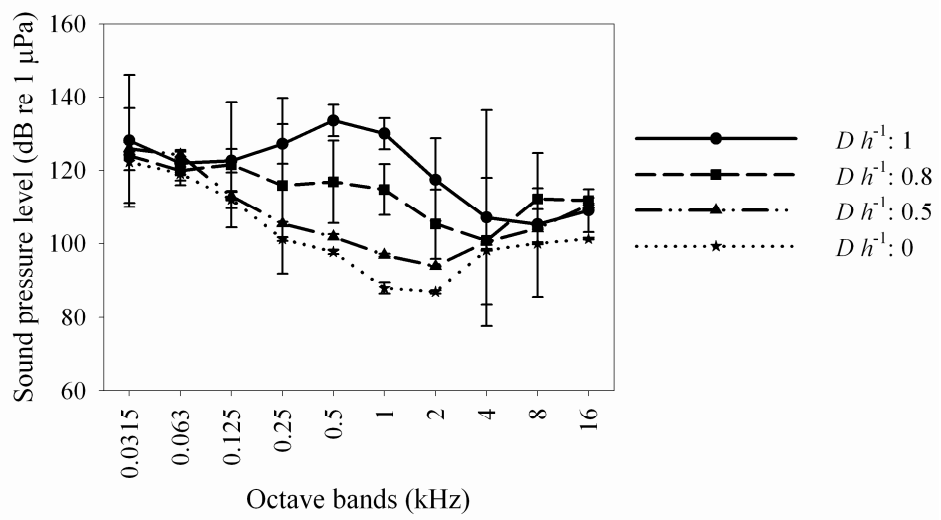

Figure 7. Sound pressure level (dB decibels, dB re 1 µPa; energetic average ± variance (as acoustic temporal variability); n = 270) for 10 octave bands at four relative submergence levels ($D\ h^{-1}$: 1, 0.8, 0.5, 0; where D submerged object size (c-axis: height) and h flow depth)) (3-D sound graphs see Figure 6).

Effect of bed structures on sound pressure level

The sound pressure level of most frequencies did not show major differences, except for 0.25, 1 and 2 kHz - which had very high variance - between the seven hydrophone positions (Figure 8A). Flow turbulence remained relatively low at positions 1 and 7 located up- and downstream of the structures with minimum values (Re = 5.28 × 10^4 and 3.52 × 10^4; Fr = 0.16 and 0.11, respectively) (Table 1). Turbulence was greatest in close proximity to flow obstruction structures, i.e. at position 3 (Re = 10.56 × 10^4; Fr = 0.33), position 4 (Re = 9.68 × 10^4; Fr = 0.30), and position 5 (Re = 10.56 × 10^4; Fr = 0.33) (Table 1). However, decreasing flow depth (Figure 8A, B), while keeping discharge, constant, increased relative submergence and water velocity, and created enough turbulence to significantly change the sound signature. This resulted in different sound pressure levels relative to frequency at different hydrophone positions (Figure 9B, C). Turbulence reached a maximum at position 3 (Re = 11.52 × 10^4) and 4 (Re = 14.40 × 10^4) (Figures 8B, 9B; Table 1). Moreover, a transition from flow with low Froude number (Position 1, Fr = 0.23; Position 2, Fr = 0.37), to flow with larger Froude number (Position 3, Fr = 0.57; Position 4, Fr = 0.72), and again to flow with smaller Froude number (Position 5, Fr = 0.50; Position 6, Fr = 0.42) was generated in the flume (Table 1). The transition zone from flow with low to large Froude numbers generated turbulent vortexes. Thus, turbulence increased and the effect of the transition zone increased the level of sound generated in the mid frequency range (0.25-2 kHz) and a narrow band of low frequency between 0.0315 and 0.063 kHz (Figures 8B, 9B).

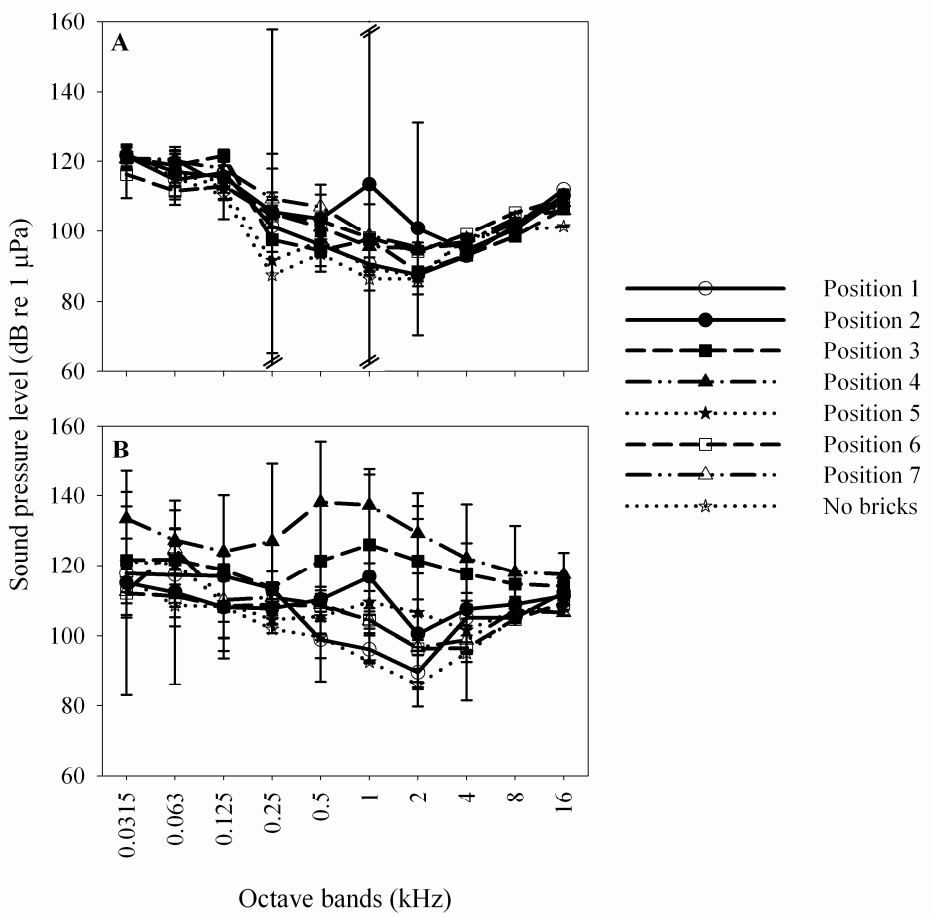

Figure 8. Sound pressure level (dB decibels; dB re 1 µPa; energetic average ± variance (as acoustic temporal variability); n = 270) for 10 octave bands at seven positions (see Figure 9A). A) Flow depth: 22 cm. B) Flow depth: 16 cm. Closed symbols correspond to the 3-D sound graphs in B, open symbols to C in Figure 9.

Sound pressure levels of midrange frequency bands (0.5-2 kHz) and the lowest frequency band (0.0315 kHz) showed positive linear correlations with both Froude and Reynolds number (Table 3). Mid-frequency range sound pressure levels quickly dissipated moving downstream from the sound source also becoming sporadic to semi-periodic at least over the sampling time frames. Low and high-frequency sound did not diminish as much as the midrange frequencies (position 5 and 6, Figures 8B and 9B, C). For midrange frequencies, the 3-D sound graph for position 7 (Figures 8B, 9C) showed a similar pattern as position 6 but with a sharp peak in the low frequency range and lower sound pressure level over the other frequencies. Position 1 (Figures 8B, 9C) showed a small but noticeable sound pressure level increase in low-frequency sound for a position upstream of the source of turbulence (compared to no structures).

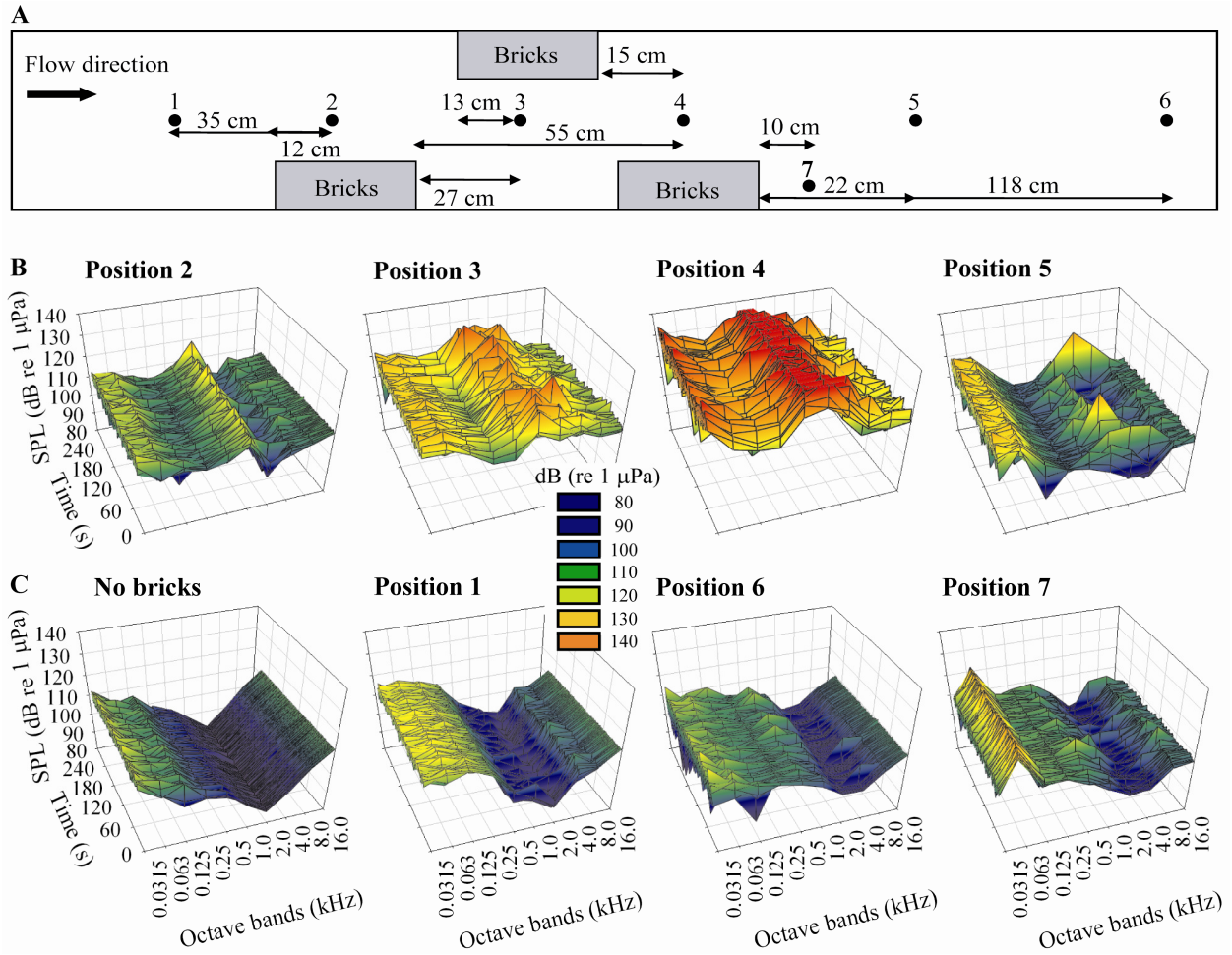

Figure 9. The 3-D sound graphs in this figure correspond to B in Figure 8. A) Arrangement of multiple structures (bricks) from a single experimental run and multiple hydrophone positions (black dots) within the flume and relative to the flow of water, position and scale of turbulence. The series of 3-D sound graphs in B shows the recorded sound pressure level per octave band in locations close to the source of turbulence and sound generation. The series of 3-D sound graphs in C shows the recorded sound pressure level per octave band in the flume without structures (first panel) compared with 3-D sound graphs from above the structures (position 1), a distance below (position 6) and in the eddy of a structure (position 7). *X*-axis: 10 octave bands; *y*-axis: analyzed time (300 s); *z*-axis: sound pressure level expressed in decibels (dB re 1 µPa).

Table 3. Pearson moment correlation analysis to test direction and strength of the relationship (*r*) between Froude number (*Fr*), respectively Reynolds number (*Re*), and sound pressure level (10 octave bands).

Octave band (kHz)	*r* (*Fr*)	*r* (*Re*)
0.0315	0.802*	0.798*
0.063	0.236	0.231
0.125	0.551	0.549
0.25	0.493	0.468
0.5	0.763*	0.756*
1	0.831*	0.825*
2	0.869*	0.865*
4	0.725	0.721
8	0.753	0.748
16	0.722	0.719

Flow depth was 16 cm (see Table 1). *$p < 0.05$.

Discussion

Physical generated underwater sound is a strong signal in flowing waters and hence should be an ecologically important habitat attribute that organisms can use to sense energetic conditions of their environment. However, the underwater acoustic characteristics of aquatic habitats have only recently received attention (Amoser and Ladich 2005; Wysocki et al. 2007). In this study, we experimentally quantified the effects of water velocity, relative submergence, bed structures, and induced turbulence on physical sound generation. Based on flume experiments, we were able to identify characteristic "soundscapes" as well as to observe phenomena that generated these soundscapes.

We found that water velocity rather than discharge explained most of the variation in sound pressure levels. The observed relationship between discharge (and the related water velocity) and generated sound is expected to also occur in rivers and streams. A discharge (i.e. turbulence) threshold seems to be necessary to influence the acoustic signature in the flume. Similarly, in a stream at low discharge and low turbulence level, one would expect low physical generated sound until discharge reaches a threshold level resulting in increased sound pressure levels over a wide range of frequencies. Hence, we expect that the underwater sound pressure level in streams and rivers may change as a consequence of the discharge (and the related water velocity) regime just as we measured in the flume. For example, some mountain rivers with discharge peak during the snow-melting period may have sound pressure level change once a year with spring run-off and flooding. On the other hand, rainfall-dominated rivers (e.g. lowland temperate rivers) can undergo multiple high flow events of

varying intensity and duration. The high rate of water level increases and decreases (and the related water velocity) would result in rapid changes in the stream sound pressure levels.

Such changes in underwater sound pressure levels could affect the behavior of fish, as well as of other organisms, by triggering migration to new positions or habitats that have different sound pressure levels. Moreover, organisms in such environments may have developed higher levels of sound perception and subsequent behavioral adaptations. Previous studies have shown that high sound pressure levels can cause damage to inner organs and induce stress responses in many fishes. However, the impact of noise exposure is based on variation in auditory capabilities of different species and consequently do not affect all fishes equally (Scholik and Yan 2001, 2002a, b; Wysocki and Ladich 2005; Wysocki et al. 2006; Vasconcelos et al. 2007). Furthermore, acoustic communication distances in aquatic organisms are influenced by physical sound stimuli in their environment (Amoser and Ladich 2005; Wysocki et al. 2007). It is clear that past studies of aquatic organisms have, at least partially, neglected the potential effects of physical generated underwater sound and the role in evolutionary and behavioral outcomes and/or adaptations.

The interaction between water velocity, relative submergence and flow obstructions can influence turbulence and bubble formation, as well as create transition zones, and therefore influence the underwater soundscape in streams. Flow obstructions created in the flume are comparable to boulders, outcrops, large trees, wood jams, bridges, and rip-rap banks. Bed structures create local vortices that entrain air and release bubbles from breaking surface water. Changes in flow depth relative to streambed structures influence relative submergence, which again has a pronounced impact on the underwater soundscape. The effect of relative submergence on the acoustic signature should be particularly prominent in low-order streams with a moderate to low ratio between depth and sediment size. A riffle may shift from a soundscape dominated by middle frequencies at low discharge and flow depth to a soundscape characterized by low frequencies at higher discharge and greater flow depth.

Our results show that an increase in turbulence and bubble formation (due to submergence and flow obstructions) lead to a distinctive increase in midrange-frequency, as well as in a narrow band of low-frequency sound pressure levels. This finding is confirmed by the work of Lugli and Fine (2003) who found that bubbles and turbulence increase sound pressure levels in midrange frequencies and low frequencies, respectively. A predominance of sound pressure levels at low frequencies (<1 kHz) is also known to be typical in underwater ambient sound, generally consisting of a combination of surf, wind and biological sound (Greene 1995). Further, the spatial heterogeneity of the underwater soundscape increased as the level

of turbulence and bubble formation increased. This sound heterogeneity across middle frequency bands is probably related to pulsating sound produced by breaking and reforming turbulent waves on flow obstructions.

The physical generated underwater sound should travel in all directions independent of the flow direction because water velocity is very low compared with sound speed that can travel at about 1,463-1,524 m s^{-1} in water, depending on temperature, salinity and pressure (Officier 1958). Moreover, because of its extraordinarily low attenuation, physical generated sound should propagate over large distances (Hawkins and Myrberg 1983). However, our results suggested that physical generated sound in the lower frequency bands travelled short distances upstream and downstream, while sound at the midrange and high frequencies quickly attenuated over very short distances beyond the scale of the flow obstruction or scale of a turbulent flow structure. Indeed, position 7 located in the lee of one of the bricks had a much different sound regime than position 4 which showed the highest level of sound across all frequencies, yet it was <1 brick distance away (Figure 9). We believe this is best explained by what is called the “cutoff phenomenon" (Officier 1958; Urick 1983), as well as to absorption and scattering processes.

We propose that the quick sound pressure level attenuation over distance in the middle frequencies was mainly a consequence of the cutoff phenomenon. A frequency corresponding to $k = 4\ h$ (where k is the wavelength and h is flow depth) is termed the cutoff frequency where sound at frequencies below this cutoff level become quickly attenuated (Urick 1983). In the bed structures experiment of the present study, flow depth was relatively low (16-22 cm). This implicated a cutoff frequency between 2.3 and 1.7 kHz (by a rigid bottom and a sound velocity of 1,500 m s^{-1}). This means that frequencies lower than the cutoff frequency could not propagate as acoustic waves and quickly decay with distance from the sound source. One of the first studies to systematically measure sound propagation in shallow water was done to examine mating call propagation of the oyster toadfish, *Opsanus tau*, which commonly call in 1 m deep water (Fine and Lenhardt 1983). Those authors found that low frequency acoustic signals in water approximately 1 m deep (over a sandy bottom) attenuated rapidly, with absorption coefficients ranging from 3 to 9 dB m^{-1}. Therefore, fish communication was restricted within a range of several meters. Moreover, Lugli and Fine (2007) reported that a 0.2 kHz tone at a flow depth of 20 cm will be reduced by 20 dB every 15 cm in distance away from the source. Therefore, high sound pressure levels in the mid-frequency range created at position 4 quickly decayed moving downstream from the sound source (position 5 and 6) (Figure 9), mainly as consequence of the cutoff phenomenon.

Because sound pressure levels of the lower octave bands had high dB levels at all positions, which is in disagreement with the cutoff effect, we suggest that a very low-frequency sound may be an artifact of the flume itself or internally generated by the recording equipment.

Sound at high frequencies has been shown to be absorbed more than low frequencies however, over short distances the effect of absorption is not a factor (UK National Physical Laboratory). Hence, sound absorption should not affect the results of this study. However, sound attenuation was probably also influenced by scattering of physical generated sound due to bubbles created by the turbulence near flow obstructions. Plumes of bubbles have been found to absorb and scatter sound (Urick 1983; Norton and Novarini 2001). Scattering is responsible for the deflection of sound energy away from the main propagation direction. This can explain the "quiet" zone (with low sound pressure levels over most frequencies) behind the bricks at position 7 (Figure 9). The high sound pressure levels created at position 4 were quickly, and over a very short distance, scattered away from the flow direction. Therefore, most of the physical generated sound energy could not reach position 7 but some of this energy reached the position 6 placed more downstream (Figure 9).

Ecological implications and conclusions

This study found that underwater soundscape in shallow running water is mainly shaped by the interaction between water velocity and relative submergence of flow obstructions and the related turbulence and bubble formation. Obstructions, which can create transition zones, are expected to generate unique acoustic signatures. In running-water habitats similar to those we created in the flume at positions 4 (e.g. riffle or cascade), 6 (e.g. run or glide), and 7 (e.g. backwater or eddy) are present at various discharge levels (Figure 9). Riffles or cascades may generate high turbulence and plenty of air bubbles in the water column, such as we created at position 4 (Figure 9). Therefore, the sound signature may be characterized by high sound pressure levels in midrange frequencies. In contrast, pools or runs, in which turbulence is generated differently and air bubble formation is less pronounced, the 3-D sound graph should resemble the ones at position 5 and 6 in the flume (Figure 9). Low-gradient streams may have lower ambient sound pressure levels than rivers with steep channels. However, quiet zones such as eddies, backwaters, and glides may have similar 3-D sound graphs as the one at position 7 (Figure 9).

We also expect that the specific physical generated sound recorded in the field remains a local phenomenon, especially in shallow waters, although very high-frequency sound may travel over longer distances (because they are less affected by the cutoff phenomenon). The effect of sound absorption and scattering should also be more marked in riffles and cascades

than in runs or pools because of a larger concentration of air bubbles in the water column and because of higher structural heterogeneity at the bottom. Therefore, physical generated sound provides a characteristic attribute of specific aquatic habitat types that organisms may use.

Organisms may obtain indirect information from the acoustic signals about the potential position of prey and predators, on how to find potential mates or competitors, and to communicate inter- and intra-specifically (Popper and Fay 1993; Lagardere et al. 1994; Myrberg and Lugli 2006). They can also receive abiotic information about waves, torrents, wind, currents or precipitation events (Popper and Fay 1993; Lagardere et al. 1994). Fish survival, for example, depends on their auditory system, which helps to accurately interpret information on the acoustic environment (Vasconcelos et al. 2007). The best hearing range and vocalization of most fish species is located below 1 kHz (Hawkins 1973; Amorim 2006). However, hearing specialists like carps can detect sound over a broader frequency range (up to several kHz), and at much lower sound pressure level (Amoser and Ladich 2005). Fishes and most likely other aquatic organisms could use their auditory system to detect typical physical generated sounds or to find preferred feeding locations such as the downstream end of riffles. The present study showed that high sound pressure levels in running waters can be generated by high water velocity as well as by the presence of submerged flow obstructions. Therefore, rivers and streams may show high sound pressure levels, especially during high flow events. Thus, eddies, pools, backwaters and glides could serve as an important hydraulic refuge where aquatic organisms can attain a positive energetic balance as well as quiet zones, for example, for intraspecific communication.

On the other hand, human interventions may affect the acoustic signature. Channelization, for example, may decrease streambed heterogeneity and relative submergence, concurrently decrease flow depth and increase mean water velocity, and thereby reducing physical generated sound heterogeneity while increasing sound pressure level and the effect of the cutoff phenomenon. Because different habitat types may have different acoustic signatures, their alteration may affect the soundscape of rivers and streams, and therefore may impact organism behavior. However, it remains an open question as to what extent physical generated sound, submerged flow obstructions, and velocity are used, independently or in concert, for positioning or movement.

Acknowledgments

We are grateful to V. Acuña and A. N. Sukhodolov for comments and suggestions on this article, and to the Laboratory of Hydraulics, Hydrology and Glaciology (VAW) of the Swiss Federal Institute of Technology (ETH) Zurich for providing the flume for the experiments. In addition we would like to thanks two anonymous reviewers for their valuable comments. This study was supported by the MAVA foundation, the Swiss Federal Institute of Aquatic Science and Technology (EAWAG), and the Leibniz-Institute of Freshwater Ecology and Inland Fisheries (IGB). Funding for M. S. Lorang was provided by a grant from the Gordon and Betty Moore Foundation, San Francisco, CA, USA.

References

Amorim MCP. 2006. Diversity of sound production in fish. In *Communication in Fishes*, Ladich F, Collin SP, Moller P, Kapoor BG (eds). Science Publishers: Enfield; 71-104.

Amoser S, Ladich F. 2005. Are hearing sensitivities of freshwater fish adapted to the ambient noise in their habitats? *Journal of Experimental Biology* 208: 3533-3542.

Anderson L, Mulligan L, Goodman L, Regen H. 1983. Effects of sound on preferences for outdoor settings. *Enviroment and Behaviour* 15: 539-566.

Apel JR, Ostrovsky LA, Stepanyants YA, Lynch JF. 2007. Internal solitons in the ocean and their effect on underwater sound. *Journal of the Acoustical Society of America* 121: 695-722.

Carles JL, Barrio IL, Lucio JV. 1999. Sound influence on landscape values. *Landscape and Urban Planning* 43: 191-200.

Clark CW, Clapham PJ. 2004. Acoustic monitoring on a humpback whale (*Megaptera novaeangliae*) feeding ground shows continual singing into late spring. *Proceedings of the Royal Society B* 271: 1051-1057.

Da Cunha RGT, Jalles E. 2007. The roaring of southern brown howler monkeys (*Alouatta guariba clamitans*) as a mechanism of active defence of borders. *Folia Primatologica* 78: 259-271.

DiSciara GN, Gordon J. 1997. Bioacoustics: a tool for the conservation of cetaceans in the Mediterranean Sea. *Marine and Freshwater Behaviour and Physiology* 30: 125-146.

Dyck MG, Baydack RK. 2004. Vigilance behaviour of polar bears (*Ursus maritimus*) in the context of wildlife-viewing activities at Churchill, Manitoba, Canada. *Biological Conservation* 116: 343-350.

Ellinger N, Hödl W. 2003. Habitat acoustic of a neotropical lowland rainforest. *Bioacoustics* 13: 297-321.

Fine ML, Lenhardt ML. 1983. Shallow-water propagation of the toadfish mating call. *Comparative Biochemistry and Physiology A* 76: 225-231.

Forman RTT, Reineking B, Hersperger AM. 2002. Road traffic and nearby grassland bird patterns in a suburbanizing landscape. *Environmental Management* 29: 782-800.

Gibeau ML, Clevenger AP, Herrero S, Wierzchowski J. 2002. Grizzly bear response to human development and activities in the Bow River watershed, Alberta, Canada. *Biological Conservation* 103: 227-236.

Gramann J. 1999. The effects of mechanical noise and natural sounds on visitors experiences in units of the natural park system. *Social Science Research Review* 1: 1-16.

Greene CR. 1995. Ambient noise. In *Marine Mammals and Noise*, Richardson WJ, Greene CR, Malme CI, Thomson DH (eds). Academic Press: San Diego; 87-100.

Hawkins AD. 1973. The sensitivity of fish to sounds. *Oceanography Marine Biology Annual Review* 11: 291-340.

Hawkins AD, Myrberg AA. 1983. Hearing and sound communication under water. In *Bioacoustics, a Comparative Approach*, Lewis B (ed). Academic Press: London; 347-405.

IEC. 1995. *Electroacoustics - Octave-band and Fractional-octave-band Filters*. Document 61260.

Kariel H. 1990. Factors affecting response to noise in outdoor recreational environments. *Canadian Geographer* 34: 142-149.

Lagardere JP, Begout ML, Lafaye JY, Villotte JP. 1994. Influence of wind-produced noise on orientation in the sole (*Solea-Solea*). *Canadian Journal of Fisheries and Aquatic Sciences* 51: 1258-1264.

Lugli M, Fine ML. 2003. Acoustic communication in two freshwater gobies: ambient noise and short-range propagation in shallow streams. *Journal of the Acoustical Society of America* 114: 512-521.

Lugli M, Fine ML. 2007. Stream ambient noise, spectrum and propagation of sounds in the goby *Padogobius martensii*: sound pressure and particle velocity. *Journal of the Acoustical Society of America* 122: 2881-2892.

Ma BB, Nystuen JA. 2005. Passive acoustic detection and measurement of rainfall at sea. *Journal of Atmospheric and Oceanic Technology* 22: 1225-1248.

Ma BB, Nystuen JA, Lien RC. 2005. Prediction of underwater sound levels from rain and wind. *Journal of the Acoustical Society of America* 117: 3555-3565.

Mason T, Priestley D, Reeve DE. 2007. Monitoring near-shore shingle transport under waves using a passive acoustic technique. *Journal of the Acoustical Society of America* 122: 737-746.

McDonald MA, Hildebrand JA, Webb SC. 1995. Blue and fin whales observed on a sea-floor array in the Northeast Pacific. *Journal of the Acoustical Society of America* 98: 712-721.

Morse N, Bowden WB, Hackman A, Pruden C, Steiner E, Berger E. 2007. Using sound pressure to estimate reaeration in streams. *Journal of the North American Benthological Society* 26: 28-37.

Myrberg AA, Lugli M. 2006. Reproductive behavior and acoustical interactions. In *Communication in Fishes*, Ladich F, Collin SP, Moller P, Kapoor BG (eds). Science Publishers: Enfield; 149-176.

Nitsche FO, Bell R, Carbotte SM, Ryan WBF, Flood R. 2004. Process-related classification of acoustic data from the Hudson River estuary. *Marine Geology* 209: 131-145.

Norton MP. 1989. *Fundamentals of Noise and Vibration Analysis for Engineers*. Cambridge University Press: Cambridge; 619.

Norton GV, Novarini JC. 2001. On the relative role of sea-surface roughness and bubble plumes in shallow-water propagation in the low-kilohertz region. *Journal of the Acoustical Society of America* 110: 2946-2955.

Nystuen JA. 2001. Listening to raindrops from underwater: an acoustic disdrometer. *Journal of Atmospheric and Oceanic Technology* 18: 1640-1657.

Officier CB. 1958. *Introduction to the Theory of Sound Transmission*. McGraw-Hill: New York; 284.

Popper AN, Fay RR. 1993. Sound detection and processing by fish - critical-review and major research questions. *Brain Behavior and Evolution* 41: 14-38.

Popper AN. 2003. Effects of anthropogenic sounds on fishes. *Fisheries* 28: 24-31.

Porteous JD, Mastin JF. 1985. Soundscape. *Journal of Architectural and Planning Research* 2: 169-186.

Rabin LA, Coss RG, Owings DH. 2006. The effects of wind turbines on antipredator behavior in California ground squirrels (*Spermophilus beecheyi*). *Biological Conservation* 131: 410-420.

Reijnen R, Foppen R, Veenbaas G. 1997. Disturbance by traffic of breeding birds: evaluation of the effect and considerations in planning and managing road corridors. *Biodiversity and Conservation* 6: 567-581.

Rickenmann D. 1997. Sediment transport in Swiss torrents. *Earth Surface Processes and Landforms* 22: 937-951.

Rouse HL. 1994. Measurement of bedload gravel transport - the calibration of a self-generated noise system. *Earth Surface Processes and Landforms* 19: 789-800.

Ruiz-Miranda CR, Archer CA, Kleiman DG. 2002. Acoustic differences between spontaneous and induced long calls of golden lion tamarins, *Leontopithecus rosalia*. *Folia Primatologica* 73: 124-131.

Scholik AR, Yan HY. 2001. Effects of underwater noise on auditory sensitivity of a cyprinid fish. *Hearing Research* 152: 17-24.

Scholik AR, Yan HY. 2002a. Effect of boat engine noise on auditory sensitivity of the fathead minnnow, *Pimephales promelas*. *Environmental Biology of Fishes* 63: 203-209.

Scholik AR, Yan HY. 2002b. The effects of noise on the auditory sensitivity of the bluegill sunfish, *Lepomis macrochirus*. *Comparative Biochemistry and Physiology A* 133: 43-52.

Slater PJB, Catchpole CK. 1990. Responses of the 2 chaffinch species on Tenerife (*Fringilla-Teydea* and *F-Coelebs-Tintillon*) to playback of the song of their own and the other species. *Behaviour* 115: 143-152.

Southworth M. 1969. The sonic environment of cities. *Environment and Behavior* 1: 49-70.

Staples S. 1997. Public policy and environmental noise: modeling exposure or understanding effects. *American Journal of Public Health* 87: 2063-2067.

Sun JWC, Narins PA. 2005. Anthropogenic sounds differentially affect amphibian call rate. *Biological Conservation* 121: 419-427.

Terrill E, Melville WK. 1997. Sound-speed measurements in the surface-wave layer. *Journal of the Acoustical Society of America* 102: 2607-2625.

Urick RJ. 1983. *Principles of Underwater Sound*. McGraw-Hill: New York; 423.

Vagle S, Burch H. 2005. Acoustic measurements of the sound-speed profile in the bubbly wake formed by a small motor boat. *Journal of the Acoustical Society of America* 117: 153-163.

Vasconcelos RO, Amorim MCP, Ladich F. 2007. Effects of ship noise on the detectability of communication signals in the Lusitanian toadfish. *Journal of Experimental Biology* 210: 2104-2112.

Wysocki LE, Ladich F. 2005. Effects of noise exposure on click detection and the temporal resolution ability of the goldfish auditory system. *Hearing Research* 201: 27-36.

Wysocki LE, Dittami JP, Ladich F. 2006. Ship noise and cortisol secretion in European freshwater fishes. *Biological Conservation* 128: 501-508.

Wysocki LE, Amoser S, Ladich F. 2007. Diversity in ambient noise in European freshwater habitats: noise levels, spectral profiles, and impact on fishes. *Journal of the Acoustical Society of America* 121: 2559-2566.

Yang W, Kang J. 2005. Soundscape and sound preferences in urban squares: a case study in Sheffield. *Journal of Urban Design* 10: 61-80.

CHAPTER 2

A field-based investigation to examine underwater soundscapes of five common river habitats

Abstract

Aquatic river habitat types have been characterized and classified for over five decades based on hydrogeomorphic and ecological variables. However, few studies have considered the generation of underwater sound as a unique property of aquatic habitats, and therefore as a potential information source for freshwater organisms. In this study, five common habitat types along 12 rivers in Switzerland (six replicates per habitat type) were acoustically compared. Acoustic signals were recorded by submerging two parallel hydrophones and were analyzed by calculating the energetic mean as well as the temporal variance of 10 octave bands (0.0315-16 kHz). Concurrently, each habitat type was characterized by hydraulic and geomorphic variables, respectively. The average relative roughness, velocity-to-depth ratio, and Froude number explained most of the variance of the acoustic signals created in different habitat types. The average relative roughness predominantly affected middle frequencies (0.063-1 kHz), while streambed sediment transport increased high-frequency sound pressure levels (2-16 kHz) as well as the temporal variability of the recorded signal. Each aquatic habitat type exhibited a distinct acoustic signature or soundscape. These soundscapes may be a crucial information source for many freshwater organisms about their riverine environment.

Introduction

Aquatic river habitat types have traditionally been classified based on flow characteristics and geomorphic properties (Leopold and Maddock 1953; Montgomery and Buffington 1997; Wohl and Merritt 2008). The structure and dynamics of these habitat types influence, among other stream ecosystem characteristics, the composition and distribution of fish (Stuart 1953; Lamouroux et al. 2002; Vlach et al. 2005) and benthic invertebrates (Beisel et al. 1998; Brooks et al. 2005; Pastuchová et al. 2008). However, little is known about the acoustic signature of aquatic habitat types. It is not known if all habitats simply have similar "white-noise" signatures or if they have mixed or even unique signatures (e.g. do riffles and pools sound the same or different?).

Acoustically, freshwater ecosystems have been considered as large composite environments rather than as a mosaic of distinct habitat types (Amoser and Ladich 2005; Wysocki et al. 2007). Wysocki et al. (2007) noticed that physical sources of underwater sound generation depend on hydraulic conditions (flow depth and velocity, sediment transport), whereas biotic sources (e.g. created by aquatic insects) may only contribute to acoustic signals when water is stagnant or slowly flowing. Based on laboratory experiments, Tonolla et al. (2009) demonstrated that underwater sound in shallow waters may be created by turbulence resulting from the interaction of flow velocity, relative roughness (given as relative submergence), and flow obstructions. Furthermore, Tonolla et al. (2009) showed that different acoustic signatures exist at different positions in a flume course, pointing to a direct influence of morphological and hydraulic conditions on the acoustic signature, which may also be the case for different river habitat types.

Underwater sound exhibits a lower attenuation rate compared to light and chemical substances; at the same time, it is rapidly transmitted over long distances (4-5 times faster than in air; Hawkins and Myrberg 1983; Rogers and Cox 1988; Popper and Carlson 1998). Therefore, acoustic signatures most likely provide important information sources about the underwater environment for aquatic organisms. Although few fish species actively use acoustic signals for communication, almost all fish species are able to detect sound and therefore may use it for positioning, navigation, refuge detection, and prey selection (Popper et al. 2003). Therefore, underwater sound is expected to strongly influence the ecology and behavior of many aquatic organisms.

The main goal of this study was to characterize hydrogeomorphologically and acoustically common aquatic habitat types including pools, runs (with and without streambed sediment transport), riffles, and step-pools. The specific objectives were (i) to characterize river habitat

types based on acoustic signatures and (ii) to quantify the relationship between acoustic signatures and hydrogeomorphic characteristics. Specifically, we predict that (i) the five selected river habitat types can be clearly distinguished acoustically and (ii) that typical hydrogeomorphic characteristics influence single or a range of frequencies. Finally, the potential ecological relevance of different acoustic signatures for fishes is briefly discussed.

Materials and methods

Experimental design

Between April and December 2007, 30 aquatic habitats along 12 Swiss rivers were hydrogeomorphologically and acoustically investigated (Figure 1, Table 1). Five common habitat types, with six replicates each, were empirically identified: pools, riffles, runs with (run sed.) and without (run) streambed sediment transport, and step-pools.

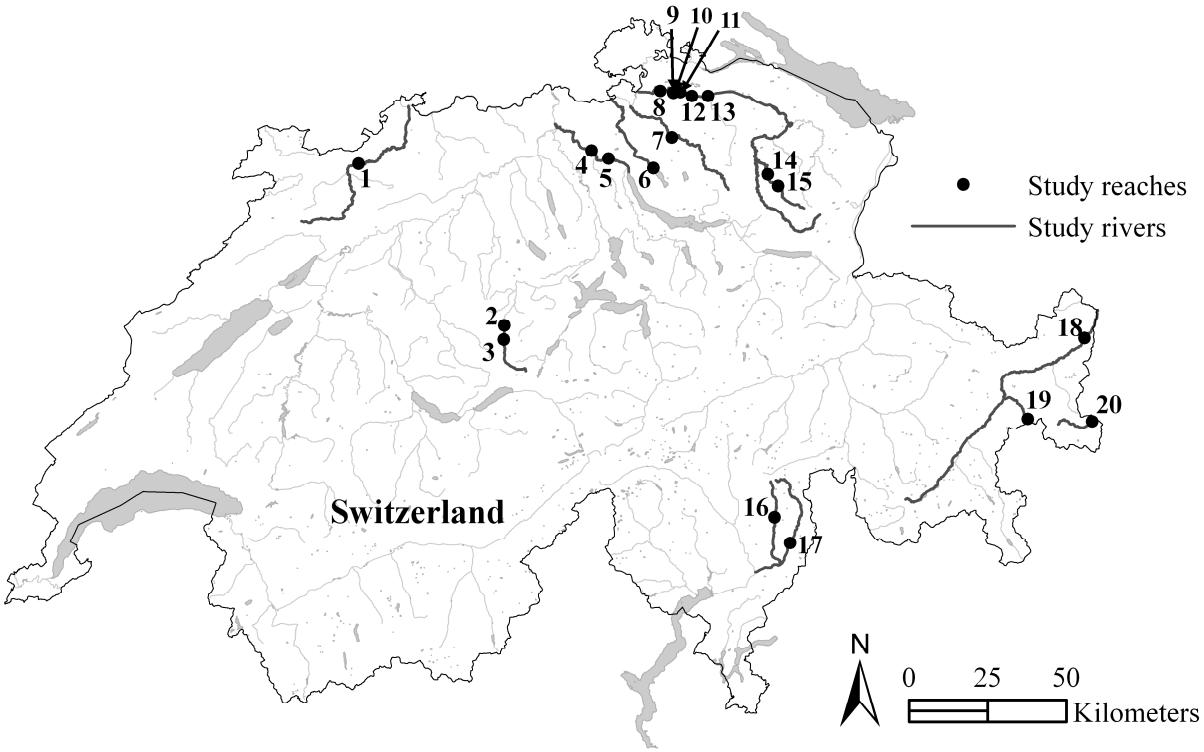

Figure 1. Location of the 20 study reaches along 12 Swiss rivers (see Table 1 for details).

Slow-flowing habitats with a smooth water surface were classified as pools; habitats with little surface agitation and no major flow obstruction as runs (runs with streambed sediment transport if this was visually clearly detectable); swiftly flowing turbulent waters with frequent surface waves as riffles, and habitats showing a single cascade of water into a boulder/cobble-forced pool as step-pools.

Table 1. Characterization of the study habitat types along 12 Swiss rivers.

Study reach	River	Habitat type	Stream order (Strahler)	Discharge (m^3 s^{-1})
1	Birs	1 run sed.	6	33.1
2	Waldemme	1 pool, 1 step-pool	6	9.6
3	Waldemme	1 pool, 2 step-pools	6	9.6
4	Limmat	1 pool	7	53.7
5	Limmat	1 run	7	48.1
6	Glatt	1 run	6	3.5
7	Töss	1 riffle	6	8.1
8	Thur	1 run sed.	7	49.9
9	Thur	1 run sed.	7	58.6
10	Thur	1 run sed.	7	58.6
11	Thur	1 riffle[A], 1 run sed.	7	13.8
12	Thur	1 run	7	13.8
13	Thur	1 run	7	11.8
14	Necker	1 pool, 2 runs	6	2.3
15	Necker	1 step-pool	5	2.3
16	Calancasca	1 step-pool	4	5.4
17	Moesa	1 pool[A], 1 run sed.	5	30.2
18	Inn	1 riffle	6	52.7
19	Spöl	1 pool[A], 2 riffles, 1 step-pool	5	13.0
20	Rom	1 riffle	4	1.7

Study reaches are indicated in Figure 1. Daily average discharge at the time of measurement are from the nearest gauging station (FOEN 2009). [A] Not in the main channel.

Data collection

Nine hydrogeomorphic variables were either directly measured in the field or calculated based on these measurements (Table 2). Flow velocity (u), using a hand-held FlowTracker (Acoustic Doppler Velocimeter, SonTek, San Diego, USA), and flow depth (h), were measured in front of the hydrophone head. The average (D_{50}) and maximum (D_{max}) particle size (c-axis: height) were calculated from 100 randomly selected substrate particles in an area of ~10 m around the hydrophones (following a modified Wolman (1954) count). The average relative roughness ($D_{50}\ h^{-1}$), maximum relative roughness ($D_{max}\ h^{-1}$), Froude number ($Fr = \frac{u}{\sqrt{g\,h}}$, where g is the acceleration due to gravity), velocity-to-depth ratio ($u\ h^{-1}$), and Reynolds number ($Re = \frac{u\,h}{\nu}$, where ν is kinematic viscosity of water) were calculated. Reynolds number is a dimensionless criterion describing the onset of turbulent flow from laminar flow conditions and Froude number indicates the energetic state of the flow (a value of 1 indicates the transition from subcritical to super-critical flow). In this study, all flow was

turbulent, hence the Reynolds number was used to scale the level of turbulence rather than describe a change in flow from laminar to turbulent conditions.

Table 2. Hydrogeomorphic variables (average ± standard deviation) of the five habitat types.

Variable	Pools (n = 6)	Runs (n = 6)	Runs Sed. (n = 6)	Riffles (n = 6)	Step-pools (n = 6)
u (m s^{-1})	0.11 ± 0.06	0.46 ± 0.10	0.66 ± 0.22	1.01 ± 0.22	0.18 ± 0.13
h (m)	0.80 ± 0.44	1.01 ± 0.36	0.74 ± 0.23	0.30 ± 0.07	0.41 ± 0.16
D_{50} (m)	0.01 ± 0.01	0.02 ± 0.02	0.03 ± 0.02	0.07 ± 0.05	0.37 ± 0.20
D_{max} (m)	0.18 ± 0.25	0.09 ± 0.11	0.09 ± 0.06	0.20 ± 0.09	0.55 ± 0.17
$D_{50}\,h^{-1}$	0.01 ± 0.01	0.03 ± 0.02	0.04 ± 0.03	0.21 ± 0.10	0.90 ± 0.37
$D_{max}\,h^{-1}$	0.19 ± 0.25	0.10 ± 0.09	0.14 ± 0.15	0.66 ± 0.19	1.37 ± 0.24
Fr	0.04 ± 0.02	0.16 ± 0.07	0.25 ± 0.08	0.62 ± 0.20	0.09 ± 0.05
$u\,h^{-1}$	0.16 ± 0.09	0.58 ± 0.47	0.93 ± 0.34	3.73 ± 1.62	0.41 ± 0.24
Re (x10^4)	9.38 ± 8.10	45.57± 17.04	50.07 ± 25.90	28.52 ± 3.40	8.68 ± 8.66

u: flow velocity; h: flow depth; D_{50}: average substrate size (c-axis: height); D_{max}: maximum substrate size (max. c-axis: max. height); $D_{50}\,h^{-1}$: relative roughness; $D_{max}\,h^{-1}$: max. relative roughness; Fr: Froude number; $u\,h^{-1}$: velocity-to-depth ratio; Re: Reynolds number. Note that flow velocity and flow depth for step-pool habitats were measured in the pool under the step. Moreover, step height had also been considered in the measurement of substrate particle. Therefore, relative roughness values >1 in step-pools occurred.

Acoustic signals were recorded using two hydrophones (Type 8103, Brüel and Kjaer, Denmark). A metal rod was placed vertically in the sediment under the water surface and a supplementary metal rod (~40 cm length) was attached at the vertical one so that the hydrophones could be positioned parallel with the heads facing upstream at 60% flow depth. The distance between the two heads was ~2 cm. An amplifier (Type Nexus 2692 OS2, Brüel and Kjaer, Denmark), with sensitivity set at 3.16 mV Pa^{-1}, was used to amplify the signal sent by the hydrophones. Finally, the signals were captured by a digital recorder (Type R-4, Edirol, Japan). The sampling frequency was 44.1 kHz and amplitude resolution was 16 bits. This setting assured a frequency range between 0.02 and 20 kHz and a dynamic range of >90 dB. The recording time was approximately 5.5 min per habitat.

Data analysis

Acoustic data reduction and analysis

The acoustic signals detected by the two hydrophones were analyzed (5 min were randomly selected) by means of a signal-processing software package specifically developed and written for this specific purpose (K. Heutschi, unpublished). A cross-spectrum analysis was used to minimize the contribution of uncorrelated noise between the two hydrophones. The data analysis used in this study followed the one recently described in Tonolla et al. (2009);

therefore, only a brief summary of the analysis is given here. In a first step, acoustic data were evaluated with a short-term third-octave band analysis over 31 frequency bands (0.020-20 kHz) and a temporal resolution of ~1.1 s. In a second step, the third-octave bands were combined in 10 octave bands. As the evaluation of a band-limited noise-like signal has uncertainty that depends reciprocally on the product of averaging time and bandwidth, the reduction of the spectral resolution from third-octave bands to octaves lowered the uncertainty significantly. One recording of approximately 5 min delivered a ~270 octave band spectra. For each octave band, the temporal variation over the 5 min recording was evaluated by calculating the variance. Furthermore, the average signal energy (energetic mean) in each octave band was evaluated. In addition to this octave band specific inspection, the variance and the average energy were calculated for the broadband signal over the whole frequency spectrum (henceforth, broadband mean value and broadband mean variance, respectively). Supplementary to the broadband mean variance, a Shannon's diversity index (*H*) was calculated using a vector-based landscape analysis tool (V-LATE 1.1 extension for ArcGis 9.2, ESRI, Redlands, USA) to represent the acoustic variability of the data (variability over time and over all octave bands). In general, the Shannon's diversity index is measured on a set of classes differing in frequency (≠ acoustic frequency; but occurrence). It increases with the evenness of the frequency of the classes and with the number of classes. In ecological studies, it is normally used to characterize species (classes) diversity in a community. The diversity analysis used in V-Late in this case focuses on acoustic classes rather than on species. The classes are sound pressure levels and their frequencies are the probability mass function of the amplitude envelope.

All data were expressed on a logarithmic scale as dB values relative to 1 µPa (dB re 1 µPa) as a reference. The calibration was performed with a Brüel and Kjaer calibrator (Type 4223, Brüel and Kjaer, Denmark), which generates a highly reproducible nominal sound pressure level of 166 dB at 0.25 kHz.

Sources of uncertainty

Potential sources of uncertainty were considered when measuring and analyzing acoustic data. These included the noise produced by the vibration of the hydrophone cable (induced by wind and/or water) and background noise produced by the suspension of the hydrophones in the water column. The metal rods placed under the water surface represented obstacles in the water flow and may have created some unwanted turbulence and vibrations, thus influencing the sound measurements. The most important external factor influencing sound measurements was wind, dominant at high frequencies. Moreover, Tonolla et al. (2009) found that, if sound

is not affected by scattering and the "cutoff phenomenon" (Officier 1958; Urick 1983; Rogers and Cox 1988), some of the energy created upstream can reach positions placed more downstream, thus sound not directly produced at the individual habitat but at more distant locations could be detected. The effect of unwanted turbulence and vibrations due to flow obstruction was reduced by the use of two hydrophones, located close to each other. This instrument set-up has been shown to provide data that can be used to reduce the background noise caused by turbulent flow around the hydrophones and internal noise of sensors and amplifiers and therefore provides an elevated signal-to-noise ratio (Tonolla et al. 2009). The advantage of this configuration is that by multiplying two signals instead of taking the square of just one sensor nullifies incoherent components between the two hydrophones (Norton 1989). This reduces internal noise components and contributions of sound from turbulence around the hydrophones, resulting in a significantly improved signal-to-noise ratio (Tonolla et al. 2009). The effect of vibration by flow was reduced by keeping the excess hydrophone cable out of the water column and securing in water cable to the metal rod. Moreover, acoustic measurements with feasible measurement artifacts such as energy peaks generated for short periods by, for example, cable movement, were identified and eliminated from the original data set.

Statistical analysis

Kolmogorov-Smirnov tests were initially used to test if variables clearly deviate from normality, and square-root-transformation applied if necessary. Principal component analyses (PCA) were performed based on hydrogeomorphic and acoustic variables. Factor loadings of the first and second principal component were extracted without rotation and used for further correlation analysis. A first PCA was used to generate habitat typology based on nine hydrogeomorphic variables (flow velocity, flow depth, average and maximum particle size, average and maximum relative roughness, Froude number, velocity-to-depth ratio, and Reynolds number). A second PCA was used to generate a habitat typology based on the sound pressure level (energetic mean) of the 10 octave bands (0.0315-16 kHz). Spearman's rank correlation analyses were used to identify the direction and strength of relationships between studied variables. Because variance of several octave bands was suspected to be inter-correlated, Spearman's rank correlation analysis was also used to determine these relationships. Analysis of variance between groups (one-way ANOVA) was performed to evaluate the effect of both habitat type and hydrogeomorphic variables on the acoustic signatures, and post hoc Tukey tests were performed for each pair-wise comparison to test for specific differences between habitat types. PCAs were performed with PRIMER 5

(version 5.2.9, Primer-E Ltd, Plymouth, UK), ANOVAs and post hoc Tukey tests were performed with SPSS (version 14.0, SPSS Inc., Chicago, USA).

Results

Hydrogeomorphic characterization of river habitat types

Based on hydrogeomorphic variables, river habitat types could be separated into four distinct groups (Figure 2). Maximum relative roughness, maximum substrate size, and average relative roughness exhibited the best correlations with the factor scores of the first component of the PCA, while velocity-to-depth ratio, Froude number, and flow velocity showed the best correlation with the factor scores of the second component (Table 3). Runs and runs with streambed sediment transport could not be clearly distinguished by the selected hydrogeomorphic variables. However, results from the present study suggest that runs with streambed sediment transport were associated with higher flow velocity, Froude number, velocity-to-depth ratio, as well as with higher Reynolds number (Table 2).

To avoid redundancy and because of the good correlation with the factor scores, the variables average relative roughness, velocity-to-depth ratio, Froude number, and Reynolds number were used for further statistical analyses.

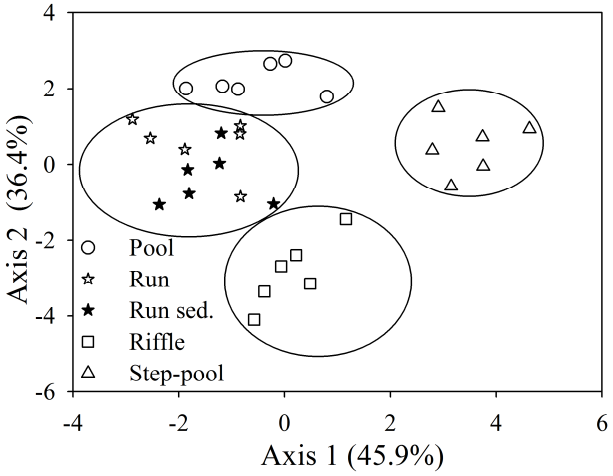

Figure 2. Principal components analysis (PCA) of the river habitats based on nine hydrogeomorphic variables (n = 6 per habitat type). The four groups separated by the PCA are indicated. Note that the percentage of explained information by each principal component is indicated in brackets.

Table 3. Spearman's rank correlation (*r*) between the nine hydrogeomorphic variables and the factor scores of the first (PCA1) and second (PCA2) components of the PCA.

Variable	PCA1 (*r*) (*n* = 30)	PCA2 (*r*) (*n* = 30)
u	-0.30	-0.89**
h	-0.52**	0.44*
D_{50}	0.80**	-0.38*
D_{max}	0.88**	-0.17
$D_{50}\,h^{-1}$	0.84**	-0.46*
$D_{max}\,h^{-1}$	0.93**	-0.34
Fr	-0.18	-0.94**
$u\,h^{-1}$	-0.01	-0.97**
Re	-0.63**	-0.48**

For abbreviations of the hydrogeomorphic variables see Table 2. *$p < 0.05$; **$p < 0.01$.

Acoustic characterization of river habitat types

Acoustically, except for one riffle outlier, river habitat types could be separated into four groups (Figure 3). The riffle outlier was at a site with high discharge (Inn River; Table 1), and had a two times higher average relative roughness than the other riffles. All 10 octave bands exhibited a significant negative correlation with the factor scores of the first component but only a weak negative (2-16 kHz) and weak positive (0.0315-1 kHz) correlation with the factor scores of the second component (Table 4).

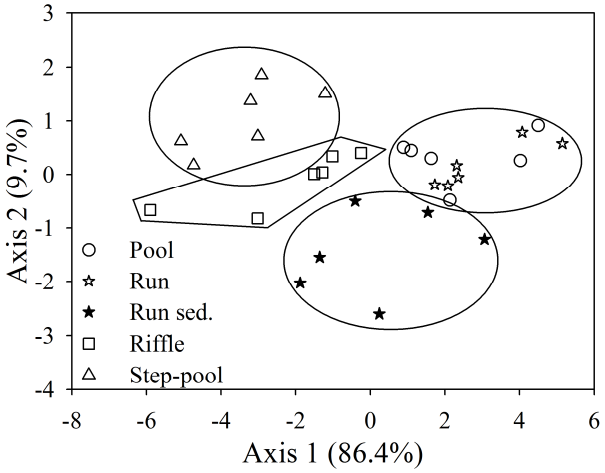

Figure 3. Principal components analysis (PCA) of the river habitats based on the sound pressure levels of 10 octave bands (*n* = 6 per habitat type). The four groups separated by the PCA are indicated. Note that the percentage of explained information by each principal component is indicated in brackets.

Table 4. Spearman's rank correlation (r) between sound pressure levels of the 10 octave bands and the factor scores of the first (PCA1) and second (PCA2) components of the PCA.

Octave band (kHz)	PCA1 (r) (n = 30)	PCA2 (r) (n = 30)
0.0315	-0.93**	0.08
0.063	-0.94**	0.19
0.125	-0.94**	0.22
0.25	-0.91**	0.27
0.5	-0.93**	0.22
1	-0.96**	0.08
2	-0.96**	-0.16
4	-0.93**	-0.31
8	-0.90**	-0.40*
16	-0.84**	-0.42*

*$p < 0.05$; **$p < 0.01$.

The Tukey pair-wise multiple comparisons test showed that the factor scores of the first and/or the second component significantly differed among habitat types ($p < 0.05$) except between pools and runs without streambed sediment transport.

The energetic mean of all octave bands, as well as of the broadband mean value, significantly differed among habitat types (one-way ANOVA: $n = 30$; $p < 0.01$). The octave bands 0.125, 0.25, and 0.5 kHz exhibited the most distinct differences ($26.72 \leq F_{4,29} \leq 26.97$; $p < 0.001$). Tukey pair-wise multiple comparisons showed that pools and runs without streambed sediment transport exhibited a similar energetic mean of all octave bands, and the broadband mean value. Pools and runs with streambed sediment transport significantly differed in the energetic mean from 2 to 8 kHz ($p < 0.05$). Runs and runs with streambed sediment transport differed in the energetic mean from 2 to 16 kHz as well as in the broadband mean value ($p < 0.05$). Step-pools and riffles significantly differed in the energetic mean of 0.125 and 0.25 kHz ($p < 0.01$). Runs with streambed sediment transport and step-pools did not significantly differ in the energetic mean from 2 to 16 kHz, and runs with streambed sediment transport and riffles also did not differ in the energetic mean of 0.125 kHz.

Each habitat type exhibited a distinct acoustic signature (Figure 4). Pools and runs showed similar acoustic signatures with low sound pressure levels over all octave bands and a main energy peak at the 0.0315 kHz octave band. Runs with streambed sediment transport showed a distinct bimodal distribution (peaks between 2 and 16 kHz as well as at 0.0315 and 0.063 kHz). Streambed sediment transport generated an energy peak in the high-frequency bands (2-16 kHz) with an increase of more than 10 dB in the broadband mean value compared to runs without sediment transport (Figure 4).

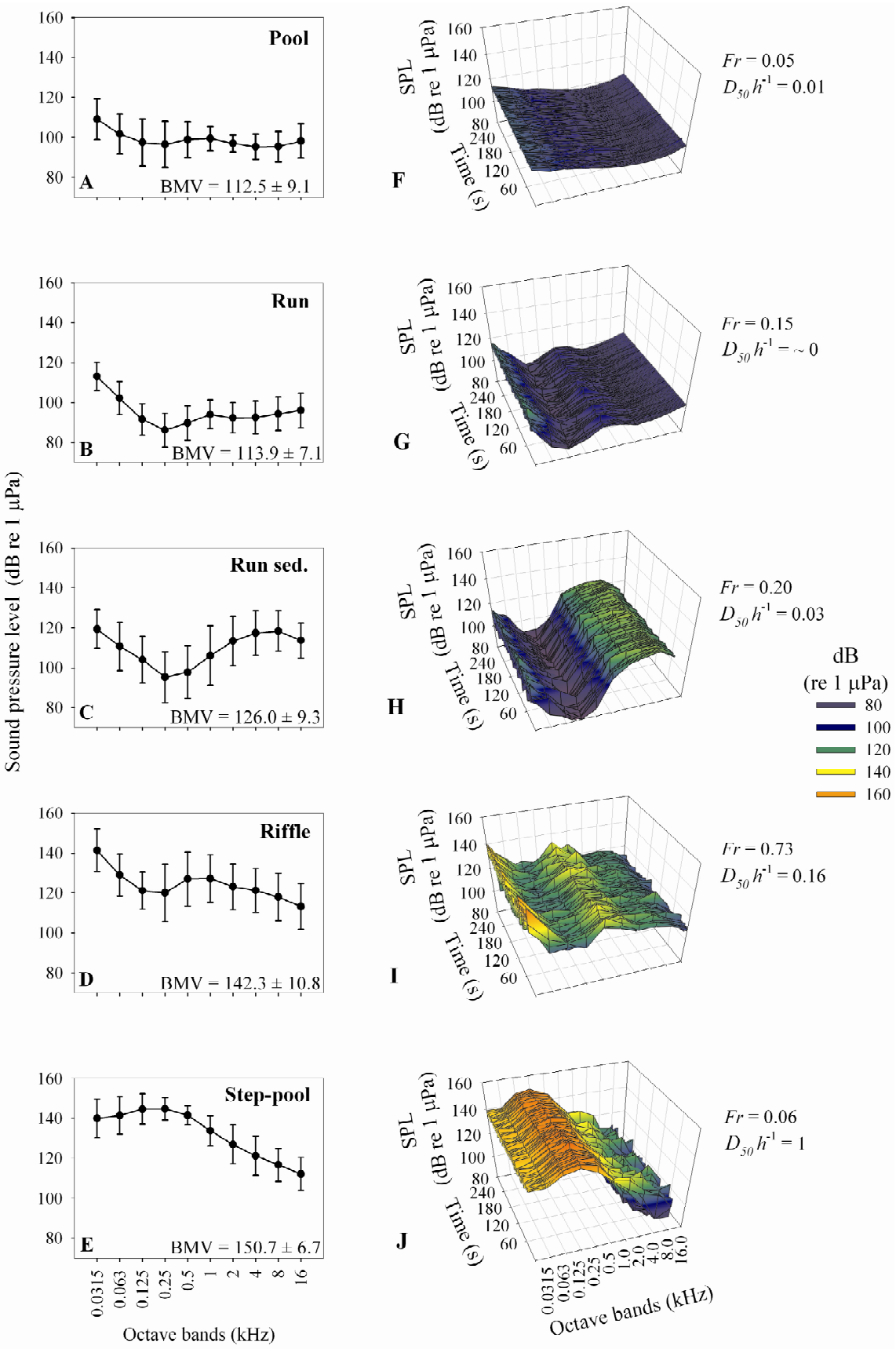

Figure 4. Acoustic signature of river habitats. Panels A-E showing sound pressure levels (average ± standard deviation) of 10 octave bands in the five habitat types (n = 6 per each habitat type); BMV: broadband mean value (average ± standard deviation). Panels F-J showing examples of 3-D sound graphs (soundscapes) for the five habitat types; SPL: sound pressure level; Fr: Froude number; $D_{50}\,h^{-1}$: relative roughness.

Riffles showed a distinct bimodal sound distribution (peaks at 0.031.5 kHz and 0.5-2 kHz) and the sound pressure level was about 20-30 dB higher than that in pools, runs, and runs with streambed sediment transport (Figure 4). There is a mid-range depression (0.125 to 0.25-0.5 kHz), a "silent" zone, in riffles, runs, runs with streambed sediment transport, and pools. However, step-pools exhibited sound pressure level peaks at these mid-range frequencies. Step-pool habitats showed by far the highest broadband mean value of all habitat types, reaching sound pressure levels of about 150 dB (Figure 4).

The acoustic temporal variability (given as variance) of the 10 octave bands could be separated into two distinct groups based on a PCA and Spearman's rank correlation analyses among dependent variables. To avoid redundancy within each of these two groups, only the variance of an octave band per group (0.125 and 2 kHz) was used for further statistical analysis. The five habitat types were significantly different based on the variance of the two selected octave bands, the broadband mean variance, as well as on the Shannon's diversity index (both variables corresponding to acoustic variability over octave bands and time). However, the Shannon's diversity index showed more pronounced differences among habitat types (Table 5). Shannon's diversity decreased from step-pools, to riffles, runs with streambed sediment transport, runs, and pools (Figure 5).

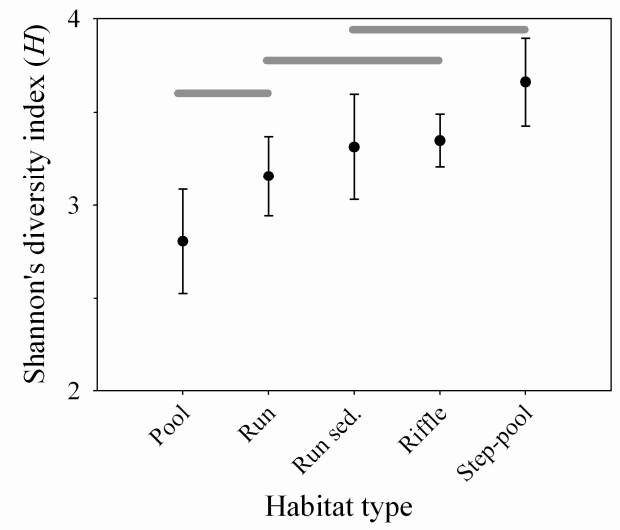

Figure 5. Shannon's diversity index (average ± standard deviation) of the five habitat types (n = 6 per habitat type). High Shannon's index values indicate high acoustic temporal and spatial (over all frequency bands) variability. Habitats plots not under the same horizontal bar are significantly different (based on Tukey pair-wise multiple comparisons test; $p < 0.01$).

Table 5. ANOVA statistic (F, p) for assessing the effect of habitat type on the variance of the two selected octave bands (0.125 and 2 kHz), the broadband mean variance (BMVa), and the Shannon's diversity index (H).

Variable	$F_{4,29}$	p
0.125 kHz	4.16	0.010*
2 kHz	5.96	0.002**
BMVa	9.82	0.000**
H	10.53	0.000**

The statistical model considered habitat type as fixed factor and 0.125 kHz, 2 kHz, BMVa, and H as dependent variables. *$p < 0.05$; **$p < 0.01$.

Out of the selected hydrogeomorphic variables, the average relative roughness explained most of the difference of the acoustic signatures of all 10 octave bands (in particular in the frequency range from 0.063 to 1 kHz), as well as of the broadband mean value (Table 6). The velocity-to-depth ratio and Froude number showed weak albeit significant correlations with 4 and 8 kHz sound pressure levels; the velocity-to-depth ratio also showed weak significant correlations with 0.0315 kHz and the broadband mean value. Reynolds number showed significant negative correlation only with 0.25 kHz (Table 6). The velocity-to-depth ratio and Froude number showed weak albeit significant correlations with 4 and 8 kHz sound pressure levels; the velocity-to-depth ratio also showed weak significant correlations with 0.0315 kHz and the broadband mean value. Reynolds number showed significant negative correlation only with 0.25 kHz (Table 6).

Table 6. Spearman's rank correlation (r) among the four selected hydrogeomorphic variables and the sound pressure level of the 10 octave bands and the broadband mean value (BMV).

Octave band (kHz)	$D_{50}\,h^{-1}$ (r) (n = 30)	Fr (r) (n = 30)	$u\,h^{-1}$ (r) (n = 30)	Re (r) (n = 30)
0.0315	0.79**	0.36	0.43*	-0.08
0.063	0.83**	0.21	0.32	-0.22
0.125	0.84**	0.16	0.28	-0.25
0.25	0.80**	0.05	0.16	-0.37*
0.5	0.84**	0.09	0.21	-0.32
1	0.82**	0.18	0.28	-0.20
2	0.74**	0.27	0.35	-0.06
4	0.68**	0.38*	0.45*	0.06
8	0.62**	0.43*	0.48**	0.15
16	0.47**	0.33	0.35	0.17
BMV	0.84**	0.27	0.37*	-0.12

For abbreviations of the hydrogeomorphic variables see Table 2. *$p < 0.05$; **$p < 0.01$.

Discussion

Aquatic river habitats have been studied and classified for decades. However, few studies have considered the generation of underwater sound as an essential feature of aquatic habitats, and therefore as a potential information signal for freshwater organisms. This is one of the first studies that acoustically characterized aquatic river habitats, and identified the main flow and geomorphic features that best explain underwater acoustic signals. Moreover, this study confirmed with stationary field experiments data that had been recently created artificially in a flume (Tonolla et al. 2009).

Based on acoustic signatures, it was possible to clearly differentiate the selected most common habitat types. Moreover, these acoustic signature groupings coincided with traditional hydrogeomorphic classifications that are typically used to distinguish habitat types. However, there was a high degree of variability within the habitat types that created a more continuous transition between habitats. Nevertheless, the common aquatic habitat types exhibited distinct acoustic signatures, although acoustic differences between pools and runs (without streambed sediment transport) were less pronounced than expected. Pools and runs exhibited low average relative roughness values due to a lack of flow obstructions, which are necessary for turbulence and air bubble formation and the subsequent sound generation (Tonolla et al. 2009). However, both run habitat types had higher sound pressure levels than pools. Higher sound pressure levels can be attributed to a combination of higher velocities, as increasing flow velocity increased sound pressure levels in a wide frequency range (Tonolla et al. 2009), and to particle collisions due to streambed sediment transport. The similarity of the acoustic signatures of step-pools and riffles might be due to the high average relative roughness that both habitat types have. High average relative roughness coupled to high flow velocity generates high turbulence and air bubbles (with related effects on sound absorption and scattering), which in turn causes broadband noise not always clearly distinguishable by the 10 octave bands.

A common characteristic of all habitat types were high sound pressure levels in the low-frequency range (0.0315 kHz), confirming previous results by Lugli and Fine (2003), Wysocki et al. (2007) and Tonolla et al. (2009). Low-frequency sound pressure levels have previously been attributed to large-scale turbulences (Lugli and Fine 2003). Thus, the highest energy was found in high turbulence habitats such as riffles and step-pools. However, even pools showed maximum sound pressure levels in the low frequencies, and a pronounced decline in middle to high frequencies, similar to lakes and backwaters (Wysocki et al. 2007). In contrast, high sound pressure levels in the mid to high frequencies were typical for fast-

flowing habitat types (riffles and runs with streambed sediment transport). This is in agreement with Wysocki et al. (2007), who also found high sound pressure level values in the high-frequency range above 1 kHz in fast-flowing habitat types.

Physical generated underwater sound is caused by specific hydraulic mechanisms including breaking waves, water plunging directly in the water column, and air bubbles that emerge from core regions of turbulent flow. In turn, turbulence is enhanced by high flow velocities, low flow depths (resulting in high velocity-to-depth ratio and Froude numbers), and high average relative roughness associated with coarse streambed particles. Therefore, differences in the acoustic signatures among habitat types were mainly determined by the average relative roughness, flow velocity, and flow depth. Similarly, Wysocki et al. (2007) attributed differences among habitat types to differences in flow velocity and type of bottom substrata. The average relative roughness influenced the acoustic signature in all frequency bands, in particular, in the 0.063-1 kHz range, as confirmed by flume experiments (Tonolla et al. 2009). The effect of the average relative roughness was more pronounced in riffles and step-pools with sound pressure level peaks between 0.5 and 2 kHz and between 0.125 and 0.5 kHz, respectively. Similar results were reported by Lugli and Fine (2003), who reported sound pressure level peaks between 0.2 and 0.5 kHz near waterfalls (equivalent to what is referred to here as step-pools) and rapids (equivalent to what is referred to here as riffles). This middle-frequency sound is attributed to processes of water breaking the surface and entraining air. The loudest sound is generated by collapsing waves and plunging chutes of water that cause a violent and forceful air entrainment. Some sound is also caused by secondary splashes and bubbles (underwater air bubbles), which are then carried by turbulent sweeps or advected vortices of current beneath the surface, which creates shear within the flow and emerges at the surface as boils, seams, and other patches of water surface roughness as turbulence dissipates. The process of rapid entrainment of air and subsequent collapse of air bubbles due to turbulence is commonly called cavitation (Urick 1983). Because of pressure changes, the bubbles of air dissolved in the water undergo dilatation and collapse after having reached a critical size, generating a short pulse of sound (Urick 1983; Lurton 2002). This process is thought to contribute to the physical underwater sound in the frequency range 0.1-1 kHz (Urick 1983; Lurton 2002). This frequency range corresponded to the sound pressure level peaks particularly found in riffles and step-pools.

High roughness coupled with high flow velocity induced breaking waves that collapsed in a rhythmic way, generating a distinct temporal sound variability. Therefore, differences in the average relative roughness were mainly responsible for differences in sound variability

among habitat types. Similarly, Tonolla et al. (2009) reported that an increase in the average relative roughness (expressed as relative submergence), and an increase in the related level of turbulence, led to an increase in acoustic variability across frequency bands and in time. Thus, the lowest variability was observed in habitat types with low average relative roughness (due to low bed heterogeneity) such as pools and runs. The sound variability was also influenced by streambed sediment transport. Sound variability in the high frequencies due to streambed sediment transport was relatively low compared to the observed variability in turbulent habitat types such as riffles and step-pools (Figure 4). Indeed, streambed sediment transport had a relevant effect on the acoustic signature, mainly on the high frequencies between 2 and 16 kHz. Higher velocity-to-depth ratio, Froude number, and flow velocity, found in runs with streambed sediment transport in contrast to "normal" runs, resulted from a higher gradient of energy across the runs, which in turn produced flow competent conditions for small particles composing the bed. Thus, the increase in the high-frequency energy was presumably caused by collisions and momentum exchange between particles in transport (mainly gravel and sand) and those resting on the bed, resulting in the production of sound and further entrainment of particle sizes larger than predicted by pure shears stress threshold conditions (Lorang and Hauer 2003). The sound produced by streambed sediments moving on the river bottom has also been successfully used by Rickenmann and McArdell (2007, 2008) to estimate the volume of coarse streambed sediment transport in mountain streams. The acoustic device used by those authors registered vibrations from gravel particle impacts passing over a metal plate, and the number of impulses per unit time was then used as a measure of bedload transport activity.

Potential ecological relevance of underwater soundscapes

Is underwater sound just an attribute of river habitats or does it provide meaningful information for organisms? Several studies have shown that reef fish larvae can detect and localize underwater sound over large distances (Tolimieri et al. 2000, 2004; Leis et al. 2002) as well as use it to migrate towards the reef (Simpson et al. 2005, 2008). Moreover, Popper et al. (2003) reported that fishes may detect and exploit complex acoustic signals. Acoustic signals in water are composed of particle motion and sound pressure components. However, certain fish taxa, the often-called hearing-generalist (e.g. salmonids, perches, eels), can only perceive the particle motion component of sound. Whereas, several group of unrelated taxa, the often-called hearing-specialists (e.g. carps, catfishes, herrings, and minnows), have additionally evolved the ability to perceive the pressure component of sound via accessory specialized anatomical structures (swim bladder or other gas-filled chambers) that transform

sound pressure waves into particle displacements. This considerably enhances their hearing sensitivity and extends their detectable auditory bandwidth to higher frequencies, Thus, hearing specialists can detect sound at frequencies up to several kilohertz and at relatively low sound pressure levels, whereas hearing generalists can only detect low-frequency sounds (<1 kHz) at a relatively high sound level (for reviews, e.g. Hawkins 1981; Fay and Simmons 1999; Ladich and Popper 2004). As a consequence, the perception and use of the typical habitat soundscapes might differ between species. In this study, only sound pressure as a component of the soundscape was considered. However, this is an important sound component in natural environments like rivers, and the shape of the sound spectrum for particle motion and pressure at noisy sites is generally similar (Lugli and Fine 2007).

Habitat types with fast-flowing water (riffles and runs with streambed sediment transport) or showing high turbulent zones (riffles and step-pools) can limit the detection of biological communication signals through high sound pressure levels. However, Lugli et al. (2003), Lugli and Fine (2003), and Wysocki et al. (2007) found a "noise window" in the <1 kHz range in fast-flowing habitats, which corresponded to the communication range of many fishes (hearing-generalists). In this study, low sound pressure levels have been recorded around 0.125 to 0.25-0.5 kHz in all habitat types, except in step-pools, supporting the "noise window" hypothesis. Moreover, Lugli and Fine (2007) found that a similar quiet zone is not only an attribute in pressure spectra but also in velocity spectra.

A major constraint in shallow waters is the limited propagation of sound. Low-frequency sounds, with long wavelengths, are relatively unaffected by scattering and absorption and may travel over great distances (Hawkins and Myrberg 1983). However, propagation of wavelengths >4 times the flow depth cannot propagate as acoustic waves owing to the cutoff phenomenon (Officier 1958; Urick 1983; Rogers and Cox 1988). Thus, sound propagation in shallow aquatic ecosystems is constrained by flow depth and the nature of the bottom material (Rogers and Cox 1988). For example, in riffles, with flow depth typically <0.4 m, low-frequency sound (<1 kHz), by a rigid bottom and a sound velocity of 1,500 m s^{-1}, rapidly decays within short distances from their source. This phenomenon has implications in the propagation of low-to-middle-frequency sounds generated in an upstream habitat, which exponentially decays with distance from its source. Lugli and Fine (2003) demonstrated that low-frequency acoustic signals (<1 kHz) generated by a waterfall disappeared within only 2 m (because of decreasing turbulence). Similarly, Fine and Lenhardt (1983) found that low-frequency acoustic signals in water approximately 1 m deep (over a sandy bottom) attenuated rapidly, with absorption coefficients ranging from 3 to 9 dB m^{-1}. Therefore, fishes that are

able to detect sound pressure may probably detect these low-frequency sounds only from sources extremely close to them. On the other hand, the strong sound pressure levels increase in the high-frequency range (2-16 kHz), generated by streambed sediment transport, could aid in refugia location by some fish taxa. The complex soundscapes detected in this study may also be influenced by the high amount of air bubbles in the water column, which can absorb and scatter the generated sound (Urick 1983; Norton and Novarini 2001; Lurton 2002), as well as by repeated reflections at the water surface and bottom, which may degrade or alter the signal quality (Hawkins and Myrberg 1983; Urick 1983; Lurton 2002).

Conclusion

This study indicates that pools, runs, riffles, and step-pools can be clearly differentiated by their acoustic signatures, therefore supporting the first hypothesis. The average relative roughness, velocity-to-depth ratio, and Froude number were the main hydrogeomorphic variables that explained the differences in acoustic signals. However, acoustic signal differences were less clear between pools and runs because of similar average relative roughness values. Hydrogeomorphic variables such as average relative roughness showed the most pronounced effects on mid-range frequencies, while streambed sediment transport strongly increased sound pressure level in the high frequencies and the temporal sound variability of the recorded signal. Therefore, the second hypothesis could be partially supported.

Distinct underwater acoustic landscapes, so-called soundscapes, exist. Soundscape perception and interpretation are expected to be highly relevant for many freshwater organisms. In a recent study, Fay (2009) suggests the possibilitiy that fishes (and probably also other aquatic organisms like insects and crustaceans) listen to much more than simply communication signals. Therefore, physically generated underwater sound may contain important information about the environment; potentially influencing the behavior and ecology of many freshwater organisms. Hence, a major future challenge is to design experiments that will allow for testing the importance of acoustic signals in fluvial ecosystems, in particular, their role as behavioral cues. Finally, in-depth research is required to understand the linkage between fluvial mechanics and physical underwater sound generation.

Acknowledgments

We are grateful to the three anonymous reviewers for their valuable comments and suggestions that helped in improving the paper. This study was supported by the MAVA foundation, the Swiss Federal Institute of Aquatic Science and Technology (EAWAG), the Leibniz-Institute of Freshwater Ecology and Inland Fisheries (IGB), and a Marie Curie Intra-European Fellowship to V. Acuña within the 6th European Community Framework Programme. Funding for M. S. Lorang was provided by a grant from the Gordon and Betty Moore Foundation (Grant Award Letter Agreement 344.01), San Francisco, CA, USA.

References

Amoser S, Ladich F. 2005. Are hearing sensitivities of freshwater fish adapted to the ambient noise in their habitats? *Journal of Experimental Biology* 208: 3533-3542.

Beisel JN, Usseglio-Polatera P, Thomas S, Moreteau JC. 1998. Stream community structure in relation to spatial variation: the influence of mesohabitat characteristics. *Hydrobiologia* 389: 73-88.

Brooks AJ, Haeusler T, Reinfelds I, Williams S. 2005. Hydraulic microhabitats and the distribution of macroinvertebrate assemblages in riffles. *Freshwater Biology* 50: 331-344.

Fay RR, Simmons AM. 1999. The sense of hearing in fishes and amphibians. In *Comparative Hearing: Fishes and Amphibians*, Fay RR, Popper AN (eds). Springer-Verlag: New York; 269-318.

Fay RR. 2009. Soundscapes and the sense of hearing in fishes. *Integrative Zoology* 4: 26-32.

Fine ML, Lenhardt ML. 1983. Shallow-water propagation of the toadfish mating call. *Comparative Biochemistry and Physiology A* 76: 225-231.

FOEN. 2009. *Swiss Federal Office for the Environment*. Hydrological data. http://www.hydrodaten.admin.ch/e/index.htm?lang=en (last accessed 25th March 2010).

Hawkins AD. 1981. The hearing abilities of fish. In *Hearing and Sound Communication in Fishes*, Tavolga WN, Popper AN, Fay RR (eds). Springer-Verlag: New York; 109-133.

Hawkins AD, Myrberg AA. 1983. Hearing and sound communication under water. In *Bioacoustics, a Comparative Approach*, Lewis B (ed). Academic Press: London; 347-405.

Ladich F, Popper AN. 2004. Parallel evolution in fish hearing organs. In *Evolution of the Vertebrate Auditory System*, Manley GA, Popper AN, Fay RR (eds). Springer-Verlag: New York; 95-127.

Lamouroux N, Poff NL, Angermeier PL. 2002. Intercontinental convergence of stream fish community traits along geomorphic and hydraulic gradients. *Ecology* 83: 1792-1807.

Leis JM, Carson-Ewart BM, Cato DH. 2002. Sound detection in situ by the larvae of a coral-reef damselfish (*Pomacentridae*). *Marine Ecology Progress Series* 232: 259-268.

Leopold LB, Maddock T. 1953. The hydraulic geometry of stream channels and some physiographic implications. *US Geological Survey Professional Paper* 252.

Lorang MS, Hauer FR. 2003. Flow competence evaluation of streambed stability: an assessment of the technique and limitations of application. *Journal of the North American Benthological Society* 22: 475-491.

Lugli M, Fine ML. 2003. Acoustic communication in two freshwater gobies: ambient noise and short-range propagation in shallow streams. *Journal of the Acoustical Society of America* 114: 512-521.

Lugli M, Yan HY, Fine ML. 2003. Acoustic communication in two freshwater gobies: the relationship between ambient noise, hearing thresholds and sound spectrum. *Journal of Comparative Physiology A* 189: 309-320.

Lugli M, Fine ML. 2007. Stream ambient noise, spectrum and propagation of sounds in the Goby *Padogobius martensii*: sound pressure and particle velocity. *Journal of the Acoustical Society of America* 122: 2881-2892.

Lurton X. 2002. *An Introduction to Underwater Acoustic: Principles and Applications*. Springer Verlag: Chichester; 347.

Montgomery DR, Buffington JM. 1997. Channel-reach morphology in mountain drainage basins. *Geological Society of America Bulletin* 109: 596-611.

Norton MP. 1989. *Fundamentals of Noise and Vibration Analysis for Engineers*. Cambridge University Press: Cambridge; 619.

Norton GV, Novarini JC. 2001. On the relative role of sea-surface relative roughness and bubble plumes in shallow-water propagation in the low-kilohertz region. *Journal of the Acoustical Society of America* 110: 2946-2955.

Officier CB. 1958. *Introduction to the Theory of Sound Transmission*. McGraw-Hill: New York; 284.

Pastuchová Z, Lehotský M, Grešková A. 2008. Influence of morphohydraulic habitat structure on invertebrate communities (Ephemeroptera, Plecoptera and Trichoptera). *Biologia* 63: 720-729.

Popper AN, Carlson TJ. 1998. Application of sound and other stimuli to control fish behavior. *Transactions of the American Fisheries Society* 127: 673-707.

Popper AN, Fay RR, Platt C, Sand O. 2003. Sound detection mechanisms and capabilities of Teleost fishes. In *Sensory Processing in Aquatic Environments*, Collin SP, Marshall NJ (eds). Springer-Verlag: New York; 3-38.

Rickenmann D, McArdell BW. 2007. Continuous measurement of sediment transport in the Erlenbach stream using piezoelectric bedload impact sensors. *Earth Surface Processes and Landforms* 32: 1362-1378.

Rickenmann D, McArdell BW. 2008. Calibration of piezoelectric bedload impact sensors in the Pitzbach mountain stream. *Geodinamica Acta* 21: 35-51.

Rogers PH, Cox M. 1988. Underwater sound as a biological stimulus. In *Sensory Biology of Aquatic Animals*, Atema J, Fay RR, Popper AN, Tavolga WN (eds). Springer-Verlag: New York; 131-149.

Simpson SD, Meekan MG, Montgomery JC, McCauley RD, Jeff A. 2005. Homeward sound. *Science* 308: 221-221.

Simpson SD, Meekan MG, Jeffs A, Montgomery JC, McCauley RD. 2008. Settlement-stage coral reef fish prefer the higher-frequency invertebrate-generated audible component of reef noise. *Animal Behaviour* 75: 1861-1868.

Stuart TA. 1953. Spawning, migration, reproduction and young stages of loch trout (*Salmo trutta* L.). *Freshwater Salmon Fisheries Research* 5: 1-39.

Tolimieri N, Jeffs A, Montgomery JC. 2000. Ambient sound as a cue for navigation by the pelagic larvae of reef fishes. *Marine Ecology Progress Series* 207: 219-224.

Tolimieri N, Haine O, Jeffs A, McCauley R, Montgomery JC. 2004. Directional orientation of pomacentrid larvae to ambient reef sound. *Coral Reefs* 23: 184-191.

Tonolla D, Lorang MS, Heutschi K, Tockner K. 2009. A flume experiment to examine underwater sound generation by flowing water. *Aquatic Sciences* 71: 449-462.

Urick RJ. 1983. *Principles of Underwater Sound*. McGraw-Hill: New York; 423.

Vlach P, Dusek J, Svatora M, Moravec P. 2005. Fish assemblage structure, habitat and microhabitat preference of five fish species in a small stream. *Folia Zoologica* 54: 421-431.

Wohl E, Merritt DM. 2008. Reach-scale channel geometry of mountain streams. *Geomorphology* 93: 168-185.

Wolman MG. 1954. A method of sampling coarse river bed material. *Transactions of the American Geophysical Union* 35: 951-956.

Wysocki LE, Amoser S, Ladich F. 2007. Diversity in ambient noise in European freshwater habitats: noise levels, spectral profiles, and impact on fishes. *Journal of the Acoustical Society of America* 121: 2559-2566.

CHAPTER 3

Underwater soundscapes along river corridors

Abstract

Underwater acoustic signals, generated by turbulent flow, are an important information source for many aquatic organisms. In this study the patterns of underwater acoustic signals, called soundscapes, were characterized at the river segment scale. A hydrophone was mounted onto the frame of an inflatable multihull raft and held just below the water's surface while floating for 5-24 km to continuously record acoustic signals along the longitudinal axis of the main channel of five hydrogeomorphologically different river segments in Italy, Switzerland, and the United States of America. The river segments could be clearly distinguished based on sound variability and the sound pressure level of 10 octave bands (0.0315-16 kHz). Hydraulically and morphologically heterogeneous segments revealed more complex soundscapes than more homogeneous ones. Higher flow levels resulted in higher sound pressure levels over all frequency bands. The acoustic variability of single octave bands increased from base to intermediate flow, while it decreased from intermediate to bankfull flow. The pulsating sound produced by breaking and reforming turbulent waves on flow obstacles was associated with sound pressure level peaks and high acoustic variability in mid-range frequency bands (0.063-0.5 kHz), whereas high-frequency sound pressure levels (1-16 kHz) were related to particle collisions during streambed sediment transport. Underwater soundscapes provide an independent measure of habitat delineation that can be applied to river corridors at the segment scale. This study has many applications from theoretical systems ecology to the monitoring of river restoration projects.

Introduction

Underwater acoustic signals in rivers are generated by turbulent flow and the nature by which air is trapped and released in the water. Hence, rapids have a different soundscape (i.e. acoustic signature) than that produced by riffles and both are distinctly different in the acoustic signature from runs and pools (Tonolla et al. 2010). Indeed, acoustic signatures provide a greater level of discrimination between aquatic habitat types than can be achieved through traditional measures of flow characteristics and morphological properties (Amoser and Ladich 2010; Tonolla et al. 2010). Underwater acoustic signals are most likely an important information source for many aquatic organisms, as most of them are able to use acoustic cues in their environment for spatial orientation and positioning within suitable habitats (Slabbekoorn and Bouton 2008; Stanley et al. 2010; Vermeij et al. 2010). Moreover, in a recent review, Fay (2009) suggested that soundscapes act as "acoustic daylight" for some fishes providing important information equal in importance to the visual assessment of their immediate surroundings.

The acoustic signatures of different freshwater ecosystems such as streams, rivers and lakes, each considered as large composite environments, have been found to vary in their spectral characteristics and sound pressure levels (Amoser and Ladich 2005; Wysocki et al. 2007; Amoser and Ladich 2010). Similarly, laboratory flume studies of various turbulent patches were also shown to produce distinct acoustic patterns (Tonolla et al. 2009). Amoser and Ladich (2010) attributed seasonal changes in the acoustic signature (sound pressure levels and spectral composition) of seven freshwater fish habitats mainly to differences in substrate types and transport, discharge and flow velocities. Moreover, Tonolla et al. (2010) showed that average relative roughness and streambed sediment transport were mainly responsible for sound generation (sound pressure levels and temporal sound variability) in the selected river habitats (pools, runs, riffles, step-pools). Thus, spatial position and complex variations in these key factors are expected to influence the composition at the source location and the radiation of acoustic signals along the longitudinal gradient of a river corridor. Furthermore, the physical structure of rivers changes across spatial and temporal scales (Thorp et al. 2006). Therefore, assessing the physical template of structural heterogeneity and process-based complexity, from small spatial scales to entire river systems, is necessary for advancing our understanding of river ecosystems (Fausch et al. 2002; Wiens 2002; Tockner et al. 2010). Thus, habitat heterogeneity and the dynamic nature of river flow create a complex network of soundscapes, which might have important implications for the distribution and behavior of

freshwater organisms. Hence, it would be valuable to examine how the complexity and arrangement of the energy gradients coupled with the nature and degree of flow obstruction (e.g. bedrock, boulders, bars, and large wood) coupled with channel form and sediment availability, and caliber and source along the river corridor affect soundscapes. The ability to measure and differentiate soundscapes provides a new, yet underexplored view of river ecosystems.

The goal of this study was to analyze underwater acoustics at the river segment scale. First, the soundscapes of five hydrogeomorphologically different river segments (5-24 km long), recorded at intermediate flow conditions, were quantified. Second, the effect of increasing flow level on the soundscape of two of the five river segments was assessed. Specifically, we expected that (i) the different river segments would be acoustically distinguishable by sound pressure level and sound variability, and (ii) that an increase in flow level would influence the acoustic variability and the sound pressure level of distinct octave bands depending on specific hydrogeomorphic characteristics of the segments.

Materials and methods

Acoustic recordings were conducted during the summers of 2007 and 2009 along five hydrogeomorphologically different rivers in Switzerland, Italy and the United States of America. The river segments were viewed as a sequence of alternating aquatic habitats (e.g. glides, runs, riffles, rapids). Generally, these habitat types and their downstream sequence (e.g. riffle-pools) differ in their hydraulic (e.g. flow depth, flow velocity), and geomorphic (e.g. slope, sediment size, bed roughness) conditions (Montgomery and Buffington 1997; Thompson et al. 2006; Wohl and Merritt 2008). In this study, river segment selection was based on three criteria: (i) the degree of channel constraint, (ii) the overall slope, and (iii) the supply and caliber of sediment. The aim was to sample a range of river types from braided and anastomosing gravel bed rivers to rivers confined by bedrock or man-made constraints.

Study river segments

The Thur River (henceforth, Thur) was constrained and stabilized by stone rip-rap as early as the 1890s. The 13-km segment consisted of a straight low-turbulent run with a few gravel point bars (mainly located between segment-km 5 and 8) and some turbulent habitats such as riffles and rapids (Figure 1, Tables 1, 2).

Figure 1. Oblique photographs of a typical section of the five river segments at intermediate flow. Arrows indicate flow direction. All photographs, except of Thur, by D. Tonolla.

The 24-km segment of the gravel-bed North Fork of the Flathead River (henceforth, North Fork) had a bedrock-constrained channel with limited alluviation for most of its length. An approximately 3-km-steep section of a semi-constrained alluviating valley was at the head of the segment, in addition to a downstream, less steep 5-km alluvial deposition section. The local sediment supply was from eroding paleoriver deposits. The segment consisted of many large rapids characterized by meter-high standing waves and large turbulent boils connected to smaller rapid-run-glide sequences and a few sand-gravel banks (Figure 1, Tables 1, 2).

Table 1. Description of the river-catchments. The Middle Fork catchment encompasses the river segments Nyack and Middle Fork (see text).

Characteristic	Thur	North Fork	Tagliamento	Middle Fork
Area (km^2)	1,700	4,010 (1,560 in Canada)	2,580	2,920
Strahler's order	7	5	7	5
Main river length (km)	130	140	170	150
Average catchment elevation (m asl)	770	NA	1.200	NA
Source elevation (m asl)	900	1,970	987	1,650
Hydrological regime	pa/a	n	p-n	n
Location	NE Switzerland	SE Canada and NW Montana	NE Italy	NW Montana

pa/a: pre-alpine/alpine with high summer precipitation; n: nival, snow dominated; p-n: flashy pluvio-nival; NA: not applicable.

The 8-km segment along the Tagliamento River (henceforth, Tagliamento) was located in an island-braided gravel-bed river floodplain (max. active width ~800 m; Tockner et al. 2003). The main channel mostly consisted of a long turbulent run broken by a few shallow rapids and a large amount of a lateral supply of sediment (Figure 1, Tables 1, 2).

Two morphologically different segments of the Middle Fork of the Flathead River were investigated. The first 12-km segment (henceforth, Nyack) was located in the anastomosing alluvial Nyack floodplain (active width up to 500 m). The main channel of the Nyack consisted of a series of sequentially linked small rapids and runs and a lateral supply of sediment (Figure 1, Tables 1, 2). The second 5-km segment investigated (henceforth, Middle Fork), was heavily bedrock constrained, had a steep slope, and no lateral supply of sediment. This segment consisted of many linked (class II-IV) whitewater rapid-run-glide sequences and a few sand-gravel banks (Figure 1, Tables 1, 2).

Table 2. Characterization of the river segments. *Q*: daily average discharge at the nearest gauging station; *u*: flow velocity (mean ± standard deviation); *h*: flow depth (mean ± standard deviation).

Characteristic	Intermediate flow					Base flow	Bankfull flow
	Thur	North Fork	Tagliamento	Nyack	Middle Fork	North Fork	Nyack
Date of recording	13 July 2007	30 June 2009	16 June 2007	29 June 2009	29 June 2009	24 August 2007	28 May 2009
Start / end Latitude (decimal degree)	47.58904 / 47.58854	48.60201 / 48.47048	46.21687 / 46.17961	48.42525 / 48.49116	48.49683 / 48.49867	48.60201 / 48.47048	48.42525 / 48.49116
Start / end Longitude (decimal degree)	8.94729 / 8.78304	-114.16109 / -114.07361	13.01836 / 12.95901	-113.77469 / -113.85826	-113.91723 / -113.96518	-114.16109 / -114.07361	-113.77469 / -113.85826
Length (km)[A]	13 (C)	24 (C)	8 (U)	12 (U)	5 (C)	24 (C)	12 (U)
Average elevation (m asl)	380	990	150	1020	980	990	1020
Average slope (m m^{-1})	0.002	0.004	0.003	0.003	0.005	0.004	0.003
Q (m^3 s^{-1})	55.4[B]	141.9[C]	29.0[D]	162.3[E]	162.3[E]	24.6[C]	447.4 [E]
u (m s^{-1})	1.5 ± 0.3	1.7 ± 0.8	2.2 ± 0.6	1.7 ± 0.5	2.0 ± 0.6	0.7 ± 0.5	2.6 ± 0.4
h (m)	1.1 ± 0.2	1.9 ± 1.0	1.3 ± 0.5	1.4 ± 0.5	3.2 ± 1.4	1.4 ± 1.1	2.1 ± 0.7
Sediment supply[F]	1	1	3	2	1	1	3
Roughness[F]	1	2	1	1	3	2	1

[A] In bracket valley form, U: unconstrained, C: constrained; [B] Average annual discharge for the year 2007 at the nearest gauging station was 45.5 m^3 s^{-1}. Discharge data from the Swiss Federal Office for the Environment, hydrological data, site number: 2044, http://www.hydrodaten.admin.ch/e/index.htm?lang=en; [C] Average annual discharges for the years 2007 and 2009 at the nearest gauging station were 84.0 and 65.2 m^3 s^{-1}, respectively. Discharge data from the US geological survey, surface-water data for the Nation, site number: 12355500, http://waterdata.usgs.gov/nwis/sw; [D] Average annual discharge for the year 2007 at the nearest gauging station was 25 m^3 s^{-1} (dry year). Stage data from the "Ufficio Idrografico", Udine, Italy; the discharge was evaluated by a flow rating curve at the Venzone hydrometric station, roughly estimated from the cross-section geometry, similar as in Bertoldi et al. (2009); [E] Average annual discharge for the year 2009 at the nearest gauging station was 67.6 m^3 s^{-1}. Discharge data from the US geological survey, surface-water data for the nation, site number: 12358500, http://waterdata.usgs.gov/nwis/sw; [F] Sediment supply and roughness (as variable for turbulence generation) were given values from an ordinal scale of 1 to 3, where 1: no-few, 2: moderate, and 3: strong sediment supply, and roughness, respectively (based on observations).

Data recording

Hydraulic flow conditions and acoustic signals were continuously collected while floating on an inflatable multihull cat-raft during intermediate flow conditions for 5-24 km along the downstream axis of the main channel of each of the five river segments. In order to determine the influence of increasing flow on the underwater soundscape, two segments (North Fork and Nyack) were again floated along during a different flow stage (Table 2). The acoustic signals were recorded by a hydrophone (type 8103, Brüel and Kjaer, Denmark) secured on a small metal rod (~40 cm length), mounted on the frame of the raft and positioned between the hulls just below the surface of the water (~30 cm) with the head facing upstream. An amplifier (type Nexus 2692 OS2, Brüel and Kjaer, Denmark) was used to amplify the signal generated by the hydrophone. Amplifier sensitivity was set to 3.16 mV Pa^{-1}, which provided good sensitivity to the acoustic instruments while minimizing overload in loud sections of the rivers (e.g. rapids). Acoustic signals were stored on a 16-bit digital recorder (type R-4, Edirol, Japan) with a sampling frequency of 44.1 kHz. This setting assured a frequency range between 0.02 and 20 kHz and a dynamic range >90 dB.

Velocity profiles and flow depths were simultaneously recorded using a 3 MHz Acoustic Doppler Current-Profiler (ADP: type RS3000, SonTek/YSI, CA, USA) and were used for a general hydraulic characterization of the five river segments (Table 2). Velocity measurements were collected within 15 cm depth bins at a nominal sampling rate of 5 seconds.

Acoustic data analysis

The recorded acoustic signals were analyzed using a signal-processing software written and optimized by K. Heutschi. The software evaluated the time-series of the hydrophone signal by using a 16,384 point Fast Fourier Transformation (FFT) that spectrally decomposed the time-series on a frame-by-frame basis into the frequency content. Three FFT frames were averaged at a time and evaluated in regard to the power spectral density. Finally, the signal power in the 10 octave bands (from 0.0315 to 16 kHz) was obtained by summing up the corresponding frequency lines and was used for further analysis. The reason for choosing octave bands instead of third-octave bands was because of the reduction of uncertainty due to the stochastic characteristic of the signal, thus, reducing a potential source of noise in the recordings. In order to reach a certain degree of confidence, the product of the parameters “analysis bandwidth” and “averaging time” had to be chosen appropriately. The length of the acoustic recording of each segment varied depending on the segment length and flow velocity.

Therefore, even though the temporal resolution of ~1.11 seconds (three FFT frames) was the same for each acoustic analysis, the sample size varied between segments ranging from n = 1,993 (Middle Fork) to n = 22,248 (North Fork at base flow) for each single octave band.

Calibration of the acoustic setting was performed by a Brüel and Kjaer calibrator (type 4223, Brüel and Kjaer, Denmark), which generates a highly reproducible nominal sound pressure level of 166 dB at 0.25 kHz, thus allowing the attribution of absolute sound pressure levels for each of the recordings. All sound pressure levels in this study are expressed on a logarithmic scale as dB values relative to 1 micro Pascal (dB re 1 μPa) as a reference.

Reduction of sources of uncertainty (noise)

The hydrophone, cable, and metal rod suspended in the water column, and their potential vibrations and turbulence generation, created a potential source of noise in the recordings. Moreover, short energy peaks generated by squeaking sounds of the raft, as well as unwanted noise produced by water bubbles and turbulence generated from the moving raft or from paddling (kept to a minimum during recording) may have affected the recorded signal. It has been shown that water breaking the surface and entraining air mainly influences sound pressure levels in the mid-frequency range (0.125-2 kHz; Lugli and Fine 2003; Tonolla et al. 2009, 2010). Some preliminary analyses of the original data set of this study showed that sound pressure level increases in the 1 kHz octave band significantly correlated with sounds caused by water breaking the surface and entraining air produced by the raft, whereas the correlation with similar sounds produced by the river (e.g. in high turbulent sections) was weak. In order to reduce the unwanted noise produced while floating and to increase the reliability of the recorded data, acoustic data over the whole acoustic range were removed if there was a step of more than 20 dB from one second to the next in the 1 kHz octave band. Furthermore, the use of octave bands instead of third-octave bands resulted in the reduction of the spectral resolution, thus significantly lowering the uncertainty. Finally, noise generated from the moving raft contributed little to the total energy (sound) produced by the river and may have only affected the recording in the quietest sections and only for short periods.

Quantification and characterization of the acoustic patterns

In order to facilitate the quantification and characterization of the underwater acoustic patterns recorded over many kilometers, a multiple-level analytical process based on visual comparisons, spatial analysis, and standard acoustic analyses was applied. Visual comparisons were applied to determine segment-long variations in sound patterns. Consequently, the acoustic signal of each river segment was plotted as a three-dimensional

graphical image (henceforth, soundscape image) that included the time period in which the sample was taken (converted to downstream distance in km; *y*-axis), frequency classes (10 octave bands in kHz; *x*-axis) and sound pressure levels (in dB re 1 µPa; *z*-axis).

Spatial indices were computed for each soundscape providing supportive indicators for the standardized comparison and interpretation of the acoustic patterns observed in the soundscape images. First, each soundscape image was converted to a raster image, with each pixel containing the corresponding sound pressure level value. The number of different sound pressure level values in each raster was used as an indicator of the amount of different sounds occurring in the soundscape. Second, two spatially explicit indices were selected and calculated: (i) an area-related index (patch density, PD) and (ii) a diversity-related index (Shannon's diversity index, SHDI). These indices provided quantitative spatial-structural information on the arrangement of acoustic signals in the soundscape. In this study, each patch was the aggregation of neighbor polygons sharing the same sound pressure level (on a 1 dB interval). The PD equaled the number of patches in the soundscape divided by the total soundscape area providing a measure of the soundscape configuration. High PD values indicate acoustic structural richness (spatial heterogeneity of sound pressure levels). The SHDI provided a measure of relative patch diversity in a soundscape, which is determined by both the number of different patch types and the proportional distribution of the area between patch types and was calculated as $-\sum_{i=1}^{k} p_i \ln p_i$ where p_i is the proportion of patch types i in the total soundscape area and k is the number of patch types. High SHDI values indicate high acoustic variability (heterogeneity) of the soundscape. These indices were originally designed to quantify landscape patterns in a variety of ecological studies, but they can also be used to characterize the composition and structure of acoustic landscapes (e.g. Mazaris et al. 2009). The selected indices were implemented in the ArcGIS extension vector-based landscape analysis tool V-LATE 1.1 (for further information see Lang and Tiede 2003; Lang and Langanke 2005; Langanke et al. 2005) and calculated within ArcGIS 9.2 (ESRI, Redlands, USA) The vector entities (polygons) considered by V-LATE represent the soundscape patches (or classes).

Traditional acoustic analyses were used to assess the amount of acoustic information and its distribution in each of the frequency classes (10 octave bands) and over the whole frequency range, in each of the river segments. Four acoustic variables were calculated over the entire sample size: (i) the average signal power in each octave band (henceforth, energetic mean), (ii) the variance, as spatial variability of the acoustic signal, of each octave band

(henceforth, variance), (iii) the average signal power, and (iv) the variance of the broadband signal over the whole frequency range (henceforth, broadband mean value and broadband mean variance, respectively). Given that variance is influenced by the sample size (n), and since this showed a strong variation between the five river segments, standardization of the variance values was necessary for comparisons. Thus, the 1,993 data points (the smallest n of a single octave band of the five segments) from each segment were randomly selected to calculate standardized variances.

All images were generated using the scientific graphing and analysis software package SigmaPlot (version 10.0, Systat Software Inc., CA, USA).

Statistical analysis

Statistical analyses were performed to test whether or not the acoustic patterns observed in the different soundscape images were the result of random changes. A Kruskal-Wallis one-way analysis of variance by rank (H-test) was performed on all raw acoustic measurements (one data point of sound pressure level every ~1.11 seconds; over the entire segment length) of each octave band (test variables) to test for differences in the median sound pressure level between the five river segments collected at intermediate flow (grouping variable). Subsequently, a Mann-Whitney (U-test) one-way analysis of variance by rank with the Bonferroni correction was performed for each pair-wise comparison to test for specific differences between segments. Additionally, separate Mann-Whitney tests were performed on the raw acoustic measurements of each octave band to test for differences in the median sound pressure level between segments collected at different flow levels.

Spearman's rank correlation analyses were used to identify the direction and strength of relationships between a broad range of hydrogeomorphic (average slope, discharge, average flow velocity, average flow depth, sediment supply, roughness) (Table 2) and acoustic (energetic mean, variance, broadband mean value, broadband mean variance, PD and SHDI) variables. All tests were performed using SPSS (version 14.0, SPSS Inc., Chicago, USA).

Results

River soundscapes at intermediate flow

At intermediate flow, the five river segments exhibited distinct soundscapes owing to segment-long variations in sound pressure level and sound variability (Figure 2).

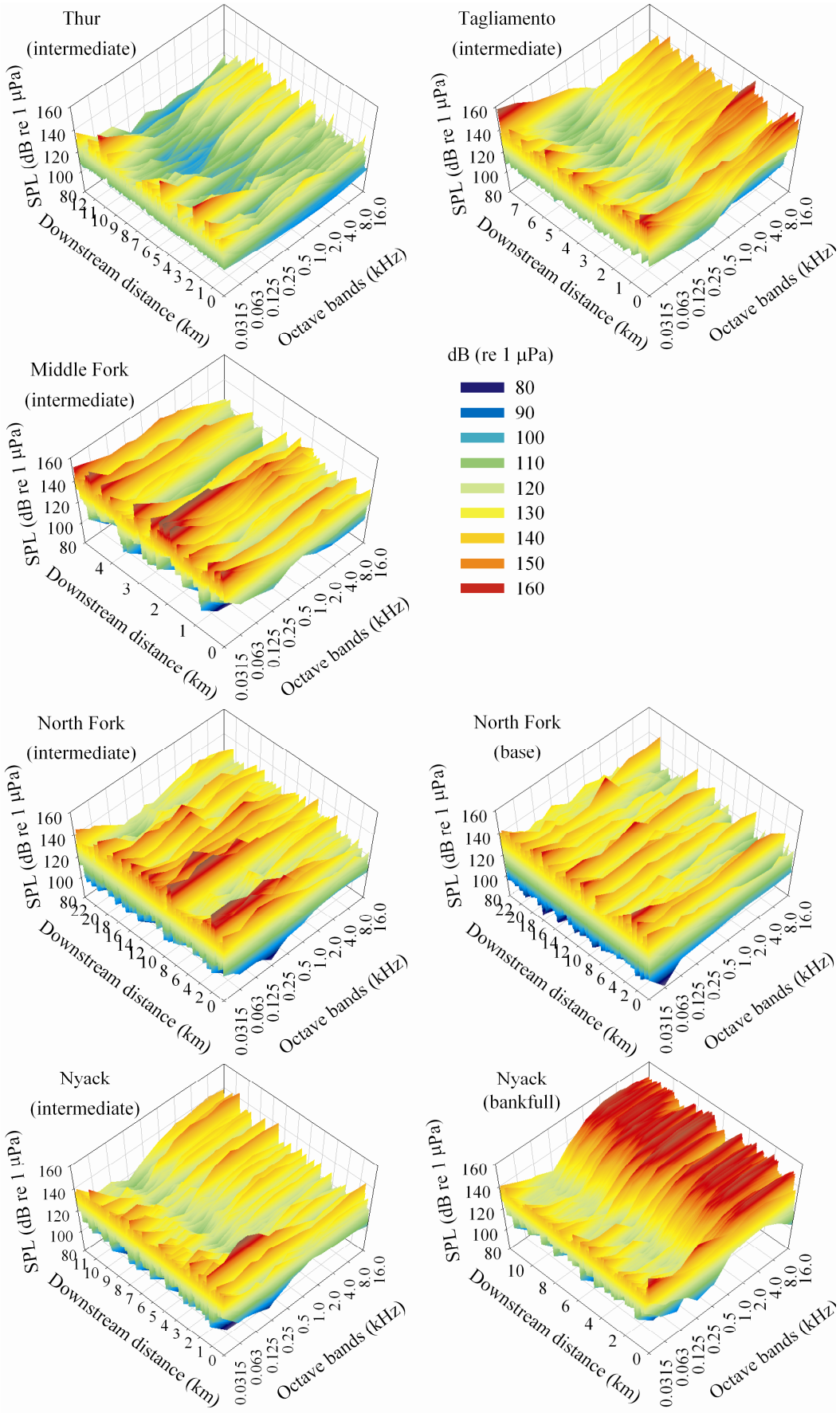

Figure 2. Soundscape images of the five river segments. *X*-axis: frequency classes (10 octave bands) in kHz; *y*-axis: downstream distance in km; *z*-axis: sound pressure level (SPL) expressed in decibels (dB re 1 µPa). Flow type in brackets.

The single characteristic common to all soundscapes were high sound pressure levels in the low-frequency range (0.0315 kHz) (Figures 2, 3). The broadband mean value differed by up to 20 dB between the soundscapes, and the difference in the energetic mean of single octave bands was up to 40 dB between soundscapes (e.g. the difference between Thur 0.5 kHz and Middle Fork 0.125 kHz) (Figure 3).

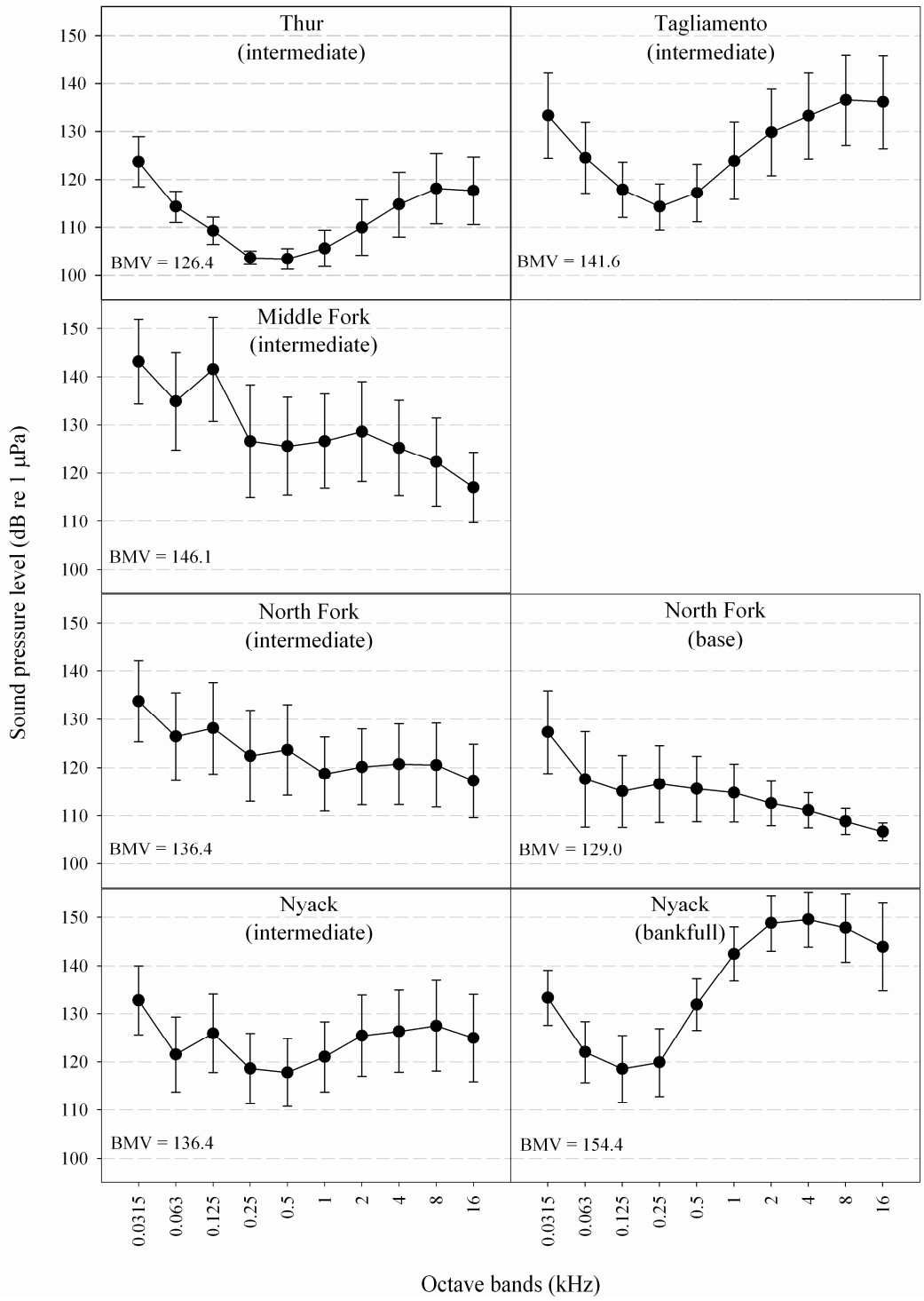

Figure 3. Sound pressure levels (energetic mean ± standard deviation) of 10 octave bands in the five river segments. Flow type in brackets. Broadband mean values (BMV) representing the average signal power of the broadband signal are indicated.

The Thur had the lowest broadband mean value and exhibited by far the most homogeneous soundscape over all octave bands (Figure 2, Table 3). Furthermore, the acoustic homogeneity of the Thur soundscape was confirmed by the lowest patch density and Shannon's diversity (Table 4), as well as by the smallest range of different sound pressure level values (Figure 4).

Table 3. Spatial variability of the acoustic signal (variance, standardized to n = 1,993) in the five river segments.

Octave band (kHz)	Intermediate flow					Base flow	Bankfull flow
	Thur	North Fork	Tagliamento	Nyack	Middle Fork	North Fork	Nyack
0.0315	29.1	71.4	78.2	55.5	78.1	71.7	32.8
0.063	11.0	83.5	55.1	65.2	102.5	93.2	39.7
0.125	8.2	88.1	33.0	70.8	117.7	52.3	47.8
0.25	2.1	87.1	23.0	54.9	136.5	60.5	49.7
0.5	5.2	86.2	34.8	52.1	102.8	44.1	28.4
1	14.7	58.0	65.3	54.6	95.5	34.5	31.7
2	32.1	61.1	80.7	71.1	108.0	19.3	33.8
4	43.9	70.6	78.2	73.5	97.2	11.6	33.1
8	51.3	75.5	86.8	90.2	84.1	5.9	51.0
16	47.2	56.7	95.2	84.5	53.5	2.4	84.8
BMVar	27.1	47.1	41.5	43.8	68.8	46.4	27.6

BMVar: Broadband mean variance.

The other four river segments exhibited a similarly high acoustic heterogeneity (Table 4) with a large range of different sound pressure level values (Figure 4). The soundscapes of the Tagliamento and Nyack (unconstrained floodplain segments) were characterized by a bimodal sound distribution with sound pressure level peaks at 1-16 kHz and 0.0315 kHz, respectively, and a distinct sound pressure level depression at mid-range frequencies (Figures 2, 3). Except for the octave band 0.0315 kHz, the two octave bands with the highest energetic means were 8 and 16 kHz and 4 and 8 kHz in the Tagliamento and Nyack, respectively (Figure 3). The broadband mean value was slightly higher in the Tagliamento than in the Nyack (Figure 3), whereas the broadband mean variance did not differ (Table 3). In the Nyack, the energetic mean peaked at 0.125 kHz as the result of very high sound pressure levels at a single location (at an approximate distance of 2.8 km downstream; Figure 2) coinciding with the location of a set of artificially added large boulders that produced a distinct zone of turbulence similar in nature to a hydraulic jump. In contrast, the North Fork and Middle Fork bedrock-constrained canyon segments exhibited many sound pressure level peaks in the mid-range octave bands (Figure 2) with a maximum sound pressure level at 0.125 kHz (Figure 3). The North Fork

exhibited an additional energetic peak at 0.5 kHz (Figure 3). Maximum variance values occurred in both segments at mid-range frequencies (Table 3). The Middle Fork showed by far the highest broadband mean value and the highest broadband mean variance (Figure 3, Table 3).

Significant differences were found in the median sound pressure level of all octave bands between the five river segments, collected during intermediate flow conditions (Kruskal-Wallis: $p < 0.001$). Furthermore, pair-wise comparison tests revealed that all river segments exhibited significantly different sound pressure levels over all octave bands (Mann-Whitney: $p < 0.001$; critical Bonferroni-corrected alpha: 0.005), except for the sound pressure level of the octave band 0.125 kHz between the North Fork and Nyack segments ($p = 0.769$) and for the sound pressure levels of the octave bands 8 and 16 kHz between the North Fork and Middle Fork segments ($p = 0.297$ and $p = 0.05$, respectively).

Effect of flow level on the river soundscapes

The effect of increasing flow level on the soundscape of two out of five river segments was assessed. An increase from base to intermediate flow in the North Fork resulted in a general increase in both sound pressure level and acoustic spatial heterogeneity (Figure 2, Tables 3, 4).

Table 4. Spatial indices for the quantitative characterization of the arrangement of acoustic signals in the five river segments.

Spatial index	Intermediate flow					Base flow	Bankfull flow
	Thur	North Fork	Tagliamento	Nyack	Middle Fork	North Fork	Nyack
Patch density (No. m^{-2})	0.62	0.79	0.71	0.80	0.82	0.55	0.72
Shannon's diversity	3.13	3.74	3.77	3.75	3.88	3.20	3.93

No.: total number of patches.

An energetic mean increase of up to 13 dB was detected in the octave band 0.125 kHz (Figure 3). The two distinct sound pressure level peaks (0.125 and 0.5 kHz) found at intermediate flow disappeared at base flow (Figure 3). The acoustic signal at base flow was mainly dominated by sound pressure levels of around 103 dB, whereas at intermediate flow a wider distribution of the sound pressure levels was detected (Figure 4).

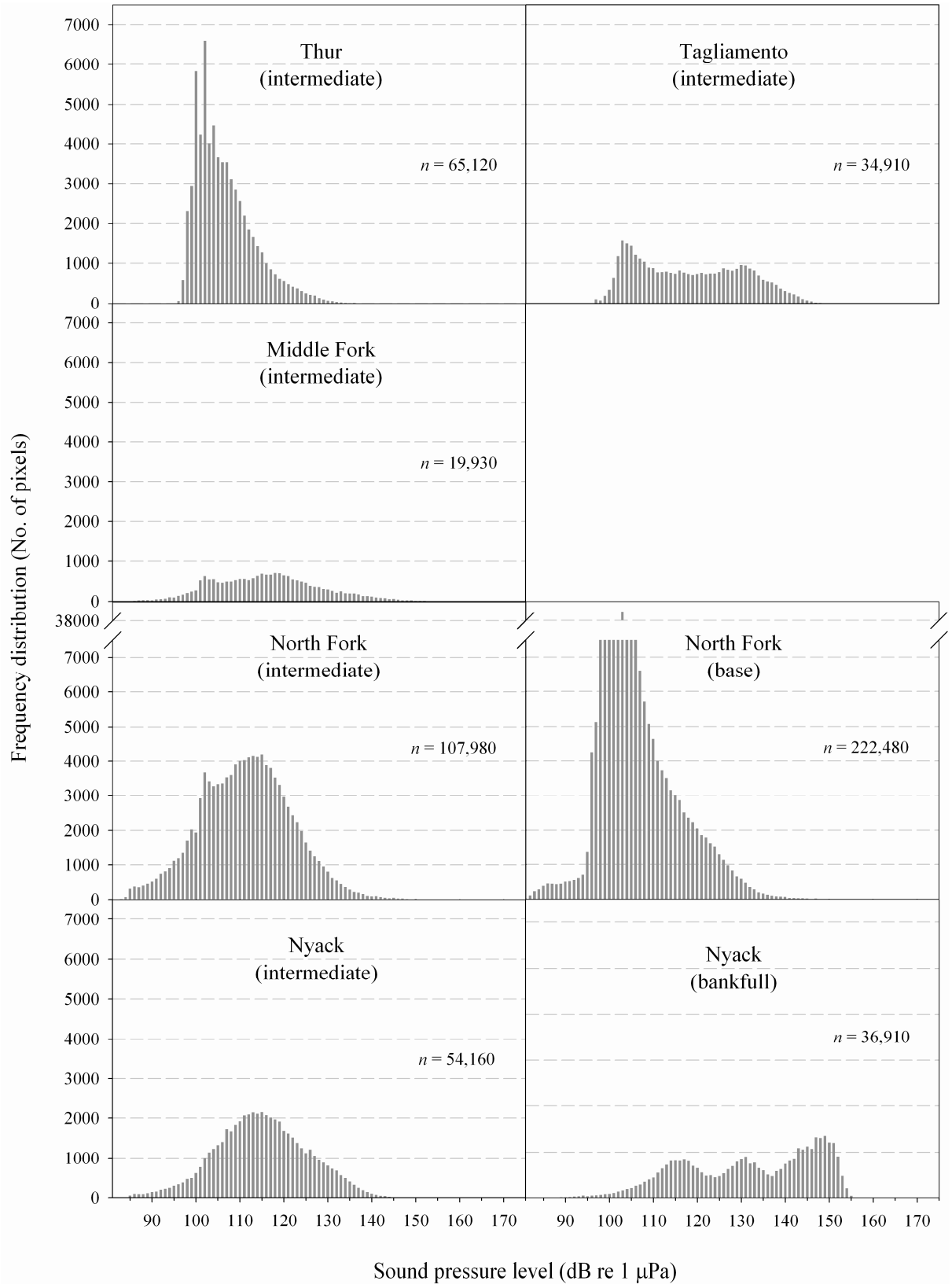

Figure 4. Frequency distribution of the sound pressure level pixels in the five river segments. Flow type in brackets. *n*: total number of pixels.

An increase from intermediate to bankfull flow in the Nyack resulted in a general increase in sound pressure levels, a decrease in sound variability of single octave bands (maximal at 2-8 kHz) and in the broadband mean variance (Figure 2, Table 3). The broadband mean value increased by 18 dB, with increases of >20 dB in the high-frequency range of 1-8 kHz (Figure 3). The mid-frequency range depression typical at intermediate flow persisted with increasing flow level. At bankfull flow, the acoustic signal was dominated by sound pressure levels of around 117 dB, 129 dB and 149 dB, whereas at intermediate flow a wider distribution of sound pressure levels was detected (Figure 4). Furthermore, the two octave bands with the highest energetic mean shifted from 4 and 8 kHz at intermediate flow to 2 and 4 kHz at bankfull flow (0.0315 kHz at intermediate flow was not considered) (Figure 3).

Pair-wise comparison tests revealed that the sound pressure levels of all octave bands were significantly different between flow levels (Mann-Whitney: $p < 0.001$).

Relationship between acoustic and hydro-geomorphological variables

River segment slope and roughness were strongly correlated with the variance of octave bands from 0.063 to 0.5 kHz and the broadband mean variance (Table 5). Flow velocity and sediment supply significantly influenced the high-frequency (1-16 kHz) energetic means and the variance of 16 kHz. Flow velocity was also strongly correlated with the broadband mean value and the Shannon's diversity index (Table 5). Flow depth was a good predictor of the low to mid-frequency (0.0315-0.5 kHz) energetic means and variances (Table 5).

Table 5. Spearman's rank correlation (*r*) between hydrogeomorphic and acoustical variables. BMV: broadband mean value; BMVar: broadband mean variance; PD: patch density; SHDI: Shannon's diversity. $n = 7$ (five at intermediate flow + two at different flow levels, North Fork and Nyack; Table 2).

		Average segment slope (*r*)	Daily average discharge (*r*)	Average flow velocity (*r*)	Average flow depth (*r*)	Sediment supply (*r*)	Roughness (*r*)
Energetic mean of each octave band (kHz)	0.0315	0.67	0.54	0.63	0.85*	0.06	0.54
	0.063	0.67	0.36	0.59	0.70	0.06	0.54
	0.125	0.67	0.61	0.41	0.81*	-0.06	0.54
	0.25	0.77*	0.63	0.36	0.95**	-0.16	0.66
	0.5	0.43	0.83*	0.74	0.90**	0.32	0.24
	1	0.24	0.68	0.92**	0.68	0.64	0.00
	2	0.09	0.56	0.95**	0.50	0.80*	-0.18
	4	-0.22	0.63	0.94**	0.29	0.90**	-0.48
	8	-0.22	0.63	0.94**	0.29	0.90**	-0.48
	16	-0.67	0.45	0.72	-0.14	0.90**	-0.84*
Variance of each octave band (kHz)	0.0315	0.62	-0.38	0.20	0.18	0.06	0.48
	0.063	0.95**	-0.09	-0.20	0.58	-0.48	0.90**
	0.125	0.86*	0.36	0.02	0.77*	-0.38	0.78*
	0.25	0.95**	0.20	-0.07	0.77*	-0.48	0.90**
	0.5	0.86*	0.18	-0.02	0.63	-0.38	0.78*
	1	0.67	0.02	0.34	0.41	0.00	0.54
	2	0.32	0.36	0.59	0.36	0.26	0.18
	4	0.24	0.22	0.41	0.18	0.10	0.18
	8	-0.06	0.22	0.31	-0.07	0.30	-0.18
	16	-0.28	0.40	0.85*	0.07	0.90**	-0.54
	BMV	0.24	0.68	0.92**	0.68	0.64	0.00
	BMVar	0.95**	0.02	-0.11	0.63	-0.48	0.90**
	PD	0.41	0.74	0.45	0.67	0.04	0.30
	SHDI	0.24	0.68	0.92**	0.68	0.64	0.00

* $p < 0.05$; ** $p < 0.01$.

Discussion

In the present study, we characterized the soundscape complexity of kilometer-long river segments. These river segments could be clearly acoustically separated based on the sound pressure level and the spatial variability of the acoustic signal. Acoustically, three stream types were distinguished: (i) the artificially channelized Thur, (ii) the unconstrained floodplains along the Tagliamento and Nyack, and (iii) the two bedrock-constrained segments of North Fork and Middle Fork. With increasing flow level and flow velocity, the pressure levels of the entire soundscape increased while the acoustic variability of single octave bands decreased (with a maximum at 2-8 kHz) from intermediate to bankfull flow, whereas it generally increased from base to intermediate flow, depending on the hydrogeomorphic

characteristics of the segments. This work provides first insights into the questions of which factors contribute to the origins and propagation of underwater ambient sound in river segments. This is an interesting area, with potentially broad impacts on the ecological studies of sound-sensitive organisms in this environment.

River soundscapes at intermediate flow

Acoustic signals travel about five times faster in water compared to air and exhibit a lower attenuation rate compared to light and chemical substances (Hawkins and Myrberg 1983; Rogers and Cox 1988), thereby providing a very effective dispersal of information about the environment. As an acoustic signal travels in flowing water it can be reflected and scattered at the bottom, at the surface, and at flow obstructions, as well as from air bubbles in the water column (Hawkins and Myrberg 1983; Urick 1983; Lurton 2002). It can also be modified by multiple sound sources, constrained or transmitted well with minimal distortion. Furthermore, sound at frequencies below the cutoff frequency (Officer 1958; Urick 1983; Rogers and Cox 1988) is rapidly attenuated (Fine and Lenhardt 1983; Lugli and Fine 2003, 2007). With respect to the cutoff theory, sound propagation is constrained by the flow depth and the nature of the bottom material; thus wavelengths can not propagate as acoustic waves in water shallower than about a quarter of the wavelength over a rigid bottom (Officer 1958; Urick 1983; Rogers and Cox 1988). Therefore, in shallow water habitats (e.g. riffles), the generation and propagation of low-frequency sounds may be subjected to a local constraining phenomenon. All of these interactions and constraints might generate complex soundscapes at different scales. For example, complex acoustic patterns with distinct pressure levels and acoustic variability have been detected at the centimeter scale along a simple flume course by placing a set of bricks that created flow obstructions (Tonolla et al. 2009). Furthermore, complex soundscapes at the meter scale were found in pools, runs, and riffles (Tonolla et al. 2010), as well as in aggregated freshwater ecosystems such as streams, rivers and lakes (Wysocki et al. 2007; Amoser and Ladich 2010).

In this study, acoustic signals were recorded at a scale of several kilometers, and typically at flow depths of >1 m. At intermediate flow, the five river segments exhibited distinct soundscapes due to different hydrogeomorphic characteristics. Specifically, the amount of available sediments, in combination with a high flow velocity, as well as the relative roughness and flow obstructions, were most likely the main factors influencing the acoustic signals. Similarly, Wysocki et al. (2007) and Amoser and Ladich (2010) suggested that acoustic signatures were determined by discharge, flow velocity, and type and transport of bed sediments. Furthermore, Tonolla et al. (2009, 2010) showed that underwater sound is

mainly generated by turbulence and air bubbles resulting from the interaction of flow velocity, relative roughness, flow obstructions, and streambed sediment transport. The typical low-frequency (0.0315 kHz) sound peaks, also found by Lugli and Fine (2003), Wysocki et al. (2007) and Tonolla et al. (2010), originating from large-scale turbulent flow are obviously a distinct component of most aquatic habitats (e.g. riffles, rapids, runs, pools, backwaters, lakes).

The Thur, with its low streambed heterogeneity and overall lack of sediment supply and transport, exhibited the most homogeneous soundscape, demonstrating that channelization not only reduces hydrogeomorphic dynamics and related ecological processes but that it also affects acoustic composition and heterogeneity. Highly complex and variable soundscapes were found in more natural river segments. In the unconstrained Tagliamento and Nyack, the unconsolidated channel banks were a major source of sediments (see Figure 1). The collision between sediment particles in transport and those on the river bed generated a sharp increase of high-frequency sound pressure levels (1-16 kHz). These sounds were audible to the human ear during the collection of data from the raft. Similarly, Tonolla et al. (2010) found that streambed sediment transport was responsible for the increases in high-frequency sound pressure levels (2-16 kHz) and acoustic variability in runs. During stationary recording, these high-frequency acoustic signals remained continuous over the entire recording period (Tonolla et al. 2010).

Along river segments, the non-uniformity in morphology, hydraulics, and intensity of streambed sediment transport truncated these signals. For example, in slow-flowing sections (e.g. glides), sediment particles might be deposited on the river bed, thus resulting in lower high-frequency sound pressure levels (e.g. the first kilometers of the Nyack; Figure 2). Moreover, the Tagliamento differed from the Nyack by a more even distribution of high-frequency sound pressure levels and a higher average signal power and variance of the broadband signal. This can be attributed to the higher energy gradient along the entire Tagliamento (higher flow velocity; Table 2), which, in turn, produced continuous flow competent conditions suitable for the sediment particles composing the bed along the entire segment. Furthermore, the sediment particles were finer in the Tagliamento than in the Nyack, thus less energy was necessary to put the particles into motion. Interestingly, this differentiation of finer and coarser sediments was reflected in the frequency distribution of the highest sound pressure levels, with the Nyack showing the highest energetic means at lower frequencies (4-8 kHz), probably generated by coarser particle collisions, as compared to the Tagliamento (8-16 kHz).

The two bedrock-constrained river segments North Fork and Middle Fork also exhibited a complex acoustic mosaic, although heterogeneity was mainly controlled by the many linked sequences of high-turbulent (rapids) and low-turbulent (glides, runs) sections (see Figure 1). Accordingly, these soundscapes were characterized by a series of patches with high sound pressure levels and high acoustic variability, especially in the mid-frequency range (rapids) followed by acoustically more silent patches (runs and glides). Rough structures such as bedrock outcrops create flow obstructions that break the water's surface, generating rapids characterized by high turbulence zones that trap air underwater, leading to sound pressure levels increase over all frequencies, with the highest increment in mid-frequency sound pressure levels (Lugli and Fine 2003; Tonolla et al. 2009, 2010).

In this study, distinctive sound pressure level peaks in the North Fork and Middle Fork were detected in the octave bands 0.125-0.5 kHz with a dominant peak at 0.125 kHz (especially pronounced in the Middle Fork, where major turbulence zones were generated by large class III-IV whitewater rapids). Similar results were reported by Lugli and Fine (2003), who found sound pressure level peaks between 0.2-0.5 kHz near rapids and waterfalls. Moreover, Tonolla et al. (2010) reported sound pressure level peaks between 0.5-2 kHz and 0.125-0.5 kHz in riffle and step-pool habitats, respectively. Distinct turbulence created at large flow obstructions shifted the sound pressure level peak to lower frequency bands. Thus, the pronounced decline in mid-range frequencies sound pressure level found in the Thur, Tagliamento and Nyack was probably due to a lack of major turbulence-sound generating sources, similar to the situation in pools, backwaters and lakes (Wysocki et al. 2007; Amoser and Ladich 2010; Tonolla et al. 2010). Pulsating sound produced by breaking and reforming turbulent waves on bedrock and non-competent boulders was probably associated with the high acoustic variability found in mid-range frequency bands of the North Fork and Middle Fork, while the limited or lacking lateral supply of sediment in the North Fork and Middle Fork resulted in significantly lower high-frequency sound pressure levels and acoustic variability with respect to the Tagliamento and Nyack floodplains.

Effect of flow level on the river soundscapes

Generally, an increase in flow level and flow velocity (Table 2) resulted in an increase in sound pressure levels over all octave bands. However, Lugli and Fine (2003) only found a sound pressure level increase in the low-frequencies during high discharge conditions. A decrease in flow level results in an increase in relative roughness. Theoretically, a high relative roughness induces stronger turbulence and a related increase in mid-range frequencies sound pressure level (Tonolla et al. 2009). However, high roughness coupled with low flow

velocities can only induce a small amount of turbulence and hence produce less sound. Therefore, the North Fork soundscape at base flow was characterized by a reduced temporal sound variability and sound pressure levels (especially at mid-range frequencies) compared to the soundscape at intermediate flow. On the other hand, very high flow conditions such as in the Nyack during bankfull conditions, led to a decrease in sound and acoustic variability in the mid-frequency range because of increasing flow depth and the related decrease in relative roughness and turbulence. Momentum exchanges between colliding particles also increase resulting in a break-up of the channel bed (Lorang and Hauer 2003). These processes resulted in higher high-frequency sound pressure levels (up to >20 dB) at bankfull flow than at intermediate flow and in a shift of the highest sound pressure level peaks to lower frequencies (from 8-16 to 2-4 kHz). Additionally, the sharp decrease in the acoustic variance in the high-frequency range coincided with bankfull flow conditions, when maximal rates of sediment can be transported from the river, thus resulting in more continuous flow competent conditions that are suitable for the transport of sediment particles composing the river bed.

High sound pressure levels (up to 150 dB) observed during bankfull flow conditions can reach or even exceed the noise caused by boating and shipping (130-160 dB, main energy content below 1.5 kHz; Vasconcelos et al. 2007; Codarin et al. 2009; Picciulin et al. 2010) and might interfere with intraspecific communication and have feasible behavioral impacts (e.g. predator-prey interactions, stress-induced fitness reduction, and disturbance of fish distribution; Popper and Hastings 2009a, b; Slabbekoorn et al. 2010). Boat traffic or loud sounds produced by strong turbulence (e.g. Middle Fork, this study, and step-pool habitats in Tonolla et al. 2010) are normally of relatively short exposure and limited area impact. In contrast, high sound pressure levels during floods (mainly as a consequence of sound production related to particle collisions due to streambed sediment transport and strong flow velocity) are constant and long-lasting (floods can persists for days or weeks), potentially impacting much larger areas (e.g. whole ecosystem) and involving much larger numbers of freshwater biota.

Nevertheless, the low-energy quiet zone found in all soundscapes (also at high flow levels) at 0.063-0.5 kHz coincides with the best hearing range of many fish species (Hawkins 1981; Fay and Simmons 1999; Ladich and Popper 2004; and reference therein), and it is similar to the one found in the pressure and velocity spectra of other studies (Lugli and Fine 2003, 2007; Tonolla et al. 2010). These quiet zones may be highly important for active communication and stress reduction in loud river sections.

In a recent study, Amoser and Ladich (2010) found that sound pressure levels (variations of up to 51 dB in single frequencies) and spectral composition may change throughout the year. In this study, we showed that a river is highly complex along its thalweg and that the spectral composition might change quite rapidly with pronounced changes dependent on the nature of the river itself (e.g. constraint vs. unconstraint). Thus, we believe that highly dynamic rivers would show different soundscapes throughout the seasons and the year, coinciding with specific climatic conditions (e.g. rainfall, snow melting, drought) and related hydrological mechanisms (flow regime).

Implications and applications

Quantifying underwater soundscapes offers new insights into the complexity of entire river segments, including the habitat types nested within these segments. Soundscape characterization could be used to assess and quantify the complexity of river corridors, hence soundscapes could be used to evaluate river restoration measures. However, in-depth research is required to better understand the hydrogeomorphic mechanisms, single and in concert, that generate complex soundscapes.

It is known that most aquatic organisms use sound as an important information source about their environment (Simpson et al. 2010; Stanley et al. 2010; Vermeij et al. 2010; and references therein). Slabbekoorn and Bouton (2008) and Fay (2009) suggested that fishes and aquatic invertebrates probably make use of acoustic scenes (soundscapes) for orientation within aquatic landscapes, and that soundscape investigation has high potential for future studies on animal orientation. Therefore, we believe that many freshwater biota probably exploit the acoustic signals of different soundscapes as a supplementary information source about their surrounding area; thus potentially influencing their behavior and ecology. Finally, changes in river and habitat acoustics over time (days to years), mostly depending on hydrogeomorphic and anthropogenic changes, are potential challenges for freshwater biota.

The insights gained through the present study may help improve future experimental designs aimed at better understanding the effects of the soundscapes on freshwater organisms as well as at formulating hypothesis-driven questions related to river ecosystems; for example, how does underwater sound influence the composition, distribution and behavior of specific aquatic organisms in specific freshwater habitats and along river corridors? Do typical acoustic signals help aquatic organisms to detect a refuge during high flow conditions?

Acknowledgments

We thank T. Mehner and the participants of the workshop "Scientific Writing" at the Leibniz-Institute of Freshwater Ecology and Inland Fisheries for helpful discussions on an early stage of the manuscript. We acknowledge V. Acuña for helpful comments. Funding for M. S. Lorang was provided by a grant (Grant Award Letter Agreement 344.01) from the Gordon and Betty Moore Foundation.

References

Amoser S, Ladich F. 2005. Are hearing sensitivities of freshwater fish adapted to the ambient noise in their habitats? *Journal of Experimental Biology* 208: 3533-3542.

Amoser S, Ladich F. 2010. Year-round variability of ambient noise in temperate freshwater habitats and its implications for fishes. *Aquatic Sciences* 3: 371-378.

Bertoldi W, Zanoni L, Tubino M. 2009. Assessment of morphological changes induced by flow and flood pulses in a gravel bed braided river: the Tagliamento River (Italy). *Geomorphology* 114: 348-360.

Codarin A, Wysocki LE, Ladich F, Picciulin M. 2009. Effects of ambient and boat noise on hearing and communication in three fish species living in a marine protected area (Miramare, Italy). *Marine Pollution Bulletin* 58: 1880-1887.

Fausch KD, Torgersen CE, Baxter CV, Li HW. 2002. Landscapes to riverscapes: bridging the gap between research and conservation of stream fishes. *Bioscience* 52: 483-498.

Fay RR, Simmons AM. 1999. The sense of hearing in fishes and amphibians. In *Comparative Hearing: Fishes and Amphibians*, Fay RR, Popper AN (eds). Springer-Verlag: New York; 269-318.

Fay RR, Popper AN. 2000. Evolution and hearing in vertebrates: the inner ears and processing. *Hearing Research* 149: 1-10.

Fay RR. 2009. Soundscapes and the sense of hearing in fishes. *Integrative Zoology* 4: 26-32.

Fine ML, Lenhardt ML. 1983. Shallow-water propagation of the toadfish mating call. *Comparative Biochemistry and Physiology A* 76: 225-231.

Hawkins AD. 1981. The hearing abilities of fish. In *Hearing and Sound Communication in Fishes*, Tavolga WN, Popper AN, Fay RR (eds). Springer-Verlag: New York; 109-133.

Hawkins AD, Myrberg AA. 1983. Hearing and sound communication under water. In *Bioacoustics, a Comparative Approach*, Lewis B (ed). Academic Press: London; 347-405.

Ladich F, Popper AN. 2004. Parallel evolution in fish hearing organs. In *Evolution of the Vertebrate Auditory System*, Manley GA, Popper AN, Fay RR (eds). Springer-Verlag: New York; 95-127.

Lang S, Tiede D. 2003. *vLATE Extension für ArcGIS: Vektorbasiertes Tool zur Quantitativen Landschaftsstrukturanalyse*. ESRI 18th European User Conference, Innsbruck, Austria.

Lang S, Langanke T. 2005. Multiscale GIS tools for site management. *Journal for Nature Conservation* 13: 185-196.

Langanke T, Rossner G, Vrscaj B, Lang S, Mitchley J. 2005. Selection and application of spatial indicators for nature conservation at different institutional levels - experiences from the SPIN project. *Journal for Nature Conservation* 13: 101-114.

Lorang MS, Hauer FR. 2003. Flow competence evaluation of streambed stability: an assessment of the technique and limitations of application. *Journal of the North American Benthological Society* 22: 475-491.

Lugli M, Fine ML. 2003. Acoustic communication in two freshwater gobies: ambient noise and short-range propagation in shallow streams. *Journal of the Acoustical Society of America* 114: 512-521.

Lugli M, Fine ML. 2007. Stream ambient noise, spectrum and propagation of sounds in the Goby *Padogobius martensii*: sound pressure and particle velocity. *Journal of the Acoustical Society of America* 122: 2881-2892.

Lurton X. 2002. *An Introduction to Underwater Acoustic: Principles and Applications*. Springer Verlag: Chichester; 347.

Mazaris AD, Kallimanis AS, Chatzigianidis G, Papadimitriou K, and Pantis JD. 2009. Spatiotemporal analysis of an acoustic environment: interactions between landscape features and sounds. *Landscape Ecology* 24: 817-831.

Montgomery DR, Buffington JM. 1997. Channel-reach morphology in mountain drainage basins. *Geological Society of America Bulletin* 109: 596-611.

Officier CB. 1958. *Introduction to the Theory of Sound Transmission*. McGraw-Hill: New York; 284.

Picciulin M, Sebastianutto L, Codarin A, Farina A, Ferrero EA. 2010. In situ behavioural responses to boat noise exposure of *Gobius cruentatus* (Gmelin, 1789; fam. Gobiidae) and *Chromis chromis* (Linnaeus, 1758; fam. Pomacentridae) living in a marine protected area. *Journal of Experimental Marine Biology and Ecology* 386: 125-132.

Popper AN, Hasting MC. 2009a. The effects of anthropogenic sources of sound on fishes. *Journal of Fish Biology* 75: 455-489.

Popper AN, Hasting MC. 2009b. The effects of human-generated sound on fish. *Integrative Zoology* 4: 43-52.

Rogers PH, Cox M. 1988. Underwater sound as a biological stimulus. In *Sensory Biology of Aquatic Animals*, Atema J, Fay RR, Popper AN, Tavolga WN (eds). Springer-Verlag: New York; 131-149.

Simpson SD, Meekan MG, Larsen NJ, McCauley RD, Jeffs A. 2010. Behavioral plasticity in larval reef fish: orientation is influenced by recent acoustic experiences. *Behavioral Ecology* 21: 1098-1105.

Slabbekoorn H, Bouton N. 2008. Soundscape orientation: a new field in need of sound investigation. *Animal Behaviour* 76: 5-8.

Slabbekoorn H, Bouton N, Van Opzeeland I, Coers A, Ten Cate C, Popper AN. 2010. A noisy spring: the impact of globally rising underwater sound levels on fish. *Trends in Ecology and Evolution* 25: 419-427.

Stanley JA, Radford CA, Jeffs AG. 2010. Induction of settlement in crab megalopae by ambient underwater reef sound. *Behavioral Ecology* 21: 113-120.

Thompson CJ, Croke J, Ogden R, Wallbrink P. 2006. A morpho-statistical classification of mountain stream reach types in southeastern Australia. *Geomorphology* 81: 43-65.

Thorp JA, Thoms MC, Delon MD. 2006. The riverine ecosystem synthesis: biocomplexity in river networks across space and time. *River Research and Applications* 22: 123-147.

Tockner K, Ward JV, Arscott DB, Edwards PJ, Kollmann J, Gurnell AM, Petts GE, Maiolini B. 2003. The Tagliamento River: an ecosystem of European importance. *Aquatic Sciences* 65: 239-253.

Tockner K, Lorang MS, Stanford JA. 2010. River floodplains are model ecosystems to test general hydrogeomorphic and ecological concepts. *River Research and Applications* 26: 76-86.

Tonolla D, Acuña V, Lorang MS, Heutschi K, Tockner K. 2010. A field-based investigation to examine underwater soundscapes of five common river habitats. *Hydrological Processes* 24: 3146-3156.

Tonolla D, Lorang MS, Heutschi K, Tockner K. 2009. A flume experiment to examine underwater sound generation by flowing water. *Aquatic Sciences* 71: 449-462.

Urick RJ. 1983. *Principles of Underwater Sound*. McGraw-Hill: New York; 423.

Vasconcelos RO, Amorim MCP, Ladich F. 2007. Effects of ship noise on the detectability of communication signals in the Lusitanian toadfish. *Journal of Experimental Biology* 210: 2104-2112.

Vermeij MJA, Marhaver KL, Huijbers CM, Nagelkerken I, Simpson SD. 2010. Coral larvae move toward reef sounds. *PLoS ONE* 5: e10660.

Wiens JA. 2002. Riverine landscapes: taking landscape ecology into the water. *Freshwater Biology* 47: 501-515.

Wohl E, Merritt DM. 2008. Reach-scale channel geometry of mountain streams. *Geomorphology* 93: 168-185.

Wysocki LE, Amoser S, Ladich F. 2007. Diversity in ambient noise in European freshwater habitats: noise levels, spectral profiles, and impact on fishes. *Journal of the Acoustical Society of America* 121: 2559-2566.

CHAPTER 4

Thermal heterogeneity in river floodplains

Abstract

River floodplains are composed of a shifting mosaic of aquatic and terrestrial habitats. Each habitat type exhibits distinct environmental and ecological properties. Temperature is a key property driving ecological processes and controlling the composition and distribution of biota. However, given the size and complexity of floodplains, ground surveys based on point measurements are spatially limited. In this study, we applied thermal infrared (IR) imagery to quantify surface temperature patterns at 12-15 min intervals over 24 h cycles in two near-natural Alpine river floodplains (Roseg, Tagliamento). Furthermore, vertical temperature distribution was measured at 3-5 min intervals in unsaturated gravel sediment deposits (at 1 cm distances; 0-29 cm depth). Each habitat type exhibited a distinct thermal signature creating a complex thermal mosaic. The diel temperature pulse and maximum daily temperature were the main thermal components that differentiated habitat types. In both floodplains, exposed gravel sediments exhibited the highest diel pulse (up to 23°C), whereas in aquatic habitats the pulse was as low as 11°C (main channel in the Roseg floodplain). In the unsaturated gravel sediment deposits, the maximum diel kinetic temperature pulse ranged from 40.4°C (sediment surface) to 2.7°C (29 cm sediment depth). Vertically, the spatiotemporal variation of temperature was about as high as horizontally across the entire floodplain surface. This study emphasized that remotely sensed thermal IR imagery provides a powerful non-invasive method to quantitatively assess thermal heterogeneity of complex aquatic and terrestrial ecosystems at a resolution required to understand ecosystem processes and the distribution of biota.

Introduction

Temperature is a master variable driving physical, chemical, and biological processes in aquatic and terrestrial ecosystems and controlling the composition, distribution, and behavior of organisms (Thyssen et al. 1987; Elliott and Hurley 2001; Acuña et al. 2008; Hannah et al. 2008; Indermaur et al. 2009a, b). In addition, temperature is gaining increasing attention because climate change has altered and will continue to alter the temperature regime at local, regional, and global scales (IPCC 2007). Thus, temperature remains a subject of worldwide environmental research (Webb et al. 2008).

The thermal regime of streams and rivers is mainly influenced by incoming shortwave solar radiation, air temperature, flow regime, riparian conditions, streambed substrata, and upwelling subsurface water (Webb and Zhang 1999; Malard et al. 2001; Webb et al. 2003). Although the seasonal, annual, and diel temperature cycles of lotic systems are well studied (for a review see Caissie 2006), little is known about the spatiotemporal heterogeneity of temperature in complex landscapes. Previous studies relied mostly on point measurements to quantify spatial thermal heterogeneity (e.g. Arscott et al. 2001; Uehlinger et al. 2003; Acuña and Tockner 2009). Distributed point measurements, using temperature loggers, reveal information at a high temporal resolution at single locations (Selker et al. 2006). However, given the size and complexity of floodplain systems, ground surveys provide spatially limited information. Quantifying thermal heterogeneity at the landscape scale is pivotal in identifying the spatiotemporal distribution of critical habitats (e.g. thermal refugia, areas of upwelling subsurface water), and to investigate the utilization of these habitats by both aquatic and terrestrial organism as well as by animals that exhibit complex life cycles (e.g. aquatic insects, amphibians). Moreover, information on thermal heterogeneity is required to scale-up ecosystem processes from point measurements to entire river floodplains.

Remotely sensed thermal infrared (IR) imagery provides an opportunity to simultaneously map surface temperature of aquatic and terrestrial ecosystems at a spatial resolution relevant for quantifying ecosystem processes and the distribution of biota. IR thermography has been used to estimate the abundance and density of terrestrial mammals such as deer, sheep, and polar bears (Naugle et al. 1996; Amstrup et al. 2004; Bernatas and Nelson 2004) as well as of aquatic mammals such as whales and walruses (Perryman et al. 1999; Udevitz et al. 2008). Thermal IR imagery has also been applied for monitoring temperature of volcanoes (Lagios et al. 2007), mapping of microbial mats in hot springs (Dunckel et al. 2009), and characterizing land surface temperature in urbanized areas (Chudnovsky et al. 2004; Hartz et al. 2006; Xian

2008). Furthermore, satellite-, airborne-, and ground-based IR images have been used to characterize the spatial heterogeneity of surface temperature of the ocean (Emery and Yu 1997; Parkinson 2003), lakes and reservoirs (LeDrewand Franklin 1985; Anderson et al. 1995; Hook et al. 2003), as well as rivers (Torgersen et al. 1999; Cherkauer et al. 2005; Kay et al. 2005; Handcock et al. 2006; Loheide and Gorelick 2006; Cardenas et al. 2008). Cardenas et al. (2008) used thermal IR images to characterize thermal heterogeneity in a small stream during different flow conditions. Smikrud et al. (2008) used thermal IR imagery, together with aerial photographs, for floodplain classification (Unuk River, SE Alaska). However, none of those studies used thermal IR imagery to characterize surface temperature of entire river landscapes at both high spatial and temporal resolution.

Floodplains may serve as excellent model systems to elaborate upon the thermal heterogeneity of complex landscapes (Tockner et al. 2000, 2010). They are composed of a shifting mosaic of aquatic and terrestrial habitat patches that differ in succession stage, flow regime characteristics, sediment, nutrients, organic matter, and thermal characteristics, all of which are critical factors influencing biological communities and ecosystem processes (Naiman et al. 2005; Stanford et al. 2005). Furthermore, the unsaturated sediments of gravel-bed rivers form the most extensive albeit neglected floodplain habitat.

The primary goals of this study were (i) to quantify the spatial and temporal thermal heterogeneity of entire river floodplains, (ii) to thermally characterize aquatic and terrestrial floodplain habitat types, and (iii) to quantify vertical temperature patterns within unsaturated gravel sediment deposits. To address these objectives, thermal IR images were collected to characterize surface spatial temperature distribution, and temperature loggers were exposed to quantify vertical temperature distribution in unsaturated gravel sediment deposits. All data were collected in two near-natural Alpine river floodplains over approximately 24 h cycles.

Materials and methods

Experimental design

Thermal IR images were taken at 12-15 min intervals over diel cycles in two Alpine floodplains (Roseg and Tagliamento Rivers) (Figure 1, Table 1). The IR camera provided surface temperature data (radiant temperature) at high spatial resolution. Concurrently, temperature loggers were deployed in various aquatic and terrestrial habitat types to estimate the difference between radiant (from IR images) and kinetic temperature (from temperature loggers). Furthermore, vertical kinetic temperature distribution was measured in the top layer (0-29 cm depth) of unsaturated gravel sediment deposits at 1 cm intervals.

Study sites

The proglacial floodplain of the second-order Roseg River (46°25'37.84'' N, 9°51'40.94'' E) is located at 2000 m asl in the Bernina massif (Eastern Swiss Alps) (Figure 1, Table 1). The floodplain is characterized by various channel types that differ in hydrology and morphology (Tockner et al. 2002; Uehlinger et al. 2003). About 85% of the floodplain is composed of exposed gravel or sparsely vegetated areas (Wellstein et al. 2003). A detailed description of the catchment and the floodplain is provided by Ward and Uehlinger (2003). Thermal characteristics of aquatic habitats have been investigated by Malard et al. (2001) and Uehlinger et al. (2003).

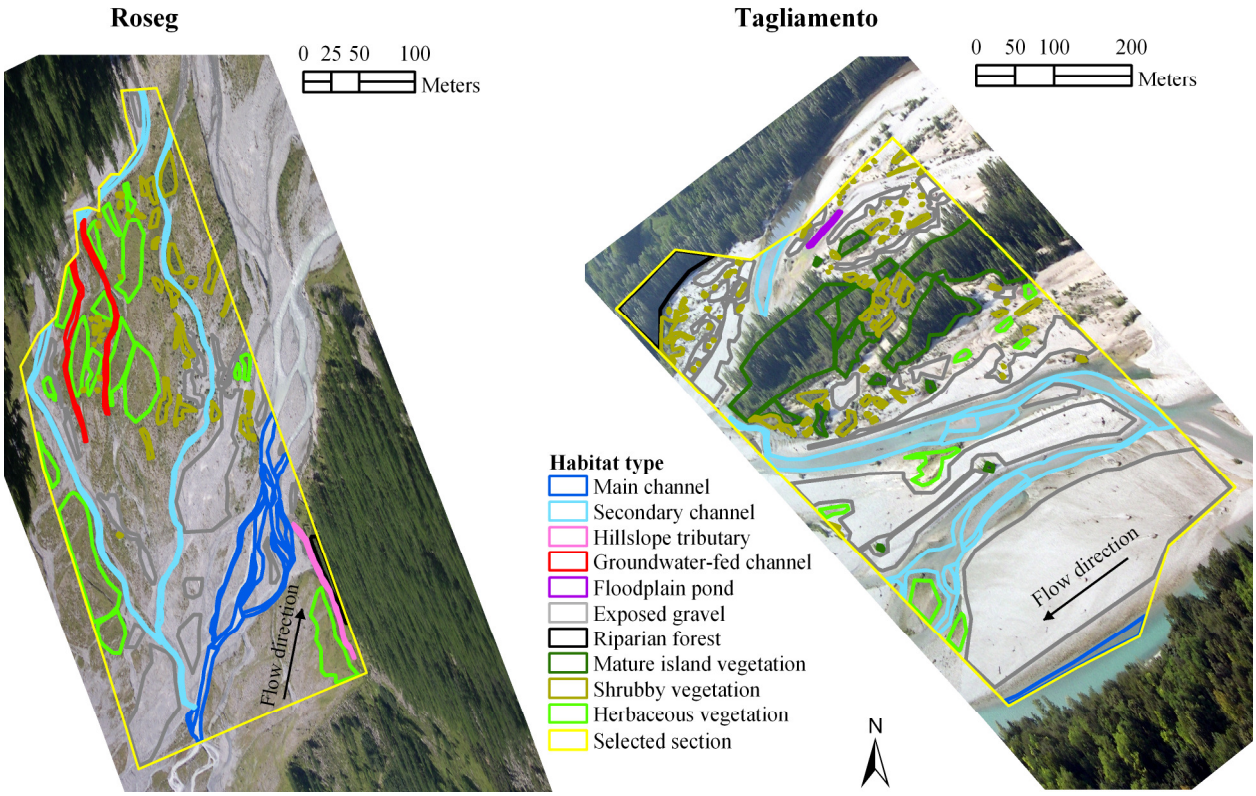

Figure 1. Distribution of aquatic and terrestrial habitat types in the Roseg and Tagliamento floodplains.

The near-natural island-braided gravel-bed river floodplain of the seventh-order Tagliamento River (46°12'3.60'' N, 12°58'26.40'' E) is located at 160 m asl at the southern fringe of the European Alps (Northeastern Italy) (Figure 1, Table 1). At base flow (approximately 20 $m^3 s^{-1}$), the floodplain contains exposed gravel habitats (42% of total area), riparian forest (35%), channel network (15%), vegetated islands (7%), as well as numerous pools and large wood accumulations (each 0.5%) (Langhans et al. 2008). Detailed information on the Tagliamento catchment and the floodplain can be found elsewhere (e.g. Tockner et al. 2003). Thermal

characteristics of aquatic habitats along the entire river corridor have been studied by Arscott et al. (2001) and Acuña and Tockner (2009).

Table 1. Characterization of the study sites (selected section, Figure 1) and information on IR imaging for the Roseg and Tagliamento floodplains.

Characteristic	Roseg	Tagliamento
Study site area (ha)	9.55	27.72
Study site width (m)	165-340	700-770
Camera altitude (m asl)	2,240	480
Camera distance (m)	545-1,130	530-1,300
Zenith angle φ (°)	65.9-79.3	82.2-84.7
Final pixel size (m)	1.66 × 1.66	2.29 × 2.29
Final number of pixels	34,502	52,531
Sampling start time	22 Aug. 2004 14:12h	31 Aug. 2005 18:00h
Sampling end time	23Aug. 2004 14:12h	01 Sep. 2005 18:00h
Sampling time interval (min)	12	15
Total number of IR images	121	97

Air temperature data for the Roseg floodplain were obtained from a meteorological station located at 1.5 km horizontal distance from the study site (1,997 m asl) (Figure 2). Solar radiation data were obtained from the Swiss Federal Office of Meteorology (Corvatsch station, 3,315 m asl, at 3.3 km horizontal distance from the study site) (Figure 2). At the Tagliamento floodplain, a portable meteorological station continuously recorded air temperatures 1.5 m above the ground (Figure 2). The Osservatorio Meteorologico Regionale dell' ARPA FVG (OSMER) provided solar radiation data from the station Campo Lessi (184 m asl, 13 km horizontal distance from the study site) (Figure 2).

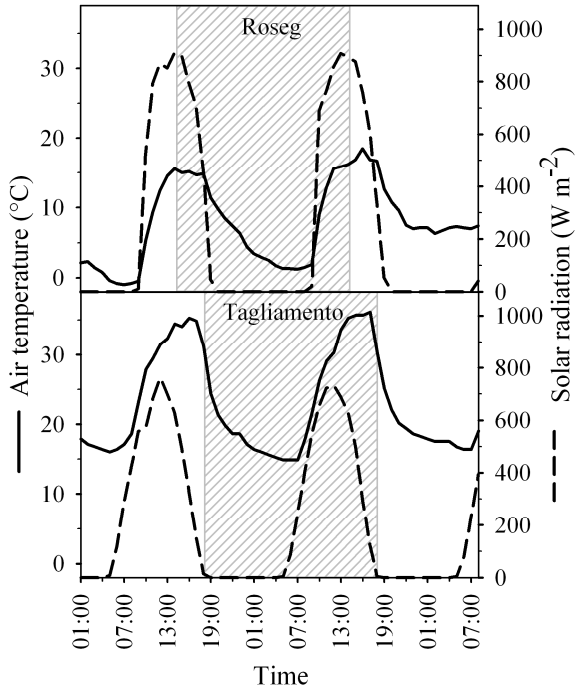

Figure 2. Air temperature and solar radiation in the Roseg (22-24.08.2004) and Tagliamento (31.08-02.09.2005) floodplains. Shaded area indicates the sampling time of IR-images.

Thermal characterization of the floodplains by IR images

IR image collection

Oblique IR images were taken with an IR camera (TH 3102 MR, NEC-San-ei Co., Japan) mounted on a tripod installed at the rim of the steep mountains fringing on the two floodplains, thereby allowing the entire valley bottom to be thermally mapped (Figure 1, Table 1). It was possible to take IR images of a floodplain segment at an exceptionally high spatial and temporal resolution that normally could not be achieved using an airborne camera. However, the large zenith angles may have affected the accuracy of the radiant temperature measurements and therefore have to be taken into consideration (Appendices A, B).

The camera was equipped with a Stirling-cooled HgCdTe detector unit operating in the 8-13 µm spectral range with a standard thermal recording range (-50-200°C). The temperature sensitivity (smallest temperature change or difference that can be detected) of the camera was 0.08 at 30°C (temperature of the camera itself during the test), the measurement accuracy (level of accuracy of the temperature measurements being recorded by the camera) was ±0.5°C (surface temperature range: 0-100°C; manufacturer's accuracy specifications). The camera used a mirror lens system for scanning a view field of 30° (horizontal) × 28.5°

(vertical) with a horizontal resolution of 1.5 mrad and an image size of 255 pixels × 207 scanning lines.

IR image processing

Thermal data were extracted using the IR image processing software PicWin-IRIS 7.1 (ebs-thermography, Munich, Germany), converted to a georeferenced raster with a specific radiant temperature for each pixel, and post-processed in ArcGIS 9.2 (ESRI, Redlands, California, USA). For further analyses, a subsection of the floodplain was selected based on two criteria: (i) to include all typical aquatic and terrestrial habitat types, and (ii) to minimize shading effects by surrounding landscape elements (Figure 1). Then a network of equally spaced points (one point every 5 m) was generated over the thermal raster to extract radiant temperature data for further analysis. This resulted in a reduced data set of approximately 3,800 points (Roseg) and approximately 11,100 points (Tagliamento), respectively. The total size differed for the two river floodplains (Figure 1, Table 1).

The key interest of this study was not to derive the most accurate temperature values at a specific point but to quantify the spatiotemporal variation at the floodplain scale. Nevertheless, because thermal remote sensing is not without shortcomings (e.g. Torgersen et al. 2001; Handcock et al. 2006), we estimated the potential errors of the collected IR imagery (Appendices A-C). In this study, the effect of atmospheric absorption was considered negligible because measurement distances were short, and humidity was low during the study period (see Anderson and Wilson 1984; Anderson et al. 1995). Moreover, there is relatively little atmospheric absorption in the 8-14 μm spectral band (Anderson and Wilson 1984). IR images were processed assuming a thermal IR emissivity of 1, which is close to the values of the targeted materials in the studied floodplains (Appendix A). In addition, radiant temperature may be influenced by reflected radiation from the sky and from the surrounding environment as well as from surface roughness (Goldstein 1978; Torgersen et al. 2001; Handcock et al. 2006). Hence, the potential error due to reflected radiation was considered in the present analyses and the effect of surface roughness was experimentally tested (Appendices B, C).

IR image analysis

Based on the radiant temperature data, six thermal variables were calculated for each point of the regular network: (i) average daily temperature, (ii) minimum daily temperature, (iii) maximum daily temperature, (iv) diel temperature pulse, (v) maximum rate of thermal heating, and (vi) maximum rate of thermal cooling (for calculations see Arscott et al. 2001).

A filter of the regular network was necessary to compare thermal characteristics of aquatic and terrestrial habitat types. Thus, polygons encompassing all typical aquatic and terrestrial habitat types were generated and sub-pixel mixing (that is, mixing of pixels from different habitats, e.g. mixing main channel pixels with exposed gravel pixels) was minimized (Figure 1). Sub-pixel mixing has been shown to affect radiant temperatures (Kay et al. 2005; Handcock et al. 2006). This resulted in 1,170 points from the regular network falling within the habitat polygons in the Roseg and 6,260 points in the Tagliamento floodplains, respectively.

At the floodplain scale, the spatial thermal structure was first assessed applying visualization techniques and then through appropriate spatial statistical analyses (Perry et al. 2002). A spatial autocorrelation analysis (Global Moran's *I*) was used to detect if high and/or low thermal values cluster together. A positive Moran's *I* index value indicates tendency toward clustering whereas a negative Moran's I index value indicates tendency toward dispersion. The *Z* score indicates whether the statistic value could be the result of random chance or is statistically significant. Spatial statistic calculations were based on Euclidian distance and performed with the six thermal variables calculated for each data point of the regular network (Spatial Statistics Tools of ArcGIS 9.2, ESRI, Redlands, California, USA).

Principal Component Analyses, PCA (R, version 2.9.2, http://www.r-project.org), based on the six thermal variables, were performed to reduce the number of variables. PCA was performed using a correlation matrix to prevent dominant variables from determining the results. Factor loadings of the first and second principal component were extracted without rotation and used for further correlation analyses. Spearman's rank correlation analyses were used to identify direction and strength of associations among the studied variables (SPSS, version 14.0, SPSS Inc., Chicago, Illinois, USA).

To validate radiant temperature values, surface kinetic temperature was concurrently recorded at 10 min intervals with VEMCO Minilog temperature loggers (TR model, AMIRIX Systems Inc., Halifax, NS, Canada; temperature range -5-35°C, accuracy ±0.3°C, resolution 0.2°C, manufacturer's specification) in selected aquatic and terrestrial habitat types. Loggers were placed in protective stainless steel casings (approximately 2.5 kg), which have minimal influence on instantaneous temperatures (±0.1°C; Malard et al. 2001).

Vertical kinetic temperature distribution in unsaturated gravel sediment deposits

To quantify the vertical kinetic temperature distribution within the top layer of unsaturated gravel sediment deposits, 30 thermocouples, mounted to a PVC frame and connected to a data logger (Squirrel 1000-Serie, Eltek, Cambridge, UK), were buried. Data recording started immediately after the installation of the thermocouples. The loggers were equally spaced between 0 and 29 cm depth at 1 cm intervals. An additional thermocouple was mounted 1 m above the ground surface and shielded against direct solar radiation. Data were recorded at 3 min (Roseg) and 5 min (Tagliamento) intervals.

Results

Spatiotemporal thermal variability at the floodplain scale

At the floodplain scale, surface radiant temperature exhibited a distinct spatiotemporal heterogeneity. Thermally, habitat types differed strongly during day time, whereas surface temperature was relatively uniform across the entire floodplain during night time (Figures 3, 4). Habitat-specific properties such as vegetation cover modified the general effect of air temperature and solar shortwave radiation on surface temperature patterns. For example, in the Tagliamento floodplain two distinct temperature peaks occurred at night time and three peaks during day time (Figure 4). During night time, cool aquatic habitats were separated from all terrestrial habitats. During day time, terrestrial habitats could be further thermally differentiated into densely vegetated (riparian forest and mature islands) and pioneer habitat types (that is, exposed gravel, herbaceous, and shrubby vegetation) (Figure 3).

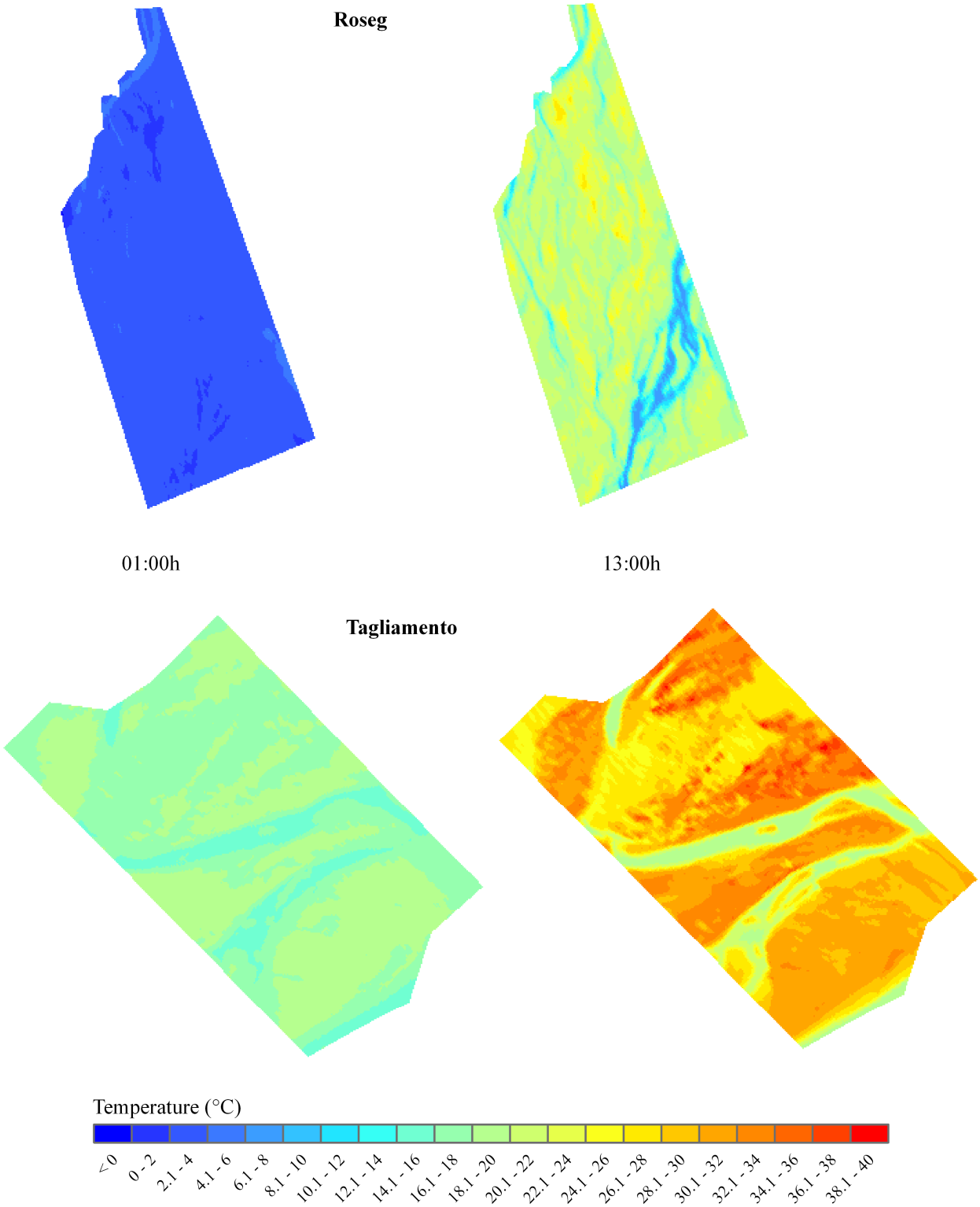

Figure 3. Spatial distribution (values per pixel) of surface radiant temperature at 01:00 hours and at 13:00 hours in the Roseg and Tagliamento floodplains.

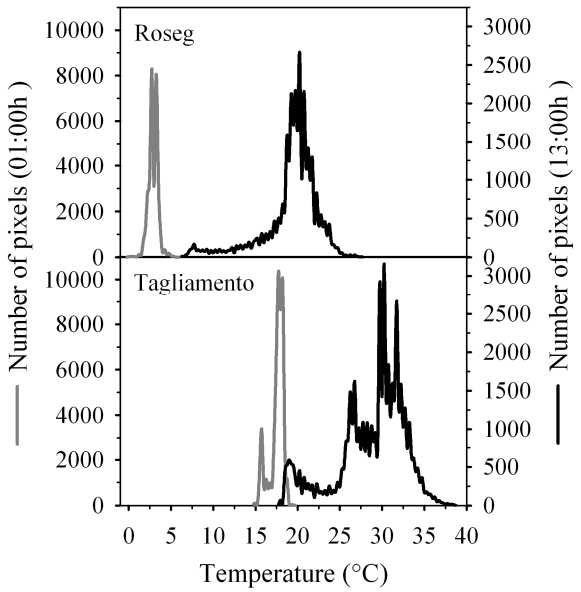

Figure 4. Frequency distribution of pixels in the Roseg and Tagliamento floodplains. Please note different *y*-scales.

At the floodplain scale, average daily temperature per pixel ranged between 3.4 and 10.5°C (Roseg floodplain) and 16.6 and 24.7°C (Tagliamento) (Figure 5). However, diel temperature pulse per pixel ranged in the Roseg from 5.5 to 28.1°C and in the Tagliamento from 4.9 to 24.4°C (Figure 5).

The global spatial statistic Global Moran's *I* confirmed that the thermal properties of the individual pixels that emerged over the 24 h cycles were not the results of random process, but exhibited a distinct degree of clustering that allowed a clear differentiation of thermal patches within the floodplains (Table 2). Moreover, the degree of clustering was higher in the Tagliamento than in the Roseg floodplain (higher *Z* scores) (Table 2).

Table 2. Spatial thermal autocorrelation (Global Moran's *I*) for each thermal variable in the Roseg and Tagliamento floodplains.

Thermal variable	Roseg		Tagliamento	
	I index	*Z* score	*I* index	*Z* score
Average	0.48	183.5*	0.48	362.7*
Minimum	0.29	110.3*	0.50	382.7*
Maximum	0.40	153.1*	0.44	337.2*
Pulse	0.39	150.5*	0.44	332.1*
Heating	0.46	176.9*	0.30	228.3*
Cooling	0.25	95.6*	0.32	243.5*

See text for calculations. *$p < 0.01$.

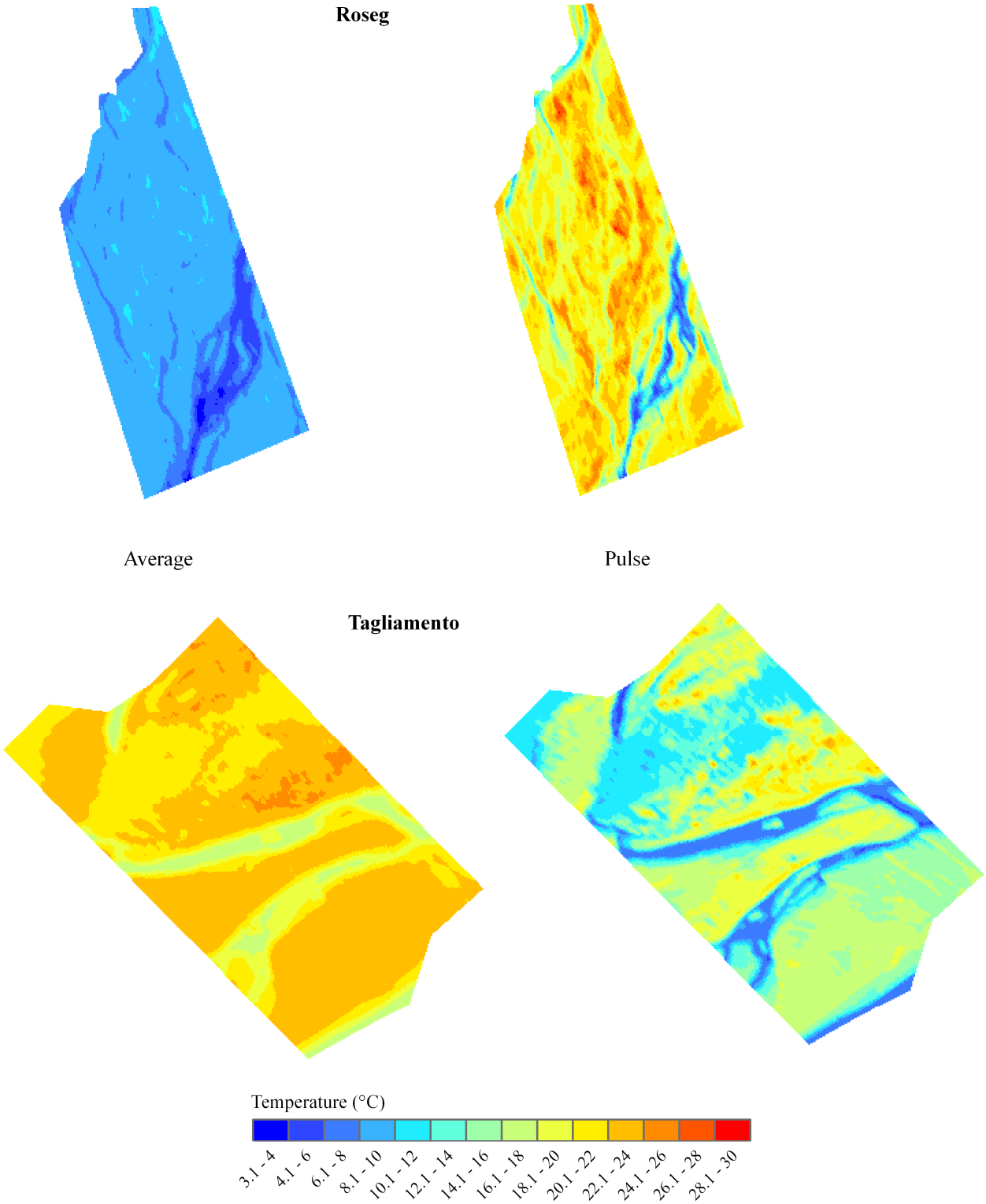

Figure 5. Spatial heterogeneity of average daily temperature and diel temperature pulse in the Roseg and Tagliamento floodplains (values per pixel).

Aquatic habitats exhibited lower average and pulse values than terrestrial habitats (Table 3). Among all the habitat types, exposed gravels exhibited the highest daily average and diel pulse temperatures. In contrast, vegetation cover attenuated the diel thermal regime (Table 3).

Table 3. Thermal characterization (average daily temperature and diel temperature pulse; average ± standard deviation; °C) of aquatic and terrestrial habitat types in the Roseg and Tagliamento floodplains.

Habitat type	Roseg		Tagliamento	
	Average	Pulse	Average	Pulse
Main channel	5.2 ± 1.1	11.2 ± 4.0	17.4 ± 0.2	6.9 ± 0.6
Secondary channel	7.6 ± 0.6	15.9 ± 3.1	18.1 ± 0.8	7.7 ± 1.4
Hillslope tributary	7.5 ± 0.7	15.2 ± 2.7	NA	NA
Groundwater-fed channel	8.1 ± 0.5	17.5 ± 2.5	NA	NA
Floodplain pond	NA	NA	21.5 ± 0.5	13.8 ± 1.3
Exposed gravel	8.9 ± 0.5	22.7 ± 1.6	23.0 ± 0.6	17.4 ± 1.4
Riparian forest	8.3 ± 0.2	14.9 ± 1.1	21.2 ± 0.3	11.0 ± 0.9
Mature islands	NA	NA	21.5 ± 0.3	11.9 ± 1.0
Shrubby vegetation	8.4 ± 0.3	19.7 ± 1.0	22.3 ± 0.6	14.4 ± 1.9
Herbaceous vegetation	8.7 ± 0.4	21.1 ± 1.3	21.9 ± 0.7	14.7 ± 1.4

NA: not applicable.

Based on six selected thermal variables, the first two components of the PCA explained 91% (75 and 16%, respectively) of the thermal variance in the Roseg floodplain and 89% (66 and 23%, respectively) in the Tagliamento floodplain (Figure 6). The factor scores of the first PCA component were strongly correlated with diel temperature pulse and maximum daily temperature (Table 4). Factor scores of the second PCA component were mainly correlated with minimum daily temperature. The aquatic and terrestrial habitat types could be better differentiated in the Tagliamento than in the Roseg floodplain (Figure 6, Table 4).

Table 4. Spearman's rank correlations (r) between thermal variables (see text) and the factor scores of the first (PCA 1) and second (PCA 2) components of the PCA.

Thermal variable	Roseg (n = 3,815)		Tagliamento (n = 11,080)	
	PCA 1 (r)	PCA 2 (r)	PCA 1 (r)	PCA 2 (r)
Average	0.80*	-0.40*	-0.88*	0.24*
Minimum	-0.53*	-0.76*	-0.26*	0.87*
Maximum	0.95*	-0.16*	-0.98*	-0.06*
Pulse	0.97*	0.01	-0.97*	-0.15*
Heating	0.78*	0.26*	-0.74*	-0.38*
Cooling	-0.81*	0.26*	0.81*	0.33*

*$p < 0.01$.

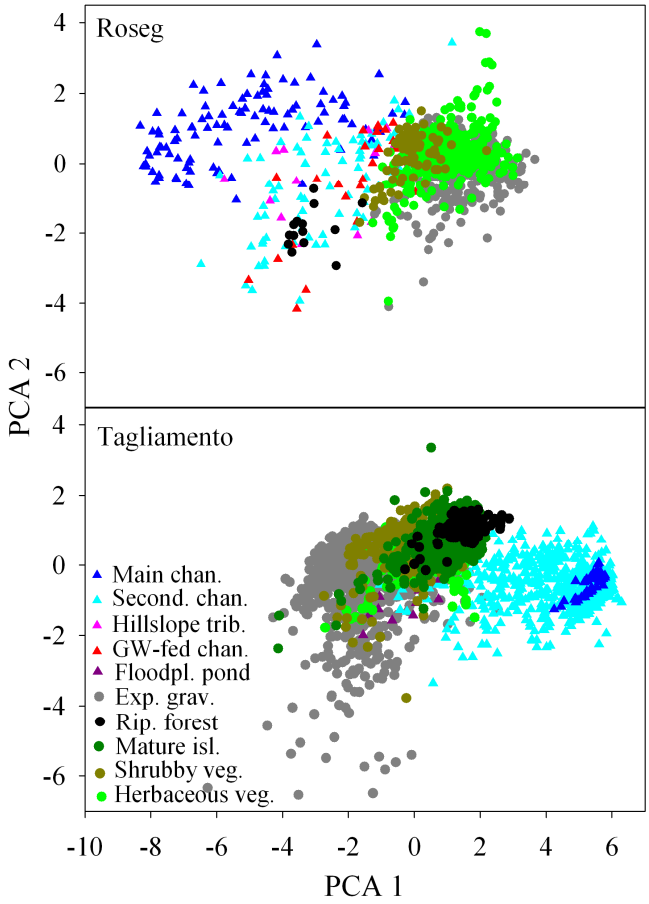

Figure 6. Principal component analysis (PCA) of the Roseg and Tagliamento floodplains based on six thermal variables (see text). Closed triangles show aquatic habitats and closed circles show terrestrial habitats. Only points from the regular network falling within the habitat polygons shown in Figure 1 are represented. For correlations among thermal variables and the factor scores of the components of the PCA see Table 4.

Vertical kinetic temperature distribution in unsaturated gravel sediment deposits

Within the unsaturated gravel sediment deposits kinetic temperature increased with sediment depth during night time, whereas during day time - after a period of rapid temperature alteration in the early morning - it sharply decreased with sediment depth (Figure 7). The diel kinetic temperature pulse ranged from 40.4°C (sediment surface) to 2.7°C (29 cm sediment depth) in the Roseg floodplain and from 28°C (sediment surface) to 2.6°C (29 cm) in the Tagliamento floodplain. Over the top 29 cm sediment layer, daily average kinetic temperature decreased by 5.2°C (Roseg) and 2°C (Tagliamento). Furthermore, maximum kinetic temperature decreased vertically by 30.4°C (Roseg) and 19.9°C (Tagliamento). The transfer time of a thermal pulse from the air (100 cm above ground level) into the sediment ranged from 100 to 300 min (both floodplains). In the Tagliamento gravel sediment deposits, there was a delay of 90 min between the maximum air temperature and the maximum kinetic temperature at the sediment surface, 130 min at 5 cm depth, 160 min at 10 cm depth, and 240

min at 15 cm depth (Figure 7). In the Roseg gravel sediment deposits, there was a delay of 60 min between the maximum air temperature and the maximum kinetic temperature at the surface, 150 min at 5 cm depth, and 260 min at 10 and 15 cm depth (Figure 7).

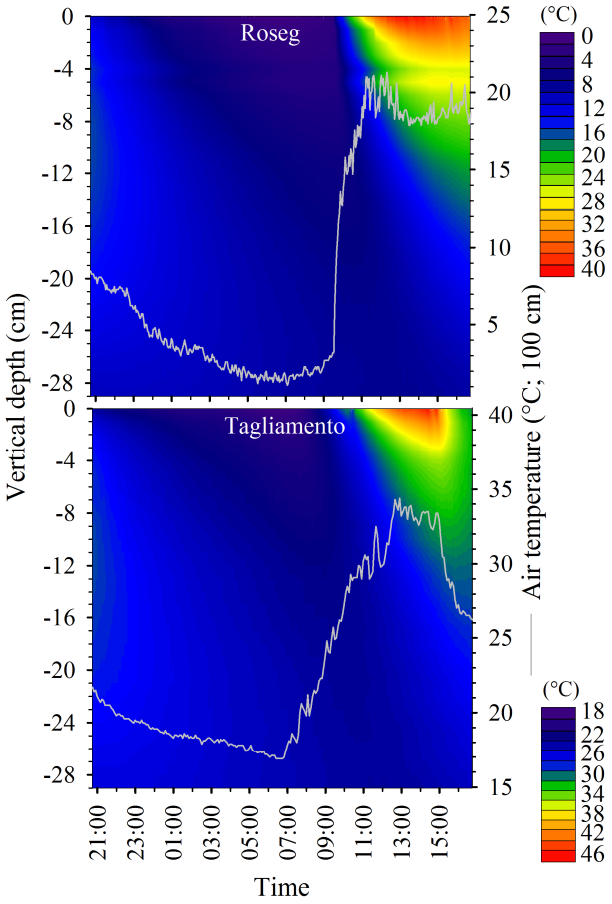

Figure 7. Vertical kinetic temperature distribution (2°C steps) in unsaturated gravel sediment deposits of the Roseg (22-23.08.2004) and Tagliamento (31.08-01.09.2005) floodplains. Surface kinetic temperature (0 cm) and air temperature (100 cm above ground level) are also shown.

Discussion

Remotely sensed IR imagery provides the capacity to map thermal heterogeneity of entire landscapes at a high spatial resolution, a capability not possible using ground-based methods (e.g. Torgersen et al. 1999, 2001; Loheide and Gorelick 2006). In this study, IR imagery allowed for quantification of surface temperature dynamics in two near-natural Alpine river floodplains characterized by a complex mosaic of habitat patches. The diel dynamics of surface temperature varied considerably across the entire river floodplain system. For example, the thermal regime of terrestrial habitat patches changed with vegetation cover, corresponding to the succession gradient characteristic for braided river floodplains (Ward et

al. 2002; Naiman et al. 2005). Among the calculated thermal variables, diel temperature pulse and maximum daily temperature separated best the individual habitat types in both river floodplains. Moreover, within the top 29 cm sediment layer of the unsaturated zone of gravel sediment deposits, spatiotemporal thermal heterogeneity was almost as high as the thermal heterogeneity across the entire floodplain surface. Results of this study clearly emphasize that traditional ground-based techniques most likely underestimate the spatiotemporal thermal heterogeneity across the river floodplain mosaic as well as within the individual habitat. This may have major consequences in calculating and interpreting the effects of temperature on biodiversity patterns and ecosystem processes.

Spatiotemporal thermal variability at the floodplain scale

For a comprehensive thermal characterization of river floodplains both aquatic and terrestrial habitats must simultaneously be investigated. Exposed gravel sediments exhibited large diel temperature fluctuations, with maximum surface temperatures of up to 45°C during a hot summer day; whereas the main channel and upwelling ground waters provided permanent cool habitat patches (see also Torgersen et al. 1999; Baxter and Hauer 2000). As expected, vegetation cover added to the thermal heterogeneity at the floodplain scale as patches of various vegetation cover exhibited distinct thermal properties. For example, woody vegetation cover leads to reduced penetration of solar shortwave radiation at the ground (increased absorption and reflection by the canopy), stores heat under the vegetation canopy, and reduces wind currents. In contrast, open surfaces (that is, exposed gravel and herbaceous vegetation cover) exhibit large diel temperature fluctuations because of distinct heat loss at night and direct exposure to solar shortwave radiation during the day. Carlson and Arthur (2000) reported that bare ground and sparsely vegetated surfaces displayed a large variation in radiant surface temperature. The variation decreased - as confirmed in this study - with increasing vegetation density. Densely vegetated habitat types such as the riparian forest exhibited higher surface temperatures during night time and cooler temperatures during day time, as well as a lower diel temperature pulse (amplitude), compared to other terrestrial habitat types (e.g. Figure 3, Table 3; Chudnovsky et al. 2004). Daytime cooling was most probably a consequence of latent heat loss through evapotranspiration resulting in reduced longwave radiation emitted from the ground and the leaves. During the night and early morning hours, heat is trapped and stored by the vegetation coverage resulting in reduced direct radiation to the sky (Dimoudi and Nikolopoulou 2003; Dousset and Gourmelon 2003; Chudnovsky et al. 2004). In contrast, the lack of an evaporative cooling effect explains the very high surface temperature variation on exposed gravel deposits.

The aquatic habitat types also contributed to the thermal complexity in both floodplains. The variation of water temperature is mainly controlled by air temperature and incoming shortwave solar radiation (e.g. Crisp and Howson 1982; Evans et al. 1998). However, because aquatic habitat types in both floodplains were characterized by channels of different hydrology and morphology, their heat budget and therefore water temperature differed over the 24 h cycles. Channel morphology, substratum material, riparian vegetation, and water source may control heat gains and losses and therefore cause strong temperature gradients over short distances (Ward 1985; Webb and Zhang 1997, 1999; Evans et al. 1998; Malard et al. 2001). For example, Arrigoni et al. (2008) found that, compared to the main channel's diel cycle, hyporheic discharge locations typically had similar daily mean temperatures, but smaller diel ranges, creating diverse daytime and nighttime mosaics of surface water temperatures across main, side, and spring channels, despite only minor differences in daily mean temperatures among the channels. Furthermore, in the present study, the complex high spatiotemporal variability was also likely related to the influence of subsurface flows to different gravel areas of the floodplains. This may explain the greater dispersion of the floodplain gravel dots in the Tagliamento PCA (Figure 6).

The Tagliamento floodplain exhibited higher average daily temperatures than the Roseg floodplain mainly because of prevailing higher air temperature. Differences between the two floodplains in terms of diel temperature pulses were most likely related to differences in the incoming solar shortwave radiation (higher in the Roseg floodplain), in the amount of water (for example, less water in the main channel and secondary channels in the Roseg floodplain), as well as in the vegetation cover (less dense in the Roseg floodplain). Higher values of diel pulses in the terrestrial habitat types of the Roseg floodplain may have been influenced by high heat loss at night, direct solar radiation during the day, and reduced evaporative cooling effect.

Vertical kinetic temperature distribution in unsaturated gravel sediment deposits

Braided gravel-bed rivers are covered by thick layers of unsaturated sediments. This unsaturated zone is likely the most extensive terrestrial habitat along gravel-bed rivers; potentially serving as an important hibernation site or as flood-refugia for terrestrial arthropods (Tockner et al. 2006). Vertical strong temperature gradients in both terrestrial (this study) and aquatic (Malard et al. 2001) habitats were found in the Roseg and Tagliamento floodplains. A maximum vertical temperature gradient of approximately 30°C over a vertical distance of 29 cm during day time in the Roseg floodplain approximately corresponds to the maximum horizontal thermal range over a distance of several hundred meters across the

floodplain surface at noon (Figure 3). In fact, in the Tagliamento a maximum vertical thermal difference of up to 20°C at a given time during the day corresponds to the observed difference along the entire 170-km long main river channel (Arscott et al. 2001).

In this study, vertical temperature patterns were only quantified in unsaturated gravel sediment deposits, but the magnitude of the observed changes over depth stresses the importance of considering the vertical dimension as a third spatial dimension in future studies. The thermal inertia observed in the unsaturated gravel layers may result from the interaction of the vertical heat transfer with the specific heat capacity of the sediments, which again was most likely influenced by the water content. The low temporal variation in temperature in the floodplain sediment deposits at the subsurface level might explain the reduction in the diel temperature pulse in emerging hyporheic flows reported elsewhere, including the same Tagliamento floodplain (Acuña and Tockner 2009).

Ecological implications

Lateral and vertical thermal heterogeneity has been recognized as an important aspect in many ecological studies (e.g. Brunke and Gonser 1997; Arscott et al. 2001; Ebersole et al. 2003; Uehlinger et al. 2003). The application of non-invasive IR imagery offers a rapid insight into the temperature regime along river corridors and helps to identify both natural and anthropogenic drivers that may influence thermal landscapes. Furthermore, this technique allows for quantification of spatiotemporal thermal heterogeneity within the individual habitat types (see PCA results and tables), to detect critical hot and cold spots as well as hot and cold moments (sensu McClain et al. 2003), to identify the key thermal properties (diel pulse and maximum temperature) that characterize these habitat patches, as well as to quantify the rapidly shifting thermal mosaic at the floodplain scale. This information is expected to be crucial for predicting the effect of environmental heterogeneity on ecosystem processes, biodiversity patterns, and animal behavior, therefore for establishing adequate conservation strategies (e.g. Fausch et al. 2002). How do organisms exploit temporally dynamic and spatially complex habitats? Does thermal heterogeneity increase the resilience of an ecosystem? How do temperature and flow dynamics interact and control ecosystem processes?

IR imagery may allow quantifying the distribution of thermal refugia, as well as the utilization of these refugia by aquatic and terrestrial animals. The provision of thermal refugia during extreme environmental conditions, such as heat waves, is crucial for the long-term survival of many aquatic (e.g. Torgersen et al. 1999; Baxter and Hauer 2000) and terrestrial (e.g. Schwarzkopf and Alford 1996; Seebacher and Alford 2002) organisms. IR imagery may

help in understanding the habitat requirements of many aquatic insects, as well as pond-breeding amphibians, which have complex life cycles with terrestrial stages. The life time fitness of these species is affected by the environmental conditions during the larval and adult stages, respectively (e.g. Bonte et al. 2008; Richter et al. 2008). Pond-breeding amphibians spend most of their life in terrestrial habitats where they actively regulate their body temperature and loss of body water through their skin using thermal shelter. Therefore, home range placement of amphibians depends on the thermal properties of the individual habitat types (e.g. large wood deposits that provide thermal refugia), as well as on the spatial configuration of these habitats, as demonstrated for the Tagliamento floodplain (Indermaur et al. 2009a, b). Moreover, sympatric species differ in their thermal preferences within the same habitat type, implying that thermal heterogeneity may facilitate the co-existence of species (Indermaur et al. 2009b). Hence, traditional methods for measuring temperature in different habitats (e.g. one or few temperature loggers per habitat type) may not provide the required spatial information for explaining the distribution and behavior of river and floodplain animals within such complex landscapes.

Ecosystem processes that are highly sensitive to temperature, such as respiration, might closely follow diel patterns of temperature (Acuña et al. 2008). In particular distinct diel temperature pulses are expected to be highly ecologically relevant - more relevant than the average daily temperature. Ecosystem processes that are controlled by microbial communities (e.g. sediment respiration or leaf litter decomposition) may quickly respond and adjust to these diel temperature pulses (Dang et al. 2009; and references therein). IR imagery can provide rapid and detailed thermal characterization of river landscapes and might help detecting spatiotemporal changes and trends in temperature patterns, therefore increasing our understanding of ecosystem processes. Furthermore, this technique can reveal information on thermal heterogeneity at a spatial and temporal resolution relevant to scale-up ecosystem processes from point measurements to entire river floodplains.

The high thermal heterogeneity within the top sediment layer may influence the spatial distribution of epigeic arthropods. Terrestrial invertebrates may actively seek refuge in deeper gravel sediment layers to avoid heat stress in summer as well as surface freezing during winter. Similarly, vertical migration in response to floods has been identified as an important survival strategy of many terrestrial invertebrates of floodplains (Adis and Junk 2002). The steep vertical temperature gradients might be also reflected in a gradient in the metabolic rates at which ecosystem processes operate, as most processes are temperature driven (Gillooly et al. 2001; Brown et al. 2004). Ignoring vertical temperature gradients might obscure the

relationship between measured ecosystem processes (that are usually integrative over depth and expressed per surface area unit; Döring 2007) and measured surface temperature. It is therefore advisable to consider those temperature gradients when studying ecosystem processes in habitats such as the bare gravel sediment deposits in floodplains.

Finally, we expect that we can greatly attenuate the effects of global warming by manipulating specific characteristics of landscape surfaces. However, ignoring small-scale and short-term thermal heterogeneity may lead to erroneous conclusions about the ecological consequences of future air temperature increases.

Acknowledgments

The authors are indebted to C. Tanner (QC-Expert, Spin-Off of the Swiss Federal Laboratories for Material Testing and Research, EMPA) for his professional support with the thermal data acquisition. We thank two anonymous reviewers for their constructive comments and suggestions that helped to improve the manuscript. This study was supported by the Swiss Federal Institute of Aquatic Science and Technology (EAWAG), the Leibniz-Institute of Freshwater Ecology and Inland Fisheries (IGB), and a Marie Curie Intra-European Fellowship to V. Acuña within the 6th European Community Framework Programme.

Appendices

Appendices A-C provide supplementary information on thermal infrared (IR) imagery and potential error sources.

Appendix A. Thermal IR emissivity of the targeted materials in the studied floodplains

All targeted materials in the studied floodplains had theoretical emissivity values (ε) close to 1 (at a zenith angle of 0° and thermal band of 8-14 μm). Water: ε = 0.983 (Cuenca and Sobrino 2004), riparian forest Roseg: ε = 0.974-0.987 (pine leaf; MODIS 2010), riparian forest and mature islands Tagliamento: ε = 0.968-0.978 (oak leaf; MODIS 2010), shrubby vegetation: ε = 0.968-0.978 (oak leaf; MODIS 2010), herbaceous vegetation: ε = 0.976-0.994 (green grass and dry leaves over a sample of organic soil approximately 40% covered; Snyder et al. 1997), exposed gravel: ε = 0.972 (Cuenca and Sobrino 2004). However, there are several aspects that can affect emittance (the terms emissivity and emittance are often used interchangeably, however, emissivity refers to the properties of a material and emittance to the properties of a particular object/surface) such as the zenith angle and the wind speed.

Zenith angle is known to have little effect at angles ≤30° (Sobrino and Cuenca 1999; Cuenca and Sobrino 2004). Results of those authors showed a general decrease of the emittance with increasing angle for different surface materials (water, clay, sand, slime, loam, gravel, and grass). For example, angular variation of relative-to-nadir emittance of water can decrease by 0.023 from 0° to 60° (Cuenca and Sobrino 2004). The effect of wind speeds less than 15 m s^{-1} (as in this study) on water surfaces is small at zenith angles ≤30° but becomes relevant at angles ≥70° (Masuda et al. 1988). It must be pointed out that tables of emissivity values of materials can provide only a rough orientation for the properties of the respective object/surface, because the emittance depends on the nature of the actual surface (e.g. surface smoothness, mix of materials, surface finish, oxide film on the surface, and so on), and therefore, might vary. However, within the long-wave spectral ranges a multitude of (non-metallic) materials show high and relatively constant emittance, regardless of surface structure. Therefore, although surface emittance may vary at high zenith angles (as in this study) and the surface properties may change between day and night, these variations are assumed to be small and therefore thermal emissivity is assumed to be uniform (ε = 1). Applying a thermal emissivity of 0.96 (similar environmental conditions, radiant temperature: 10-30°C) would lead to a temperature change of approximately -0.6 to +0.2°C, which is smaller or equal than the accuracy of the IR camera.

Appendix B. Potential error for IR temperature measurements due to reflected radiation from the sky and the surrounding environment

Theoretically, the ambient (environmental) temperature can be considered as the temperature of an adiabatic surface which is exposed to the outside air, the shortwave solar radiation and the atmospheric long-wave radiation. For this extreme situation, equation (1) gives a rough, but correct approximation for the ambient temperature T_{amb}:

$$T_{amb} = T_{air} + (\alpha_s \cdot I_s - \varepsilon \cdot \Delta IR) / h_\varepsilon \quad (1)$$

where T_{air} is air temperature (°K), α_s is the solar absorption of the surface, I_s is solar radiation (W m^{-2}), ε is the hemispherical surface emissivity, ΔIR is IR heat sink of the sky calculated with the procedure given by Frank (1986), and h_e is the external surface heat transfer coefficient (W m^{-2} $°K^{-1}$). The deviation between radiant surface temperature and kinetic surface temperature of the targeted objects can be estimated using equations (2) and (3):

$$T_{rad} = \sqrt[n]{\varepsilon(\varphi) \cdot T_{sur}^n + (1 - \varepsilon(\phi)) \cdot T_{amb}^n} \quad (2)$$

$$T_{sur} = \sqrt[n]{\frac{T_{rad}^n - (1 - \varepsilon(\phi)) \cdot T_{amb}^n}{\varepsilon(\varphi)}} \quad (3)$$

where $\varepsilon(\varphi)$ is the angular emissivity as function of the zenith angle (φ). T_{rad} is the radiant (measured with the IR camera) surface temperature (°K) of the targeted object, and T_{sur} is the kinetic surface temperature of the object (°K). In the applied Stefan Boltzmann law in equations (2) and (3), the exponent n is 4 for an unlimited IR spectrum. For the limited spectral band from 8-13 µm the value used is 5 according to Goldstein (1978).

These equations were used to correct the radiant temperatures from one of the studied aquatic habitats, a secondary channel in the Roseg floodplain (Figure 8). Thus, radiant temperatures for this secondary channel overestimated the kinetic temperatures (measured with temperature loggers) during the day (maximum difference of 6.7ºC) and underestimated them during the night (maximum difference of -4.6ºC). During the night the error was smaller because ambient temperature and target surface temperature were more similar. The errors in the estimations persisted despite the correction performed with equations (2) and (3), but the kinetic temperatures were only overestimated by 1-3ºC during the day and <2ºC during the night (Figure 8). This kind of correction of the radiant temperatures was not always possible as several variables could only be estimated (e.g. solar absorption of the ambient surface, part-shading on the terrain). Accordingly, this correction was not applied to all the radiant temperatures, so that only the uncorrected radiant temperatures are discussed in this study. Even though this error may reduce the validity of absolute temperature measurements, temperature differences in the same image or temperature variation in image sequences could be well characterized.

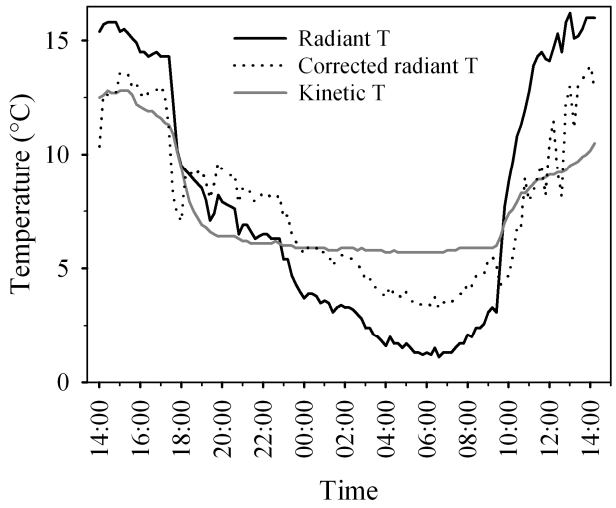

Figure 8. Uncorrected radiant and kinetic temperatures, and corrected radiant temperatures for a secondary channel in the Roseg floodplain (22-23.08.2004; with an assumption of $\varepsilon(\varphi)$ = 0.80 and φ = 75°). Corrected radiant temperatures were calculated using equations (2) and (3).

Average temperatures in aquatic habitat types were slightly overestimated by the IR measurements in main and secondary channels in both floodplains (average difference between 0.4 and 0.9ºC), while radiant temperature in groundwater-fed channels in the Roseg floodplain was slightly underestimated (Table 5).

Table 5. Average (± standard deviation) difference between radiant and kinetic temperature (radiant - kinetic; °C) in selected habitat types.

Floodplain	Habitat	Average
Roseg	Main channel	0.4 ± 1.7
	Secondary channel	0.7 ± 3.1
	Groundwater-fed channel	-1.1 ± 3.2
	Exposed gravel	-4.8 ±6.0
Tagliamento	Main channel	0.9 ± 0.6
	Secondary channel	0.9 ± 0.6
	Exposed gravel	-2.8 ± 1.8
	Riparian forest	1.6 ± 1.3
	Mature islands	0.1 ± 1.3
	Shrubby vegetation	-0.6 ± 1.9

Positive values imply overestimation by radiant temperature and negative values imply underestimation.

Average temperature overestimation in aquatic habitats was similar in magnitude (0.1-1.9°C; images taken from aircraft or handheld cameras with pixel sizes from 0.2-5 m) to those reported in other studies (Torgersen et al. 2001; Cherkauer et al. 2005; Handcock et al. 2006; Loheide and Gorelick 2006; Cardenas et al. 2008). The highest underestimation of average surface temperature was found in exposed gravel in both floodplains (Table 5). High standard deviation values were probably related to the difference between night and day temperature differences.

Appendix C. Potential error for IR temperature measurements due to the effect of surface roughness

Because of the important differences between kinetic and radiant temperatures on exposed gravel especially during sun hours, the effect of coarse sediment surface roughness (which could be one of the reasons for those differences) on the accuracy of temperatures obtained from the IR images was experimentally tested. Digital and IR images were taken at three different positions with respect to the sun (with the sun behind, at the side, and in front), to simulate the daily solar cycle, on an area of approximately 0.5 × 0.5 m containing gravel and some pebbles. By incrementing the contrast of the digital pictures with the freely available

image processing software XnView (version 1.21, by Pierre-e Gougelet) and using histograms, the fraction of "dark surfaces" (essentially shadows) was calculated.

Zenith angle of the IR camera was approximately 45°, weather was sunny (sun was at approximately 44.5º) with an air temperature of 23.5°C and low wind velocities (<3 m s^{-1}). Results showed that when the camera had the sun in front or at the side, many substrate particles appeared shaded, and this was in turn detected by the IR camera as a geometrical cold fraction, which thus had a strong influence on the recorded radiant temperature (Figure 9). Consequently, given certain roughness conditions, the deviation due to surface roughness will show a daily and a seasonal variation due to changes in the sun's position, with minimum deviations during summer midday and no effect a few hours after sunset.

Finally, additional research is needed for improving the accuracy and reducing the uncertainties associated with IR imagery in a landscape as complex as the studied floodplains.

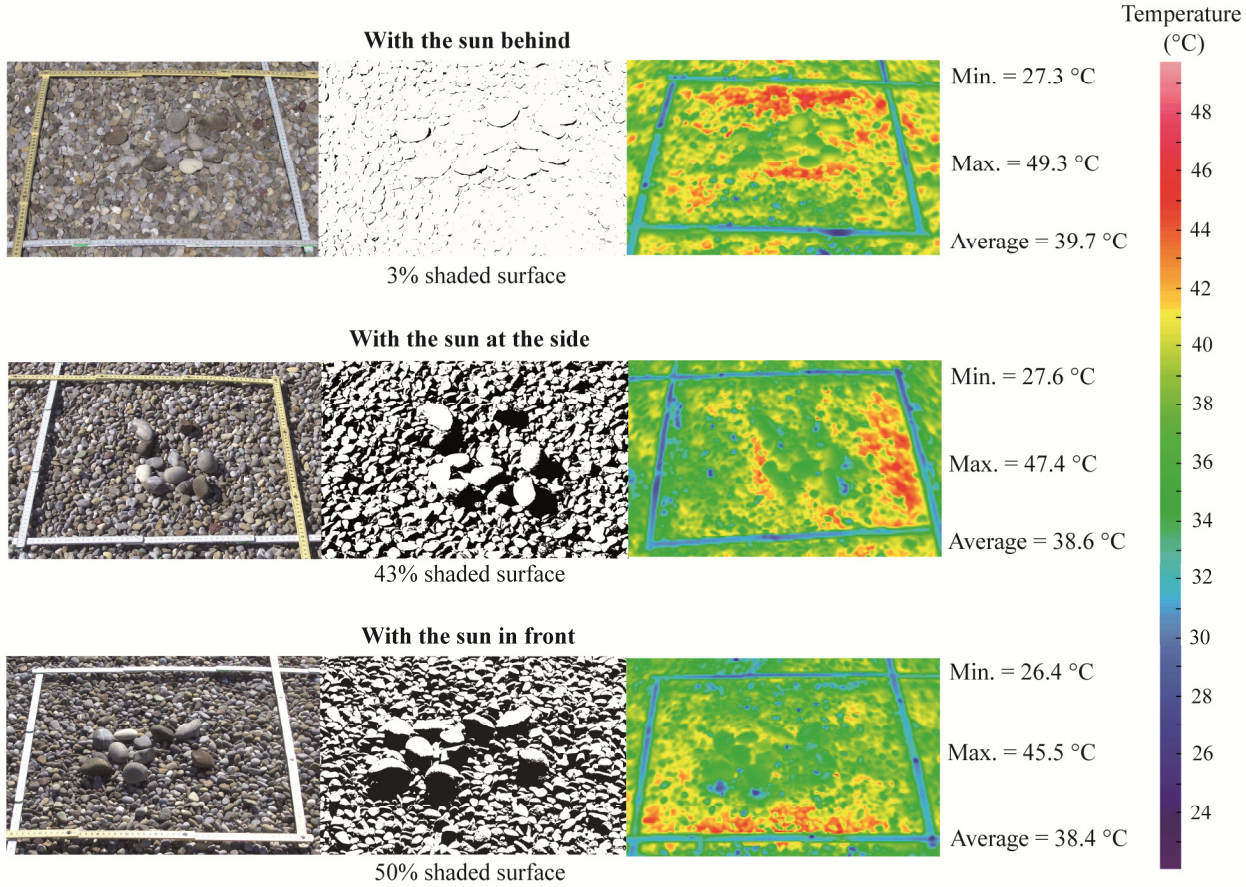

Figure 9. Effect of surface roughness on radiant temperature based of three different camera positions with respect to the position of the sun. Frame: 0.5 × 0.5 m.

References

Acuña V, Wolf A, Uehlinger U, Tockner K. 2008. Temperature dependence of stream benthic respiration in an Alpine river network with relevance to global warming. *Freshwater Biology* 53: 2076-2088.

Acuña V, Tockner K. 2009. Surface-subsurface water exchange rates along alluvial river reaches control the thermal patterns in an Alpine river network. *Freshwater Biology* 54: 306-320.

Adis J, Junk WJ. 2002. Terrestrial invertebrates inhabiting lowland river floodplains of Central Amazonia and Central Europe: a review. *Freshwater Biology* 47: 711-731.

Amstrup SC, York G, McDonald TL, Nielson R, Simac K. 2004. Detecting denning polar bears with forward-looking infrared (FLIR) imagery. *Bioscience* 54: 337-344.

Anderson JM, Wilson SB. 1984. The physical basis of current infrared remote-sensing techniques and the interpretation of data from aerial surveys. *International Journal of Remote Sensing* 5: 1-18.

Anderson JM, Duck RW, McManus J. 1995. Thermal radiometry - a rapid means of determining surface-water temperature - variations in lakes and reservoirs. *Journal of Hydrology* 173: 131-144.

Arrigoni AS, Poole GC, Mertes LAK, O'Daniel SJ, Woessner WW, Thomas SA. 2008. Buffered, lagged, or cooled? Disentangling hyporheic influences on temperature cycles in stream channels. *Water Resources Research* 44: W09418.

Arscott DB, Tockner K, Ward JV. 2001. Thermal heterogeneity along a braided floodplain river (Tagliamento River, northeastern Italy). *Canadian Journal of Fisheries and Aquatic Sciences* 58: 2359-2373.

Baxter CV, Hauer FR. 2000. Geomorphology, hyporheic exchanges, and selection of spawning habitat by bull trout (*Salvelinus confluentus*). *Canadian Journal of Fisheries and Aquatic Sciences* 57: 1470-1481.

Bernatas S, Nelson L. 2004. Sightability model for California bighorn sheep in canyonlands using forward-looking infrared (FLIR). *Wildlife Society Bulletin* 32: 638-647.

Bonte D, Travis JMJ, De Clercq N, Zwertvaegher I, Lens L. 2008. Thermal conditions during juvenile development affect adult dispersal in a spider. *Proceedings of the National Academy of Sciences* 105: 17000-17005.

Brown JH, Gillooly JF, Allen AP, Savage VM, West GB. 2004. Toward a metabolic theory of ecology. *Ecology* 85: 1771-1789.

Brunke M, Gonser T. 1997. The ecological significance of exchange processes between rivers and groundwater. *Freshwater Biology* 37: 1-33.

Caissie D. 2006. The thermal regime of rivers: a review. *Freshwater Biology* 51: 1389-1406.

Cardenas MB, Harvey JW, Packman AI, Scott DT. 2008. Ground-based thermography of fluvial systems at low and high discharge reveals potential complex thermal heterogeneity driven by flow variation and bioroughness. *Hydrological Processes* 22: 980-986.

Carlson TN, Arthur ST. 2000. The impact of land use - land cover changes due to urbanization on surface microclimate and hydrology: a satellite perspective. *Global and Planetary Change* 25: 49-65.

Cherkauer KA, Burges SJ, Handcock RN, Kay JE, Kampf SK, Gillespie AR. 2005. Assessing satellite-based and aircraft-based thermal infrared remote sensing for monitoring Pacific Northwest river temperature. *Journal of the American Water Resources Association* 41: 1149-1159.

Chudnovsky A, Ben-Dor E, Saaroni H. 2004. Diurnal thermal behaviour of selected urban objects using remote sensing measurements. *Energy and Buildings* 36: 1063-1074.

Crisp DT, Howson G. 1982. Effect of air-temperature upon mean water temperature in streams in the Northern Pennines and English Lake District. *Freshwater Biology* 12: 359-367.

Cuenca J, Sobrino JA. 2004. Experimental measurements for studying angular and spectral variation of thermal infrared emissivity. *Applied Optics* 43: 4598-4602.

Dang CK, Schindler M, Chauvet E, Gessner MO. 2009. Temperature oscillation coupled with fungal community shifts can modulate warming effects on litter decomposition. *Ecology* 90: 122-131.

Dimoudi A, Nikolopoulou M. 2003. Vegetation in the urban environment: microclimatic analysis and benefits. *Energy and Buildings* 35: 69-76.

Döring M. 2007. *Environmental Heterogeneity and Respiration in a Dynamic River Corridor: Structural Properties and Functional Performance*. Dissertation ETH-Zurich no. 17046.

Dousset B, Gourmelon F. 2003. Satellite multi-sensor data analysis of urban surface temperatures and landcover. *ISPRS Journal of Photogrammetry and Remote Sensing* 58: 43-54.

Dunckel AE, Cardenas MB, Sawyer AH, Bennett PC. 2009. High-resolution in situ thermal imaging of microbial mats at El Tatio Geyser, Chile, shows coupling between community color and temperature. *Geophysical Research Letters* 36: L23403.

Ebersole JL, Liss WJ, Frissell CA. 2003. Cold water patches in warm streams: physicochemical characteristics and the influence of shading. *Journal of the American Water Resources Association* 39: 355-368.

Elliott JM, Hurley MA. 2001. Modelling growth of brown trout, *Salmo trutta*, in terms of weight and energy units. *Freshwater Biology* 46: 679-692.

Emery WJ, Yu Y. 1997. Satellite sea surface temperature patterns. *International Journal of Remote Sensing* 18: 323-334.

Evans EC, McGregor GR, Petts GE. 1998. River energy budgets with special reference to river bed processes. *Hydrological Processes* 12: 575-595.

Fausch KD, Torgersen CE, Baxter CV, Li HW. 2002. Landscapes to riverscapes: bridging the gap between research and conservation of stream fishes. *Bioscience* 52: 483-498.

Frank T. 1986. *Surface Temperatures of Sunlit Glazing and their Impact on the Indoor Climate and Comfort*. NEFF Research Report 266 (in German), EMPA, Dübendorf, Switzerland.

Gillooly JF, Brown JH, West GB, Savage VM, Charnov EL. 2001. Effects of size and temperature on metabolic rate. *Science* 293: 2248-2251.

Goldstein RJ. 1978. Application of aerial infrared thermography to the measurement of building heat loss. *ASHRAE Transactions* 84: 207-226.

Handcock RN, Gillespie AR, Cherkauer KA, Kay JE, Burges SJ, Kampf SK. 2006. Accuracy and uncertainty of thermal-infrared remote sensing of stream temperatures at multiple spatial scales. *Remote Sensing of Environment* 100: 427-440.

Hannah DM, Webb BW, Nobilis F. 2008. River and stream temperature: dynamics, processes, models and implications - preface. *Hydrological Processes* 22: 899-901.

Hartz DA, Prashad L, Hedquist BC, Golden J, Brazel AJ. 2006. Linking satellite images and hand-held infrared thermography to observed neighborhood climate conditions. *Remote Sensing of Environment* 104: 190-200.

Hook SJ, Prata FJ, Alley RE, Abtahi A, Richards RC, Schladow SG, Pálmarsson SO. 2003. Retrieval of lake bulk and skin temperatures using Along-Track Scanning Radiometer (ATSR-2) data: a case study using Lake Tahoe, California. *Journal of Atmospheric and Oceanic Technology* 20: 534-548.

Indermaur L, Gehring M, Wehrle W, Tockner K, Näf-Dänzer B. 2009a. Behavior-based scale definitions for determining individual space use: requirement of two amphibians. *The American Naturalist* 173: 60-71.

Indermaur L, Winzeler T, Schmidt BR, Tockner K, Schaub M. 2009b. Differential resource selection within shared habitat types across spatial scales in sympatric toads. *Ecology* 90: 3430-3444.

IPCC. 2007. *Intergovernmental Panel on Climate Change*. Fourth assessment report on climate change. http://www.ipcc.ch/ (last accessed 20th April 2010).

Kay JE, Kampf SK, Handcock RN, Cherkauer KA, Gillespie AR, Burges SJ. 2005. Accuracy of lake and stream temperatures estimated from thermal infrared images. *Journal of the American Water Resources Association* 41: 1161-1175.

Lagios E, Vassilopoulou S, Sakkas V, Dietrich V, Damiata BN, Ganas A. 2007. Testing satellite and ground thermal imaging of low-temperature fumarolic fields: the dormant Nisyros volcano (Greece). *ISPRS Journal of Photogrammetry and Remote Sensing* 62: 447-460.

Langhans SD, Tiegs SD, Gessner MO, Tockner K. 2008. Leaf decomposition heterogeneity across a riverine floodplain mosaic. *Aquatic Sciences* 70: 337-346.

LeDrew EF, Franklin SE. 1985. The use of thermal infrared imagery in surface current analysis of a small lake. *Photogrammetric Engineering and Remote Sensing* 51: 565-573.

Loheide SP, Gorelick SM. 2006. Quantifying stream-aquifer interactions through the analysis of remotely sensed thermographic profiles and in situ temperature histories. *Environmental Science and Technology* 40: 3336-3341.

Malard F, Mangin A, Uehlinger U, Ward JV. 2001. Thermal heterogeneity in the hyporheic zone of a glacial floodplain. *Canadian Journal of Fisheries and Aquatic Sciences* 58: 1319-1335.

Masuda K, Takashima T, Takayama Y. 1988. Emissivity of pure and sea waters for the model sea-surface in the infrared window regions. *Remote Sensing of Environment* 24: 313-329.

McClain ME, Boyer EW, Dent CL, Gergel SE, Grimm NB, Groffman PM, Hart SC, Harvey JW, Johnston CA, Mayorga E, McDowell WH, Pinay G. 2003. Biogeochemical hot spots and hot moments at the interface of terrestrial and aquatic ecosystems. *Ecosystems* 6: 301-312.

MODIS. 2009. *Moderate Resolution Imaging Spectrometer*. UCSB (University of California, Santa Barbara, CA, USA) emissivity library. http://www.icess.ucsb.edu/modis/EMIS/html/em.html (last accessed 20th April 2010).

Naiman RJ, Décamps H, McClain ME. 2005. *Riparia: Ecology, Conservation, and Management of Streamside Communities*. Elsevier Academic Press: Amsterdam; 430.

Naugle DE, Jenks JA, Kernohan BJ. 1996. Use of thermal infrared sensing to estimate density of white-tailed deer. *Wildlife Society Bulletin* 24: 37-43.

Parkinson CL. 2003. Aqua: an earth-observing satellite mission to examine water and others climate variables. *IEEE Transactions on Geoscience and Remote Sensing* 41: 173-183.

Perry JN, Liebhold AM, Rosenberg MS, Dungan J, Miriti M, Jakomulska A, Citron-Pousty S. 2002. Illustrations and guidelines for selecting statistical methods for quantifying spatial pattern in ecological data. *Ecography* 25: 578-600.

Perryman WL, Donahue MA, Laake JL, Martin TE. 1999. Diel variation in migration rates of eastern pacific gray whales measured with thermal imaging sensors. *Marine Mammal Science* 15: 426-445.

Richter O, Suhling F, Mueller O, Kern D. 2008. A model for predicting the emergence of dragonflies in a changing climate. *Freshwater Biology* 53: 1868-1880.

Schwarzkopf L, Alford RA. 1996. Desiccation and shelter-site use in a tropical amphibian: comparing toads with physical models. *Functional Ecology* 10: 193-200.

Seebacher F, Alford RA. 2002. Shelter microhabitats determine body temperature and dehydration rates of a terrestrial amphibian (*Bufo marinus*). *Journal of Herpetology* 36: 69-75.

Selker JS, Thévenaz L, Huwald H, Mallet A, Luxemburg W, van de Giesen N, Stejskal M, Zeman J, Westhoff M, Parlange MB. 2006. Distributed fiber-optic temperature sensing for hydrologic systems. *Water Resources Research* 42: W12202.

Smikrud KM, Prakash A, Nicholos JV. 2008. Decision-based fusion for improved fluvial landscape classification using digital aerial photographs and forward looking infrared images. *Photogrammetric Engineering and Remote Sensing* 74: 903-911.

Snyder WC, Wan ZM, Zhang YL, Feng YZ. 1997. Thermal infrared (3-14 μm) bidirectional reflectance measurements of sands and soils. *Remote Sensing of Environment* 60: 101-109.

Sobrino JA, Cuenca J. 1999. Angular variation of thermal infrared emissivity for some natural surfaces from experimental measurements. *Applied Optics* 38: 3931-3936.

Stanford JA, Lorang MS, Hauer FR. 2005. The shifting habitat mosaic of river ecosystems. *Verhandlungen der Internationalen Vereinigung für Theoretische und Angewandte Limnologie* 29: 123-136.

Thyssen N, Erlandsen M, Jeppesen E, Ursin C. 1987. Reaeration of oxygen in shallow, macrophyte rich streams: I. Determination of the reaeration rate coefficient. *Internationale Revue der gesamten Hydrobiologie und Hydrographie* 72: 405-429.

Tockner K, Malard F, Ward JV. 2000. An extension of the flood pulse concept. *Hydrological Processes* 14: 2861-2883.

Tockner K, Malard F, Uehlinger U, Ward JV. 2002. Nutrients and organic matter in a glacial river-floodplain system (Val Roseg, Switzerland). *Limnology and Oceanography* 47: 266-277.

Tockner K, Ward JV, Arscott DB, Edwards PJ, Kollmann J, Gurnell AM, Petts GE, Maiolini B. 2003. The Tagliamento River: an ecosystem of European importance. *Aquatic Sciences* 65: 239-253.

Tockner K, Karaus U, Paetzold A, Claret C, Zettel J. 2006. Ecology of braided rivers. In: *Ecology of Braided Rivers*, Sambrook Smith GH, Best JL, Bristow C, Petts GE (eds). IAS Special Publication, Blackwell Science: Oxford; 339-358.

Tockner K, Lorang MS, Stanford JA. 2010. River flood plains are model ecosystems to test general hydrogeomorphic and ecological concepts. *River Research and Applications* 26: 76-86.

Torgersen CE, Price DM, Li HW, McIntosh BA. 1999. Multiscale thermal refugia and stream habitat associations of chinook salmon in northeastern Oregon. *Ecological Applications* 9: 301-319.

Torgersen CE, Faux RN, McIntosh BA, Poage NJ, Norton DJ. 2001. Airborne thermal remote sensing for water temperature assessment in rivers and streams. *Remote Sensing of Environment* 76: 386-398.

Udevitz MS, Burn DM, Webber MA. 2008. Estimation of walrus populations on sea ice with infrared imagery and aerial photography. *Marine Mammal Science* 24: 57-70.

Uehlinger U, Malard F, Ward JV. 2003. Thermal patterns in the surface waters of a glacial river corridor (Val Roseg, Switzerland). *Freshwater Biology* 48: 284-300.

Ward JV. 1985. Thermal-characteristics of running waters. *Hydrobiologia* 125: 31-46.

Ward JV, Malard F, Tockner K. 2002. Landscape ecology: a framework for integrating pattern and process in river corridors. *Landscape Ecology* 17: 34-45.

Ward JV, Uehlinger U. 2003. *Ecology of a Glacial Flood Plain*. Kluwer Academic Publisher: Dordrecht; 320.

Webb BW, Zhang Y. 1997. Spatial and seasonal variability in the components of the river heat budget. *Hydrological Processes* 11: 79-101.

Webb BW, Zhang Y. 1999. Water temperatures and heat budgets in Dorset chalk water courses. *Hydrological Processes* 13: 309-321.

Webb BW, Clack PD, Walling DE. 2003. Water-air temperature relationships in a Devon river system and the role of flow. *Hydrological Processes* 17: 3069-3084.

Webb BW, Hannah DM, Moore RD, Brown LE, Nobilis F. 2008. Recent advances in stream and river temperature research. *Hydrological Processes* 22: 902-918.

Wellstein C, Uehlinger U, Zah R. 2003. Terrestrial floodplain vegetation. In: *Ecology of a Glacial Flood Plain*, Ward JV, Uehlinger U (eds). Kluwer Academic Publisher: Dordrecht; 109-121.

Xian G. 2008. Satellite remotely-sensed land surface parameters and their climatic effects for three metropolitan regions. *Advances in Space Research* 41: 1861-1869.

CHAPTER 5

Thermal heterogeneity and fish assemblages in a dynamic river floodplain mosaic (Oder River, Germany)

Abstract

River floodplains are heterogeneous landscapes composed of a mosaic of aquatic and terrestrial habitats. While flow has frequently been considered as a master variable that controls aquatic biodiversity and species behavior in river floodplains, little is known about thermal heterogeneity and its effect on aquatic biota in complex landscapes. However, quantifying thermal patch dynamics at the river floodplain scale remains a challenging task. In this study, we applied airborne thermal infrared (IR) imagery to characterize the thermal heterogeneity at two flow conditions in a lowland river floodplain (Oder River, Germany). In addition, the kinetic temperature was measured at 20 min intervals for four months, across the entire range of floodplain water bodies. At the same time we also electro-fished all major water bodies to identify the composition of associated fish assemblages. In spring (high flow) and summer (mean flow) the floodplain revealed a complex mosaic of thermal patches. Cumulative degree-days and average and maximum temperatures were the main variables that differentiated individual water bodies. The water body types delineated based on spatial and seasonal thermal signatures also contained distinct fish assemblages. Distinct temperature gradients at the floodplain scale and both within and across distinct water body types were resolved with airborne thermal data, providing a fully spatial and concurrently available temperature mosaic that constitutes an important factor in ecosystem processes and which is virtually inaccessible by point measurements of temperature at larger scales. This study demonstrates the great potential of airborne remotely sensed thermal IR imagery as a non-invasive method for detecting and quantifying spatial heterogeneity and ecologically relevant temperature gradients in complex landscapes, thereby facilitating the “up-scaling” of ecosystem processes and biodiversity to the landscape scale.

Introduction

High-resolution satellite and airborne remote sensing are rapidly evolving tools for accurately quantifying the structure and dynamics of complex river landscapes, a prerequisite for improving our understanding of ecosystem processes and biodiversity at various scales (Mertes 2002; Goetz et al. 2008; Marcus and Fonstad 2008; Johnson and Host 2010; and references therein). Remote sensing sensors include (i) multispectral imagers (e.g. CASI, QuickBird, Ikonos, GeoEye) for quantifying suspended sediment concentrations, chlorophyll *a*, turbidity, and water depth; (ii) laser scanners (e.g. LIDAR) for the generation of digital topographic maps and for water surface classification and delineation; and (iii) thermal infrared cameras (e.g. FLIR) for measuring surface temperatures.

River floodplains are heterogeneous landscapes composed of a shifting mosaic of interconnected aquatic and terrestrial habitats. The composition, configuration, and degree of hydrological connectivity of these habitats determine biodiversity and ecosystem processes (Ward et al. 1998; Tockner and Stanford 2002). Moreover, they determine the diversity of fish assemblages (Welcomme 1979; Van den Brink et al. 1996; Schomaker and Wolter 2011), fish reproduction, and juvenile recruitment (Bischoff and Wolter 2001; Bischoff 2002; Grift et al. 2003), as well as fish production (Welcomme 1979).

Temperature is a master variable that influences physical, chemical, biological, and ecological processes in aquatic ecosystems (Magnuson et al. 1979; Webb 1996; Caissie 2006; and references therein), triggers the dispersal of ectothermic organisms, such as fish (Buisson et al. 2008; Tiffan et al. 2009), and determines the behavior and survival of fish (Buisson et al. 2008; Pörtner and Farrell 2008; McCullough et al. 2009). In complex river floodplain mosaics temperature is inherently highly variable in space and time (Caissie 2006; Tonolla et al. 2010), and, therefore, difficult to quantify using conventional in-situ methods.

Thermal infrared (IR) imagery has been successfully used to determine the spatial heterogeneity of stream and river temperatures (Faux et al. 2001; Torgersen et al. 2001; Cristea and Burges 2009), to identify areas of groundwater-surface water interactions (Loheide and Gorelick 2006; Deitchman and Loheide 2009), to calibrate and validate stream temperature models (Loheide and Gorelick 2006; Cristea and Burges 2009), and to monitor the success of restoration projects (Shuman and Ambrose 2003; Loheide and Gorelick 2006). Moreover, thermal IR imagery has been employed to identify warm and cold water refugia that are critical for the survival of many biota, including fish (Torgersen et al. 1999, 2006; Madej et al. 2006). However, up to now, most studies have used thermal IR imagery at the

micro- and meso-habitat level, or for mapping the temperature along river corridors. So far, we are only aware of two studies that have used IR imagery to quantify thermal heterogeneity at the landscape scale (Alpine landscapes: Scherrer and Körner 2010, braided river floodplains: Tonolla et al. 2010).

The main aim of the present study was to quantify the spatiotemporal heterogeneity of temperature (during two different flow conditions) at the river floodplain scale by applying aerial thermal IR imagery together with in-situ temperature recording using conventional loggers. The second aim was to evaluate the potential link between thermal heterogeneity and the structure of fish assemblages at the river floodplain scale. We further hypothesized that ectothermic fish strongly respond to high temperatures, especially in spring.

Materials and methods

Experimental design

Thermal long-wavelength infrared (LWIR) and visible spectrum images were remotely collected during two low altitude flights to spatially map continuous patterns of surface temperature and water extent at two different flow conditions in a dynamic river floodplain segment along the lowland Oder River (Figure 1). At the same time, all major river and floodplain habitats were electro-fished to assess the composition of fish assemblages. In addition, temperature loggers were deployed from March to July in various water bodies, distributed across the entire floodplain, to assess temperature at 20 min intervals (Figure 1).

Study area

The 854 km long Oder River drains a catchment of 118,861 km^2. The average discharge at the mouth is 522 $m^3 s^{-1}$ (LUABB 1998). Detailed information on the Oder catchment can be found elsewhere (Dohle et al. 1999; Pusch et al. 2009). The study area was located on the German bank between river-km 603.8 and 608 (52°30’31’’ N, 14°36’30’’ E) at 15 m asl. The floodplain covered 347.5 ha with a maximum width of 1.1 km (Figure 1). The floodplain is bordered by dikes. The main channel is regulated by groynes and its banks are fortified with rip-rap. The floodplain contains a set of water bodies that differ in the degree of hydrological connectivity with the main channel. In the study area, the main river channel exhibits a mean annual water temperature of 11.4°C (range: -0.1 to 25.8°C), a mean annual discharge of 240 $m^3 s^{-1}$ (range: 96.3 to 476 $m^3 s^{-1}$), and a mean annual water depth of 213 cm (range: 116 to 320 cm) (Water and Navigation Authority Eberswalde 2008, unpublished).

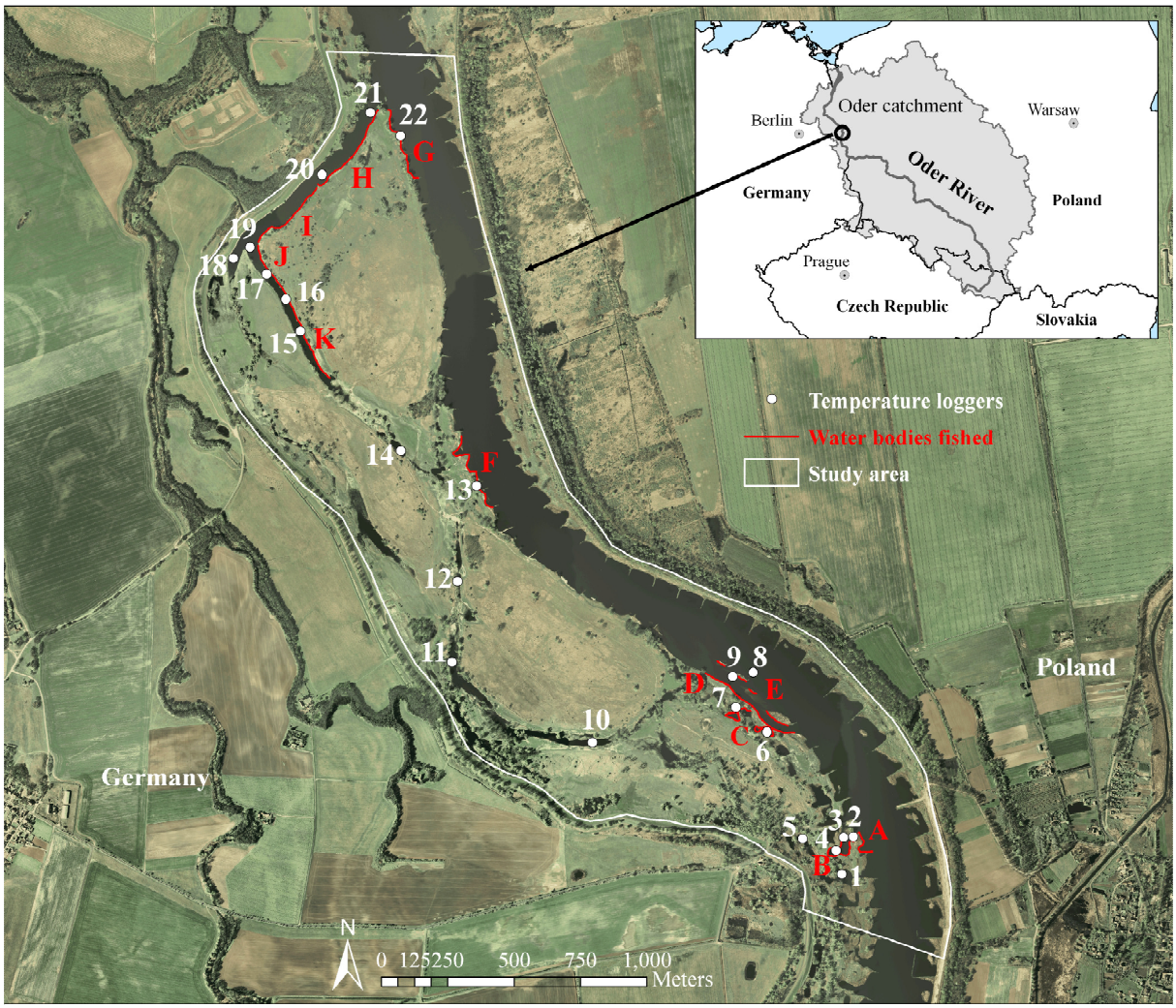

Figure 1. Study area, water bodies fished, and locations of in-situ temperature loggers in the River Oder floodplain at "Reitwein" (map data source: 20 cm resolution digital orthophoto, Geodata infrastructure Berlin-Brandenburg, Germany).

Airborne remote sensing surveys

Setting for airborne remote sensing image collection

The main channel and the fringing floodplain were mapped on two days with clear skies from early to mid-afternoon (Table 1). At this time of the day the relative humidity is normally constant and low, and it coincides with the maximum daily temperature. Flights were scheduled for the end of March (high flow) and mid-July 2010 (mean flow) (Table 1). On each date, 15 parallel flight lines with an average length of 8 km were required in order to cover the entire study area. Remotely sensed images were collected over a period of approximately 80 min during each flight period (Table 1).

Table 1. Characterization of the hydraulic and meteorological conditions during the remote sensing surveys (values averaged over the entire flying period).

Characteristic	25 March (high flow)	14 July (mean flow)
Time of remote sensing survey[A]	13:40-15.00	11:50-13:10
Discharge (m^3 s^{-1})[B]	476.0	204.7
Flow depth (cm)[B]	334.0	203.3
Water temperature (°C)[B]	8.1	25.8
Rel. Humidity (%)[C]	44.5	51.0
Wind velocity (m s^{-1})[C]	4.4	2.5
Air temperature (°C)[C]	19.9	29.0
Cloud cover (% clouded)[C]	0.05	0.15

[A] Flight start and end times (UTC, hh:min); [B] Discharge recorded at the gauging station "Eisenhüttenstadt" (river-km 554.1); flow depth and water temperature recorded at the gauging station "Frankfurt-Oder" (river-km 585.3). Data source: Water and Navigation Authority Eberswalde; [C] Recorded from a meteorological station near the village "Manschnow" (an approximate aerial distance of 7 km downstream from the study area). Data source: http://www.wetteronline.de/.

The images were collected with an airborne research platform (modified Cessna 207T, owned by the Institute of Space Science of the Freie Universität, Berlin, Germany), flying at a consistent altitude (~300 m agl) and at constant speed (~200 km h^{-1}). The Cessna was equipped with an internally calibrated LWIR (7.5-14 μm) camera (VarioCAM high resolution head, InfraTec, Dresden, Germany) and a visible near-infrared (VNIR, 0.4-1.0 μm) compact airborne spectrographic imager (CASI 550, Itres Research Limited, Calgary, Canada; owned by ARSF, Nerc, UK). The two sensors were aligned and mounted in a vertical (nadir) position on a real- time three-axis hydraulically stabilized platform (GSM3000, Zeiss, Jena, Germany). This setting minimized image distortions associated with aircraft motion, side winds, and air turbulence (Appendix A).

Each LWIR and VNIR image frame was digitally collected and stored directly in-flight from the sensors on an on-board computer at a rate of 500 and 75 ms, respectively. Finally, the images were tagged with the acquisition time as well as the position and orientation data provided by an inertial navigation system (Aerocontrol, IGI Airborne Systems, Kreuztal, Germany), which combines a fiber-optic gyro-based inertial measurements unit (IMU-IId) and an airborne computer unit with an integrated 12-channel L1/L2 GPS receiver for the precise determination of the absolute position and the attitude of the airborne sensors.

The LWIR images were used to provide surface temperature data (T_r: radiant temperature) at a high spatial resolution (0.25 × 0.25 m nominal ground pixel size), whereas images within the visible spectrum (derived from the VNIR images, see below) were used to provide a visual overview of the study area at high and mean flow conditions, as well as to help

delineate the floodplain water bodies in the LWIR images. Supplementary information on the sensors and their setting is provided in Appendix A.

LWIR image processing

The individual LWIR image frames (n = 1,540 (spring) and n = 1,250 (summer)) were digitally stored with each pixel containing the radiance values measured by the detector. Sensor internal calibration software converted the thermal radiance values to radiant temperature values (T_r) using Planck's radiation law and sensor calibration curves by considering the emissivity of water, atmospheric transmissivity and ambient background reflections (Appendix B). The LWIR images were processed assuming a thermal IR emissivity of water of 0.98 (0.983 at a zenith angle of 0° and thermal band of 8-13 µm; Cuenca and Sobrino 2004).

The main interest of this study was to quantify the relative temperature patterns at the floodplain scale rather than derive absolute temperature values at specific points. The potential inaccuracies of thermal remote sensing for absolute temperature measurements have to be balanced with the pixel resolution in favor of the large-scale data provided by such techniques (Marcus and Fonstad 2008). The LWIR sensor had a high thermal sensitivity allowing for the detection of relative temperature differences of <0.06°K (manufacturer's accuracy specification). We estimated the potential errors of the IR images collected because thermal remote sensing is not without shortcomings (e.g. Torgersen et al. 2001; Kay et al. 2005; Handcock et al. 2006) and because the remote thermal surveys covered a large area with probable changes in atmospheric and ambient conditions (Appendix B). In-situ recording with temperature loggers (see below) showed an average water temperature change throughout the duration of the flight of 0.4 ± 0.2°C (both dates). Thus, the IR images were not corrected for temperature changes due to elapsing time. The major source of error for absolute temperature recording was thermal stratification of water, which was detected during the summer (mean flow) survey in all of the measured water bodies, except in the main channel (Appendix B). Thermal stratification was absent during the spring (high flow) survey. During stratification in the summer, the temperature cannot be considered as being indicative of the overall water column temperature or of cold water areas near the bottom.

LWIR and VNIR image post-processing workflow

In order to generate single IR-image mosaics of the entire floodplain, three main post-processing steps were required. First, T_r values were extracted as ASCII files using the IR analyzing software IRBIS 3 professional (InfraTec, Dresden, Germany) and converted into

floating point rasters in ArcGIS 9.3 (ESRI, Redlands, CA, USA). Second, each raster image frame was manually scaled, rotated and individually aligned using the navigation data as a reference. Third, multiple overlapping raster image frames were manually assembled and registered in a final single raster mosaic using the nearest neighbor function to conserve the original values.

The processing chain of the VNIR instrumentation was written in IDL 7.1 (ITT-VIS, Boulder, CO, USA) by T. Ruhtz et al. (unpublished) using navigation data to geocorrect the VNIR image strips (which corresponded to the flight lines). The images were not corrected for atmospheric effects. The geocorrected image strips were then saved as RGB images (only three spectral bands were selected to generate the RGB images, no further spectral analyses were performed; Appendix A) and stitched together to generate a single mosaic of the entire floodplain. Finally, the LWIR and RGB mosaics were georeferenced using a 20 cm resolution digital orthophoto (Geodata infrastructure Berlin-Brandenburg, Germany) as a reference.

Missing parts in the final mosaics were due to sensor and/or GPS malfunctions during the survey. Visible striped patterns in the mosaics were the result of exposure and illumination artifacts associated with image joining and atmospheric effects but they did not significantly affect the thermal IR imagery (temperature differences: 0.1-0.3°C).

Field surveys

Kinetic water temperature

The kinetic water temperature (T_k) was continuously recorded at 20 min intervals using temperature loggers (TR model 12 bit, AMIRIX Systems Inc., Halifax, NS, Canada; temperature range -5 to 40°C, resolution 0.015°C, accuracy ± 0.1ºC, manufacturer's specification). In total, 30 loggers were used in all of the representative water bodies (recording period: March 24 17:00 until July 21 23:40 2010) (Figure1). Prior to and after the sampling period, the loggers were calibrated in a temperature-controlled water bath for their working range (maximum error: 0.05°C). A handheld GPS receiver (GPSmap 60CS, Garmin international, Inc., Olathe, KS; average accuracy during the surveys 3.3 ± 1.8 m) was used to determine the position of the loggers. The loggers were placed in a water depth of 0.2-0.5 m to measure the surface water temperature, which was estimated by means of IR thermography (thermal radiation emitted from the upper ~50 µm surface; Lillesand et al. 2008). In the main channel, two loggers were attached to buoys marking the fairway for inland vessels. These were the only possible logger positions in the channel thalweg. Eight loggers were lost due to either a major flood event (maximum: 1,950 $m^3 s^{-1}$, 28 May 2010) or to human intervention.

Another two loggers (No. 1 and 12, Figure 1) went dry for a maximum of 70 days, resulting in approximately 60% of missing data. The data from these two loggers and from another that was stolen from the channel thalweg (No. 8, Figure 1) could only be used to cross-check the accuracy of the T_r derived from the LWIR mosaics (Appendix C) and were excluded from further analyses.

The T_k values from the gauging station "Frankfurt-Oder", located at river-km 585.3, were used to characterize the temperature variation in the channel thalweg (location: G). A preliminary Spearman's rank correlation analysis revealed a strong correlation between the T_k from the available data of logger No. 8 in the channel thalweg and the gauging station (r = 0.99, $p < 0.001$, n = 683, R-project, version 2.9.2). Therefore, further temperature analyses were performed using the data of the remaining 19 loggers and from the gauging station (Figure 1).

Recording the T_k enabled seasonal temperature patterns to be quantified. Furthermore, the T_k values were used to cross-check the accuracy of the T_r derived from the LWIR mosaics (Appendix C). Relative temperature values were used for further analysis because this study aimed to analyze patterns of temperature distribution in floodplain habitats rather than absolute temperatures, which were always well above and below the critical lower and upper temperature thresholds for fish, respectively.

Fish sampling and characterization of the water bodies fished

At the same time as the remote sensing surveys, fish were sampled from 10:00 to 19:00, with a sampling break during the flights. Eleven representative water bodies (Figure 1) were sampled by two teams from along the banks using two DC electro-fishing gear (Types EFKO 7000 and EFKO 8000, EFKO Fischfanggeräte, Leutkirch, Germany) with 7 and 8 kW power, respectively, and a handheld ring anode of 0.4 m diameter each. This type of equipment allows a representative sampling of fish ≥5 cm in total length. Therefore, smaller fish were excluded from further analyses. All water bodies were single-pass electro-fished from a boat without stop nets along a bank length of between 70-480 m depending on the size of the water body during high and mean flow. Stunned fish were immediately collected by a second operator using a separate dip net. All of the fish caught were identified to species level, counted, measured (total length), and returned to the water. During the two fish surveys, the following environmental variables were recorded at each site: dissolved oxygen concentration, pH, and water surface temperature, measured using handheld multi-parameter water quality meters (U-10, Horiba Ltd., Kyoto, Japan; temperature accuracy ± 0.3°C, dissolved O_2 accuracy ± 0.1 mg l^{-1}, pH ± 0.05, manufacturer's specifications), and substrate

type, submerged and emerged macrophytes, woody debris, water depth, and type of embankment were visually estimated (Table 2). The water velocity along the banks during electro-fishing was observed as being at similarly low in all of the water bodies sampled.

Table 2. Environmental characteristics of the 11 water bodies fished (see Figure 1). Unless stated otherwise, the classes were the same during both field surveys.

Sampling day	Characteristic	Water bodies fished										
		A	B	C	D	E	F	G	H	I	J	K
25 March (high flow) & 14 July (mean flow)	Sand[I]	3	2	2	3	3	3	3	3	3	3	3
	Silt[I]	2	3	3	1	1	1	1	2	2	2	2
	Organic substrate[I]	1	3	3	1	1	2	2	3	3	3	3
	Submerged macrophytes[II]	1	2	2	2	2	2	1	1	2	2	2
	Emerged macrophytes[II]	2	2	2	1	2	1	1	1	1	1	1
	Woody debris[II]	1	2	2	1	1	1	1	2	2	2	2
	Water depth[III]	3	2	2[IV]	3	3	3	3	3	3	2	2
	Embankment[I]	1	1	1	1	1	3	3	2	2	1	1
25 March (high flow)	T_k (°C)	8.8	9.2	9.0	7.9	7.9	8.7	8.1	8.8	9.8	10.2	14.0
	Dissolved O_2 (mg l^{-1})	12.1	12.0	11.5	10.8	10.8	12.5	12.2	15.3	15.5	16.5	19.1
	Water pH	9.6	9.3	9.3	9.3	9.3	9.4	9.3	9.3	9.3	9.5	9.7
14 July (mean flow)	T_k (°C)	26.0	29.2	29.4	26.8	26.8	26.9	26.7	28.0	28.8	30.5	30.1
	Dissolved O_2 (mg l^{-1})	8.1	12.9	13.5	9.8	9.8	13.2	10.4	9.8	10.2	12.0	12.2
	pH	8.7	8.9	8.9	8.9	8.9	8.4	8.3	8.3	8.3	8.4	8.3

[I] 1: absent/insignificant, 2: moderate, 3: dominant; [II] 1: cover ≤ 10%, 2: cover > 10%; [III] 1: 0.5-1 m, 2: 1-2 m, 3: 2-5 m; [IV] Class 1 on 14 July.

Data analysis

Spatial patterns of surface temperature

At the floodplain scale, the spatial thermal patterns were first investigated using visualization techniques and then subsequently through appropriate data analyses. First, the T_r of each pixel falling in the study area was extracted and used to quantify the T_r pixel frequency distribution. The emissivity of the materials targeted in the floodplain (e.g. grass, shrubs, mature

vegetation, sand) had theoretical emissivity values close to that of water (0.96-0.98, at a zenith angle of 0° and a thermal band of 8-14 µm; Cuenca and Sobrino 2004; MODIS 2011). Second, an old side channel was subsequently selected and analyzed further. Then, polygons were generated in ArcGIS 9.3, and T_r values of each pixel falling in these polygons (for advantages of this technique see Appendix B) were then extracted. We calculated: (i) total number of pixels, (ii) minimum T_r, (iii) maximum T_r, (iv) average T_r, and (v) T_r amplitude. Temperature categories with fewer than 10 pixels were omitted. Third, T_r gradients were analyzed by extracting the T_r values of each pixel spaced by 0.5 m falling in the thalweg of an old side channel. Fourth, polygons (width: 3 m) were generated for each water body, representing the effective electric field, i.e. the area fished along the banks (Figure 1). The T_r of each pixel within the polygons was then extracted and the average T_r was calculated and used for further investigations into the effect of spatial temperature on fish assemblages.

Seasonal dynamics of water temperature

Seasonal dynamics of water temperature were investigated using six thermal variables calculated for the T_k of each temperature logger and the gauging station over the four-month period: (i) minimum T_k, (ii) maximum T_k, (iii) the average T_k, (iv) T_k pulse (amplitude), (v) maximum kinetic rate of thermal heating, and (vi) maximum kinetic rate of thermal cooling (for calculations see Arscott et al. 2001). In addition, two temperature-related metrics of specific relevance to fish were calculated: (vii) cumulative kinetic degree-days (kinetic temperature sum), and (viii) cumulative kinetic degree-days above 12°C (for calculations see Wolter 2007). Because variables (v) and (vi) are strongly affected by sampling intervals, the logger data were averaged to the gauging station sampling interval of 1 h. In order to calculate the degree-day variables, days with no data (e.g. if the logger went dry) were eliminated for all loggers; thus 96 days out of 119 days were used for the calculations. Furthermore, the average T_k was calculated over 24 h of the two survey days and used for further investigations into the effect of the seasonal dynamics of water temperature on fish assemblages.

Fish assemblages

The fish catches were standardized as catch per unit effort, CPUE (fish caught per 100 m). The CPUE data were log-transformed (x + 1) prior to analysis. Furthermore, two additional metrics were calculated for each water body fished: (i) total number of species S, and (ii) Shannon's diversity index H, calculated as $-\sum_{i=1}^{S} p_i \ln p_i$, where p_i is the proportion of each species i relative to S in the water body.

Statistical analysis

Differences in the seasonal dynamics of water temperature and fish assemblages among the locations studied were analyzed using non-metric multidimensional scaling (NMS), providing between-location (dis)similarity for each group of variables (eight kinetic thermal variables, CPUE of species). Only species with three or more individuals were included in the fish assemblage ordination, since species with only a few individuals provide little reliability when assigning them to groups (McCune et al. 2000). NMS avoids the error produced by the "zero truncation" problem (where the absence of a species from a water body provides no information about how unfavorable the environment is for that species) common to heterogeneous ecological data sets (Clarke 1993), and is commonly regarded as the most robust, unconstrained ordination method in community ecology (Minchin 1987). All NMS solutions were calculated using the Sørensen (Bray-Curtis) distance measure and 250 runs of real data with up to 500 iterations to evaluate the stability; 250 Monte Carlo runs with randomized data evaluated the probability ($p < 0.05$) that the ordination axes explained more variation than could be expected by chance. One or two-dimensional ordinations with a final stress <10 (highly reliable graphical representation of the data; Clarke 1993; McCune and Mefford 2006) were finally used. The axes were rotated, if necessary, to show the maximum amount of variation on the first axis.

Joint plots were constructed to identify environmental factors that might influence the fish assemblage structure. NMS was used in combination with joint plots to ordinate the fish assemblages in the sample space and to evaluate the association between a fish assemblage and the water temperature, in particular. Three temperature variables were used: (i) temperature measured during electro-fishing, (ii) average daily temperature measured with the loggers, and (iii) average temperature derived from the LWIR mosaic, representing the area of the water bodies fished. Nine out of the eleven initial water bodies were used for this analysis because of a loss of loggers in water bodies A and D (Figure 1).

Quantitative variables were plotted as vector fits against fish assemblage ordinations. Before the analyses, the secondary matrix (environmental variables) was standardized by calculating the zero-unit mean variance ($z' = \frac{x - \bar{x}}{\mathrm{SD}}$, where $\bar{x}$ is the mean and SD the standard deviation) within each variable. Pearson's correlation coefficients were used as relative means to compare the strength of correlations between variables and the ordination axis. Mantel's tests were conducted with Monte Carlo simulations (10,000 randomization runs) and the Sørensen distance measure for both matrices (CPUE of species and environmental variables)

to evaluate the correspondence (significance) between dissimilarity matrices. A significant correlation would indicate that, for example, thermally similar locations tend to exhibit similar fish assemblages.

All statistical analyses were performed using PC-ORD (version 5.01; McCune and Mefford 2006).

Results

Spatial thermal heterogeneity at the floodplain scale

A distinct variation in surface water extent and surface temperature was detected at the floodplain scale (Figure 2). At high flow (spring), most water bodies were hydrologically connected, as reflected in the thermal properties (Figure 2). For example, an old side channel was fully connected to the main channel over its entire length (3,900 m) during high flow, whereas it was only connected downstream for 1,700 m during mean flow (from "a" to "b", Figure 2). Furthermore, thermal IR imagery was able to delineate the flooded area. At high flow, both groynes and sand islands were submerged (zone "c" for the latter in Figure 2) and most of the floodplain ponds were connected (e.g. zone "d" in Figure 2).

The radiant temperature (pixel $n > 12 \times 10^6$) at the floodplain scale (including terrestrial and aquatic habitats) was very variable during the summer survey (mean flow), whereas it was more uniform during the spring survey (high flow) (Figure 2). From spring to summer, the average surface temperature and temperature amplitude at the floodplain scale increased by approximately 13.5°C and 2.5°C, respectively (Figure 2). Two distinct temperature peaks occurred during both surveys (Figure 2). A cool peak (aquatic habitats) with an average temperature of 8.5°C and a warmer peak (terrestrial surfaces, mainly exposed sand) with an average temperature of 25.5°C in spring (high flow) (Figure 2). In summer (mean flow), one peak reflected the water temperature of the main channel (26.5°C), and a second peak reflected the water temperature of the old side channel, ponds, as well as of mature vegetation patches (28-29°C) (Figure 2). In the old side channel (water bodies H-K, Figure 1), the water temperature increased by 0.6-0.7°C (spring) and 0.9-1°C (summer) per 500 m distance, with a sharp increase starting at about 800 m distance from the confluence area with the main channel (zones "b" and "e" in Figure 3). The water temperature ranged between 8.6 and 12.2°C (spring) and 25.8 and 28.7°C (summer) in the proximal part of the old channel and between 9.3 and 13.9°C (spring) and 27.3 and 29.2°C (summer) in the distal part (Figure 3).

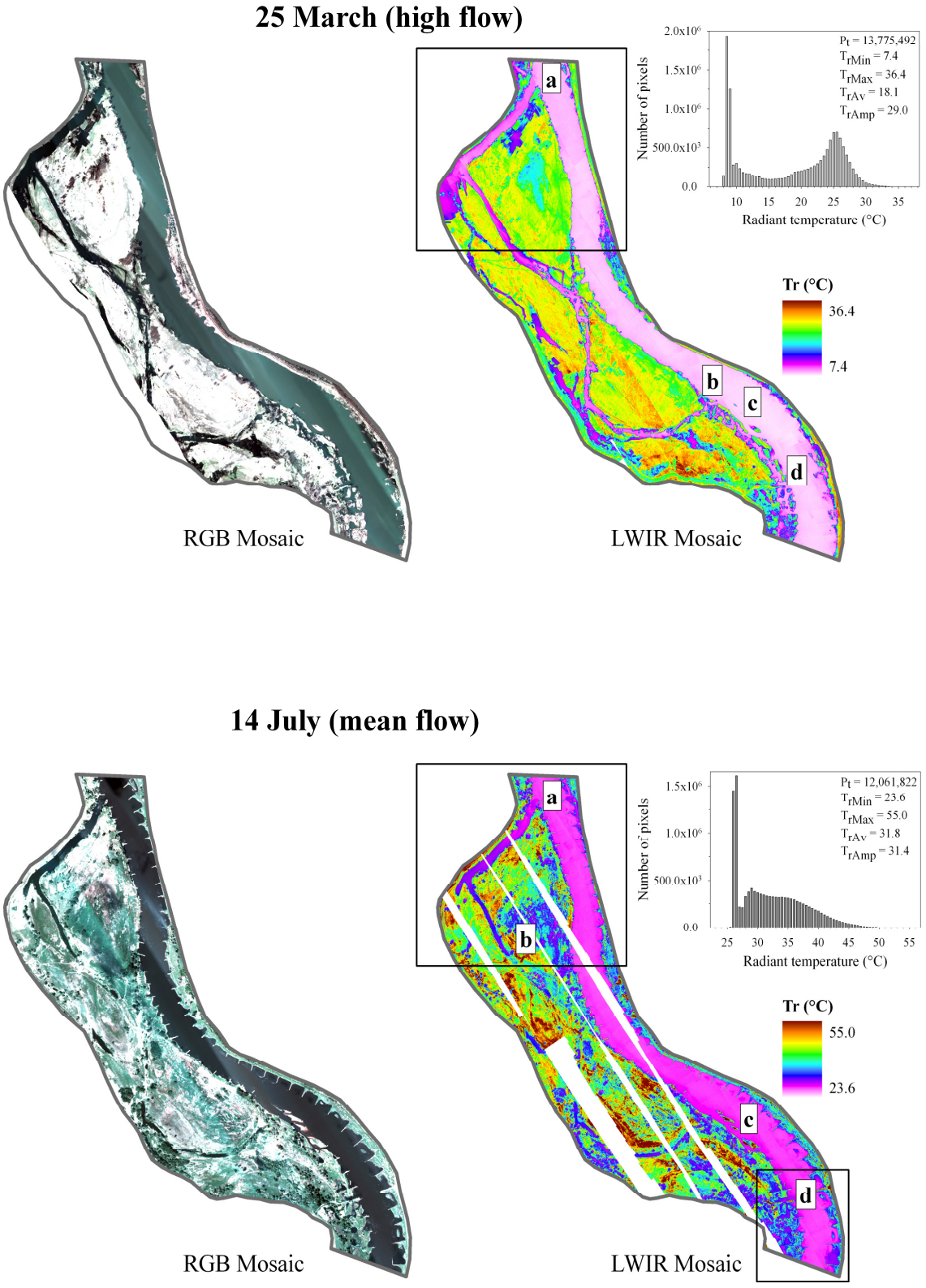

Figure 2. 16-bit RGB mosaic and corresponding 32-bit LWIR mosaic (spatial distribution of surface radiant temperature, T_r, values per pixel) of the entire floodplain at high and mean flow conditions (missing parts due to sensor and/or GPS malfunctions during the survey). Statistics for each histogram (pixel frequency distribution of radiant temperature over the entire floodplain) include total number of pixels (P_t), minimum radiant temperature (T_{rMin}), maximum radiant temperature (T_{rMax}), average radiant temperature (T_{rAv}), and radiant temperature amplitude (T_{rAmp}). Framed sections are shown in detail in Figures 3 and 4. Lower case letters indicate interesting zones.

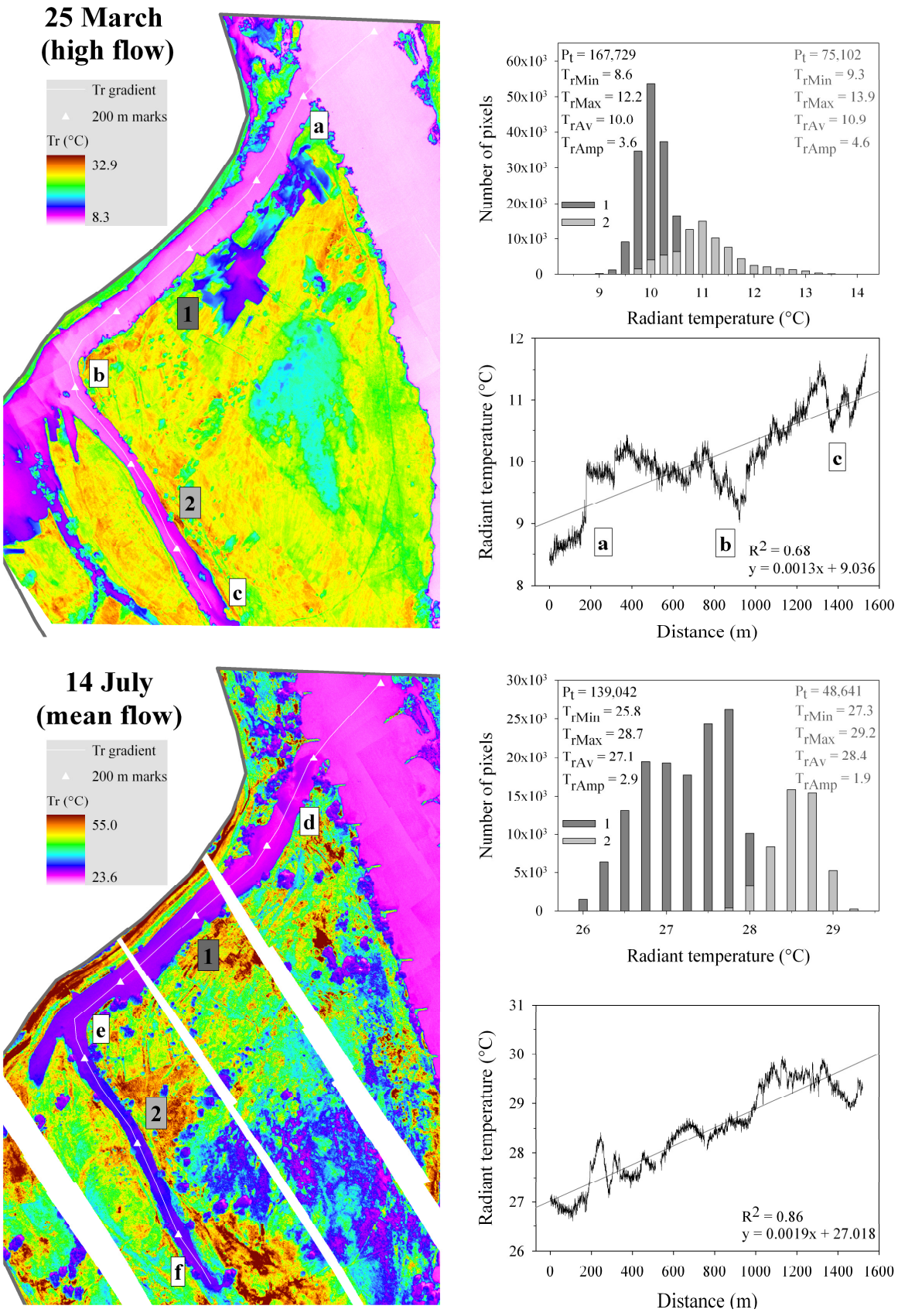

Figure 3. Spatial distribution of surface radiant temperature (T_r, values per pixel) of the old side channel (water bodies H-K, Figure 1) at high and mean flow. Pixel frequency distributions of water T_r (histograms; see Figure 2 for abbreviations) and T_r gradients (line plots) are illustrated. Lower case letters indicate interesting zones in the line plots and bordered numbers refer to the histograms.

Mixing processes at the confluence zone between the main channel and the old side channel generated sharp water temperature differences over short distances, especially in summer (zones “a” and “d” in Figure 3). At the terminus of the old side channel, where the water depth was shallower, thermal heterogeneity of the water was also high (zones “c” and “f” in Figure 3). In the main channel (summer), the water temperature was about 2°C higher in the groyne fields than in the channel thalweg, and was similar to the temperature in the connected ponds (Figure 4).

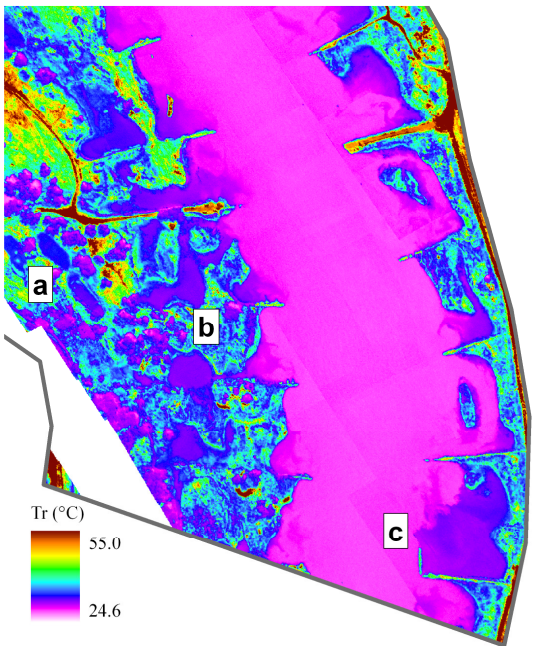

Figure 4. Spatial distribution of surface radiant temperatures (T_r, values per pixel) during the mean flow of an area including “a” isolated and “b” connected ponds, and “c” the main channel regulated by perpendicular groynes.

Seasonal dynamics of water temperature

At the floodplain scale, the kinetic water temperature (measured by conventional loggers) ranged from 7.3 to 31.6°C during the recording period (Table 3).

Non-metric multidimensional scaling (NMS), based on eight thermal variables, ordinated the water bodies where temperature loggers were deployed along a distinct spatial gradient corresponding to a decreasing degree of hydrological connectivity (i.e. decreasing temperature, except for the maximum rate of thermal cooling) (Figure 5). The channel thalweg (G, Figure 5) represented the coldest point along the gradient, followed by the water bodies located along the banks of the main channel (No. 9, 13, 22), the permanently connected ponds (No. 2, 3, 4, 6), the ponds that became isolated at low-mean flow (No. 7, 10, 11), and the water bodies located in the old side channel or in its prolongation (No. 14-21) (Figure 5). Cumulative degree-days and the average and maximum temperatures correlated

best with the factor score of the first components of the NMS (Figure 5). The average temperature and cumulative degree-days were strongly correlated with the variables temperature pulse (amplitude) and cumulative degree-days above 12°C. Furthermore, the maximum temperature was correlated with maximum rate of thermal heating (Spearman's rank correlations, $0.51 < r < 0.95$, $p < 0.05$, $n = 20$).

Table 3. Characterization of the seasonal dynamics of water temperature by each logger and the gauging station (G, representative of logger No. 8, Figure 1). See Figure 1 for the locations of the loggers.

Logger No.	Temperature variables							
	T_{kMin}	T_{kMax}	T_{kAv}	T_{kAmp}	T_{kHeat}	T_{kCol}	T_{kCum}	T_{kCum12}
2	7.5	29.5	16.5	22.0	1.3	-0.6	1546.7	68
3	7.6	29.7	16.5	22.2	1.4	-0.9	1547.3	68
4	7.6	29.5	16.5	21.9	1.4	-0.8	1548.6	68
5	7.8	30.3	16.3	22.5	1.5	-1.2	1518.7	62
6	7.6	28.1	16.5	20.5	0.8	-0.5	1543.1	68
7	7.6	30.4	16.7	22.8	1.3	-2.0	1557.8	68
G	7.3	26.6	15.9	19.3	0.3	-0.3	1492.4	64
9	7.7	28.4	15.9	20.7	1.0	-1.1	1535.7	67
10	7.5	30.4	16.7	22.8	2.3	-3.0	1558.8	67
11	7.7	31.6	16.7	24.0	1.4	-1.5	1561.4	68
13	7.6	27.7	16.0	20.1	0.4	-0.3	1536.0	67
14	7.6	31.5	17.1	23.9	1.3	-0.6	1584.3	68
15	7.6	30.8	16.9	23.2	1.5	-0.9	1572.4	68
16	7.6	31.2	17.0	23.6	2.1	-1.0	1580.2	68
17	7.6	31.4	16.9	23.7	1.8	-0.9	1578.2	68
18	8.4	31.6	17.1	23.2	1.8	-1.4	1598.2	68
19	8.2	31.3	17.1	23.1	1.4	-1.8	1593.7	68
20	8.5	30.1	16.9	21.6	1.3	-0.7	1580.3	69
21	8.2	28.9	16.7	20.7	1.2	-1.1	1565.9	69
22	7.7	27.8	15.9	20.1	2.0	-3.2	1537.2	67

T_{kMin}: minimum kinetic temperature; T_{kMax}: maximum kinetic temperature; T_{kAv}: average kinetic temperature; T_{kAmp}: kinetic temperature amplitude; T_{kHeat}: maximum kinetic rate of thermal heating; T_{kCol}: maximum kinetic rate of thermal cooling; T_{kCum}: cumulative kinetic degree-days; T_{kCum12}: cumulative kinetic degree-days above 12°C.

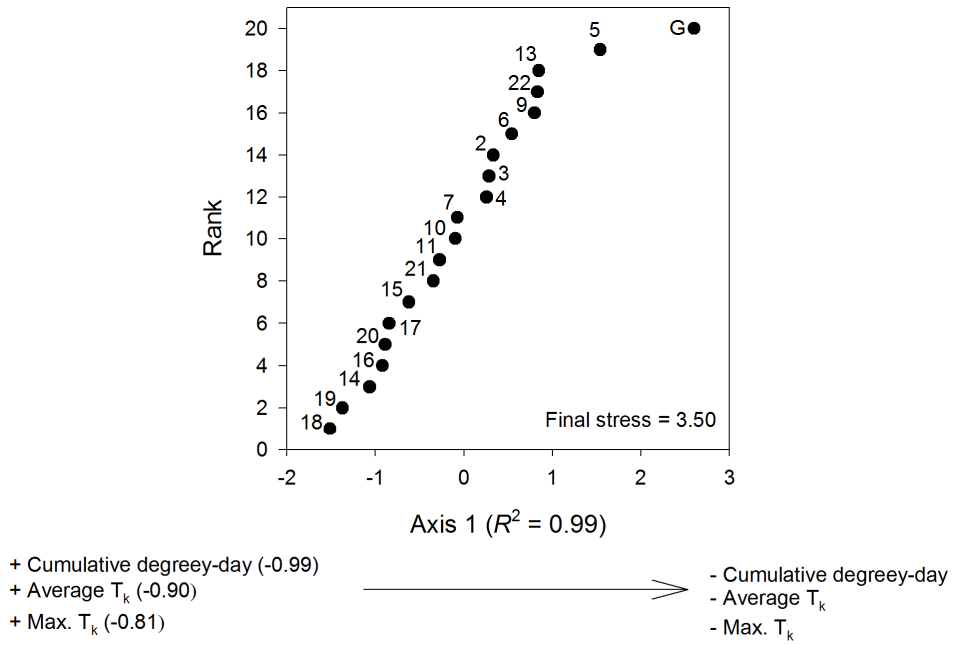

Figure 5. NMS ordination of the 20 logger locations (see Figure 1) according to the eight temperature variables calculated for the four-month sampling period. The amount of variation explained by the ordination axis (R^2, $p < 0.05$) and the three temperature variables that were most highly correlated with the ordination axis are given in parentheses (Pearson's correlation coefficients). G: gauging station "Frankfurt-Oder" represents the main channel thalweg.

Fish assemblages

During the spring (high flow) and summer (mean flow) surveys, 1,339 and 5,192 fish were collected, respectively, representing a total of 26 native species (Table 4). Barbel (*Barbus barbus*), pikeperch (*Sander lucioperca*), and crucian carp (*Carassius carassius*) were only found during the spring survey, whereas golden loach (*Sabanejewia baltica*), asp (*Aspius aspius*), and European catfish (*Silurus glanis*) were only caught during the summer (Table 4). The total number of fish species per individual water body varied between 7 and 15 (spring) and between 10 and 18 (summer) (Table 5). The dominant species were gudgeon (*Gobio gobio*) and roach (*Rutilus rutilus*) in spring and spined loach (*Cobitis taenia*) and roach in summer (Table 4). In the old side channel the total number of species decreased with increasing distance from the main channel (Table 5).

Table 4. Fish species recorded (TI: total bumber of individual caught) during spring (high flow) and summer (mean flow) in the 11 water bodies fished. Fish species grouped according to flow preference.

Scientific name	Abbr.	Common name	25 March (high flow) TI	14 July (mean flow) TI
Rheophils A				
Barbatula barbatula (L.)	BABA	Stone loach	4	3
Barbus barbus (L.)	BABA2	Common barbell	2	0
Leuciscus cephalus (L.)	LECE	Chub	59	416
Leuciscus leuciscus (L.)	LELE	Dace	10	166
Romanogobio belingi (Slastenenko)	ROBE	River gudgeon	21	4
Sabanejewia baltica (Witkowski)	SABA	N. golden loach	0	27
Rheophils B				
Abramis ballerus (L.)	ABBA	Blue bream	1	2
Aspius aspius (L.)	ASAS	Asp	0	117
Cobitis taenia (L.)	COTA	Spined loach	40	1,163
Gobio gobio (L.)	GOGO	Gudgeon	239	38
Leuciscus idus (L.)	LEID	Ide	11	226
Lota lota (L.)	LOLO	Burbot	28	52
Eurytops				
Abramis brama (L.)	ABBR	Common bream	24	17
Alburnus alburnus (L.)	ALAL	Bleak	94	205
Blicca bjoerkna (L.)	BLBJ	Silver bream	14	319
Esox lucius (L.)	ESLU	Pike	57	410
Gymnocephalus cernuus (L.)	GYCE	Ruffe	7	3
Perca fluviatilis (L.)	PEFL	Perch	164	721
Rutilus rutilus (L.)	RURU	Roach	396	1,038
Sander lucioperca (L.)	SALU	Pikeperch	2	0
Silurus glanis (L.)	SIGL	European catfish	0	6
Limnophils				
Carassius carassius (L.)	CACA	Crucian carp	1	0
Misgurnus fossilis (L.)	MIFO	Weatherfish	1	7
Rhodeus amarus (Bloch)	RHAM	Bitterling	137	38
Scardinius erythrophthalmus (L.)	SCER	Rudd	21	164
Tinca tinca (L.)	TITI	Tench	6	5

Abbr.: Abbreviation.

Table 5. Fish metrics at high and mean flows in the 11 water bodies that were fished (see Figure 1).

Sampling day	Variable	Water bodies fished										
		A	B	C[I]	D	E[II]	F	G	H	I	J	K
25 March (high flow)	Length fished (m)	120	300	480	400	80	400	400	300	300	250	250
	CPUE	33	55	73	19	56	30	42	52	21	29	35
	H	1.3	1.3	1.6	2.0	1.7	2.1	1.4	2.0	1.8	1.8	1.5
	S	7	12	14	10	9	15	12	12	11	10	9
14 July (mean flow)	Length fished (m)	140	250	70	380	200	460	400	400	330	400	270
	CPUE	275	254	430	306	159	119	176	103	87	58	77
	H	1.9	1.6	1.7	2.1	1.9	2.1	2.1	1.9	1.9	1.9	2.2
	S	15	14	14	18	13	18	17	13	13	11	10

CPUE: No. fish per 100 m (not log-transformed); *H*: Shannon's diversity index; *S*: total number of species.
[I] Length fished with respect to the water body connected to the main channel at different flow conditions
[II] Length fished with respect to the emerging bank length of the islands at different flow conditions.

Three main fish assemblages were distinguished (Figure 6): (i) in the old side channel (water bodies H-K) the assemblage was dominated by eurytopic species, (ii) in the connected ponds (water bodies B and C) limnophilic species dominated, and (iii) in the main channel (water bodies A and D-G) the fish assemblage was characterized by rheophilic species. The differences between the assemblages were stronger in summer than in spring (Figure 6).

Kinetic water temperature (spring, summer), dissolved oxygen (spring) and pH (summer) were strongly correlated with the NMS axis (Table 6). However, Mantel's tests showed that during both surveys the relationship was only significant for dissolved oxygen (Table 7). The strongest significant correlation between the categorical environmental variables and fish assemblages was observed for the dominant water body substrate (Table 7). The fish species most strongly correlated with the primary axis were chub (*Leuciscus cephalus*) and river gudgeon (*Romanogobio belingi*) in spring and chub and rudd (*Scardinius erythrophthalmus*) in summer (Figure 6, Table 6).

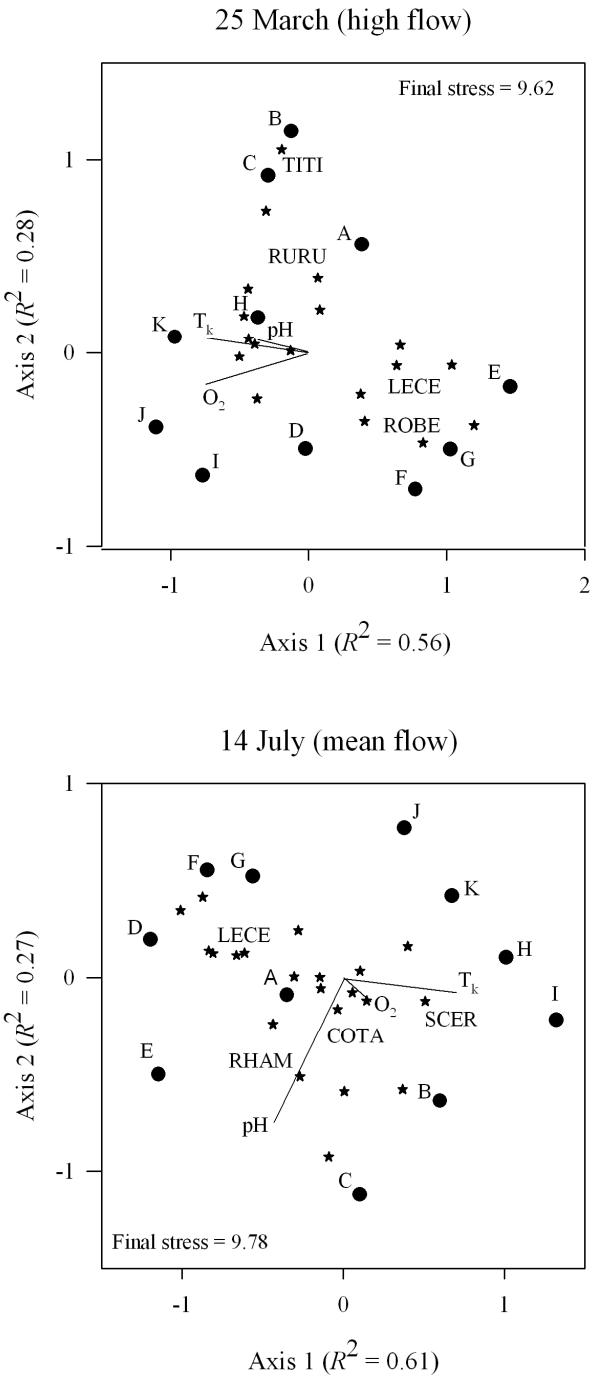

Figure 6. NMS ordination of the 11 water bodies fished (see Figure 1) according to their fish assemblages (log-transformed CPUE of species) on the two sampling dates. Dots represent water bodies, stars represent fish species. Joint plot overlays (lines radiating from the centroid) indicate the relative strength and direction of the Pearson's correlations of quantitative environmental variables with the ordination axis (exact values: see Table 6). The amount of variation explained by the ordination axis (R^2, $p < 0.05$) and the four fish species (abbreviations: see Table 4) that were most highly correlated with the ordination axis are indicated.

Table 6. Pearson's correlation coefficients of species and quantitative environmental variables versus the axis scores from the NMS ordinations of fish assemblage structures on the two sampling dates. Ordinations were calculated from log-transformed CPUE of species in the 11 water bodies fished (see Figure 1) using NMS. See Table 4 for species abbreviations.

Variable	25 March (mean flow) $n = 11$		14 July (mean flow) $n = 11$	
	Axis 1	Axis 2	Axis 1	Axis 2
Species				
Rheophils A				
BABA	0.79	-0.32	-0.64	0.46
LECE	0.83	0.11	-0.92	0.24
LELE	0.76	-0.06	-0.88	0.20
ROBE	0.82	-0.60	-0.32	0.32
SABA	NA	NA	-0.36	-0.30
Rheophils B				
ASAS	NA	NA	0.20	0.10
COTA	-0.58	-0.49	-0.11	-0.76
GOGO	0.73	-0.54	-0.62	0.32
LEID	-0.45	0.07	-0.82	0.02
LOLO	0.74	0.06	-0.78	0.24
Eurytops				
ABBR	-0.39	0.09	0.42	0.25
ALAL	-0.72	-0.04	-0.49	0.64
BLBJ	-0.40	0.39	-0.37	-0.23
ESLU	0.17	0.61	0.32	-0.65
GYCE	0.28	-0.32	-0.04	-0.62
PEFL	-0.57	0.06	0.45	-0.56
RURU	0.12	0.94	-0.90	0.01
SIGL	NA	NA	-0.54	0.14
Limnophils				
MIFO	NA	NA	0.29	-0.68
RHAM	-0.67	0.36	-0.28	-0.80
SCER	-0.22	0.68	0.92	-0.33
TITI	-0.11	0.80	0.01	-0.67
Environmental				
T_k	-0.67	0.08	0.69	-0.05
O_2	-0.74	-0.16	0.16	-0.11
pH	-0.36	0.07	-0.42	-0.73

NA: not applicable.

Table 7. Standardized Mantel's statistics (r_m) of the dissimilarity matrices for the categorical and quantitative variables and fish assemblages (log-transformed CPUE of species) in the 11 water bodies fished (see Figure 1).

Variable	25 March (high flow) r_m (n = 11)	14 July (mean flow) r_m (n = 11)
Categorical		
Sand	0.17	0.14
Silt	0.56***	0.54***
Organic substrate	0.37*	0.50**
Submerged macrophytes	0.05	0.02
Emerged macrophytes	0.32*	0.12
Woody debris	0.11	0.48**
Water depth	0.27*	0.09
Embankment	0.04	0.02
Quantitative		
T_k	0.18	0.36*
O_2	0.29*	-0.24*
pH	-0.04	0.30*

Significance levels for the Mantel's statistics: * < 0.05; ** < 0.01; *** < 0.001.

Relationship between fish assemblages and water temperature

In general, the fish assemblages in spring (high flow) exhibited a stronger correlation with temperature than they did in summer (mean flow) (Figure 7, Tables 8, 9). The water body groups and fish species that were most strongly correlated with the two axes were similar to those in the NMS ordination based on 11 water bodies (Figure 7, Table 8). Significant correlations (Mantel's tests) indicated that thermally similar locations tended to contain similar fish assemblages. Variations in fish assemblage structure correlated best with the daily (24 h data from the survey days) average kinetic temperature in spring and with the average radiant temperature in summer (Tables 8, 9). Average radiant temperature was the only temperature variable that was significantly correlated with differences in fish assemblage between the water bodies in spring and summer (Table 9).

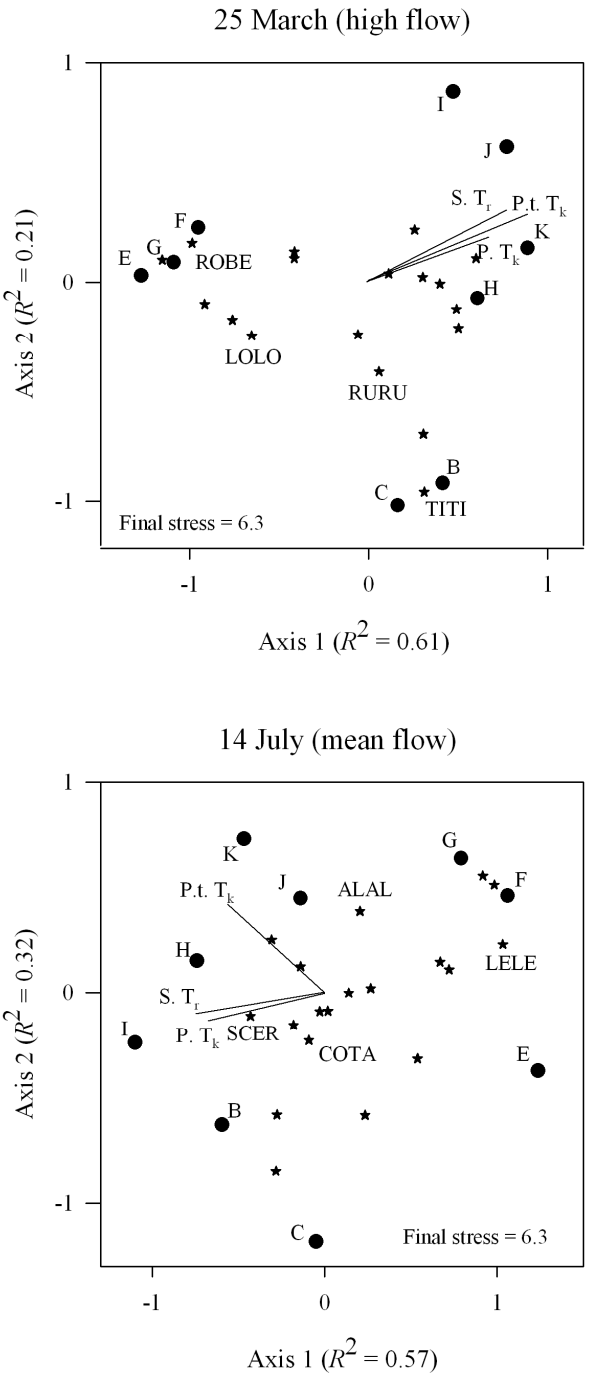

Figure 7. NMS ordination of the nine water bodies fished with temperature loggers according to their fish assemblages (log-transformed CPUE of species) on the two sampling dates. Dots represent water bodies, stars represent fish species. Joint plot overlays (lines radiating from the centroid) indicate the relative strength and direction of the Pearson's correlations of water temperature with the ordination axis (exact values: see Table 8). P. T_k: "punctual" kinetic temperature measured during electro-fishing, P.t. T_k: "punctual-temporal" average daily kinetic temperature measured by the loggers, S. T_r: "spatial" average radiant temperature derived from the LWIR mosaic (representing the area of the water bodies fished). The amount of variation explained by the ordination axis (R^2, $p < 0.05$) and the four fish species (see Table 4 for abbreviations) that were most highly correlated with the ordination axis are indicated.

Table 8. Pearson's correlation coefficients of species and three temperature measurements versus the axis scores from the NMS ordinations of fish assemblage structures on the two sampling dates. Ordinations were calculated from log-transformed CPUE of species in the nine water bodies fished with temperature loggers (see Figure 1) using NMS. See Table 4 for species abbreviations.

Variable	25 March (high flow) $n = 9$		14 July (mean flow) $n = 9$	
	Axis 1	Axis 2	Axis 1	Axis 2
Species				
Rheophils A				
BABA	-0.86	0.10	0.62	0.48
LECE	-0.86	-0.27	0.92	0.18
LELE	-0.76	-0.12	0.92	0.27
ROBE	-0.96	0.24	0.47	0.27
SABA	NA	NA	0.41	-0.31
Rheophils B				
ASAS	NA	NA	-0.25	0.29
COTA	0.42	0.54	-0.29	-0.93
GOGO	-0.74	-0.34	0.60	0.40
LEID	0.42	0.04	0.74	0.07
LOLO	-0.87	-0.45	0.73	0.21
Eurytops				
ABBR	0.41	-0.01	-0.33	0.35
ALAL	0.77	0.19	0.35	0.86
BLBJ	0.52	-0.30	0.05	-0.33
ESLU	-0.12	-0.66	-0.18	-0.73
GYCE	-0.33	0.12	-0.02	-0.68
PEFL	0.54	0.26	-0.55	-0.61
RURU	0.10	-0.95	0.86	-0.02
SIGL	NA	NA	0.47	0.27
Limnophils				
MIFO	NA	NA	-0.26	-0.72
RHAM	0.76	-0.26	0.26	-0.83
SCER	0.25	-0.77	-0.93	-0.31
TITI	0.20	-0.86	-0.20	-0.79
Temperatures				
Punctual T_k	0.67	0.20	-0.68	-0.12
Punctual-temporal T_k	0.89	0.32	-0.57	0.42
Spatial T_r	0.78	0.32	-0.73	-0.10

Punctual T_k: kinetic temperature measured during electro-fishing; punctual-temporal T_k: average daily kinetic temperature measured by the loggers; spatial T_r: average radiant temperature derived from the LWIR mosaic (representing the area of the water bodies fished). NA: not applicable.

Table 9. Standardized Mantel's statistic (r_m) of dissimilarity matrices for the temperature variables and fish assemblages (log-transformed CPUE of species) in the nine water bodies fished with temperature loggers (see Figure 1).

Variable	25 March (high flow) r_m (n = 9)	14 July (mean flow) r_m (n = 9)
Punctual T_k	0.29	0.37*
Punctual-temporal T_k	0.69***	0.13
Spatial T_r	0.45**	0.37*

Punctual T_k: kinetic temperature measured during electro-fishing; punctual-temporal T_k: average daily kinetic temperature measured by the loggers; spatial T_r: average radiant temperature derived from the LWIR mosaic (representing the area of the water bodies fished). Significance levels for the Mantel's statistics: * < 0.05; ** < 0.01; *** <0.001.

Discussion

In this study, we quantified thermal heterogeneity during two different flow conditions at the floodplain scale and related it to fish assemblage structure. Based on the thermal properties and the fish assemblage structure, three main habitat types were distinguished: (i) main channel habitat types, (ii) connected and isolated ponds, and (iii) old side channel habitat types. These water bodies were best separated by the thermal variables of cumulative degree-days, and average and maximum temperatures. A high congruency between spatial thermal properties and fish assemblages showed that temperatures derived from thermal IR imagery enabled better discrimination between the floodplain water bodies than in-situ temperature measurements.

Spatiotemporal thermal heterogeneity at the floodplain scale

The present study demonstrated that the application of spatially continuous airborne remotely sensed thermal IR imagery, with a sub-meter resolution, provides a very reliable method for identifying thermal heterogeneity and ecologically relevant warm and cold water patches (see also Torgersen et al. 1999, 2001; Cristea and Burges 2009; Deitchman and Loheide 2009; Tonolla et al. 2010). Furthermore, the in-situ temperature measurements provided critical information on the temporal thermal dynamics of floodplain water bodies (see also Arscott et al. 2001; Malard et al. 2001; Uehlinger et al. 2003). We showed that for a comprehensive thermal characterization of complex river floodplains, and in order to assess thermal patterns that could affect the distribution of biota and ecosystem processes both spatially and temporally, extensive temperature surveys are required.

In this study, a shifting habitat mosaic (sensu Stanford et al. 2005) of thermal patches, mainly influenced by the degree of hydrological connectivity, was detected across the

floodplain. Hydrological connectivity, which determines the extent of flooded surfaces, the emergence and submergence of distinct habitat structures (e.g. sandbars, groynes), and the size of individual patches, was identified as the main factor determining thermal heterogeneity at the floodplain scale. The season (i.e. higher air temperature in summer than in spring) was found to be less relevant for explaining the overall thermal heterogeneity, although it does influence the maximum temperature. In summer (mean flow), the Oder floodplain (composed of aquatic and terrestrial habitats) not only exhibited a much higher average temperature but also larger spatial temperature heterogeneity (amplitude) than in spring (high flow). While high surface temperatures in summer are obviously the result of high air temperatures and solar short-wave radiation, differences in the spatial variability were most likely related to the degree of hydrological connectivity, to the water width to depth ratio, and to surface and sub-surface water exchange rates (Malard et al. 2001; Uehlinger et al. 2003; Poole et al. 2008), as well as to vegetation cover (e.g. Tonolla et al. 2010). Similarly, Cardenas et al. (2008), who collected surface temperatures of a stream at base flow and peak flood using a handheld IR camera, found lower thermal heterogeneity under high flow than low flow conditions and stressed that periphyton anchored to the streambed, logs and partially exposed sandbars significantly contributs to thermal heterogeneity during low flow conditions.

Complex thermal mosaics exhibiting distinct diel dynamics were identified using thermal imagery in braided river floodplains (Tonolla et al. 2010) and alpine terrestrial landscapes (Scherrer and Körner 2010). The temperature gradient (amplitude) of approximately 30°C across the entire Oder floodplain (considering both terrestrial and aquatic habitats) during spring (high flow) and summer (mean flow) corresponds well to the thermal range over a distance of several hundred meters across the Roseg and Tagliamento floodplain surfaces at noon in fall (Tonolla et al. 2010). Hydrologically dynamic water bodies such as the main channel provided relatively cool patches (see also Torgersen et al. 1999; Tonolla et al. 2010). In contrast, standing water bodies such as ponds and most of the old side channel exhibited larger temperature amplitudes with maximum temperatures of up to 31.5°C (Table 3) during hot summer days. The difference of 17°C between the two temperature peaks (aquatic vs. terrestrial surfaces) across the entire Oder floodplain in spring corresponds well with the spatial variation of peak noon temperatures across the Tagliamento and Roseg floodplains (Tonolla et al. 2010). However, differences between the individual water bodies of the Oder floodplain were smaller than across the Tagliamento (Arscott et al. 2001) and Austrian Danube floodplains (Ward et al. 2002).

The thermal images provided accurate details of a distinct spatial gradient in an old side channel and of the thermal effect of groyne fields. Spatial heterogeneity in the old side channel (a 5.3°C difference between the maximum and minimum radiant temperatures; Figure 3) in spring was almost as high as the temporal heterogeneity across the water bodies of the entire floodplain (a 5°C difference between the maximum kinetic temperatures; Table 3). The groyne fields in the main channel generated large eddies with very low flowing central habitats fostering a significant temperature increase of up to 2°C compared to the main channel. This finding emphasizes the utility of airborne remotely sensed thermal IR imagery as a tool for large-scale spatial temperature mapping and quantification for a more complete ecological understanding from a riverscape perspective.

Fish assemblages and the effect of thermal patchiness on fish distribution

A total of 26 fish species were caught in this study, which is in agreement with other studies in the lower Oder River (19-26 species; Wolter and Freyhof 2005; Wolter 2007) and which can be considered as being representative of the study area. The same three water body types, distinguished according to their temperature patterns, could also be separated according to their common fish assemblages. Thermally similar water bodies tended to have similar fish assemblages. However, differentiation between the water body types was clearer in summer (mean flow) than in spring (high flow), whereas, in contrast, the response of the fish to temperature gradients was stronger in spring. These seemingly contradictory findings were a result of the generally lower temperatures that were below the optimum values for fish and the higher temperature homogeneity between the interconnected water bodies under the higher flow conditions in spring.

Many fish species are capable of tracking small differences in water temperature over a short distance and respond to these very small-scale differences by moving to more favorable areas (Wootton 1990; Mather et al. 2008), which has been particularly well studied in cold-water preferring salmonid fishes (Ebersole et al. 2001; Madej et al. 2006). On the other hand, temperate fishes actively seek out warm thermal refugia to take advantage, in terms of activity and metabolism, of their warmer conditions (Peterson and Rabeni 1996; Meka et al. 2003). Similarly, most fish species in the study area tolerate high water temperatures and were thus expected to migrate into warm water areas such as the old side channel in spring (average temperature of the main channel was 8.5°C). Increasing temperatures in side waters should induce activity by promoting metabolic rates and triggering spawning. In spring, the old side channel showed a distinct thermal gradient with water temperatures up to 5.5°C warmer than in the main channel. However, the hypothesis that fish, as ectotherms, strongly respond to

patterns of higher temperatures could not be confirmed. The total number of fish species decreased with increasing distance from the main channel, despite an increasing temperature gradient. Therefore, it must be concluded that most fish overwinter in the main channel and deep side waters, which were still cold during the spring survey and were probably too cold for most of the fish species to start being active. Accordingly, species with low temperature thresholds for activity have a higher probability of approaching and taking advantage of early patches of water with higher temperatures. Correspondingly, Wolter (2007) found that the temperature increase in March in the Oder River only promoted the spawning of perch, whereas other species did not substantially benefit from this early warming.

Outlook

Temperature drives the major life history traits of fishes (Wolter 2007; Buisson et al. 2008; Pörtner and Farrell 2008; Jonsson and Jonsson 2009; McCullough et al. 2009), is pivotal for floodplain animals such as pond-breeding amphibians by determining their reproductive success and body size (McMenamin et al. 2008; Indermaur et al. 2010), influences community structure, abundance, and the emergence of many invertebrates (Mouthon and Daufresne 2006; Durance and Ormerod 2007; Richter et al. 2008), and controls key ecosystem processes such as organic matter decomposition as well as soil and sediment respiration (Langhans et al. 2008; Döring et al. 2011).

High resolution thermal IR imagery provides a unique opportunity to quantify and study thermal heterogeneity at spatial scales relevant to ecosystem processes and biota distribution in entire ecosystems. Thermal IR imagery can be used to identify critical habitats such as cold and warm water refugia, groundwater upwelling areas, and confluence and mixing areas. All of these areas can become critical bottlenecks during periods of low flow or critical temperatures. This might become particularly relevant for management and conservation issues upon predicted temperature increases and changes in discharge and the seasonality of precipitation due to global climate change. Furthermore, high resolution thermal IR imagery allows research questions to be addressed concerning the effect of river regulation (e.g. groyne fields), water abstraction and industrial water discharge on the thermal regimes of rivers regarding effective river restoration and management for the conservation of freshwater biodiversity in large floodplain river systems.

Acknowledgments

The authors are especially indebted to the generous field support provided by C. Schomaker and our electro-fishing field crew (A. Türck, H. Zwadlo, A. Weber, and J. Hallermann). We would like to thank M. S. Lorang for insightful comments and an editorial review. Furthermore, we acknowledge the pilot of the Cessna, C. Lindemann, for his skills and helpfulness during the remote sensing flights.

Appendices

Appendix A. Supplementary information on the stabilizing platform and the sensors used during the remote sensing aerial surveys

Stabilizing platform

The platform provided ± 5° for pitch and roll and ± 25° for yaw attitude corrections. Furthermore, in combination with the IGI Aerocontrol System, the platform provided (in most cases) a residual error in the nadir pointing of less than 0.02°. Aircraft motion effects were reduced by a factor of 50:1 (Somag GSM3000 specification).

Thermal long-wavelength infrared (LWIR)

The sensor was equipped with a 16-bit amorphous Silicon (α-Si) uncooled microbolometer focal-plan-array (FPA) detector (single cell size: 25 μm) operating in the 7.5-14 μm single broad band spectral range and configured for the standard thermal recording range (-40 to 120°C). The sensor used a normal 30 mm lens (germanium, with antireflective coating, transmittance >90%) for a fiel of view (FOV) of 30° (lateral) × 23° (vertical) with an instantaneous field of view (IFOV: spatial, geometric, resolution of the camera's FPA detector) of 0.8 mrad and an image size of 640 (lateral) × 480 (vertical) infrared (IR) pixels. The thermal resolution (sensitivity) of the camera (NETD: Noise Equivalent Temperature Difference, which describes the change in object temperature relative to the effective value of the device's own noise; considered as the minimum detectable temperature difference) in the selected temperature range measured was <0.06°K and the absolute thermal accuracy was ± 1.5°K (max. error allowed, manufacturer's accuracy specifications). Calibration of the sensor was carried out by the manufacturer prior to the survey (from reference measurements of the sensor and from a calibrated pyrometer in blackbody radiators set at a known temperature).

Approximately 1,250-1,540 single images from each flight were necessary to cover the entire study area. Ground image size was approximately 160 (lateral) × 120 (vertical) m with

a pixel size (i.e. spatial resolution) of 0.25 × 0.25 m, and 30% and 77% image overlap across tracks and along tracks, respectively. Georectification of the mosaic yielded a final pixel size of 0.5 × 0.5 m.

Visible near-infrared (VNIR)

The VNIR sensor was a push-broom imaging spectrometer system measuring visible and near IR nadir radiances. The sensor was equipped with a 14-bit two-dimensional CCD array detector with 512 spatial pixels perpendicular to the flight direction and 288 spectral detector lines (pixels) covering a spectral range of 545 nm adjustable between 400 and 1,000 nm, a spectral pixel distance of 1.9 nm and a spectral resolution (FWHM: full width at half maximum, nominal bandwidth) of 2.2 nm. Images were collected using a lens with a field of view of 54.4° (across tracks) and 0.069 (along tracks). The noise floor (measure of the signal created from the sum of all noise sources and unwanted signals within the measurement system) of the sensor was 1 DN and it had a calibration accuracy of ± 2% absolute (470-800 nm, manufacturer's accuracy specifications).

For this study, the sensor was configured to achieve full spatial resolution with a reduced band setting of 35 (first flight) and 15 (second flight) non-overlapping spectral channels covering wavelength ranges between 424-941 nm and 412-902 nm, respectively. The spectral and radiometric calibration of the sensor was carried out in the laboratory at the Freie Universität Berlin, prior to and following each survey. A 1.0 × 1.0 m ground pixel size was obtained after post-processing. Finally, only three spectral bands were selected to generate the RGB images: bands 5 (blue: 483.8 nm), 7 (green: 513.9 nm) and 17 (red: 665.6 nm) from the first flight and bands 3 (blue: 490.4 nm), 4 (green: 511.1 nm) and 7 (red: 664.7 nm) from the second flight. No further spectral analyses were performed in this study.

Appendix B. Major potential error sources for the IR measurements of water surface temperature

The LWIR used an internal calibration procedure with a near to ideal blackbody as the internal temperature reference and internal software to correct for single image point deviations from the temperature of the blackbody. The detector was thermally stabilized using a Peltier element and was thus independent of the ambient temperature. However, the accuracy of thermal remote sensing of flowing water can be affected by various physical factors such as atmospheric absorption and emission, reflected long-wave radiation, emissivity, surface characteristics, vertical thermal stratification, sub-pixel mixing, and near-bank shade (Torgersen et al. 2001; Kay et al. 2005; Handcock et al. 2006). In an effort to take

into account the radiative properties of the surrounding environment and the physical qualities of the aquatic habitats we made the following assumptions and performed ground-truth measurements to cross-check the LWIR images.

The LWIR images were corrected for atmospheric transmissivity and ambient background conditions using the post-acquisition analysis software IRBIS 3 professional (InfraTec, Dresden, Germany) with the user-defined calibration variables of ambient temperature, sensor-target distance, and relative humidity. Ambient temperature, which is the temperature reflected from all objects the camera detects (this is not necessarily equal to the temperature of the camera itself or of its immediate environment), was approximated by measuring the temperature in the opposite direction to the floodplain (in the reflection direction, in this case the sky) during the flights. Sensor-target distance and relative humidity might also influence transmissivity. However, these two last parameters have a small impact as the long-wavelength IR spectrum is optimal in terms of atmospheric transmission and the images were acquired at low altitude (see below).

Atmospheric and ambient background effects

The long-wavelength IR spectrum (8-14 μm) is optimal in terms of atmospheric transmission because it is least affected by the absorption of atmospheric gases (at short distances, mainly water in the form of vapor or aerosol droplets) and atmospheric scattering is negligible for IR wavelengths (Anderson and Wilson 1984; Lillesand et al. 2008). Moreover, the IR energy emitted predominates at long wavelengths over reflected energy and natural objects, such as water, have temperatures with radiation peaks emitted in the long-wavelength region of the spectrum (Anderson and Wilson 1984; Lillesand et al. 2008). Furthermore, in this study, the measurement distances were relatively short (300 m) and humidity was moderately low (≤50% relative humidity) during the two flights; thus further reducing the effect of atmospheric absorption (Anderson et al. 1995). The two flights were conducted during conditions of clear skies (no or moderate fluctuations in sky radiation) so that only the cold reflections from the sky on smooth water surfaces (which makes these surfaces appear colder than they actually are) would have played a significant role in the radiant temperature (T_r) measurements. However, the reflection (direct and scattered) of radiation from the near environment (e.g. trees) may also have partially affected the T_r measurements. However, this effect is normally small compared to the temperature (and emitted radiation) of water surfaces (Handcock et al. 2006). Thus, the atmospheric absorption effects of IR radiation, atmospheric radiance and ambient background conditions were considered to be minimal. Additionally,

these effects were roughly corrected using inbuilt functions of the LWIR camera software (see above).

Emissivity and water surface characteristics

Differences in water turbidity, surface roughness, and wind velocity, which affect surface roughness, have also been found to affect emissivity and thus IR temperature measurements (Wenyao et al. 1987; Masuda et al. 1988). The effect of wind speeds less than 15 m s^{-1} (<5 m s^{-1} in this study) on water surfaces is small at zenith angles ≤30° (Masuda et al. 1988; the zenith angle in this study was nadir, i.e ~0°), and tap water emissivity (water with high turbidity has a higher reflectance in comparison to clear water) remains essentially invariant at 0.98 (thermal band of 8-14 µm) over a wide range of inorganic sediment (clay-silt) concentrations (from pure tap water to 50,000 mg l^{-1}, within the temperature range of 10-35°C; Wenyao et al. 1987). In the present study, all of the water bodies were more or less turbid with an estimated depth of visibility between 0.5 and 0.9 m. Furthermore, water surface roughness was minimal in the study area (no riffles or rapids; some roughness was due to wind or turbulence caused by the groynes or rip-rap along the main channel). Thus, these effects were considered as negligible. Furthermore, the small zenith angle minimized reflection from the near-bank environment (e.g. vegetation), reflections due to different levels of water surface roughness, and variations in emissivity and wind influence (Masuda et al. 1988; Torgersen et al. 2001; Handcock et al. 2006). Wind-induced evaporative cooling, lower T_r as kinetic temperature (T_k), at the surface layer was also expected; however, the magnitude of this error was probably much smaller than the other errors and was therefore not considered.

Vertical thermal stratification

The LWIR sensor detects thermal radiation emitted from the surface (upper ~50 µm; Lillesand et al. 2008) and may not be indicative of the temperature of the overall water column. Therefore, thermal stratification, as can occur in water bodies that are not well mixed, such as in floodplain ponds and behind within-stream impoundments, might lead to important errors in the interpretation of IR images (Torgersen et al. 2001; Kay et al. 2005; Handcock et al. 2006). Consequently, measurements of thermal stratification were conducted one week after the final survey (22 July 2010, 09:30-15:30). Water T_k were measured at each temperature logger location at 10 and 100 cm below the water surface with a handheld universal meter (Multi 340i, WTW Measurement Systems, Weilheim, Germany; accuracy ± 0.2°C, resolution 0.1°C, manufacturer's specifications). Thermal stratification was then

calculated as surface T_k minus bottom T_k = T_s. Water bodies were considered stratified when T_s exceeded the ± 0.2°C accuracy of the sensor. Significant thermal stratification in summer (mean flow) was detected in most of the locations measured (T_s = 2.0 ± 1.7°C, max. T_s = 5.7°C) (Table 10). As expected, thermal stratification was most pronounced in the water bodies with low flow velocities (and thus little mixing), such as the ponds and the old side channel, whereas no stratification was detected in the three locations within the main channel (No. 9, 13, 22) (Table 10). Additionally, T_k at 10 and 100 cm below the water surface was measured in eight of the eleven habitats fished during the first (25 March 2010), high flow, survey and no significant thermal stratification was found (T_s = 0.0 ± 0.04°C, max. T_s = 0.1°C).

Table 10. Thermal stratification at individual logger locations during the summer survey (14 July 2010, mean flow). See Figure 1 for locations of the loggers.

Logger No.	T_s (°C)
1	4.3
2	1.5
3	5.0
4	5.7
5	2.8
6	5.0
7	2.4
8	NA
9	0.1
10	3.7
11	1.7
12	1.6
13	0.1
14	1.5
15	1.4
16	1.5
17	1.2
18	1.0
19	0.9
20	1.0
21	0.5
22	0.1

T_s = surface T_k (10 cm) – bottom T_k (100 cm), representing the stratification temperature threshold (i.e. stratified when T_s > 0.2°C, see text). NA: not applicable.

Although hydrologists, ecologists, and resource managers are ultimately interested in the kinetic temperature of water within the entire water column - since this is both biologically important and is also the definition of temperature used for management purposes - the

measurements of T_r shown in thermal images can be used to evaluate spatially extensive patterns of surface temperature in riverine landscapes.

Sub-pixel mixing

The accuracy of thermal IR surface temperatures depends on the IR-ground pixel size and the size of the survey object or habitat (Torgersen et al. 2001; Kay et al. 2005; Handcock et al. 2006). Torgersen et al. (2001) suggested the use of ≥10 pure-water IR pixels to prevent compromising surface water temperature measurements due to sub-pixel mixing, i.e. the mixing of both water and land surface pixels at the margins (Torgersen et al. 2001; Kay et al. 2005; Handcock et al. 2006). The final ground pixel resolution of 0.5 × 0.5 m used in our study resulted in thousands of pixels in the investigated water bodies, which was sufficient for accurate measurements of T_r. Furthermore, using the RGB mosaics and polygons for delineation of water body boundaries, it was possible to discriminate between pure water isothermal pixels and mixing with sub-pixel objects such as within-river impoundments, sandbars, and major macrophytes; thus considerably reducing the uncertainty of sub-pixel mixing and emissivity differences (of different materials).

Near-bank shade

If vegetation canopies obscure the water surface, the near-surface layer of water will be cooler than areas warmed by direct solar irradiance. This effect will only be visible in the LWIR images if the stream has been shaded for a sufficient period of time to make a discernable change in the surface temperature and if the water is not sufficiently mixed (Handcock et al. 2006). In this study, it was possible to exclude all major shaded surfaces (visible in the RGB mosaics) from the analysis by using polygons. Moreover, because water has a high thermal inertia and therefore temperature changes occur slowly in response to shadows from vegetation and/or clouds, the thermal contrast between the surface of shadow-free and shadowed water is low to non-existent (Smikrud et al. 2008), thus further minimizing this possible error source.

Appendix C. Supplementary information on the cross-checking of T_r through T_k measurements

The T_r was calculated by averaging all IR pixels that fell within a circular region (the radius was set to 5 m to account for the inaccuracy of the handheld GPS receiver and the georeferenced LWIR mosaic) around the location of the temperature logger. The T_k measured

by the in-situ temperature loggers was calculated as the average temperature throughout the duration of the flight. The difference in temperature was then calculated as $T_k - T_r$.

In spring (high flow), the difference between T_k and T_r at most logger locations was between -0.5 and + 0.3°C (Table 11), which is consistent with results of studies conducted over the past 10 years (±0.5°C, e.g. Torgersen et al. 1999, 2001; Rayne and Henderson 2004; Loheide and Gorelick 2006; Cardenas et al. 2008; Deitchman 2009). However, at single locations, especially in water bodies with a low level of turbulence, the error could rise to a maximum of -3.4°C (No. 5, Table 11). During the summer (mean flow) survey only well-mixed locations (e.g. the main channel) showed an error of around ±0.5°C (Table 11).

Table 11. Differences between T_k and T_r at individual logger positions. See Figure 1 for locations of the loggers.

Logger No.	25 March 2010 (high flow) $T_k - T_r$ (°C)	14 July 2010 (mean flow) $T_k - T_r$ (°C)
1	-2.1	-2.1
2	-0.4	-1.3
3	0.0	-1.6
4	0.1	-1.2
5	-3.4	-1.8
6	0.1	-1.9
7	-0.3	-1.0
8	0.3	0.4
9	0.2	0.6
10	-0.8	-1.1
11	-1.4	-0.9
12	-0.7	-2.6
13	-0.2	0.5
14	0.1	1.4
15	-1.1	-1.5
16	-0.9	-1.2
17	-1.3	-0.5
18	-0.5	0.7
19	-0.5	0.9
20	-0.4	1.1
21	-0.4	-0.2
22	-0.3	-0.1

T_k: kinetic temperature measured by in-situ temperature loggers; T_r: radiant temperature estimated from the LWIR images.

The differences in the range of errors were probably due to the depth of the logger in the water column (it was not always possible to keep them at exactly the same water depth) and stratification (Appendix B). Furthermore, microthermal variability in the water column

temperature tends to be most pronounced in summer months under conditions of stronger solar heating and lower discharge volumes (see Webb et al. 2008 for a review).

References

Anderson JM, Wilson SB. 1984. The physical basis of current infrared remote-sensing techniques and the interpretation of data from aerial surveys. *International Journal of Remote Sensing* 5: 1-18.

Anderson JM, Duck RW, McManus J. 1995. Thermal radiometry - a rapid means of determining surface-water temperature-variations in lakes and reservoirs. *Journal of Hydrology* 173: 131-144.

Arscott DB, Tockner K, Ward JV. 2001. Thermal heterogeneity along a braided floodplain river (Tagliamento River, northeastern Italy). *Canadian Journal of Fisheries and Aquatic Sciences* 58: 2359-2373.

Bischoff A, Wolter C. 2001. The flood of the century on the River Oder: effects on the 0+ fish community and implications for flood plain restoration. *Regulated Rivers: Research and Management* 17: 171-190.

Bischoff A. 2002. *Juvenile Fish Recruitment in the Large Lowland River Oder: Assessing the Role of Physical Factors and Habitat Availability*. Shaker Verlag: Aachen; 192.

Buisson L, Blanc L, Grenouillet G. 2008. Modelling stream fish species distribution in a river network: the relative effects of temperature versus physical factors. *Ecology of Freshwater Fish* 17: 244-257.

Caissie D. 2006. The thermal regime of rivers: a review. *Freshwater Biology* 51: 1389-1406.

Cardenas MB, Harvey JW, Packman AI, Scott DT. 2008. Ground-based thermography of fluvial systems at low and high discharge reveals potential complex thermal heterogeneity driven by flow variation and bioroughness. *Hydrological Processes* 22: 980-986.

Clarke KR. 1993. Non-parametric analyses of changes in community structure. *Australian Journal of Ecology* 18:117-143.

Cristea NC, Burges SJ. 2009. Use of thermal infrared imagery to complement monitoring and modeling of spatial stream temperatures. *Journal of Hydrologic Engineering* 14: 1080-1090.

Cuenca J, Sobrino JA. 2004. Experimental measurements for studying angular and spectral variation of thermal infrared emissivity. *Applied Optics* 43: 4598-4602.

Deitchman RS, Loheide SP. 2009. Ground-based thermal imaging of groundwater flow processes at the seepage face. *Geophysical Research Letters* 36: L14401.

Döring M, Uehlinger U, Ackermann T, Woodtli M, Tockner K. 2011. Spatiotemporal heterogeneity of soil and sediment respiration in a river-floodplain mosaic (Tagliamento, NE Italy). *Freshwater Biology*. In press: Doi:10.1111/j.1365-2427.2011.02569.x.

Dohle W, Bornkamm R, Weigmann G. 1999. *Das Untere Odertal: Auswirkungen der periodischen Überschwemmungen auf Biozönosen und Arten*. Limnologie aktuell 9. Schweizerbart'sche Verlagsbuchhandlung: Stuttgart; 442.

Durance I, Ormerod SJ. 2007. Climate change effects on upland stream macroinvertebrates over a 25-year period. *Global Change Biology* 13: 942-957.

Ebersole JL, Liss WJ, Frissell CA. 2001. Relationship between stream temperature, thermal refugia, and rainbow trout (*Oncorhynchus mykiss*) abundance in arid-land streams, northwestern United States. *Ecology of Freshwater Fish* 10: 1-11.

Faux RN, Maus P, Lachowsky H, Torgersen CE, Boyd MS. 2001. *New Approaches for Monitoring Stream Temperature: Airborne Thermal Infrared Remote Sensing*. Inventory and monitoring project report, integration of remote sensing, Remote sensing applications center, USDA Forest service engineering.

Goetz SJ, Gardiner N, Viers JH. 2008. Applications of remote sensing to monitoring freshwater and estuarine systems. *Remote Sensing of Environment* (special issue containing 15 articles) 112: 3993-4166.

Grift RE, Buijse AD, Van Densen WLT, Machiels MAM, Kranenbarg J, Klein Breteler JGP, Backx JJGM. 2003. Suitable habitats for 0-group fish in rehabilitated floodplains along the lower River Rhine. *River Research and Applications* 19: 353-374.

Handcock RN, Gillespie AR, Cherkauer KA, Kay JE, Burges SJ, Kampf SK. 2006. Accuracy and uncertainty of thermal-infrared remote sensing of stream temperatures at multiple spatial scales. *Remote Sensing of Environment* 100: 427-440.

Indermaur L, Schmidt BR, Tockner K, Schaub M. 2010. Spatial variation in abiotic and biotic factors in a floodplain determine anuran body size and growth rate at metamorphosis. *Oecologia* 163: 637-649.

Johnson LB, Host GE. 2010. Recent developments in landscape approaches for the study of aquatic ecosystems. *Journal of the North American Benthological Society* 29: 41-66.

Jonsson B, Jonsson N. 2009. A review of the likely effects of climate change on anadromous Atlantic Salmon Salmo salar and brown trout Salmo trutta, with particular reference to water temperature and flow. *Journal of Fish Biology* 75: 2381-2447.

Kay JE, Kampf SK, Handcock RN, Cherkauer KA, Gillespie AR, Burges SJ. 2005. Accuracy of lake and stream temperatures estimated from thermal infrared images. *Journal of the American Water Resources Association* 41: 1161-1175.

Langhans SD, Tiegs SD, Gessner M, Tockner K. 2008. Leaf decomposition heterogeneity across a riverine floodplain mosaic. *Aquatic Sciences* 70: 337:346.

Lillesand TM, Kiefer RW, Chipman JW. 2008. Multispectral, thermal, and hyperspectral sensing. In: *Remote sensing and image interpretation*, Lillesand TM, Kiefer RW, Chipman JW (eds). John Wiley and Sons: New York; 325-391.

Loheide SP, Gorelick SM. 2006. Quantifying stream-aquifer interactions through analysis of remotely sensed thermographic profiles and in-situ temperature histories. *Environmental Science and Technology* 40: 3336-3341.

LUABB. 1998. *Landesumweltamt Brandenburg: das Sommerhochwasser an der Oder 1997*. Studien und Tagungsberichte 16.

Madej MA, Currens C, Ozaki V, Yee J, Anderson DG. 2006. Assessing possible thermal rearing restrictions for juvenile coho salmon (*Oncorhynchus kisutch*) through thermal infrared imaging and in-stream monitoring, Redwood Creek, California. *Canadian Journal of Fisheries and Aquatic Sciences* 63: 1384-1396.

Magnuson JJ, Crowder LB, Medvick PA. 1979. Temperature as an ecological resource. *American Zoologist* 19: 331-343.

Malard F, Mangin A, Uehlinger U, Ward JV. 2001. Thermal heterogeneity in the hyporheic zone of a glacial floodplain. *Canadian Journal of Fisheries and Aquatic Sciences* 58: 1319-1335.

Marcus WA, Fonstad MA. 2008. Optical remote mapping of rivers at sub-meter resolutions and watershed extents. *Earth Surface Processes and Landforms* 33: 4-24.

Masuda K, Takashima T, Takayama Y. 1988. Emissivity of pure and sea waters for the model sea-surface in the infrared window regions. *Remote Sensing of Environment* 24: 313-329.

Mather ME, Parrish DL, Campbell CA, McMenemy JR, Smith JM. 2008. Summer temperature variation and implications for juvenile Atlantic salmon. *Hydrobiologia* 603: 183-196.

McCullough DA, Bartholow JM, Jager HI, Beschta RL, Cheslak EF, Deas ML, Ebersole JL, Foott JS, Johnson SL, Marine KR, Mesa MG, Petersen JH, Souchon Y, Tiffan KF, Wurtsbaugh WA. 2009. Research in thermal biology: burning questions for coldwater stream fishes. *Reviews in Fisheries Science* 17: 90-115.

McCune B, Rosentreter R, Ponzetti JM, Shaw DC. 2000 Epiphyte habitats in an old conifer forest in western Washington, USA. *Bryologist* 103: 417-427.

McCune B, Mefford MJ. 2006. *PC-ORD. Multivariate Analysis of Ecological Data*. Version 5. MjM Software, Gleneden Beach, Oregon, USA.

McMenamin SK, Hadly EA, Wright CK. 2008. Climatic change and wetland desiccation cause amphibian decline in Yellowstone National Park. *Proceedings of the National Academy of Sciences* 105: 16988-16993.

Meka JM, Knudsen EE, Douglas DC, Benter RB. 2003. Variable migratory patterns of different adult rainbow trout life history types in a southwest Alaska watershed. *Transactions of the American Fisheries Society* 132: 717-732.

Mertes LAK. 2002. Remote sensing of riverine landscapes. *Freshwater Biology* 47: 799-816.

Minchin PR. 1987. An evaluation of relative robustness of techniques for ecological ordinations. *Vegetatio* 69: 89-107.

MODIS 2011. *Moderate Resolution Imaging Spectrometer*. UCSB (University of California, Santa Barbara, CA, USA) emissivity library. http://www.icess.ucsb.edu/modis/EMIS/html/em.html (last accessed 10th February 2011).

Mouthon J, Daufresne M. 2006. Effects of the 2003 heatwave and climatic warming on mollusc communities of the Saone: a large lowland river and of its two main tributaries (France). *Global Change Biology* 12: 441-449.

Peterson JT, Rabeni CF. 1996. Natural thermal refugia for temperate warmwater stream fishes. *North American Journal of Fisheries Management* 16: 738-746.

Poole GC, O'Daniel SJ, Jones KL, Woessner WW, Bernhardt ES, Helton AM, Stanford JA, Boer BR, Beechie TJ. 2008. Hydrologic spiralling: the role of multiple interactive flow paths in stream ecosystems. *River Research and Applications* 24: 1018-1031.

Pörtner HO, Farrell AP. 2008. Physiology and climate change. *Science* 322: 690-692.

Pusch M, Andersen HE; Bäthe J, Behrendt H, Fischer H, Friberg N, Gancarczyk A, Hoffmann CC, Hachol J, Kronvang B, Nowacki F, Pedersen ML, Sandin L, Schöll F, Scholten M, Stendera S, Svendsen LM, Wnuk-Glawdel E, Wolter C. 2009. Rivers of the central European highlands and plains. In *Rivers of Europe*, Tockner K, Uehlinger U. Robinson CT (eds). Academic Press: Amsterdam; 525-576.

Rayne S, Henderson GS. 2004. Airborne thermal infrared remote sensing of stream and riparian temperatures in the Nicola River watershed, British Columbia, Canada. *Journal of Environmental Hydrology* 12: 1-11.

Richter O, Suhling F, Mueller O, Kern D. 2008. A model for predicting the emergence of dragonflies in a changing climate. *Freshwater Biology* 53: 1868-1880.

Scherrer D, Körner C. 2010. Infra-red thermometry of alpine landscapes challenges climatic warming projections. *Global Change Biology* 16: 2602-2613.

Schomaker C, Wolter C. 2011. The contribution of long-term isolated water bodies to floodplain fish diversity. *Freshwater Biology*. In press: Doi:10.1111/j.1365-2427.2011.02583.x.

Shuman CS, Ambrose RF. 2003. A comparison of remote sensing and ground-based methods for monitoring restoration success. *Restoration Ecology* 11: 325-333.

Smikrud KM, Prakash A, Nicholos JV. 2008. Decision-based fusion for improved fluvial landscape classification using digital aerial photographs and forward looking infrared images. *Photogrammetric Engineering and Remote Sensing* 74: 903-911.

Stanford JA, Lorang MS, Hauer FR. 2005. The shifting habitat mosaic of river ecosystems. *Verhandlungen der internationalen Vereinigung für theoretische und angewandte Limnologie* 29: 123-136.

Tiffan KF, Kock TJ, Connor WP, Steinhorst RK, Rondorf DW. 2009. Behavioural thermoregulation by subyearling fall (autumn) Chinook salmon *Oncorhynchus tshawytscha* in a reservoir. *Journal of Fish Biology* 74: 1562-1579.

Tockner K, Stanford JA. 2002. Riverine floodplains: present state and future trends. *Environmental Conservation* 29: 308-330.

Tonolla D, Acuña V, Uehlinger U, Frank T, Tockner K. 2010. Thermal heterogeneity in river floodplains. *Ecosystems* 13: 727-740.

Torgersen CE, Price DM, Li HW, McIntosh BA. 1999. Multiscale thermal refugia and stream unit associations of chinook salmon in northeastern Oregon. *Ecological Applications* 9: 301- 319.

Torgersen CE, Faux RN, McIntosh BA, Poage NJ, Norton DJ. 2001. Airborne thermal remote sensing for water temperature assessment in rivers and streams. *Remote Sensing of Environment* 76: 386-398.

Torgersen CE, Baxter CV, Li HW, McIntosh BA. 2006. Landscape influences on longitudinal patterns of river fishes: spatially continuous analysis of fish-habitat relationships. In: *Landscape Influences on Stream Habitats and Biological Assemblages*, Hughes RM, Wang L, Seelbach PW (eds). American Fisheries Society, Symposium 48: Bethesda, Maryland; 473-492.

Uehlinger U, Malard F, Ward JV. 2003. Thermal patterns in the surface waters of a glacial river corridor (Val Roseg, Switzerland). *Freshwater Biology* 48: 284-300.

Van den Brink FWB, Van der Velde G, Buijse AD, Klink AG. 1996. Biodiversity in the lower Rhine and Meuse river-floodplains: its significance for ecological river management. *Netherlands Journal of Aquatic Ecology* 30: 129-149.

Ward JV. 1998. Riverine landscapes: biodiversity patterns, disturbance regimes, and aquatic conservation. *Biological Conservation* 83: 269-278.

Ward JV, Tockner K, Arscott DB, Claret C. 2002. Riverine landscape diversity. *Freshwater Biology* 47: 517-539.

Webb BW. 1996. Trends in stream and river temperature. *Hydrological Processes* 10: 205-226.

Webb BW, Hannah DM, Dan Moore R, Brown LE, Nobilis F. 2008. Recent advances in stream and river temperature research. *Hydrological Processes* 22: 902-918.

Welcomme RL. 1979. *Fisheries Ecology of Floodplain Rivers*. Longman: London; 317.

Wenyao L, Field RT, Gantt RG, Klemas V. 1987: Measurements of the surface emissivity of turbid waters. *Remote Sensing of Environment* 21: 97-109.

Wolter C, Freyhof J. 2005. Die Fischbesiedelung des Oder-Einzugsgebietes. *Nationalpark-Jahrbuch Unteres Odertal*: 37-63.

Wolter C. 2007. Temperature influence on the fish assemblage structure in a large lowland river, the lower Oder River, Germany. *Ecology of Freshwater Fish* 16: 493-503.

Wootton RJ. 1990. *Ecology of teleost fishes*. Chapman and Hall: London; 404.

GENERAL DISCUSSION AND OUTLOOK

This doctoral thesis focused on the acoustic and thermal characterization of river landscapes; two little-explored and poorly understood features in river science. It was demonstrated that advanced application of acoustic sensors and thermal infrared (IR) imagery are appropriate techniques for the characterization and quantification of river landscape heterogeneity. The concurrent integration of data from different kinds of surveys on one ecosystem (e.g. remote sensing and species-based field research) and across broad spatial and temporal scales increases the probability of discovering unexpected findings about the natural environment. Detecting ecological "surprises" has been recognized as critical in advancing ecology (Lindenmayer et al. 2010a). Moreover, the studies presented here contributed towards unraveling the complex nature of river ecosystems, providing useful insights into the key natural and anthropogenic drivers that shape the composition and configuration of acoustic and thermal patches, which in turn may influence biota and ecosystem processes. The outputs of this thesis may have broad application to multiple disciplines including those studying impacts of river restoration and conservation, river and habitat modification, river modeling, and landscape dynamics. Furthermore, the results of this study can guide researchers in designing and executing field experiments aimed at better understanding ecosystem processes and the ecology and behavior of freshwater organisms, as well as in making predictions on the ecological consequences of changing landscapes. Finally, I believe that studies at the landscape scale can be enhanced through a stronger collaboration between ecologists, engineers and informatics scientists.

Acoustic characterization of river landscapes

Ecological relevance of underwater soundscapes

Even though all fishes studied to date are able to hear sound (Fay and Popper 2000), hearing data in the literature are only available for about 100 out of 30,000 described fish species (Ladich and Popper 2004). Acoustic signals in water are composed of two physically related components: directional (vectorial) particle velocity and propagating scalar pressure waves (Michelsen 1983). Hearing among fishes differs in spectral range (bandwidth) and absolute sensitivity depending on the presence or absence of specially evolved anatomical structures (e.g. Weberian ossicles: modified bones of the vertebral column) (Ladich and Popper 2004; Popper and Fay 2010). These structures connect (i.e. otophysic connection) the inner ear with

the swim bladder, thus enhancing the ability of a fish to detect and use sound pressure signals (Popper and Fay 2010).

The majority of fish species is expected to respond principally to the particle motion of sound, namely to particle acceleration, and hear best within 0.030-1 kHz. Species with special adaptations (e.g. carps, catfishes, herrings, minnows) can detect sounds up to 3-5 kHz (Ladich and Popper 2004; Webb et al. 2008b; and references therein). Few species, however, are sensitive to ultrasound up to 180 kHz (e.g. some fishes in the order Clupeiformes; Mann et al. 1997; Higgs et al. 2004; Popper et al. 2004) or to infrasound down to below 1 Hz (e.g. Atlantic cod, plaice, perch, Atlantic salmon, European silver eels; Sand and Karlsen 2000; Sand et al. 2001). Nevertheless, we have scarce information about the relevance of the individual sound components (Horodysky et al. 2008). There is a lack of data supporting the concept that only species with obvious morphological specializations detect the pressure component; most species are expected to have pressure detection capabilities (Popper and Fay 2010). Furthermore, recent studies showed that the general shape of the particle velocity spectrum of studied fish species and of ambient sound are generally similar to the sound pressure spectrum (Lugli and Fine 2007; Horodysky et al. 2008; Wysocki et al. 2009). Wysocki et al. (2009) reported that particle velocity and sound pressure levels increase and decrease proportionally to each other. Accordingly, the general spectrum shape and best hearing range of fishes are independent of the physical unit measured.

Despite the fact that in this thesis (Chapters 1 to 3) only the pressure component of the aquatic sound field was measured, some considerations can be given to the potential ecological relevance of river soundscapes.

From an ecological perspective, rivers are differentiated by many attributes such as temperature conditions, food availability, and flow regime. However, the acoustic signature is potentially a pivotal and integrating component of the river environment. Underwater sounds may originate from biotic sources such as fish and invertebrates; from natural abiotic sources such as the movement of flowing water and its interaction with geomorphic structures, collapsing air bubbles in the water column, and wind; and from anthropogenic sources such as shipping and boating. In Chapters 1 to 3 the importance of hydrogeomorphic variables - especially water velocity, relative roughness, flow obstructions, and streambed sediment transport - and of fluctuating flow conditions in shaping the acoustic pattern of rivers were quantified. A dynamic river exhibits different soundscapes throughout the year coinciding with specific climatic conditions (e.g. rainfall, snow melting, drought) and related hydrological mechanisms (flow regime). On the other hand, human interventions like

channelization not only reduce geomorphic and hydraulic dynamics (e.g. reducing connectivity and habitats diversity) and the related ecological processes, but also strongly affect acoustic heterogeneity (Chapter 3).

Natural sounds of up to 150-160 dB (Chapters 2 and 3) can exceed the sound pressure level caused by boating and shipping (130-160 dB, main energy content <1.5 kHz; Vasconcelos et al. 2007; Codarin et al. 2009; Picciulin et al. 2010). A sound pressure level of 160 dB in water corresponds to 134 dB sound pressure level in the air (because of the different reference values: 1 µPa in the water and 20 µPa in the air). As comparison, a normal conversation is 60-70 dB, city traffic (inside a car) is 85 dB, a rock concert is 115 dB, and a gun blast is 140 dB (≥140 dB: level at which even short term exposure can cause permanent damage to the human ear) (all data for about 1 m distance; GCA 2011). Popper and Hastings (2009a, b) as well as Slabbekoorn et al. (2010) recently summarized the feasible behavioral impacts of anthropogenic noise on fishes such as predator-prey interactions, stress-induced fitness reduction, and disturbance of fish distribution (e.g. removal from important feeding and reproduction areas). For example, high sound pressure levels might elevate the hearing threshold, interfere with intraspecific communication among individual fish (Wysocki and Ladich 2005; Vasconcelos et al. 2007; Picciulin et al. 2010), increase stress levels, and impact the immune system, resulting in an increase in the secretion of the stress hormone cortisol or in an increase in the heart rate (Wysocki et al. 2006; Graham and Cooke 2008).

Boat traffic or loud sounds produced by strong turbulence (e.g. rapids, riffles, step-pools) are normally of relatively short exposure and limited areal impact. Thus, fishes may respond to stress caused by loud sounds by avoiding these areas. In contrast, high sound pressure levels during floods (mainly due to streambed sediment transport) are long-lasting (floods can persist for days to weeks), thereby impacting large areas and affecting various freshwater biota. However, Vasconcelos et al. (2007) and Codarin et al. (2009) demonstrated that the hearing abilities of teleost families are well adapted to the local background ambient sound. These authors also showed that hearing is only slightly masked by ambient sound and thus does not impact detection thresholds of intraspecific sounds. However, these authors recorded ambient sound in a river estuary and in a calm sea, respectively. Consequently, sound pressure levels (100-110 dB, main energy content <1 kHz) were well below the levels recorded in this thesis (Chapters 2 and 3). Thus, auditory sensitivities may change in relation to higher conditions of sound pressure levels. The low-energy quiet zone found at 0.063-0.5 kHz (Chapters 1 to 3), even found at high flow, coincides with the best hearing range of many fish species (Hawkins 1981; Fay and Simmons 1999; Ladich and Popper 2004; and references

therein). A similar "noise window" was found in fast-flowing waters in both pressure and velocity spectra (Lugli and Fine 2003, 2007). These quiet zones may be very important for active communication in loud river sections because the strength of a biological sound signal must exceed that of the ambient soundscapes in order to be detectable (Kingsford et al. 2002; Vasconcelos 2007).

Active fish communications are most likely masked in zones showing high-turbulent conditions (e.g. rapids, riffles) characterized by high middle-frequency sound pressure levels. Along natural rivers, quiet zones such as glides, runs, eddies, pools, and backwaters occur. Fishes may exploit these zones for intraspecific communication. Moreover, in shallow zones such as riffles and rapids, the propagation of low-frequency sounds may be subjected to a local constraining phenomenon. Sound at frequencies below the cutoff (i.e. wavelengths > four times the flow depth) cannot propagate as acoustic waves over a rigid bottom (Officier 1958; Urick 1983; Rogers and Cox 1988) and therefore is rapidly attenuated (Fine and Lenhardt 1983; Lugli and Fine 2003, 2007). On the other hand, high frequencies are more affected by absorption than low frequencies (approximately 0 dB km^{-1} for 0.0315 kHz and 1.8-2.4 dB km^{-1} for 16 kHz; data obtained from the UK National Physical Laboratory). Irrespective of those constraints, the unique river and habitat sounds may allow organisms to acoustically interpret their surrounding space.

Organisms use all their senses to perceive their environment. Acoustic signals travel about five times faster in water compared to air and exhibit a lower attenuation rate compared to light and chemical substances (Hawkins and Myrberg 1983; Rogers and Cox 1988), thereby are very efficient carriers of information. All sounds audible to a species are significant in the sense that fitness of the species would depend upon its capacity to segregate the relevant sources from the irrelevant ones (Fay and Popper 2000). The ability to discern sound source characteristics in the usual environments containing multiple sources may have been a key selective factor in the evolution of hearing specializations, and the auditory system of many organisms may have adapted to several types of acoustic constraints (Fay and Popper 2000).

Communication between individuals or groups of animals is certainly not the only role of sound (Popper and Hastings 2009b). It is well known that many aquatic organisms like crustacean larvae (Montgomery et al. 2006; Radford et al. 2007; Stanley et al. 2010), settlement-stage coral fish larvae (Tolimieri et al. 2004; Simpson et al. 2005; Wright et al. 2010), free-swimming coral fish larvae (Vermeij et al. 2010) as well as frogs (Bee 2007; Swanson et al. 2007), and newts (Diego-Rasilla and Luengo 2007; Pupin et al. 2007) can detect and localize underwater soundscapes and are able to use this signal for spatial

orientation, for solving directional movement challenges, and for facilitating detection and selection of preferred locations in their environment. Furthermore, in a recent work, Simpson et al. (2010) suggested that settlement-stage coral reef fish larvae not only are influenced by, but also can retain information from recent acoustic experiences. Indeed, some fish species are able to obtain information about wind or water currents (Popper and Fay 1993; Lagardere et al. 1994) as well as detect complex acoustic landscapes with distinct landmarks and information about distant structures beyond the range of vision (Popper et al. 2003).

Slabbekoorn and Bouton (2008) and Fay (2009) suggested that fishes and other aquatic organisms probably make use of acoustic scenes (soundscapes) for orientation within aquatic landscapes. Thus, freshwater biota probably exploit the acoustic signals of different soundscapes as a supplementary information source about their surrounding area to orient themselves within the water course (e.g. migration) and to locate and navigate to habitat types with favorable attributes (e.g. for resting, feeding, and breeding). Moreover, typical acoustic signals may help aquatic organisms to detect refuges within high flow conditions, thus potentially influencing their behavior and ecology. Finally, changes in river and habitat acoustics over time (days to years), depending mostly on hydrogeomorphic and anthropogenic changes, are potential challenges for biota.

Outlook

Recently, Pijanowski et al. (2011) suggested that soundscape ecology be considered as a new research field, which emphasizes the ecological characteristics of sounds and their spatiotemporal patterns as they emerge from landscapes. Those authors, among others, have emphasized the need for more research aimed at measuring and quantifying spatiotemporal dynamics across different scales and the potential impact of soundscapes on organisms. Both tasks were studied and discussed in this thesis (Chapters 1 to 3).

In this study, the application of underwater soundscape analysis at different spatial scales offered first insights into the direct relationship between hydrogeomorphology and underwater sound generation. Additional field research linking physical parameters of flow (e.g. Froude number, Reynolds number, turbulent kinetic energy, shear stress, stream power), river morphology (e.g. relative roughness, sediment size and volume, slope) and their relationship to the origin and propagation (e.g. cutoff, absorption, scattering) of acoustic signals are crucial and explicitly needed for a proper understanding of the underwater acoustic environment of flowing waters. For example, the exact measures of flow hydraulics (e.g. flow velocity and depth) recorded every 5 seconds with an ADP (Acoustic Doppler Current Profiler) could be related to the acoustic signals, instead of using the average value of the

entire segment length (see Chapter 3). This would facilitate a more exact relationship between hydrogeomorphic parameters and sound generation.

Streambed sediment transport was related to high sound pressure levels and sediment grain sizes influenced unique frequencies (Chapter 3). The sound produced by streambed sediments moving on the river bottom can be used to estimate the intensity and particle composition of streambed sediment. To test this, the acoustic equipment should be completed with a sonar (to make real-time video images of the bottom substrate), ADP, and GPS equipment to simultaneously measure acoustic signals, substrate size composition, and flow hydraulics. Those simultaneous measurements would allow the assessment of how closely the sound pressure level is related to the intensity of streambed sediment transport and what particle sizes are reflected at what frequency or frequency range. If sound measurements produce reliable results for the estimation of streambed sediment transport, exciting research questions emerge about which kind of sediment grain size is transported and deposited along a river course and where potential areas of sediment erosion and accumulation are. Furthermore, sound equipment could be installed in automatic gauging stations, thus providing important information about real-time streambed sediment transport activity. It would also be possible to use fiber-optic cables buried in the river bed to continuously record bedload motion (see Selker et al. 2006 for an example of the use of fiber-optic cables). Those data would allow major advancements in the field of fluvial geomorphology and landscape dynamics.

Soundscape analysis could be used to differentiate aquatic habitats and, as such, serve as an indicator of river system complexity because it reflects important hydrogeomorphic dynamics of river habitats. It may provide a quick yet accurate means of monitoring river restoration measures aimed at re-naturalizing river structure and function, manipulating flow regimes, ecosystem changes, and negative impacts such as channelization and shipping. The power of this approach is that river ecologists could potentially use soundscapes to characterize spatial heterogeneity in a more direct (i.e. less biased) and potentially more cost-effective manner than visual classification by observers in the field.

We may increase or decrease acoustic heterogeneity by manipulating specific hydrogeomorphic characteristics of the river. There is a need to conserve, protect, and value natural soundscapes as it is done for other aspects of nature (Pijanowski et al. 2011). Finally, the alteration of the river acoustic environment could impact the behavior of aquatic organisms, and therefore, have general ecological implications.

I believe that soundscape investigation has very good potential for future studies on animal behavior (see also Slabbekoorn and Bouton 2008; Fay et al. 2009). Furthermore, given the possible relevance of ultrasonic and infrasonic signals for aquatic biota (Popper and Carlson 1998), it would be interesting to extend the analyzed frequency range in future studies. However, because of the complexity of sound in rivers, and because there is a major step between characterizing soundscapes and interpreting their meaning ecologically, particular attention must be paid to physical process and ecological response. As recently stressed by Popper and Hastings (2009a, b), there are indications that some types of sounds, under certain conditions and with different species, can cause variable species response. Therefore it is important to note that at this stage of our knowledge, extrapolation of species response to the same sounds under different environmental conditions, or to other organisms is nearly impossible. Moreover, laboratory observations do not always indicate how an unrestrained animal would behave when exposed to the same sound in its natural environment.

In Chapters 1 to 3 I showed that kilometers-long river segments and the habitat types nested within these segments have unique acoustic characteristics and I provided important information on the most relevant hydraulic and geomorphic variables that can influence the heterogeneity of the acoustic signals in rivers. This information is expected to improve the understanding of the possible impact of such complex sound signals on animal behavior and will help to develop innovative experiments to address the ecological questions raised.

Thermal characterization of river landscapes

Ecological relevance of thermal landscapes

The predicted increase of air temperature of 0.2°C per decade (IPCC 2007) is a critical stressor in river floodplains (Tockner et al. 2010). A significant water temperature increase in the last 100 years was found in many streams and rivers in the USA (up to 0.077°C yr^{-1}, Kaushal et al. 2010) and, to a lesser extent, in Austrian rivers (Webb and Nobilis 2007). The future increases in air temperature and the concurrent decrease in flow during summer is expected to increase the thermal distinctiveness of aquatic and terrestrial habitats across river floodplains and lead to higher temperature in isolated water bodies. This will increase physiological stress for aquatic organisms, may shift community structures, and will accelerate ecosystem processes. For example, an increase in temperature may reduce the suitability of habitats for many fish species. This might improve the conditions for mosquito breeding habitats by reducing predation.

Because of the ecological importance of temperature, preventing or mitigating anthropogenic thermal degradation is a common concern for resource managers, and it is therefore addressed by the European Water Framework Directive. Understanding the ecological responses of organisms and ecosystems to changes in climate and temperature requires a good understanding of spatial and temporal trends in temperature variation in river floodplains.

Thermal IR imagery provides a unique opportunity to simultaneously map and quantify the surface temperature of aquatic and terrestrial habitats at a spatial scale relevant to ecosystem processes and biota distribution. This technique adds critical information on broad spatial scales and allows the detection and quantification of complex thermal mosaics (see Chapters 4 and 5). Moreover, it provides a means to scale-up ecosystem processes from point measurements to the entire river floodplain system.

Many physical and biochemical processes are controlled by temperature and flow (Caissie 2006; Pörtner and Farrell 2008; Buisson et al. 2008; Jonsson and Jonsson 2009; Olden and Naiman 2010; and references therein). Temperature regulates the solubility of oxygen and other gases, the availability of nutrients and toxic substances, primary production, and decomposition (Magnuson et al. 1979; Webb 1996; Caissie 2006), as well as protein synthesis, photosynthesis, energy conversion, and respiration (Jonsson and Jonsson 2009; McCullough et al. 2009). As a result, temperature and thermal heterogeneity exert direct or indirect control over the distribution of aquatic and terrestrial organisms, and influence ecosystem processes.

For ectothermic organisms such as fish, temperature determines all major life history traits (Wolter 2007; Buisson et al. 2008; Pörtner and Farrell 2008; Jonsson and Jonsson 2009; McCullough et al. 2009). Furthermore, growth, development, composition, and distribution of aquatic invertebrates are all influenced by temperature (Brittain and Campbell 1991; Chadwick and Feminella 2001; Daufresne et al. 2004; Chinnayakanahalli et al. 2011). Increasing temperature (+1.5°C and heatwaves) reduced richness and changed community structure of macroinvertebrates in the lowland Saône River (Mouthon and Daufresne 2006). Similarly, Durance and Ormerod (2007) stressed that macroinvertebrate abundance in British headwaters might decline by 21% for every 1°C rise in water temperature, and already scarce species would risk local extinction. Richter et al. (2008) found that a 1°C winter water temperature increase in northern German streams accelerated the emergence of dragonflies by 6-7 days. Moreover, Harper and Peckarsky (2006) found that water temperature predicted the onset of emergence in the mayflies *Baetis bicaudatus*. They speculated that large-scale climate change could cause significant shifts in the timing of mayfly metamorphosis.

Temperature is also critical for pond-breeding amphibians. For example, McMenamin et al. (2008) found that recent climatic warming and resultant pond desiccation are causing dramatic declines in amphibian population density and species richness. Further, amphibians' survival depends on certain cool terrestrial habitat types such as large wood deposits for thermal shelter (Indermaur et al. 2009). Temperature determines habitat quality and thereby influences anuran body size at metamorphosis (Indermaur et al. 2010). Thermal heterogeneity may also facilitate the co-occurrence of amphibian species (Indermaur et al. 2009).

Temperature preferences can change during an organism life cycle. Young stages may prefer different temperature niches than adults and, therefore, take advantage of thermal heterogeneity (e.g. Bonte et al. 2008). Aquatic organisms generally have to face a narrower range of temperature fluctuations than terrestrial organisms. Thus, mobile terrestrial organisms may take advantage of the spatial thermal heterogeneity by actively avoiding unfavorable hot or cold zones. Moreover, diel and seasonal changes in the thermal surface heterogeneity may imply differences over time in the patch use by biota. Thermal boundaries between patches can constrain animals' movement and composition among habitats and thereby influence migration, local extinction, invasion of non-native species, and/or (re)colonization, as well as overall biodiversity.

Temperature-dependent ecosystem processes like respiration, primary production, denitrification, and organic matter decomposition will also differ between thermal patch units, thereby influencing river energetics (Richardson 1992). Langhans et al. (2008) found that floodplain heterogeneity generates spatial variability in the decomposition of coarse-particulate organic matter. Higher temperatures may promote leaf decomposition and respiration in aquatic habitats. Temperature was also identified as the main factor controlling the high spatiotemporal heterogeneity of soil and sediment respiration within various floodplain habitat types (Döring et al. 2011). Moreover, Acuña et al. (2008) stressed that an increase of 2.5°C in water temperature will increase river respiration by an average of 20 ± 1.6%. When assessing the consequences of temperature changes for ecosystem processes (especially those controlled by microbial communities; see Dang et al. 2009 and references therein), not only spatial temperature heterogeneity but also diel temperature oscillations need to be considered.

Although thermal IR imagery is not without constraints (and therefore not suited for every research purpose), it provides information about the spatial patterns of fine- and large-scale habitat temperature. For example, Scherrer and Körner (2010a, b) found that fine-scale thermal mosaics of alpine landscapes reflect changes of otherwise several hundred meters of

elevation. These small patches are inhabited by plant species with different thermal preferences, creating key thermal refuges against warming. Thermal heterogeneity is expected to reduce the distance that biota need to move because of temperature rise. Maintaining thermal heterogeneity of river floodplains is pivotal for conserving biodiversity. Based on the results of the present study (Chapters 4 and 5) it is clear that the spatiotemporal thermal heterogeneity in river floodplains will most likely be underestimated by using only in-situ point measurements.

Outlook

The continuous and rapid development of thermal IR sensors may serve as a major stimulus for future studies on the thermal heterogeneity of aquatic and terrestrial ecosystems. However, additional research is also needed to improve the accuracy and reduce the uncertainties associated with thermal IR imagery in complex river landscapes such as floodplains.

In Chapters 4 and 5 I showed the value of thermal IR imagery as a non-invasive method to quantify thermal heterogeneity, to identify thermal refugia, and to detect thermal gradients, all at a spatial resolution relevant for predicting ecosystem processes and the distribution of biota. Broad-scale thermal mosaics provide the required spatial overview of surface temperature for better understanding the consequences of changes in landscape and climate. Supplementary research aimed at better understanding how thermal patches are recognized and utilized by various organisms at various times during the day and season is explicitly needed. The thermal IR images might also assist scientists to more effectively translate conservation and restoration strategies into management and policy by providing pictoral representation of habitat heterogeneity rather than more abstract statistical or graphical representations.

For the successful conservation and restoration of river floodplains we need to document how the spatiotemporal thermal heterogeneity and the physical factors that generate it (like inundation dynamics) govern species diversity and ecosystem processes at multiple spatial scales. I encourage the inclusion of terrestrial habitats as well as the vertical and temporal components of the temperature regime in future studies of thermal heterogeneity and the temperature regime of river floodplains. Expanding the spatial and temporal scales may complicate the interpretation of thermal IR images due to varied effects of differing surface materials and atmospheric conditions, but there is much to be gained from viewing the entire thermal landscape of rivers, laterally, longitudinally, vertically, and temporally.

Remote sensing techniques such as thermal IR imagery can also be used to study and gain valuable insights into major events such as floods. Floods can shape river landscapes,

influence key ecological processes, and affect biota. Usually, research is performed before or after a flood using in-situ survey techniques. Hence, almost nothing is known about the processes occurring during the flood event. Conventional remote sensing surveys can not be done using commercial providers of airborne imagery because this requires scheduling around other clients; hence observing a flood event is often simply not possible. Finally, to assess temporal changes several flights should be performed, which is not financially affordable.

High accuracy images for detailed assessment of flood events could be collected using Unmanned Aerial Systems(UAS). UAS are capable of autonomous flight, are time- and cost-effective, are flexible in mission planning, can fly at low altitude (allowing sub-centimeter resolution and avoiding the cloud canopy), and will permit more measurements to be taken at different daily, seasonal, and annual conditions. Extensive spatial and temporal surveys could then be feasible. The flexibility of such systems would also allow ecological research to begin quickly, for example the moment a flood occurs, and may help obtain unexpected and pivotal results, develop new ecological theories and concepts, and significantly improve our ecological understanding (Lindenmayer et al. 2010b).

Further applications of UAS and appropriate sensors in river landscape research could be: (i) quantifying the effect of anthropogenic alterations of the flow regime (water abstraction for industrial and agricultural use) on the surface temperature (using a thermal IR camera), (ii) mapping of mammals such as wild pigs or deer in wetlands (using a thermal IR camera), (iii) detecting upwelling and downwelling zones (using a thermal IR camera), (iv) quantifying light pollution (using light sensors), (v) three-dimensional mapping and reconstruction of river landscapes (using a laser scanner), and (vi) quantifying suspended sediment concentration, chlorophyll *a*, and turbidity (using hyper- and multispectral cameras). I expect that UAS will be able to complement point monitoring and in-situ approaches by providing spatially and temporally extensive and affordable data in the near feature.

References for the introduction and discussion section

Acuña V, Wolf A, Uehlinger U, Tockner K. 2008. Temperature dependence of stream benthic respiration in an Alpine river network and its relevance to global warming. *Freshwater Biology* 53: 2076-2088.

Acuña V, Tockner K. 2009. Surface-subsurface water exchange rates along alluvial river reaches control the thermal patterns in an Alpine river network. *Freshwater Biology* 54: 306-320.

Amoser S, Ladich F. 2005. Are hearing sensitivities of freshwater fish adapted to the ambient noise in their habitats? *Journal of Experimental Biology* 208: 3533-3542.

Amoser S, Ladich F. 2010. Year-round variability of ambient noise in temperate freshwater habitats and its implications for fishes. *Aquatic Sciences* 3: 371-378.

Arscott DB, Tockner K, Ward JV. 2001. Thermal heterogeneity along a braided floodplain river (Tagliamento River, northeastern Italy). *Canadian Journal of Fisheries and Aquatic Sciences* 58: 2359-2373.

Bee MA. 2007. Selective phonotaxis by male wood frogs (*Rana sylvatica*) to the sound of a chorus. *Behavioral Ecology and Sociobiology* 61: 955-966.

Belknap W, Naiman RJ. 1998. A GIS and TIR procedure to detect and map wall-base channels in Western Washington. *Journal of Environmental Management* 52: 147-160.

Benson BJ, Bond BJ, Hamilton MP, Monson RK, Han R. 2010. Perspectives on next-generation technology for environmental sensor networks. *Frontiers in Ecology and the Environment* 8: 193-200.

Bonte D, Travis JMJ, De Clercq N, Zwertvaegher I, Lens L. 2008. Thermal conditions during juvenile development affect adult dispersal in a spider. *Proceedings of the National Academy of Sciences* 105: 17000-17005.

Brittain JE, Campbell IC. 1991. The effect of temperature on egg development in the Australian mayfly genus *Coloburiscoides* (Ephemeroptera: *Coloburiscidae*) and its relationship to distribution and life history. *Journal of Biogeography* 18: 231-235.

Buisson L, Blanc L, Grenouillet G. 2008. Modelling stream fish species distribution in a river network: the relative effects of temperature versus physical factors. *Ecology of Freshwater Fish* 17: 244-257.

Caissie D. 2006. The thermal regime of rivers: a review. *Freshwater Biology* 51: 1389-1406.

Chadwick MA, Feminella JW. 2001. Influence of salinity and temperature on the growth and production of a freshwater mayfly in the Lower Mobile River, Alabama. *Limnology and Oceanography* 46: 532-542.

Chinnayakanahalli KJ, Hawkins CP, Tarboton DG, Hill RA. 2011. Natural flow regime, temperature and the composition and richness of invertebrate assemblages in streams of the western United States. *Freshwater Biology*. In press: Doi: 10.1111/j.1365-2427.2010.02560.x.

Codarin A, Wysocki LE, Ladich F, Picciulin M. 2009. Effects of ambient and boat noise on hearing and communication in three fish species living in a marine protected area (Miramare, Italy). *Marine Pollution Bulletin* 58: 1880-1887.

Cristea NC, Burges SJ. 2009. Use of thermal infrared imagery to complement monitoring and modeling of spatial stream temperatures. *Journal of Hydrologic Engineering* 14: 1080-1090.

Dang CK, Schindler M, Chauvet E, Gessner MO. 2009. Temperature oscillation coupled with fungal community shifts can modulate warming effects on litter decomposition. *Ecology* 90: 122-131.

Daufresne M, Roger MC, Capra H, Lamouroux N. 2004. Long-term changes within the invertebrate and fish communities of the Upper Rhone River: effects of climatic factors. *Global Change Biology* 10: 124-140.

Diego-Rasilla FJ, Luengo RM. 2007. Acoustic orientation in the palmate newt, *Lissotriton helveticus*. *Behavioral Ecology and Sociobiology* 61: 1329-1335.

Döring M, Uehlinger U, Ackermann T, Woodtli M, Tockner K. 2011. Spatiotemporal heterogeneity of soil and sediment respiration in a river-floodplain mosaic (Tagliamento, NE Italy). *Freshwater Biology*. In press: Doi:10.1111/j.1365-2427.2011.02569.x.

Durance I, Ormerod SJ. 2007. Climate change effects on upland stream macroinvertebrates over a 25-year period. *Global Change Biology* 13: 942-957.

Fausch KD, Torgersen CE, Baxter CV, Li HW. 2002. Landscapes to riverscapes: bridging the gap between research and conservation of stream fishes. *Bioscience* 52: 483-498.

Faux RN, Maus P, Lachowsky H, Torgersen CE, Boyd MS. 2001. *New Approaches for Monitoring Stream Temperature: Airborne Thermal Infrared Remote Sensing*. Inventory and monitoring project report, integration of remote sensing, Remote sensing applications center, USDA Forest service engineering.

Fay RR, Simmons AM. 1999. The sense of hearing in fishes and amphibians. In *Comparative Hearing: Fishes and Amphibians*, Fay RR, Popper AN (eds). Springer-Verlag: New York; 269-318.

Fay RR, Popper AN. 2000. Evolution and hearing in vertebrates: the inner ears and processing. *Hearing Research* 149: 1-10.

Fay RR. 2009. Soundscapes and the sense of hearing in fishes. *Integrative Zoology* 4: 26-32.

Fine ML, Lenhardt ML. 1983. Shallow-water propagation of the toadfish mating call. *Comparative Biochemistry and Physiology A* 76: 225-231.

Frissell CA, Liss WJ, Warren CE, Hurley MD. 1986. A hierarchical framework for stream habitat classification: viewing streams in a watershed context. *Environmental Management* 10: 199-214.

GCA 2011. *Galen Carol Audio*. http://www.gcaudio.com/resources/howtos/loudness.html (last accessed 15th April 2011).

Graham AL, Cooke SJ. 2008. The effects of noise disturbance from various recreational boating activities common to inland waters on the cardiac physiology of a freshwater fish, the largemouth bass (*Micropterus salmoides*). *Aquatic Conservation: Marine Freshwater Ecosystems*: 18: 1315-1324.

Harper MP, Peckarsky BL. 2006. Emergence cues of a mayfly in a high-altitude stream ecosystem: potential response to climate change. *Ecological Applications* 16: 612-621.

Hawkins AD. 1981. The hearing abilities of fish. In *Hearing and Sound Communication in Fishes*, Tavolga WN, Popper AN, Fay RR (eds). Springer-Verlag: New York; 109-133.

Hawkins AD, Myrberg AA. 1983. Hearing and sound communication under water. In *Bioacoustics, a Comparative Approach*, Lewis B (ed). Academic Press: London; 347-405.

Higgs DM, Plachta DTT, Rollo AK, Singheiser M, Hastings MC, Popper AN. 2004. Development of ultrasound detection in American shad (*Alosa sapidissima*). *Journal of Experimental Biology*: 207: 155-163.

Horodysky AZ, Brill RW, Fine ML, Musick JA, Latour RJ. 2008. Acoustic pressure and particle motion thresholds in six sciaenid fishes. *Journal of Experimental Biology*: 211: 1504-1511.

Illies J, Botosaneau L. 1963. Problèmes et méthodes de la classification et de la zonation écologiques des eaux courantes considerées surtout du point de vue faunistique. *Mitteilungen der Internationalen Vereinigung für theorische und angwandte Limnologie* 12: 1-57.

Indermaur L, Gehring M, Wehrle W, Tockner K, Näf-Dänzer B. 2009. Behavior-based scale definitions for determining individual space use: requirement of two amphibians. *The American Naturalist* 173: 60-71.

Indermaur L, Schmidt BR, Tockner K, Schaub M. 2010. Spatial variation in abiotic and biotic factors in a floodplain determine anuran body size and growth rate at metamorphosis. *Oecologia* 163: 637-49.

IPCC. 2007. *Intergovernmental Panel on Climate Change*. Fourth assessment report on climate change. http://www.ipcc.ch/ (last accessed 25th February 2011).

Jonsson B, Jonsson N. 2009. A review of the likely effects of climate change on anadromous Atlantic Salmon *Salmo salar* and brown trout *Salmo trutta*, with particular reference to water temperature and flow. *Journal of Fish Biology* 75: 2381-2447.

Kaushal SS, Likens GE, Jaworski NA, Pace ML, Sides AM, Seekell D, Belt KT, Secor DH, Wingate RL. 2010. Rising stream and river temperatures in the United States. *Frontiers in Ecology and the Environment* 8: 461-466.

Kingsford MJ, Leis JM, Shanks A, Lindeman KC, Morgan SG, Pineda J. 2002. Sensory environments, larval abilities and local self-recruitment. *Bulletin of Marine Science*: 70: 309-340.

Ladich F, Popper AN. 2004. Parallel evolution in fish hearing organs. In *Evolution of the Vertebrate Auditory System*, Manley GA, Popper AN, Fay RR (eds). Springer-Verlag: New York; 95-127.

Lagardere JP, Begout ML, Lafaye JY, Villotte JP. 1994. Influence of wind-produced noise on orientation in the sole (*Solea-Solea*). *Canadian Journal of Fisheries and Aquatic Sciences* 51: 1258-1264.

Langhans SD, Tiegs SD, Gessner M, Tockner K. 2008. Leaf decomposition heterogeneity across a riverine floodplain mosaic. *Aquatic Sciences* 70: 337:346.

Leopold LB, Maddock T. 1953. The hydraulic geometry of stream channels and some physiographic implications. *US Geological Survey Professional Paper* 252.

Lindenmayer DB, Likens GE, Krebs CJ, Hobbs RJ. 2010a. Improved probability of detection of ecological "surprises". *Proceedings of the National Academy of Sciences*: 21957-21962.

Lindenmayer DB, Likens GE, Franklin JF. 2010b. Rapid responses to facilitate discoveries from major disturbances. *Frontiers in Ecological Environments* 8: 527-532.

Loheide SP, Gorelick SM. 2006. Quantifying stream-aquifer interactions through the analysis of remotely sensed thermographic profiles and in situ temperature histories. *Environmental Science and Technology* 40: 3336-3341.

Lugli M, Fine ML. 2003. Acoustic communication in two freshwater gobies: ambient noise and short-range propagation in shallow streams. *Journal of the Acoustical Society of America* 114: 512-521.

Lugli M, Fine ML. 2007. Stream ambient noise, spectrum and propagation of sounds in the Goby *Padogobius martensii*: sound pressure and particle velocity. *Journal of the Acoustical Society of America* 122: 2881-2892.

Lurton X. 2002. *An Introduction to Underwater Acoustic: Principles and Applications*. Springer Verlag: Chichester; 347.

Madej MA, Currens C, Ozaki V, Yee J, Anderson DG. 2006. Assessing possible thermal rearing restrictions for juvenile coho salmon (*Oncorhynchus kisutch*) through thermal infrared imaging and in-stream monitoring, Redwood Creek, California. *Canadian Journal of Fisheries and Aquatic Sciences* 63: 1384-1396.

Magnuson JJ, Crowder LB, Medvick PA. 1979. Temperature as an ecological resource. *American Zoologist* 19: 331-343.

Malard F, Mangin A, Uehlinger U, Ward JV. 2001. Thermal heterogeneity in the hyporheic zone of a glacial floodplain. *Canadian Journal of Fisheries and Aquatic Sciences* 58: 1319-35.

Mann DA, Lu Z, Popper AN. 1997. A clupeid fish can detect ultrasound. *Nature*: 389: 341.

Marcus WA, Fonstad MA. 2008. Optical remote mapping of rivers at sub-meter resolutions and watershed extents. *Earth Surface Processes and Landforms* 33: 4-24.

Marcus WA, Fonstad MA. 2010. Remote sensing of rivers: the emergence of a subdiscipline in the river science. *Earth Surface Processes and Landforms* 35: 1867-1872.

McCullough DA, Bartholow JM, Jager HI, Beschta RL, Cheslak EF, Deas ML, Ebersole JL, Foott JS, Johnson SL, Marine KR, Mesa MG, Petersen JH, Souchon Y, Tiffan KF, Wurtsbaugh WA. 2009. Research in thermal biology: burning questions for coldwater stream fishes. *Reviews in Fisheries Science* 17: 90-115.

McMenamin SK, Hadly EA, Wright CK. 2008. Climatic change and wetland desiccation cause amphibian decline in Yellowstone National Park. *Proceedings of the National Academy of Sciences* 105: 16988-16993.

Mertes LAK. 2002. Remote sensing of riverine landscapes. *Freshwater Biology* 47: 799-816.

Michelsen A. 1983. Biophysical basis of sound communication. In *Bioacoustics, a Comparative Approach*, Lewis B (ed). Academic Press: London; 3-38.

Montgomery DR, Buffington JM. 1997. Channel-reach morphology in mountain drainage basins. *Geological Society of America Bulletin* 109: 596-611.

Montgomery JC, Jeffs A, Simpson SD, Meekan M, Tindle C. 2006. Sound as an orientation cue for the pelagic larvae of reef fishes and decapod crustaceans. *Advances in Marine Biology* 51: 143-196.

Mouthon J, Daufresne M. 2006. Effects of the 2003 heatwave and climatic warming on mollusc communities of the Saône: a large lowland river and of its two main tributaries (France). *Global Change Biology* 12: 441-449.

Officier CB. 1958. *Introduction to the Theory of Sound Transmission*. McGraw-Hill: New York; 284.

Olden JD, Naiman RJ. 2010. Incorporating thermal regimes into environmental assessments: modifying dam operations to restore freshwater ecosystem integrity. *Freshwater Biology* 55: 86-107.

Picciulin M, Sebastianutto L, Codarin A, Farina A, Ferrero EA. 2010. In situ behavioural responses to boat noise exposure of *Gobius cruentatus* (Gmelin, 1789; fam. Gobiidae) and *Chromis chromis* (Linnaeus, 1758; fam. Pomacentridae) living in a marine protected area. *Journal of Experimental Marine Biology and Ecology* 386: 125-132.

Pijanowski BC, Villanueva-Rivera LJ, Dumyahn SL, Farina A, Krause BL, Napoletano BM, Gage SH, Pieretti N. 2011. Soundscape Ecology: the science of sound in the landscape. *BioScience* 61: 203-216.

Popper AN, Fay RR. 1993. Sound detection and processing by fish - critical-review and major research questions. *Brain Behavior and Evolution* 41: 14-38.

Popper AN, Carlson TJ. 1998. Application of sound and other stimuli to control fish behavior. *Transactions of the American Fisheries Society* 127: 673-707.

Popper AN, Fay RR, Platt C, Sand O. 2003. Sound detection mechanisms and capabilities of Teleost fishes. In *Sensory Processing in Aquatic Environments*, Collin SP, Marshall NJ (eds). Springer-Verlag: New York; 3-38.

Popper AN, Plachta DTT, Mann DA, Higgs DM. 2004. Response of clupeid fish to ultrasound: a review. *ICES Journal of Marine Science* 61: 1057-1061.

Popper AN, Hasting MC. 2009a. The effects of anthropogenic sources of sound on fishes. *Journal of Fish Biology* 75: 455-489.

Popper AN, Hasting MC. 2009b. The effects of human-generated sound on fish. *Integrative Zoology* 4: 43-52.

Popper AN, Fay RR. 2010. Rethinking sound detection by fishes. *Hearing Research* 273: 25-36.

Porter JH, Nagy E, Kratz TK, Hanson P, Collins SL, Arzberger P. 2009. New eyes on the world: advanced sensors for ecology. *BioScience* 59: 385-397.

Pörtner HO, Farrell AP. 2008. Physiology and climate change. *Science* 322: 690-692.

Pupin F, Sacchi R, Gentilli A, Galeotti P, Fasola M. 2007. Discrimination of toad calls by smooth newts: support for the heterospecific attraction hypothesis. *Animal Behaviour* 74: 1683-1690.

Radford C, Jeffs AG, Montgomery J. 2007. Directional swimming behaviour by five species of crab post-larvae in response to reef sound. *Bulletin of Marine Science* 80: 369-378.

Richardson JS. 1992. Coarse particulate detritus dynamics in small montane streams of the southwestern British Columbia. *Canadian Journal of Fisheries and Aquatic Sciences* 49: 337-346.

Richter O, Suhling F, Mueller O, Kern D. 2008. A model for predicting the emergence of dragonflies in a changing climate. *Freshwater Biology* 53: 1868-1880.

Rogers PH, Cox M. 1988. Underwater sound as a biological stimulus. In *Sensory Biology of Aquatic Animals*, Atema J, Fay RR, Popper AN, Tavolga WN (eds). Springer-Verlag: New York; 131-149.

Sand O, Karlsen HE. 2000. Detection of infrasound and linear acceleration in fishes. *Philosophical Transactions of the Royal Society B* 355: 1295-1298.

Sand O, Enger PS, Karlsen HR, Knudsen FR. 2001. Detection of infrasound in fish and behavioral responses to intense infrasound in juvenile salmonids and European silver eels: a minireview. *American Fisheries Society Symposium* 26: 183-193.

Scherrer D, Körner C. 2010a. Infra-red thermometry of alpine landscapes challenges climatic warming projections. *Global Change Biology* 16: 2602-2613.

Scherrer D, Körner C. 2010b. Topographically controlled thermal-habitat differentiation buffers alpine plant diversity against climate warming. *Journal of Biogeography* 38: 406-416.

Selker JS, Thévenaz L, Huwald H, Mallet A, Luxemburg W, van de Giesen N, Stejskal M, Zeman J, Westhoff M, Parlange MB. 2006. Distributed fiber-optic temperature sensing for hydrologic systems. *Water Resources Research* 42: W12202.

Simpson SD, Meekan MG, Montgomery JC, McCauley RD, Jeff A. 2005. Homeward sound. *Science* 308: 221-221.

Simpson SD, Meekan MG, Larsen NJ, McCauley RD, Jeffs A. 2010. Behavioral plasticity in larval reef fish: orientation is influenced by recent acoustic experiences. *Behavioral Ecology* 21: 1098-1105.

Slabbekoorn H, Bouton N. 2008. Soundscape orientation: a new field in need of sound investigation. *Animal Behaviour* 76: 5-8.

Slabbekoorn H. Bouton N, Van Opzeeland I, Coers A, Ten Cate C, Popper AN. 2010. A noisy spring: the impact of globally rising underwater sound levels on fish. *Trends in Ecology and Evolution* 25: 419-427.

Stanley JA, Radford CA, Jeffs AG. 2010. Induction of settlement in crab megalopae by ambient underwater reef sound. *Behavioral Ecology* 21: 113-120.

Swanson EM, Tekmen SM, Bee MA. 2007. Do female frogs exploit inadvertent social information to locate breeding aggregations? *Canadian Journal of Zoology* 85: 921-932.

Thorp JA, Thoms MC, Delon MD. 2006. The riverine ecosystem synthesis: biocomplexity in river networks across space and time. *River Research and Applications* 22: 123-147.

Tiffan KF, Kock TJ, Connor WP, Steinhorst RK, Rondorf DW. 2009. Behavioural thermoregulation by subyearling fall (autumn) Chinook salmon *Oncorhynchus tshawytscha* in a reservoir. *Journal of Fish Biology* 74: 1562-1579.

Tockner K, Pusch M, Borchardt D, Lorang MS. 2010. Multiple stressors in coupled river-floodplain ecosystems. *Freshwater Biology* 55: 135-151.

Tolimieri N, Haine O, Jeffs A, McCauley R, Montgomery JC. 2004. Directional orientation of pomacentrid larvae to ambient reef sound. *Coral Reefs* 23: 184-191.

Torgersen CE, Price DM, Li HW, McIntosh BA. 1999. Multiscale thermal refugia and stream habitat associations of chinook salmon in northeastern Oregon. *Ecological Applications* 9: 301-19.

Torgersen CE, Faux RN, McIntosh BA, Poage NJ, Norton DJ. 2001. Airborne thermal remote sensing for water temperature assessment in rivers and streams. *Remote Sensing of Environment* 76: 386-398.

Uehlinger U, Malard F, Ward JV. 2003. Thermal patterns in the surface waters of a glacial river corridor (Val Roseg, Switzerland). *Freshwater Biology* 48: 284-300.

Urick RJ. 1983. *Principles of Underwater Sound*. McGraw-Hill: New York; 423.

Vannote RL, Minshall GW, Cummins KW, Sedell JR, Cushing CE. 1980. River continuum concept. *Canadian Journal of Fisheries and Aquatic Sciences* 37: 130-137.

Vasconcelos RO, Amorim MCP, Ladich F. 2007. Effects of ship noise on the detectability of communication signals in the Lusitanian toadfish. *Journal of Experimental Biology* 210: 2104-2112.

Vermeij MJA, Marhaver KL, Huijbers CM, Nagelkerken I, Simpson SD. 2010. Coral larvae move toward reef sounds. *PLoS ONE* 5: e10660.

Webb BW. 1996. Trends in stream and river temperature. *Hydrological Processes* 10: 205-226.

Webb BW, Zhang Y. 1999. Water temperatures and heat budgets in Dorset chalk water courses. *Hydrological Processes* 13: 309-321.

Webb BW, Clack PD, Walling DE. 2003. Water-air temperature relationships in a Devon river system and the role of flow. *Hydrological Processes* 17: 3069-3084.

Webb BW, Nobilis F. 2007. Long-term changes in river temperature and the influence of climatic and hydrological factors. *Hydrological Sciences Journal* 52: 74-85.

Webb BW, Hannah DM, Moore RD, Brown LE, Nobilis F. 2008a. Recent advances in stream and river temperature research. *Hydrological Processes* 22: 902-918.

Webb JF, Fay RR, Popper A. 2008b. *Fish Bioacoustics*. Springer-Verlag: New York; 322.

Wiens JA. 2002. Riverine landscapes: taking landscape ecology into the water. *Freshwater Biology* 47: 501-515.

Wohl E, Merritt DM. 2008. Reach-scale channel geometry of mountain streams. *Geomorphology* 93: 168-185.

Wolter C. 2007. Temperature influence on the fish assemblage structure in a large lowland river, the lower Oder River, Germany. *Ecology of Freshwater Fish* 16: 493-503.

Wright KJ, Higgs DM, Cato DH, Leis JM. 2010. Auditory sensitivity in settlement-stage larvae of coral reef fishes. *Coral Reefs* 29: 235-243.

Wysocki LE, Ladich F. 2005. Hearing in fishes under noise conditions. *Journal of the Association for Research in Otolaryngology*: 6: 28-36

Wysocki LE, Dittami JP, Ladich F. 2006. Ship noise and cortisol secretion in European freshwater fishes. *Biological Conservation* 128: 501-508.

Wysocki LE, Amoser S, Ladich F. 2007. Diversity in ambient noise in European freshwater habitats: noise levels, spectral profiles, and impact on fishes. *Journal of the Acoustical Society of America* 121: 2559-2566.

Wysocki LE, Codarin A, Ladich F, Picciulin M. 2009. Sound pressure and particle acceleration audiograms in three marine fish species from the Adriatic Sea. *Journal of the Acoustical Society of America* 126: 2100-2107.

STATEMENT OF ACADEMIC INTEGRITY

I hereby certify that the submitted thesis “Acoustic and thermal characterization of river landscapes” is my own work, and that all published or other sources of material consulted in its preparation have been indicated. Where any collaboration has taken place with other researchers, I have clearly stated my own personal share in the investigation (see Introduction). I confirm that this work, in the same or a similar form, has not been submitted to any other university or examining body for a comparable academic award.

Berlin, 28 April 2011

Diego Tonolla

ACKNOWLEDGMENTS

Most people say that it is the intellect which makes a great scientist. They are wrong: it is character (Albert Einstein).

I would like to thank Klement Tockner for mentoring my dissertation, being a supportive and constructive advisor, providing the opportunity to work on several interdisciplinary projects at the EAWAG (Swiss Federal Institute of Aquatic Science and Technology) and at the IGB (Leibniz-Institute of Freshwater Ecology and Inland Fisheries), and for giving me a lot of freedom. I would also like to thank Mark Lorang for co-advising my dissertation, for giving me the opportunity to work for a couple of months at the Flathead Lake Biological Station in Montana, for teaching me the principles of hydraulic and morphology, for his extensive scientific and personal support, and for some gorgeous river rafting. I wish to thank Vicenç Acuña (ICRA, Catalan Institute for Water Research) for teaching me so much, for sharing his ideas and experience regarding manuscript writing, data analysis and presentation skills, and for his general support, never-ending enthusiasm and friendship.

The manuscripts presented in this thesis have strongly benefited from my interactions with the bright minds of many other co-authors from various research groups. Kurt Heutschi (EMPA: Swiss Federal Laboratories for Materials Science and Technology; Laboratory of Acoustics) provided excellent advice on environmental acoustic data analysis and acoustic methodology. Christian Wolter (IGB; Department of Biology and Ecology of Fishes) introduced me to the fascinating world of fishes, and supported me in conducting electro-fishing surveys in the Oder River. Thomas Ruhtz (FU: Freie Universität Berlin; Institute for Space Sciences) assisted in the collection and processing of huge amounts of remotely-sensed images, and spent a lot of time with me in interesting discussions on the potential and limitations of remote-sensing imagery and unmanned aerial systems. Urs Uehlinger collected and provided the temperature data of the Roseg and Tagliamento floodplains. Chris Gotschalk supported the sound data collection process in the USA, introduced me to Matlab, and cooked me the best wild salmon I have ever eaten. Thomas Frank (EMPA; Laboratory of Building Science and Technology) advised me on IR methodology and IR data analysis at the beginning of my thesis. Furthermore, I would also like to express my deepest gratitude to Alexander Sukhodolov for his comments and suggestions on general hydraulics questions which arose during the construction of the flume manuscript, Christoph Tanner for his

professional support with IR thermal data acquisition in the Roseg and Tagliamento floodplains, and the Cessna pilot Carsten Lindemann for providing flight support and for his skills during remote-sensing flights over the Oder River. I have always felt comfortable while working with all of you, and I feel lucky and grateful to have shared ideas with you during the developpment of my thesis. All of you contributed a great deal to the accomplishment of this work.

I would like to express my special gratitude to all of the people who helped out so generously during the field data collection process, sometimes under harsh environmental conditions. In particular, I would like to acknowledge Christian Schomaker, Alexander Türck, Henrik Zwadlo, Arnd Weber, Jan Hallermann (all IGB), Christopher Kyba (FU), Michael Döring (EAWAG), Fabian Peter, Diego and Claudio Cruciat, Oliver Siegrist and Prisca Beeli. I am also deeply grateful to Lukas Indermaur (EAWAG) for sharing relevant data on the Tagliamento floodplain, as well as to Michael Monaghan and Stefano Larsen (both IGB) for the final English review of the general introduction and discussion section. Further, I acknowledge all IGB and EAWAG colleagues and many friends spread across the world for their general support. I am especially thankful to Maria Alp, Nike Sommerwerk and Stefano Larsen, for their good company, general support and friendship, as well as for making me laugh during some tough times.

I would like to express my gratitude for the essential logistics, administrative and financial support provided by the EAWAG, the IGB and the MAVA foundation. Many thanks also to the Laboratory of Hydraulics, Hydrology and Glaciology (VAW) for providing the flume for my initial experiments on underwater acoustic.

Finally, I would like to thank my mother Emilia, my father Giancarlo and my sister Maura, as well as my fiancée Prisca for their never-ending encouragement, their presence and love, and for their ability to lower my stress level throughout my academic career. You kept me going and this thesis is lovingly dedicated to you!

CURRICULUM VITAE

„Der Lebenslauf ist in der Online-Version aus Gründen des Datenschutzes nicht enthalten“

Publications

Peer-reviewed publications

Tonolla D, Wolter C, Ruhtz T, Tockner K. 2011. Thermal heterogeneity and fish assemblages in a dynamic river floodplain mosaic (Oder River, Germany). Submitted to *Ecography: Pattern and Diversity in Ecology*.

Tonolla D, Lorang MS, Heutschi K, Gotschalk CC, Tockner K. 2011. Underwater soundscapes along river corridors. *Limnology and Oceanography*. In revision.

Tonolla D, Acuña V, Uehlinger U, Frank T, Tockner K. 2010. Thermal heterogeneity in river floodplains. *Ecosystems* 13: 727-740.

Tonolla D, Acuña V, Lorang MS, Heutschi K, Tockner K. 2010. A field-based investigation to examine underwater soundscapes of five common river habitats. *Hydrological Processes* 24: 3146-3156.

Tonolla D, Lorang MS, Heutschi K, Tockner K. 2009. A flume experiment to examine underwater sound generation by flowing water. *Aquatic Sciences* 71: 449-462.

Book chapters

Tockner K, Uehlinger U, Robinson CT, **Tonolla D**, Siber R, Peter FD. 2009. Introduction to European Rivers. In *Rivers of Europe*, Tockner K, Uehlinger, U, Robsinson CT (eds). Elsevier Publisher: London; 1-21.

Tockner K, Uehlinger U, Robinson CT, Siber R, **Tonolla D**, Peter FD. 2009. European Rivers. In *Encyclopedia of inland waters*, Likens GE (ed). Elsevier Publisher: Oxford; 366-377.

Popular articles

Tockner K, **Tonolla D**, Junker B, Heutschi K. 2009. Der Klang der Flüsse. *Nationalpark* 1: 20-21.

Tonolla D. 2008. Lauschangriff unter Wasser. *Der Spiegel* 2: 135.

Tonolla D, Tockner K, Junker B, Heutschi K. 2008. The sound of rivers. *EAWAG Annual Report*: 29.

Tockner K, Uehlinger U, Robinson CT, **Tonolla D**, Siber R, Peter FD. 2008. European rivers under pressure. *EAWAG Annual Report*: 31.

Tonolla D. 2007. Fliessgeflüster, Wellenrauschen. *Geo*: 20-26.

Moretti M, **Tonolla D**, Altenburger I, Duelli P. 2004. Biodiversità delle selve castanili del Mont Grand (Soazza, Grigioni). *Quaderni Grigionitaliani* 73: 355-362.